

The
University
Of
Sheffield.

Increasing the Imaging Speed of Stochastic Optical Reconstruction Microscopy

Mary Louise Snape

The University of Sheffield

Department of Physics and Astronomy

Thesis submitted for the degree of Doctor of Philosophy

Supervised by Ashley Cadby and Andrew Furley

September 2016

Abstract

This thesis investigates methods of increasing the imaging speed of Stochastic Optical Reconstruction Microscopy (STORM); a superresolution imaging technique which breaks the diffraction limit by imaging single molecules. Initially the imaging conditions were optimised to maximize both the Signal-to-Noise Ratio (SNR) and the number of molecules localised in order to push the system to image at the fastest rate possible. It was found that the lowest readout laser power possible should be used at a frame rate between 100 - 150 fps. The optimum concentration of MEA - a component of the STORM imaging buffer - was found to be 100 mM.

Whilst the optimized conditions afford some speed increase, there is a more fundamental question to be investigated: how many localisations are required for an accurate reconstruction of the sample? The answer to this question will allow a reduction in the image acquisition time by only imaging until the minimum number of molecules have been localised.

The density of localisations was studied over time and a simple histogram analysis suggested that using a trade off between density and localisation limited regimes is a valid method to increase the imaging speed by determining a "finishing point". The localisation density increased linearly over time for all samples tested, however some areas reached the cut off density more quickly than others. Using several analysis methods and simulated data it was shown that the blinking behaviour of molecules is a random process and that the variability in resolution across an image is mostly due to a non uniform labelling distribution.

Finally, dual colour samples were imaged, as labelling the target structure with two coloured dyes was hypothesised to double the imaging speed. This was found to be true, however there was no overall reduction in acquisition time as dual labelled samples have a slower increase in localisation density over time.

Acknowledgements

I would not have been able to undertake a PhD if it were not for my supervisors, Ashley Cadby and Andrew Furley. Thank you for all the guidance and encouragement, for all the support and patience over the years - it means a lot to me. I would never have made it this far without all your help!

To my family: the parents and the sibs, thank you so much. You've always been there for me whenever I need it, thank you for believing in me and encouraging me, especially over the last four years of my PhD. You guys are the best!

I would like to thank the members of my physics group ("Group Ash"), past and present, for all their help and support: Amy, Tania, Nic C, Nic R, Sam & James ("Sames"), Liyana, Adrian, Dawn and Charlotte. Our socials are always excellent and the trip to FOM was a blast! There's no other group of people I'd like to be stuck with in a stuffy darkened room for hours at a time. To my biology group: Ora, Basudha and Alex, thank you for being so friendly and teaching me the ropes when I was new and knew nothing.

Thank you to Bob Tuner, who wrote the initial STORM analysis code, Victoria Lund who helped prepare *staphylococcus aureus* samples and Miguel Juárez for maths and statistics knowledge.

Thank you to my office mates: Theo, Bracher, Ben, Stringer, Tom, James and Jon for providing ample distractions and tea breaks.

To the rest of my friends, thank you all for being there through the good times and the bad. I definitely wouldn't have made it through this without you!!! Emma and Bryony, you girls have been so great and I'm so glad that I met you both! I know I can always count on you to cheer me up when I'm having a bad day. To the BMS crew, thank you for all the after work drinks (and after after work drinks). To Nic and Nikki, thank you for the lunch dates and for taking me out to poptarts all the time! To Mandi and Nat (and Em and MK), you guys are hilarious! Thanks for brightening up the long nights spent writing my thesis, and yelling at me to get back to work when I got too distracted chatting. To my home squad: Naomi, Jane and Laura. I'm so grateful to have met you guys and that we've stayed friends throughout school, university and beyond. Cheers for all the top bants over the years!

Finally, special thanks goes out to Amy and Nikki, who helped proofread sections of my thesis.

Publications

S. F. H. Barnett, M. L. Snape, M. Juarez, A. J. Cadby. '*A Novel Application of Non-Destructive Readout Technology to Localization Microscopy*', *Scientific Reports*, 7:42313 doi:10.1038/srep42313. (2017)

A. J. Parnell, A. L. Washington, O. O. Mykhaylyk, C. J. Hill, A. Bianco, S. L. Burg, A. J. C. Dennison, M. L. Snape, A. J. Cadby, A. Smith, S. Prevost, D. M. Whittaker, R. A. L. Jones, J. Patrick. A. Fairclough, A. R. Parker. '*Spatially modulated structural colour in bird feathers*', *Scientific Reports*, 5:18317. doi: 10.1038/srep18317. (2015)

B. Chapa-y-Lazo, E. G. Allwood, I. I. Smaczynska-de Rooij, M. L. Snape, K. R. Ayscough. '*Yeast endocytic adaptor AP-2 binds the stress sensor Mid2 and functions in polarized cell responses*', *Traffic*, 15, pp. 546-557. doi:10.1111/tra.12155. (2014)

Conference Presentations

CMIAD Retreat, Sheffield, UK, 2016 (Poster, Flash Presentation)

Focus On Microscopy, Göttingen, Germany, 2015 (Poster)

CMIAD Retreat, Sheffield, UK, 2015 (Poster, Flash Presentation)

CMIAD Retreat, Sheffield, UK, 2013 (Flash Presentation)

Table of Contents

| | |
|-------------------------------|-----|
| Abstract..... | II |
| Acknowledgements..... | III |
| Publications..... | IV |
| Conference Presentations..... | IV |
| Table of Contents..... | V |

Chapter 1: Introduction and Background

| | |
|---|----|
| 1.1 – Lenses, Microscopes and Geometric Optics..... | 2 |
| 1.1.1 - Refraction..... | 2 |
| 1.1.2 – Diffraction..... | 8 |
| 1.1.3 – Compound Microscopes..... | 16 |
| 1.1.4 – Light Detection..... | 19 |
| 1.2 - Electron Microscopy..... | 25 |
| 1.3 - Fluorescence Microscopy..... | 27 |
| 1.3.1 – Fluorescence..... | 29 |
| 1.3.2 – Biological Labelling..... | 32 |
| 1.3.3 - TIRF Microscopy..... | 33 |
| 1.4 – Ensemble Superresolution Imaging..... | 34 |
| 1.4.1 - NSOM..... | 34 |
| 1.4.2 - SIM..... | 36 |
| 1.4.3 - STED..... | 37 |
| 1.4.4 - Single Molecule Localisation..... | 38 |
| 1.5 – Stochastic Optical Reconstruction Microscopy..... | 40 |
| 1.5.1 – Principles of STORM..... | 40 |
| 1.5.2 – Reconstruction Algorithms..... | 42 |
| 1.6 – Aims and Reasons for Project..... | 44 |
| 1.7 - References..... | 46 |

Chapter 2: Materials and Methods

| | |
|--|----|
| 2.1- Cell-Line Culture..... | 52 |
| 2.1.1 - NIH3T3-GL Culture..... | 52 |
| 2.1.2 - Staphylococcus Aureus Culture..... | 52 |
| 2.2 - Primary Culture..... | 52 |
| 2.2.1 - Animals..... | 52 |
| 2.2.2 - Dorsal Root Ganglion Dissection..... | 52 |
| 2.2.3 - DRG Culture..... | 53 |
| 2.3 - Preparation of Cover slips..... | 53 |
| 2.3.1 - Cover Slips for Cell Line Culture..... | 53 |
| 2.3.2 - Cover Slips for Primary Culture..... | 53 |
| 2.4 - Fluorescent Labelling..... | 53 |
| 2.4.1 - Mammalian Cell Labelling..... | 53 |
| 2.4.2 - Bacterial Cell Labelling..... | 54 |
| 2.5 - Mounting Cover Slips..... | 55 |
| 2.6 - Microscopy..... | 55 |
| 2.6.1 - Wide Field Microscopy..... | 55 |
| 2.6.1 - STORM..... | 55 |
| 2.6.2 - STORM Reconstruction Algorithm..... | 55 |
| 2.7 - Tables of Reagents..... | 58 |
| 2.7.1 - Mammalian Cell Culture Media..... | 58 |
| 2.7.2 - List of Buffers and Fixatives for Mammalian Culture..... | 59 |
| 2.7.3 - List of Buffers and Fixatives for Bacterial Culture..... | 60 |
| 2.7.4 - STORM Buffer..... | 61 |
| 2.7.5 - List of Fluorescently Conjugated Labels..... | 61 |
| 2.8 - References..... | 62 |

Chapter 3: Building and Optimisation

| | |
|--|----|
| 3.1 - Introduction..... | 64 |
| 3.2 – Results..... | 69 |
| 3.2.1 – Measuring the Point Spread Function..... | 70 |

| | |
|---|----|
| 3.2.2 – Optimisation of Readout Laser Power..... | 71 |
| 3.2.3 - Optimisation of Frame Rate..... | 81 |
| 3.2.4 - Effect of changing the STORM buffer concentrations..... | 85 |
| 3.3 - Conclusions..... | 89 |
| 3.4 - References..... | 91 |

Chapter 4: Reconstruction Density Limit

| | |
|--|-----|
| 4.1 - Introduction..... | 93 |
| 4.2 – Results..... | 101 |
| 4.2.1 - Simple Image Quality Analysis (small section analysis) | 101 |
| 4.2.2 - Image Quality Analysis: Radial Distances Histograms..... | 106 |
| 4.2.3 - Image Quality Analysis: Actin Cables..... | 111 |
| 4.2.4 - Cut-off Point Analysis in Staphylococcus Cells..... | 115 |
| 4.2.5 - Cut-off Point Analysis in Actin..... | 122 |
| 4.2.7 - Dependence of Cut Off Density with Laser Power..... | 124 |
| 4.3 - Conclusions..... | 128 |
| 4. 4 - References..... | 131 |

Chapter 5: Imaging with Dual Labelled Samples

| | |
|---|-----|
| 5.1 – Introduction..... | 134 |
| 5.2 – Results..... | 138 |
| 5.2.1 - Selection of Secondary Fluorophore..... | 139 |
| 5.2.2 - Testing the Increase in Imaging Speed..... | 142 |
| 5.2.3 - Investigation of Dual Labelled Blinking Dynamics..... | 146 |
| 5.3 – Conclusions..... | 148 |
| 5.4 - References..... | 150 |

Chapter 6: Discussion and Conclusions

| | |
|---------------------------------------|-----|
| 6.1 - Discussion and Conclusions..... | 153 |
| 6.2 - References..... | 158 |

Appendix

| | |
|---------------------------------|-----|
| Matlab Functions..... | 160 |
| 1 - Binned_cutoff..... | 160 |
| 2 - Kmeans_column..... | 164 |
| 3 - Kmeans_position..... | 168 |
| 4 - KmeansGroup..... | 172 |
| 5 - LM_actin_density_new..... | 176 |
| 6 - LM_BlinksPerSec..... | 180 |
| 7 - LM_CircularAreaDensity..... | 182 |
| 8 - LM_findPSF..... | 184 |
| 9 - LM_radialdistances..... | 186 |
| 10 - Make_binary..... | 189 |
| 11 - Simulate_seaweed..... | 190 |
| 12 - Simulate_seaweed_2..... | 192 |
| 13 - Simulate_seaweed_3..... | 194 |
| 14 - SNR_finder..... | 196 |
| 15- Sortemitters..... | 197 |
| 16 - LM_blinkofftime..... | 199 |

1: Background and Theory

Contents

| | |
|---|----|
| 1.1 – Lenses, Microscopes and Geometric Optics | 2 |
| 1.1.1 - Refraction..... | 2 |
| 1.1.2 – Diffraction | 8 |
| 1.1.3 – Compound Microscopes | 16 |
| 1.1.4 – Light Detection..... | 19 |
| 1.2 - Electron Microscopy | 25 |
| 1.3 - Fluorescence Microscopy | 27 |
| 1.3.1 – Fluorescence | 29 |
| 1.3.2 – Biological Labelling..... | 32 |
| 1.3.3 - TIRF Microscopy..... | 33 |
| 1.4 – Ensemble Superresolution Imaging | 34 |
| 1.4.1 - NSOM..... | 34 |
| 1.4.2 - SIM | 36 |
| 1.4.3 - STED | 37 |
| 1.4.4 - Single Molecule Localisation..... | 38 |
| 1.5 – Stochastic Optical Reconstruction Microscopy..... | 40 |
| 1.5.1 – Principles of STORM..... | 40 |
| 1.5.2 – Reconstruction Algorithms | 42 |
| 1.6 – Aims and Reasons for Project | 44 |
| 1.7 - References | 46 |

1.1 – Lenses, Microscopes and Geometric Optics

There are many ways that scientists can observe the world around them both directly and indirectly, but the simplest way – employed successfully throughout history – is to observe phenomena visually through sight.

The smallest object the naked human eye can discern is around 0.07mm in diameter¹, which corresponds to approximately the width of a single human hair. In order to see objects any smaller, tools are required to magnify the object, hence the invention of the microscope and telescope.

1.1.1 - Refraction

Simple microscopes (or magnifying glasses) - consisting of a single convex lens - have been used since classical antiquity if not earlier. The earliest surviving reference of a glass “burning lens” used to focus light and cauterize wounds is from the comedy *'The Clouds'* written by Aristophanes in 423 B.C.^{2,3} and the first explicit reference to the magnifying properties of lenses can be found in Seneca's *'Naturales Quaestiones'* (65 A. D.)^{4,5}:

Letters, however small and dim, are comparatively large and distinct when seen through a glass globe filled with water.

Lenses work via a property of light known as refraction, which is described using *Snell's Law*, first discovered by Ibn Sahl in 984 A.D.⁶ in Baghdad but is credited to the experimental work of Dutch Astronomer Snellius in 1621⁷. Snell's Law states:

$$n_1 \sin \theta_1 = n_2 \sin \theta_2 \quad (1.1)$$

where n = refractive index of material, θ_1 = angle of incidence and θ_2 = angle of refraction (Figure 1.1).

Refraction occurs when a beam of light moves into or out-of media with differing refractive indices. The refractive index of a material is defined as:

$$n = \frac{c}{v} \quad (1.2)$$

where n = refractive index, c = speed of light in a vacuum and v = phase velocity of light in the material.

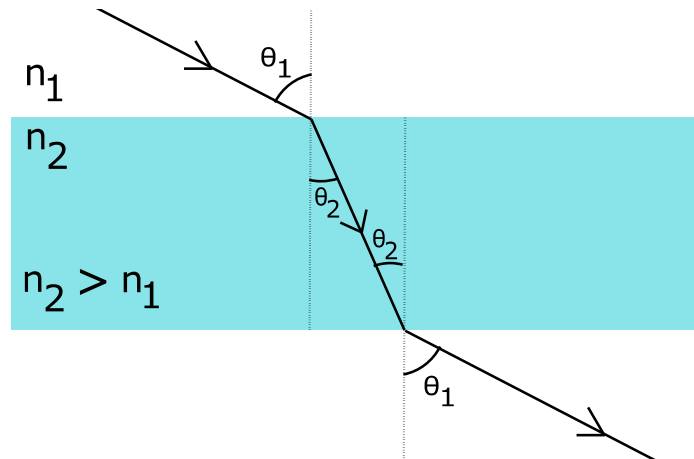


Figure 1.1: A beam of incident light is refracted towards the normal when entering a medium with a higher refractive index ($n_2 > n_1$). The light is refracted away from the normal upon travelling back into a lower n material.

The refractive index is therefore a measure of how much slower light travels in different media compared to light in a vacuum. When light travels across the interface between two different media it bends either towards or away from the normal. This is because of the differences in the speeds at which light propagates through the two materials.

When travelling from a lower refractive index material (n_1) such as air to a higher refractive index material (n_2) such as glass, the light beam bends towards the normal (figure 1.2). If the beam is incident at 0° , there is no refraction.

An analogy for the refraction of light is of driving a car from tarmac into sand. If driving at an angle, the tyre that hits the sand first will slow down. The other wheel will continue at the same speed until it also hits the sand, causing the car to bend towards the normal. Once both tyres are in the sand and travelling at the same speed the car will continue in a straight line. The reverse occurs when travelling in the opposite direction- the car or light beam bends away from the normal.

Snell's law can be derived by considering figure 2.2 – a wave front undergoing refraction, moving from a lower density material to a higher density material. D_1 is the extra distance the far end of the wave front travels in the lower density material before reaching the material interface – D_2 is the corresponding distance the near end of the wave front travels in the same amount of time, Δt .

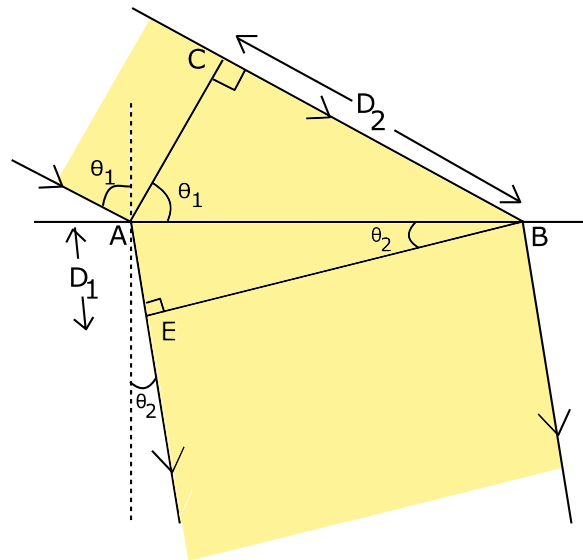


Figure 1.2: Diagram for the derivation of Snell's Law depicting a wave front travelling from a less- to a more-dense medium.

As the distance travelled is equal to the velocity multiplied by the time taken for travel:

$$D_1 = v_1 \Delta t \qquad D_2 = v_2 \Delta t \qquad (1.3)$$

As the two triangles ABC and ABE share a hypotenuse

$$\frac{\sin \theta_1}{D_1} = \frac{\sin \theta_2}{D_2} \qquad (1.4)$$

Substituting in equations (1.3) and (1.2) into (1.4) produce Snell's Law (1.1).

The bending of light rays via refraction can be exploited by changing the shape of the interface between the two different materials, e.g. in a microscope lens.

A lens can be shaped with non-refracting, convex or concave edges. A lens with only one refracting edge is known as a simple lens; a lens with larger number of refracting edges is known as a compound lens⁸. A convex or convergent lens focuses light into a point whereas a concave or dispersive lens bends the light such that it appears to be coming from a virtual focus point (figure 1.3). In microscopes, convex lenses are used most commonly.

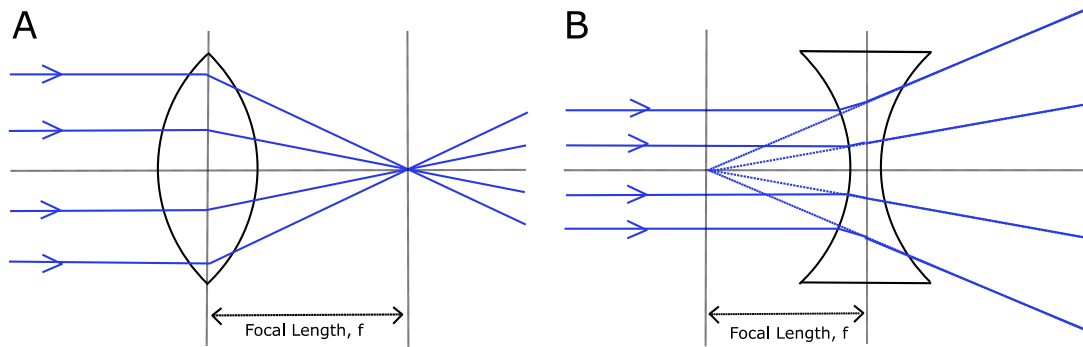


Figure 1.3: Focusing ray diagrams for (A) a convex lens and (B) a concave lens.

Both the curvature and the refractive index of the lens defines how much the light refracts, and therefore where the focus point will be located. The larger the difference between n_{glass} and n_{air} , the more the light refracts and the shorter the focal length will be. Similarly, the larger the curvature of the lens, the larger the change in direction of the light wave and therefore the shorter the focal length.

The *Lensmaker's formula* or *thin-lens equation* for a thin lens in air is given by:

$$\frac{1}{s_0} + \frac{1}{s_i} = \frac{1}{f} = (n_i - 1) \left(\frac{1}{R_1} - \frac{1}{R_2} \right) \quad (1.5)$$

Where R_1 and R_2 are the radius of curvature of the lens (figure 1.4), n_i is the refractive index of the lens, f is the focal length of the lens, s_0 is the distance from the object to the lens and s_i is the distance from the lens to the image.

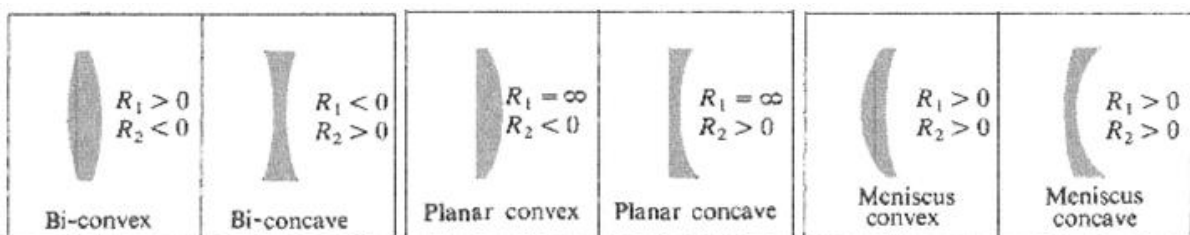


Figure 1.4: Diagram⁸ showing different lens shapes depending on the radius of curvature, R_1 and R_2

Lenses not only focus light – they can also be used to magnify objects, making them appear to be larger without changing the real size of the object.

The principle of magnification using a simple convex lens is demonstrated in the ray diagram in figure 1.5. The average human eye has a minimum 'working distance' of $\sim 250 \text{ mm}^1$ (also known as

the least distance of distinct vision, LDDV) at which it can produce a sharp image. If two close-together objects $O-O^1$ (indicated by red arrows) are placed at the LDDV, the visual angle subtended by the eye in this case is small (I , dashed line, blue arrow) and so the image at the eye is also small.

However, if a convex lens is introduced and the objects are moved (purple arrows) to the focal distance, f , this effectively increases the visual angle - causing a larger image to be formed at the retina. The image has therefore been magnified¹.

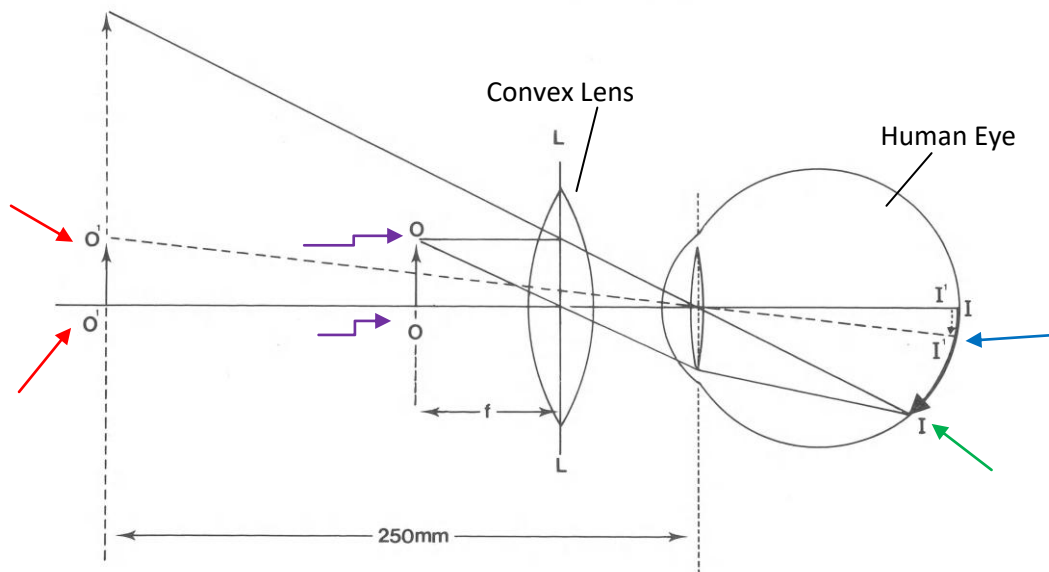


Figure 1.5: Diagram demonstrating the magnification properties of lenses¹

Magnification can be calculated using similar triangles ABE and CDE (figure 1.6)

$$M = \frac{h_i}{h_o} = -\frac{d_i}{d_o} \quad (1.6)$$

$$M = \frac{f}{d_o - f} = \frac{d_i - f}{f} \quad (1.7)$$

where M = magnification, h_i = image height, h_o = object height, d_i = distance from lens to image and d_o = distance from lens to object.

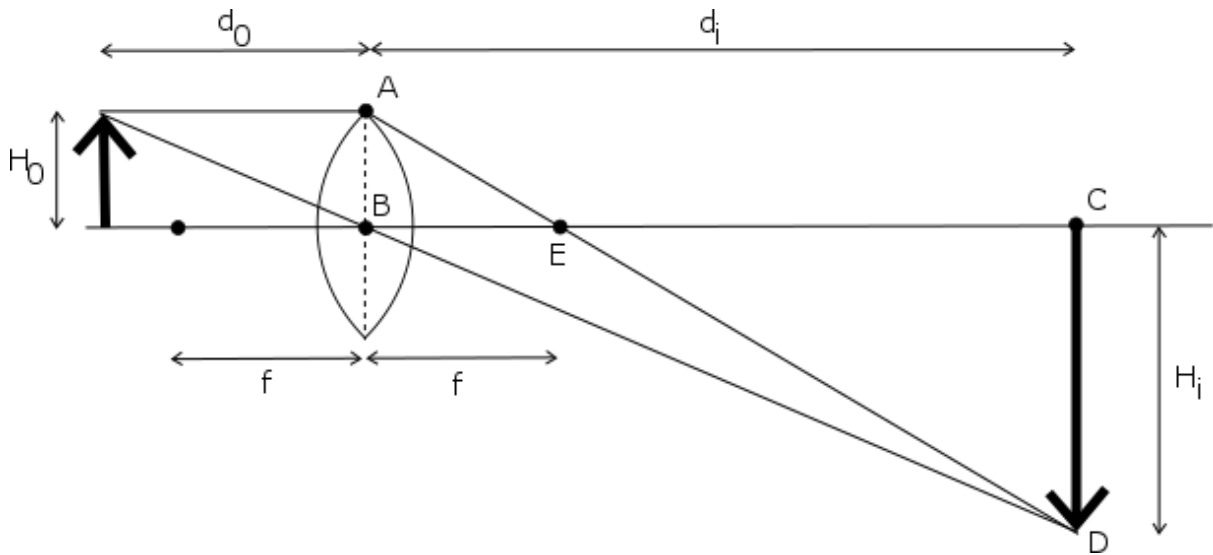


Figure 1.6: *Magnifying Glass Ray Diagram. An object (H_o) is magnified by the lens and an image is formed (H_i).¹*

Magnification with a single lens depends on distance from the lens and is therefore not a fixed quantity. However, for two or more lenses the magnification is defined as:

$$M = \frac{f_1}{f_2} \quad (1.8)$$

1.1.2 - Diffraction

Diffraction is the spreading out of light as it passes the edges of an object or travels through a small aperture. Classically, electromagnetic radiation - light - can be described as a wave. The light wave spreads out and bends around the object. As the light spreads out the waves interfere with each other, causing constructive and destructive interference fringes. This band pattern, seen at far distances, is due to Fraunhofer diffraction. Figure 1.7 shows the diffraction pattern for light travelling through a single slit. Bright bands are formed where light interferes constructively, and dark bands where the waves interfere destructively.

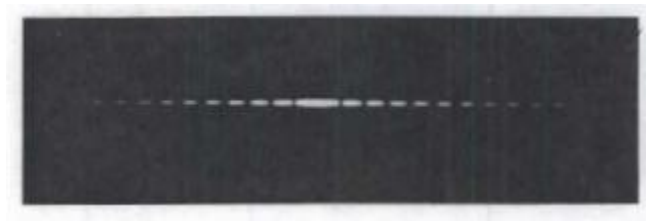


Figure 1.7: *Diffraction pattern of light through a single slit (taken from⁸). A central bright fringe can be seen, with smaller bright bands of decreasing intensity on either side.*

For the case of light travelling through a single slit, the positions of the interference maxima and minima can be calculated. Consider a coherent beam of light shone through a slit of width a onto a screen placed at a distance D , such that $D \gg a$. An interference minimum is seen at point y .

The *Huygens-Fresnel Principle* states:

“Every unobstructed point of a wave front, at a given instant, serves as a source of spherical secondary wavelets (with the same frequency as that of the primary wave). The amplitude of the optical field at any point beyond is the superposition of all these wavelets (considering their amplitudes and relative phases).”⁸

In order to form a minima, all sources of wavelets must cancel at point y . If the wave front at the slit is split into N sections, consider the point where $N = 1$ and the point at $N/2$, located just below the midpoint of the slit. As $D \gg a$, $\theta \approx \theta'$. The path difference, δ , travelled by a wave from these two locations can be calculated (Figure 1.8 B):

$$\delta = \frac{a}{2} \sin \theta \quad (1.9)$$

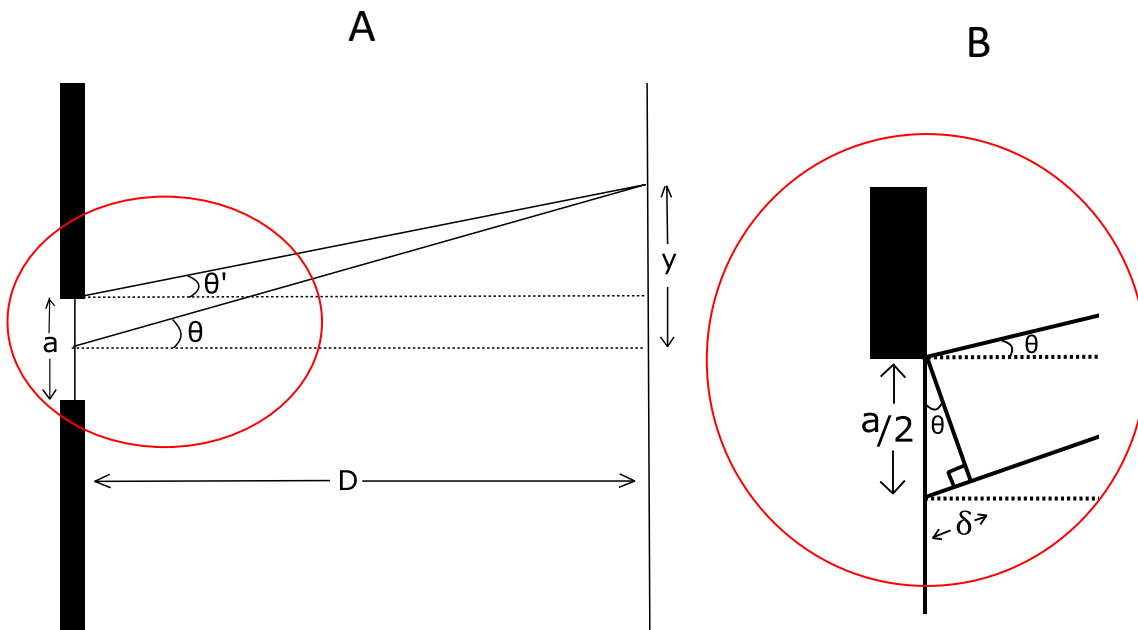


Figure 1.8: Diagram for Single Slit Diffraction. (A) Light is shone through a single slit of width a and is viewed on a screen at a distance D . The light beam diffracts and interferes with itself to form a minima on the screen at point y . (B) Close up of the red circled region, δ represents the extra path length travelled

In order for the two waves to interfere destructively, the path distance must be a whole number of half wavelengths.

$$\frac{a}{2} \sin \theta = \frac{m\lambda}{2} \quad (1.10)$$

$$\sin \theta = \frac{m\lambda}{a} \quad (1.11)$$

All N sections can be paired up in this way, such that all waves cancel and there is a minimum intensity at y .

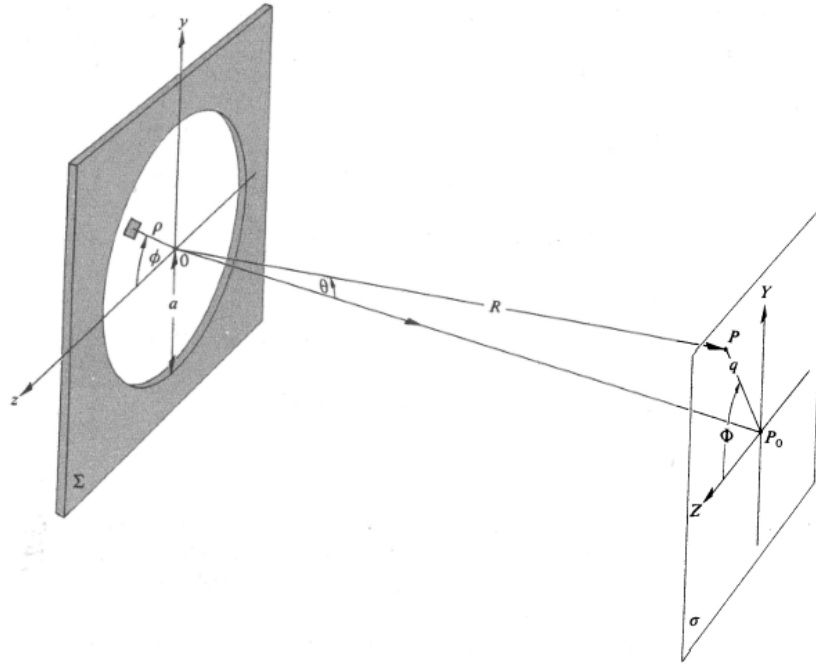


Figure 1.9: Diagram for diffraction through a circular aperture.⁸

For the case of diffraction through a circular aperture, the diffraction pattern is known as an *airy disk* and forms a bright central spot, surrounded by concentric circular bands which decrease in intensity as the radius increases (figure 1.10). This diffraction pattern as it appears on the viewing screen/camera sensor is known as the Point Spread Function (PSF).

The intensity across the airy disk can be calculated. Again, using the Huygens-Fresnel principle, each point at the aperture, dS , can be treated as a coherent point source of spherical light waves (figure 1.9). The optical disturbance at point P is:

$$dE = \left(\frac{\varepsilon_A}{r}\right) e^{i(\omega t - kr)} dS \quad (1.12)$$

Where ε_A is the source strength per unit area, r is the distance from dS to point P and $e^{i(\omega t - kr)}$ is the equation for a plane wave.

Writing this in spherical coordinates and integrating to find E gives the equation:

$$\tilde{E} = \frac{\varepsilon_A e^{i(\omega t + kR)}}{r} \int_{\rho=0}^a \int_{\Phi=0}^{2\pi} e^{i\left(\frac{k\rho q}{R}\right) \cos(\varphi - \Phi)} \rho \, d\rho \, d\Phi \quad (1.13)$$

Due to the axial symmetry, can assume the disturbance at any point P is independent of Φ . The equation can therefore be simplified by setting $\Phi = 0$.

Equation (1.13) includes a term which is in the form of a Bessel function – a slowly decreasing oscillatory function. The first order Bessel function term is given by:

$$J_0(u) = \frac{1}{2\pi} \int_0^{2\pi} e^{iu \cos(v)} dv \quad (1.14)$$

Using properties of the Bessel function, this allows equation (1.13) to be rewritten as:

$$\tilde{E}(t) = \frac{\epsilon_A e^{i(\omega t + kR)}}{r} 2A \left(\frac{R}{kaq} \right) J_1 \left(\frac{kaq}{R} \right) \quad (1.15)$$

Where A is the aperture area. Taking the real part of equation (1.15) gives the irradiance. Again, using the properties of the Bessel function, this can be rewritten as:

$$I(\theta) = I(0) \left[\frac{2J_1(kaq/R)}{(kaq/R)} \right] \quad (1.16)$$

The first minima of the airy disk occurs at the first 0 of the $J_1(u)$ term, i.e. when $J_1(u) = 0$. From tables, this occurs when $(kaq/R) = 3.38$. This therefore gives the radius to the first minima, q_1 , as:

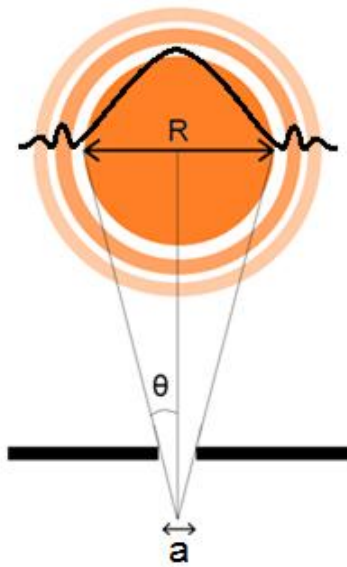
$$q_1 = 1.22 \frac{R\lambda}{2a} \quad (1.17)$$

If the diffracting aperture is a lens focused on a screen, $R \approx f$, the focal length of the lens. Therefore, the radius to the first minima is given by:

$$q_1 = 1.22 \frac{f\lambda}{D} \quad (1.18)$$

Decreasing apertures (D) and increasing wavelengths (λ) increase the distance to the first minima i.e. cause the light beam to be diffracted more. Derivation taken from Hecht (2014)⁸.

A



B

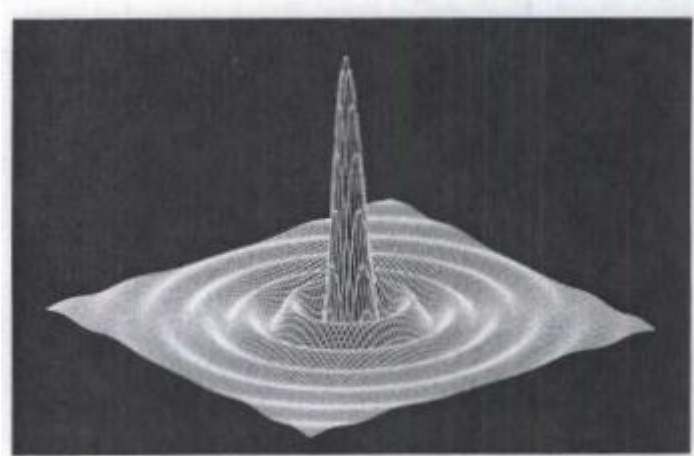


Figure 1.10: Diffraction patterns for a circular aperture. (A) The orange concentric circles represent the diffraction pattern seen on a screen, the black trace represents the intensity function of the light. θ is the angular resolution - that is, the angle to the first minima. (B) A 3D representation of the intensity pattern of an airy disk⁸

Diffraction affects microscopy as light diffracts as it travels through lenses in an optical system. In a non-diffracting system, a lens would focus light down to a perfect spot (Figure 2.11 A)- however, due to diffraction the focus point becomes enlarged (Figure 2.11 B). The size of the focus area is dependent on the wavelength of light, as this determines how much the light diffracts.

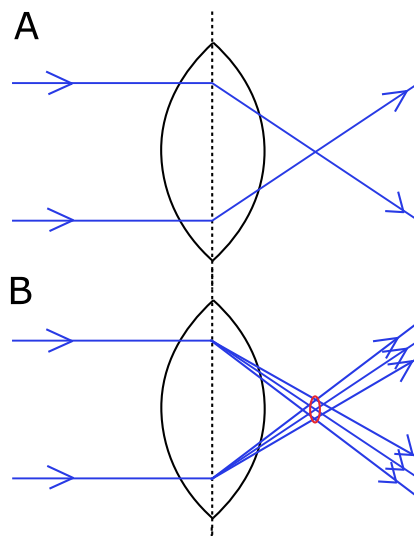


Figure 1.11: Light diffracting through a lens. (A) In a non-diffracting system light focuses to a point. (B) Light diffracts – spreads out – and the focus point is now spread over an area (denoted in red)

This spreading out of light also works in reverse - point sources of light when viewed through a lens are subject to diffraction. The resolution of a microscope is often defined by the *Rayleigh Criterion*. This is defined as the minimum distance between two point sources of light such that they are still resolvable. The minimum distance occurs when the first minima of one point occurs at the central maximum of the second point (figure 1.12 - D).

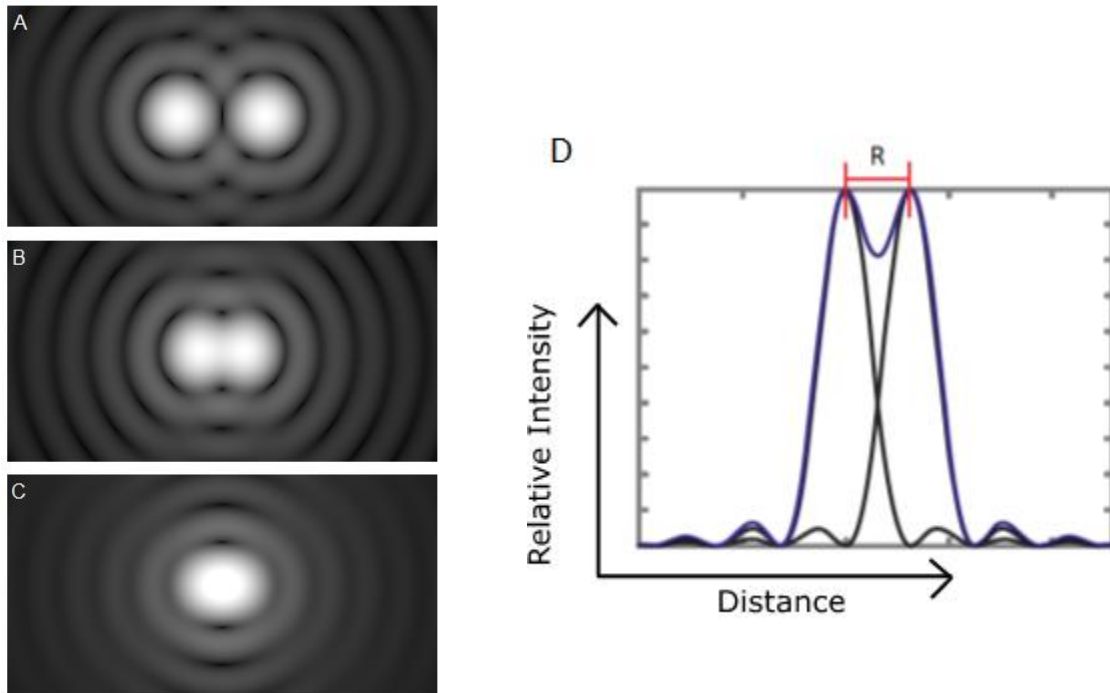


Figure 1.12: The Rayleigh Criterion is defined as the minimum distance between two points such that they are visibly two points. Images A-C⁹ show the airy disks of two molecules that are (A) well separated, (B) at the Rayleigh Criterion and (C) too close to be resolved as separate. The Rayleigh Criterion occurs when the central maximum of the first point overlaps with the first minima of the second(D)¹⁰. The distance between the two maxima, R, is the resolution or minimum length scale visible.

The Rayleigh criterion - the minimum resolvable distance, R, - is therefore the same quantity as q_1 from equation (1.18). The quantity of f/D is known as the 'f-number' of the lens. This can be rewritten in terms of the Numerical Aperture of the lens (NA), which gives the Rayleigh Criterion for the resolution in an image as:

$$R \approx 0.61 \frac{\lambda}{NA} = 0.61 \frac{\lambda}{n \sin \theta} \quad (1.19)$$

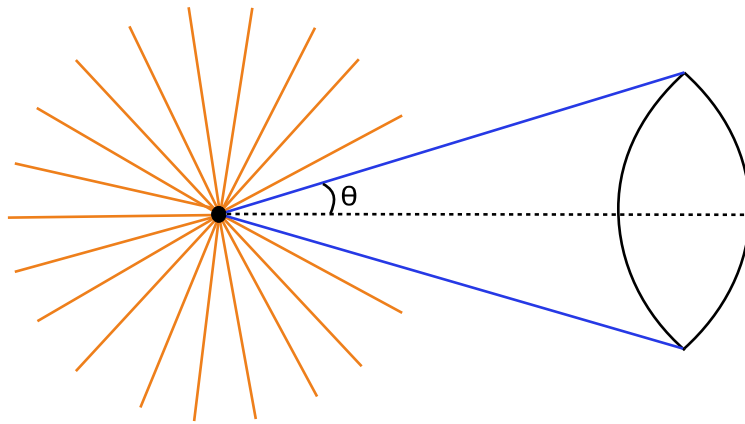


Figure 1.13: The Numerical Aperture of a lens is a measure describing the angle, ϑ , of incoming light rays (yellow) from an object that are able to pass through the lens.

The NA of a lens describes how much light the lens can collect from a sample, or the angle at which light rays from a sample will be collected by the lens and are able to travel through the microscope to be imaged (figure 1.13). It changes depending on the refractive index of the material: with higher refractive indices, the light entering the lens will refract more enabling a larger amount of the wave front to be captured by the lens. The amount a ray of light will diffract also depends on its wavelength – shorter wavelengths will diffract – spread out – less than longer wavelengths resulting in a higher resolution image.

Light diffracts whenever it travels past or through an object – this means it diffracts through microscopy samples. Diffraction through a 3D array of differently sized structures, as in a cell, causes light to be spread out according to the sizes of the periodic structures in the sample. Higher order frequencies – at larger angles of θ – represent smaller periodic structures within the sample. Due to the NA of a lens, the higher frequencies of light are lost. This is demonstrated in figure 1.14. This loss of the higher frequencies of light can be thought of as losing the higher frequency components of the Fourier series which makes up the image.

Equation 1.19 shows that the resolution is determined by the NA of the lens and the wavelength of light. The NA of the lens is limited by the refractive index - whilst this can be increased slightly by using a water ($n = 1.33$)¹⁰, oil ($n \approx 1.5$)¹⁰ or solid ($n \approx 2$)¹⁰ immersion lens it cannot be increased further. The wavelength of visible light ranges from approximately 390 - 700nm. Using the middle value of green light ($\lambda \approx 500$ nm) and $NA = 1$, this gives a maximum resolution of around 250nm. This is what is known as the *diffraction limit*. The diffraction limit determines the minimum length-scales visible in an image – any two points which are closer together than this will “blur” together and be seen as a single shape. The diffraction limit is the limiting factor in the size of details which can be

viewed through a microscope – although an image can be magnified as much as desired, the detail within the image is fixed by the diffraction of light. Details below the diffraction limit of $\sim 250\text{nm}$ are impossible to be viewed using standard optical microscopes.

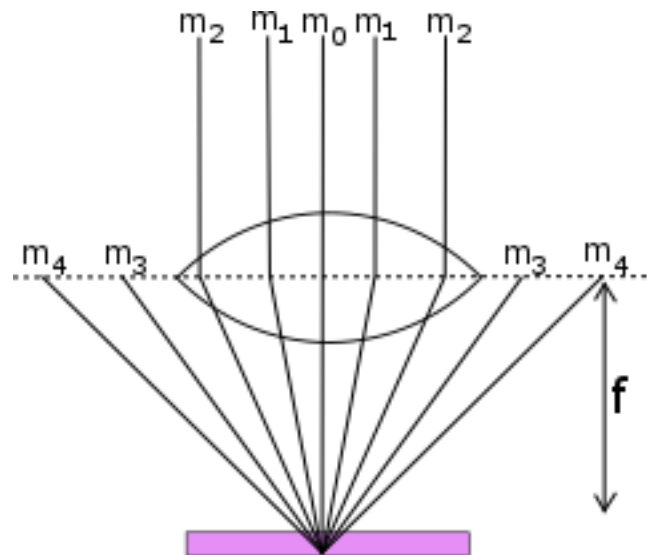


Figure 1.14: Diffraction of light through a sample. Smaller structures in the sample will diffract light more than larger structures. Due to the NA of a lens, higher frequency light (here, $m=3$ and upwards) is lost and is not collected. This limits the maximum resolution of the image

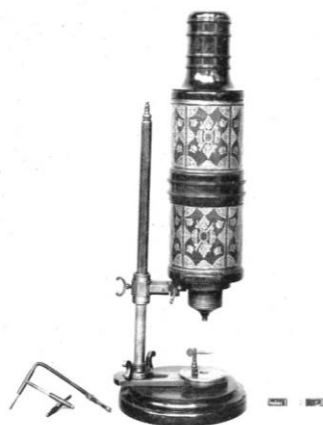
1.1.3 – Compound Microscopes

The magnification properties of lenses were known at least since the time of the Romans, and the first formal discussion of the use of convex lenses was written by Arab scientist Ibn al-Haytham (Alhazen) in *'The Book of Optics'* between 1011 – 1021⁵. However, it was not until the late 16th century when glass making and grinding techniques were starting to advance that the microscope and the telescope as we know them today were invented. The inventor of the first compound microscope is disputed but generally attributed to the Dutch spectacle makers, Zacharias and Hans Janssen in 1595⁵. Their design is thought to have been a simple tube consisting of a bi-convex eye lens and a plano-convex objective lens set in a sleeve enabling the lenses to be moved relative to each other for focusing purposes.

Compound microscopes use a system of multiple lenses in order to achieve higher levels of magnification. For a single lens, the maximum magnification possible is limited for the LDDV of the eye. This means that generally, the maximum magnification possible from a single lens is ~X25. By combining multiple lenses, the total magnification is increased and becomes the product of the individual lenses.

Although the compound microscope was first invented at the end of the 16th Century, the early prototypes were quite blurry and were seen merely as amusements, rather than a serious scientific tool⁵. The first real pioneer of microscopy was perhaps Robert Hooke, who published *'Micrographia'* in 1665¹¹ some 70 years later. Hooke used a simple compound microscope (figure 1.15 A) to make his observations, and is credited with the discovery of cells, first seen in a slice of cork (figure 1.15 B).

A



B

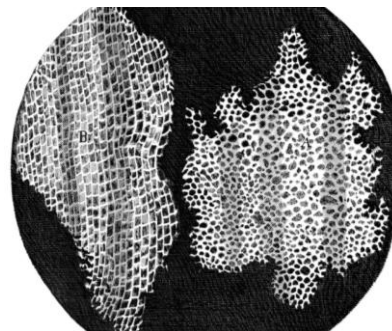


Figure 1.15: (A) A compound microscope, believed to have been used by Hooke⁵, (B) Hooke's discovery of the cell in a slice of cork¹¹

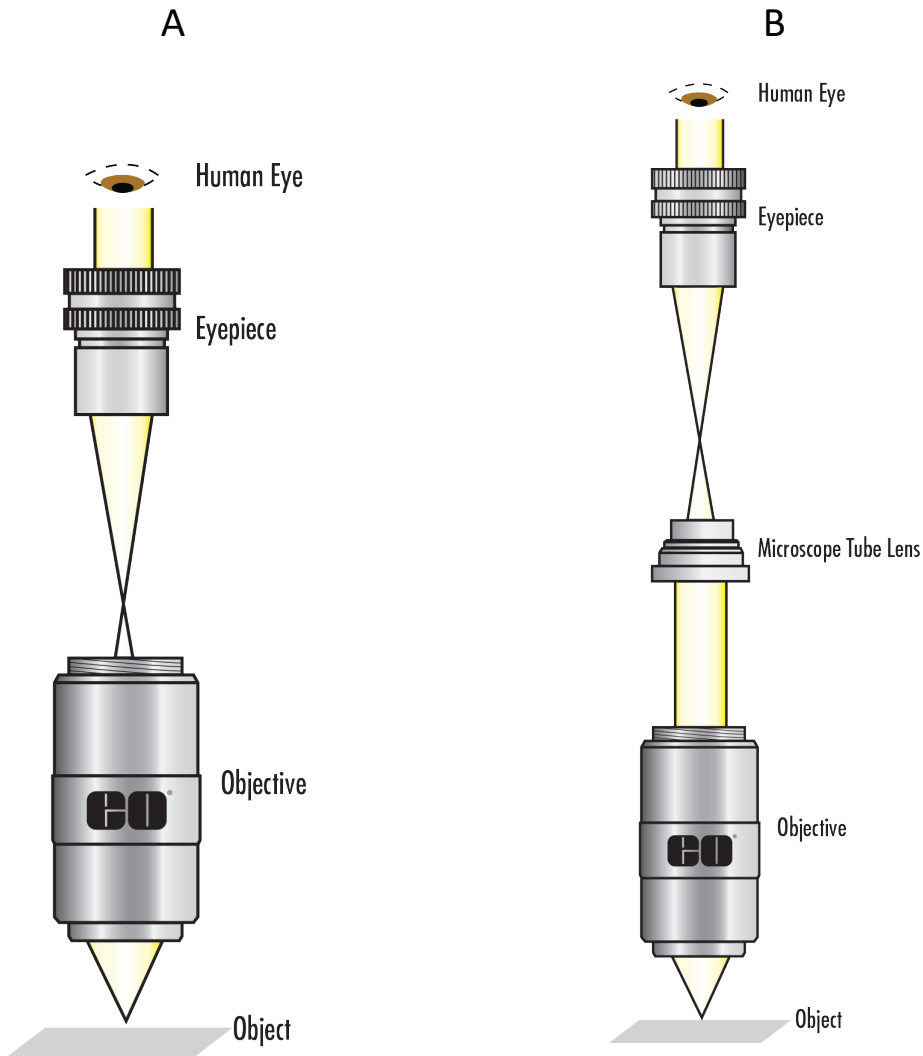


Figure 1.16: Ray diagrams for (A) a finite and (B) an infinity-corrected compound microscope¹²

Two-lens microscopes consist of an objective lens used to collect light from the sample and form a real, inverted image at the focus point of the objective. This is then paired with an eyepiece lens that collects the light diverging from the real image and is used to magnify the image and display an enlarged virtual image for the viewer. This type of microscope is also known as a finite compound microscope. A ray diagram of this set-up can be seen in figure 1.16 A.

Most modern microscopes however use the set-up as seen in figure 1.16 B – they are infinity corrected. In finite compound microscopes, the distance between objective and eyepiece – the tube length – is fixed, which means that no new optical components can be added to the light path. In infinity corrected microscopes, light emerges from the objective in parallel, which allows the addition of extra optics in the light path without changing the focus¹³. The tube lens then converges

the light to a focus which is again picked up with the eyepiece lens. The magnification of the objective is the ratio of the tube lens focal length and the objective focal length – this means the overall magnification can be changed by changing the focal length of the tube lens¹³. The limiting factor in these microscopes for NA is the thread-size or the diameter of the objective aperture. For a fixed NA, the longer the tube length the larger the diameter of the aperture must be.

In addition to the three lenses in a compound microscope, objective lenses are often much more complicated than a single lens; they are made from many individual lenses. Figure 1.17 shows an example objective lens. It is desirable to collect as much incoming light as possible, so the lens has a very wide incoming angle or numerical aperture (also see figure 1.14). However, this angle is so large all the light cannot be focused into a point immediately so the first few lenses in the system bend the light by a small amount until it can be focused. Other lenses in the system are used to correct for aberrations such as chromatic, astigmatism and comatics. Chromatic aberrations occur as different colours of light are diffracted through different angles causing blurring of the focal point⁸, astigmatism of the lens causes light travelling in different planes to have different focal lengths and comatic aberrations cause distortion of off-axis objects. Correcting for all these aberrations requires precision engineering of the glass and is the reason why the microscope did not become popular for over 2000 years after the first mention of focusing lenses in literature.

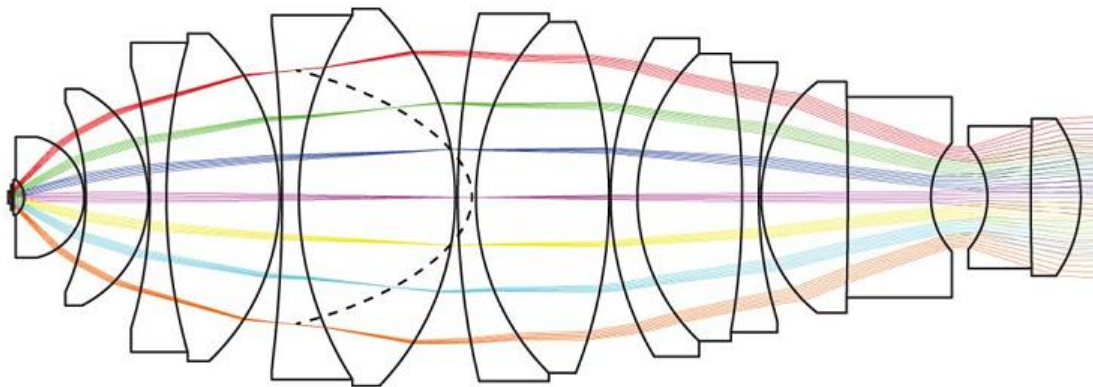


Figure 2.17: *Objective Lens Diagram*¹⁴. An objective lens is made up of a series of different lenses.

1.1.4 - Light Detection

Before the digital age, scientists had to draw what they saw down a microscope in order to share their discoveries (figure 1.15 B). However, in modern times the image from the microscope is now projected onto the sensory array of a digital camera. Cameras collect incoming photons and convert them into an electrical signal which can be read by a computer.

There are two main types of camera used in scientific imaging – Electron Multiplying Charge-Coupled Devices (EMCCD) and Scientific Complementary Metal-Oxide Semiconductors (sCMOS). Both of these cameras detect photons via the same basic principles but information is read out to the computer differently.

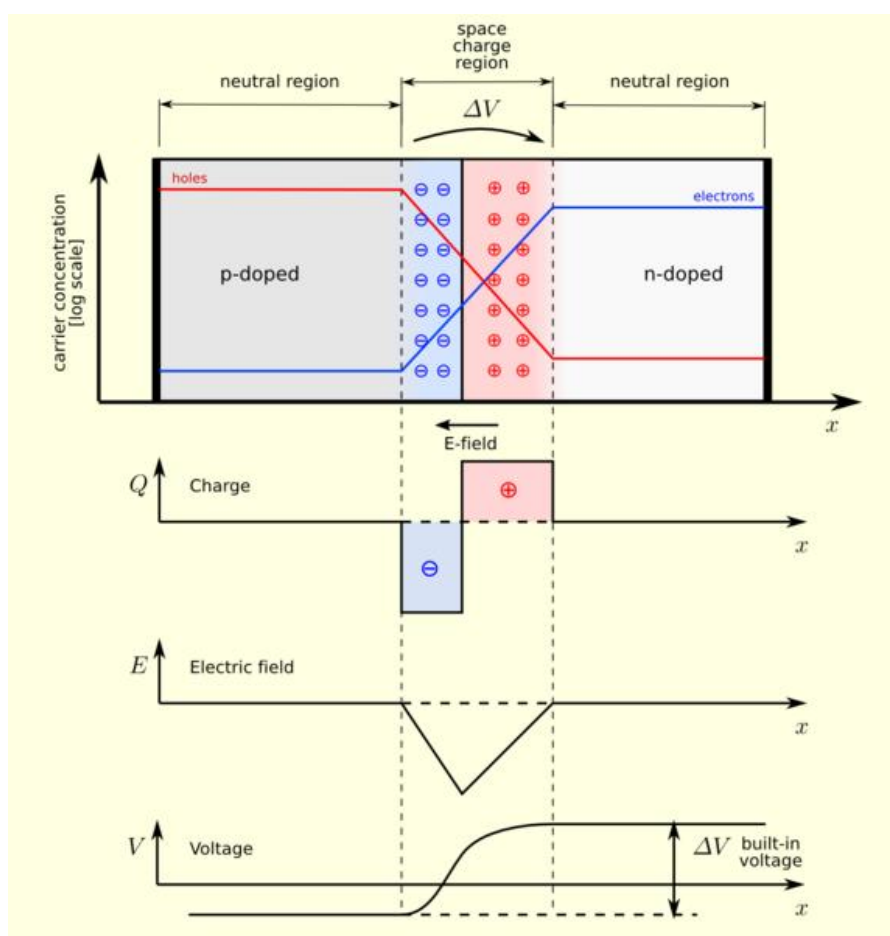


Figure 1.18: Diagram of a p-n junction. Negative electrons and positive holes are attracted to each other and form a potential well¹⁵

The sensor array of a camera is made up of many pixels. Each pixel is made up of a photodiode, which consists of a semiconductor p-n junction. The p-n junction is the boundary between p-doped (a material with an excess of positively charged holes) and n-doped (a material with an excess of negatively charged electrons) semiconductor layers. Due to diffusion, negative free electrons in the

n-region move into the p-region, leaving positively charged holes in their absence. This build-up of charge at the junction causes the formation of an electric field which opposes the movement of charge due to diffusion. The system is in equilibrium when the net movement of charge is equal to zero.

The build-up of charge leaves the photodiode with a natural potential difference across the junction, forming a potential well. The area at the junction where there are no free charges is known as the depletion region or space charge region.

Photodiodes are designed to be run in reverse bias – this is when the p-doped material is connected to the negative terminal and the n-doped material is connected to the positive terminal. Reverse bias acts to increase the voltage drop over the depletion region – that is, increase the width of the depletion region. This ensures that there is very little current in the system when no light is incident as it is difficult for a charge to flow across the depletion region. Any current (movement of charge) which does flow in the absence of any incoming photons is called the dark current.

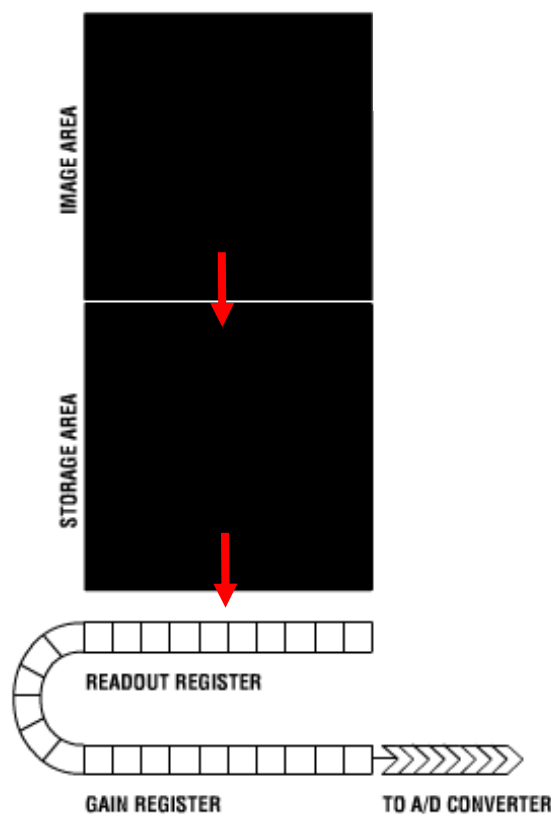


Figure 1.19: Diagram of an EMCCD Chip. Photons are incident on the sensing (image) area and are turned into electrons. Once an image has been built up, the electrons are downshifted into the storage area which is shielded from incoming photons. The electrons are then sent through the readout and gain registers before being digitised in the A/D converter¹⁶

If an incoming photon strikes on or near the depletion region, an electron-hole pair is formed due to the photoelectric effect. The photoelectric effect occurs when an incoming photon with sufficient energy excites an electron from the valence band into the conduction band of the semiconductor. The electron is then collected in the quantum well formed by the p-n junction.

Each pixel is 'open' for a certain amount of time to collect photons – this corresponds to the frame rate the camera is run at. Each pixel collects electrons, the number of which is proportional to the number of photons that were incident on that area. Once the sensor has been exposed to the light for the correct amount of time, the pixels are downshifted and emptied row-by-row using a sinusoidally varying voltage to shift the electrons from one quantum well to another (figure 1.19) to the storage area – the sensing area is then free to start collecting photons for the next image in the series.

Each row is then shifted through the read-out register and through the electron-multiplication register (also known as the gain register) before being amplified and turned into electrical signals read by the computer. The gain register is unique to EMCCD cameras and works via a process known as clock-induced charge or impact ionisation, in a similar way to avalanche photodiodes. The gain register increases the signal via a process whereby energetic electrons trapped in the quantum well collide with another electron, allowing it to escape from the valence band as an electron-hole pair. The electron is then trapped in the quantum well, creating 'extra' signal (figure 1.20). In the gain register, the electrons are run through a series of pixels where the clocked voltage to transfer electrons between pixels is much higher than required. This higher voltage accelerates the electrons more quickly, allowing impact ionisation to occur. The gain in an EMCCD camera is controlled by controlling the voltage of the gain register electrodes and is calculated by

$$G = (1 + g)^N \quad (1.20)$$

Where G = gain, g = probability of impact ionisation occurring (dependent on the voltage) and N = number of pixels in the gain register¹⁷.

The probability of impact ionisation occurring is dependent on voltage and temperature. The electron-multiplication stage of an EMCCD camera can cause over a gain increase of x1000, vastly increasing the signal detected by the camera¹⁷.

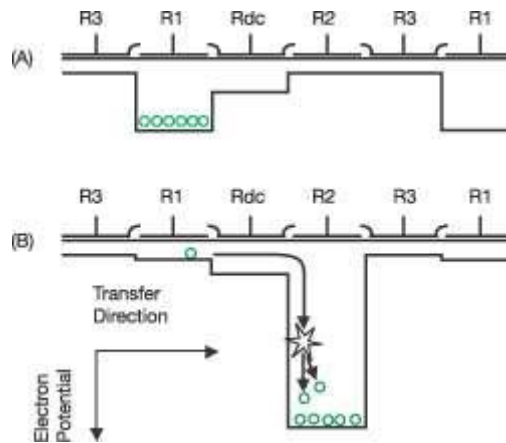


Figure 1.20: Diagram showing an EMCCD Gain register. (A) Electrons are caught in a quantum well. (B) Electrons are accelerated by a voltage causing impact ionisation¹⁸

In comparison, in a sCMOS camera the photoelectrons are converted into voltage at the pixel¹⁹. Each row of pixels is read out separately and immediately after the image has been taken as each row of pixels has its own charge amplifier to digitise the signal. This allows for much faster frame rates as electrons do not have to be carefully transferred over a large number of pixels – EMCCD cameras need to be careful they do not run at too high speeds, as this causes the electrons to gain too much energy and be lost from the quantum wells or cause excess noise due to impact ionisation. sCMOS cameras are therefore significantly cheaper to produce than EMCCD cameras, whose sensor chips must be carefully grown as one single device. However, as sCMOS cameras have an array of charge amplifiers which all work at slightly different quantum efficiencies, this means that not all pixels are exactly the same: some may amplify the signal more or less than others.

Both EMCCD and sCMOS cameras are subject to thermal noise or the dark current. This is the noise that is present when there is no light incident on the camera sensor. Thermal noise is caused by energetic electrons which escape the semiconductor sea of electrons and collect in the pixel potential wells, causing a current to flow through the readout read-out register hence the name ‘the dark current’. The thermal noise increases over time as more and more electrons accumulate in the pixel wells. Thermal noise also increases at higher temperatures. To counteract this, cameras are often cooled.

Each pixel quantum well can only hold a certain amount of electrons before becoming saturated. Saturating the pixels causes a loss of information as electrons are lost from the well. The electrons that escape may cause a ‘bleeding’ effect if they travel far enough to spill into neighbouring pixels. Reducing the exposure time will counteract this problem.

The quantum efficiency (QE) of a camera refers to the percentage of incoming photons that are detected and turned into signal. In a perfect sensor, this would be 100%, however in reality the QE value for an EMCCD camera is slightly lower at ~92% and for a sCMOS ~72%²⁰. This value is lower for sCMOS cameras mainly because they are designed to be cheap to process, and are therefore less accurately built.

The read-out noise of a camera is inherent to both EMCCD and sCMOS cameras and is caused by the digitisation step where the electron charges are amplified and turned into a digital signal which can be read by a computer. The noise associated with the charge amplifier increases with readout speed. In an EMCCD camera all pixels are run through the same read-out register and therefore have the same read-out noise. In an sCMOS camera, each row of pixels is read-out by a different charge amplifier so read-out noise is not constant throughout the sample. Typical read-out noises for EMCCD cameras are $< 0.1 e^-$, and around $1.3 e^-$ for sCMOS²⁰. The read noise is so low for EMCCD cameras because of the electron-multiplying step. The gain multiplies the number of electrons by such a large amount that the number of electrons lost in the digitisation step is negligible compared to the signal.

There is also noise associated with the gain register of an EMCCD camera – this is known as the excess noise factor (ENF) and comes from the fact that the electron multiplication is a random process and the same number of extra electrons will not be generated each time through the gain register.

Shot noise originates from the fact light travels as discrete photons. Photons originating from the laser are created at random. Over large time-scales the fluctuations in photon intensity is negligible, however at very low counts this variation becomes more important.

EMCCD cameras have very low read noises and high quantum efficiencies and therefore appear to be the best choice of camera for super resolution imaging. However, any noise within the sensor is amplified along with the signal in the gain register which reduces the Signal-to-Noise Ratio (SNR). This causes the effective QE to be “approximately $\frac{1}{2}$ of the nominal QE”²⁰. Figure 1.21 shows the relative SNR for varying numbers of incident photons. In all but very low light conditions (< 10 input photons per pixel) sCMOS cameras actually produce a better SNR. The green shaded section of the graph represents typical photon counts for all imaging. Therefore, sCMOS cameras will be used throughout this project.

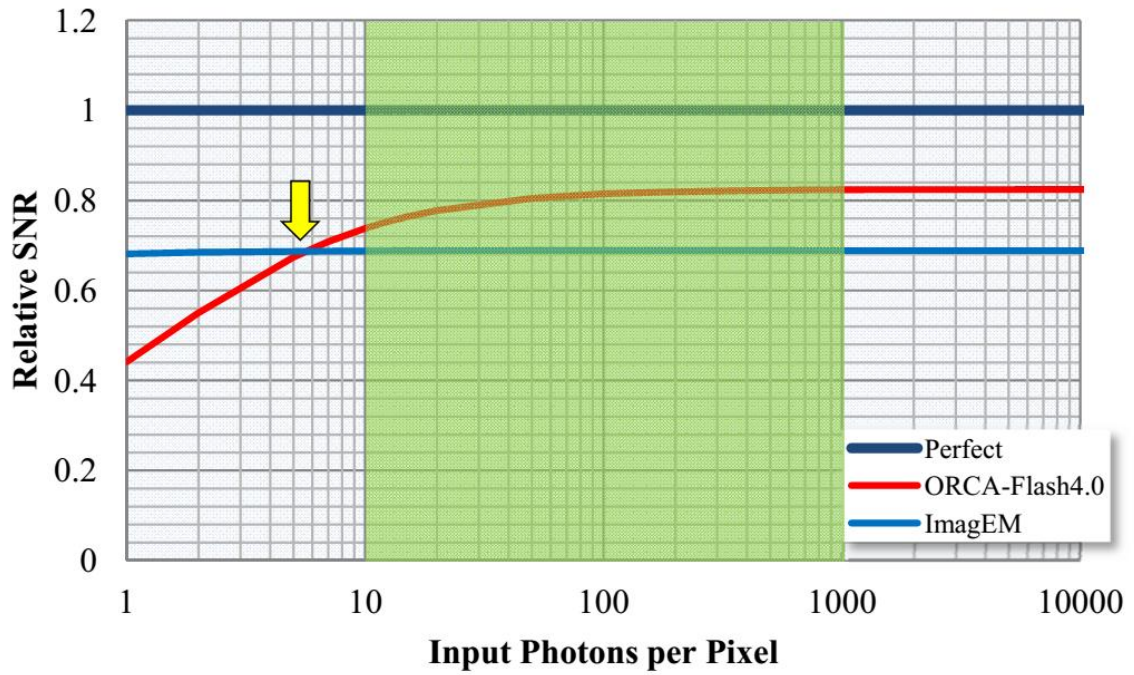


Figure 1.21: Performance comparison of EMCCD vs sCMOS cameras – testing the Signal-to-Noise Ratio over different numbers of incident photons per pixel²⁰. Green shaded area represents typical photon counts for fluorescence microscopy.

1.2 - Electron Microscopy

After the optical microscope, the next big advancement in the field of microscopy came in the 1930's with the invention of the electron microscope. Using the Rayleigh Criterion (equation 1.19), the resolution can be improved by using shorter wavelengths to illuminate the sample (λ) – shorter wavelengths of light diffract less, resulting in a better resolution. This can be done with UV light or x-rays however these are not often used for several reasons. UV light is of a higher energy than visible light and therefore causes more background fluorescence in the cell, as well as causing physical damage. UV light also causes fluorophores to bleach out more quickly. As an additional concern, cameras tend to perform better with light towards the red end of the spectrum.

In the early 20th century the wave-particle duality theory was postulated, which gives rise to the concept of particles having a wavelength. The wave-particle duality theory is a part of quantum mechanics which states that particles - such as the electron - can exist and display properties of both particles and waves. The 1929 Nobel Prize in physics went to Louis-Victor de Broglie, for the discovery of the wave-like properties of electrons. His doctoral thesis in 1924, *Recherches sur la Théorie des Quanta* (Researches on the Quantum Theory)²¹ proposed an equation to calculate the wavelength of any particle, known as the de Broglie wavelength:

$$\lambda = \frac{h}{p} \quad (1.21)$$

where λ = wavelength, h = Planck's Constant (6.63×10^{-34} J) and p = momentum.

The wave-like nature of electrons was confirmed in 1927 by Davisson and Germer²² when they observed diffraction of electrons through crystal lattices.

The wavelength of an electron depends entirely on its momentum - therefore if the momentum is high, the wavelength will be very small. For example, if an electron is accelerated using 100kV of energy, it will have a wavelength of 3.89 pm - this is 10^5 times smaller than light in the visible spectrum (500nm). This means that electron microscopes have a much higher resolution than standard optical microscopes: detail on the atomic scale is visible. There are however several downsides to electron microscopy (EM), despite the resolution gain.

EM must be performed in a vacuum as electrons are small, highly charged particles and therefore interact strongly with their surroundings. If EM was carried out in air, the electron beam would interact with air molecules instead of the sample. Unfortunately, this means that live EM is not

possible – cells cannot survive a vacuum environment. Preparing samples for EM is difficult as they must be fixed and thinly sectioned. Fixation can cause the introduction of undesirable artefacts into the image due to effects such as membrane deformation and shrinkage²³. Samples are required to be thinly sectioned as the behaviour of the electrons means that they are not very penetrating. EM can also be expensive, and is not as accessible for everyday scientific experiments in the way that optical microscopy is. An example Transmission Electron Microscope image of a staphylococcus aureus cell is shown in figure 1.22.

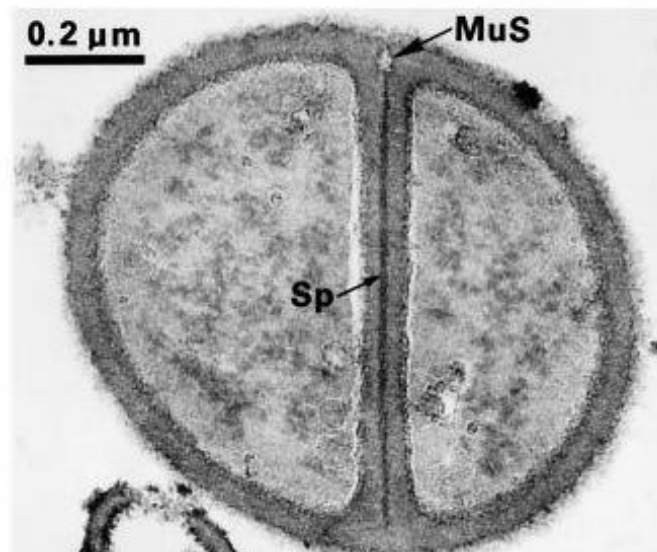


Figure 1.22: Example Transmission Electron Microscope Image of a Staphylococcus Aureus cell undergoing cell division (*Sp* labels the splitting system, *MuS* labels a murosome)²⁴

1.3 - Fluorescence Microscopy

In the years 1911-1913 the fluorescence microscope was invented. Fluorescence is to the ability of a material to emit photons after absorbing light. The term fluorescence was first coined in 1852 by George Gabriel Stokes²⁵ after conducting experiments on fluorspar.

Fluorescence microscopy refers to the technique in which a fluorescently-labelled sample is illuminated with specific wavelengths of light and the resulting fluorescence is selectively detected. Fluorescence Microscopy is regularly used to image biological samples: fluorescent dyes and proteins are attached to specific targets within the cell, which allows the location and movement of these targets to be studied.

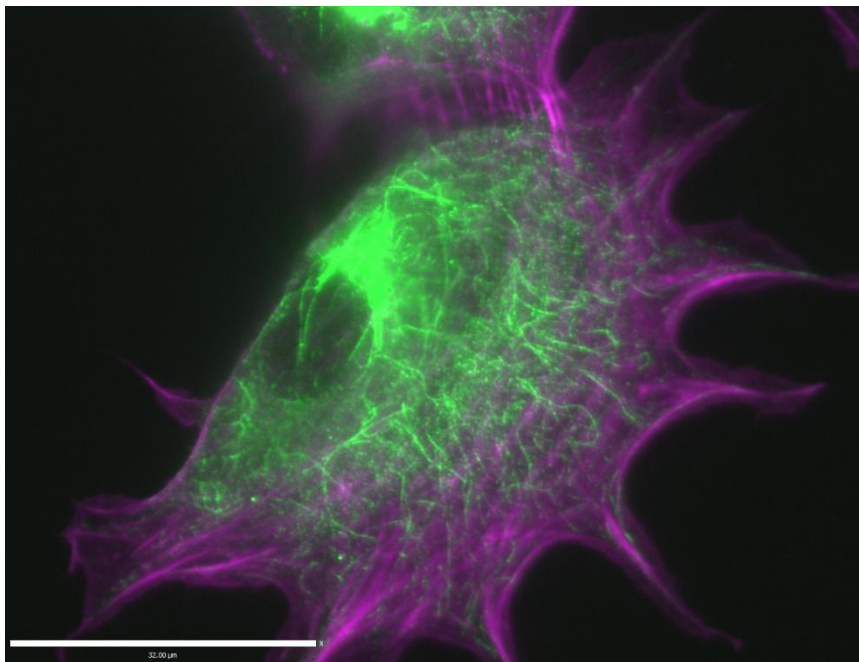


Figure 1.23: Example widefield fluorescence image of a mouse fibroblast (NIH 3T3) cell, labelled with fluorescent dyes attached to actin (purple) and acetylated tubulin (green). Scale bar is 32 μ m.

Despite its current popularity, fluorescence microscopy did not become widely used in the biological sciences until the discovery of Green Fluorescent Protein (GFP) in 1962 by Shimomura²⁶, which won the 2008 Nobel Prize in Chemistry³⁴. GFP was first extracted from *Aequorea victoria* jellyfish and since then has become a hugely powerful tool - biologists are able to manipulate the DNA of organisms such that they grow and express GFP. This allows biologists to study the location of various proteins throughout an organism as it grows. Fluorescent dye molecules are also widely used, and these can be attached to specific targets using antibodies or other methods. Fluorescent labelling of samples is further discussed in chapter 1.3.2.

Whilst fluorescent microscopy is an immensely powerful and important tool it is still limited by the *diffraction* of light. The size of an average human cell is around $10\ \mu\text{m}^2$, but many structures within a cell are on the scale of the diffraction limit or smaller and are therefore unresolvable under optical techniques.

Several methods of fluorescence microscopy have been developed. Widefield microscopy illuminates the entire sample at the same time. This means that out of focus light originating from excited molecules outside of the focal plane reaches the camera as well as emission from fluorophores at the focal plane: this causes a further reduction in resolution, on top of the diffraction of light. Total Internal Reflection Fluorescence (TIRF) and Confocal microscopy were invented to remove out of focus light in an attempt to increase the obtainable resolution.

1.3.1 - Fluorescence

A fluorescent dye emits light due to two processes - absorption and emission. Absorption occurs when a molecule is excited into a higher energy state by gaining energy from absorbing a photon. In order to relax from the higher energy state, the molecule emits a photon. The energy of the emitted photon is determined by the energy drop between the excited state and the ground state. A simple Jablonski diagram for this transition is shown in figure 1.24.

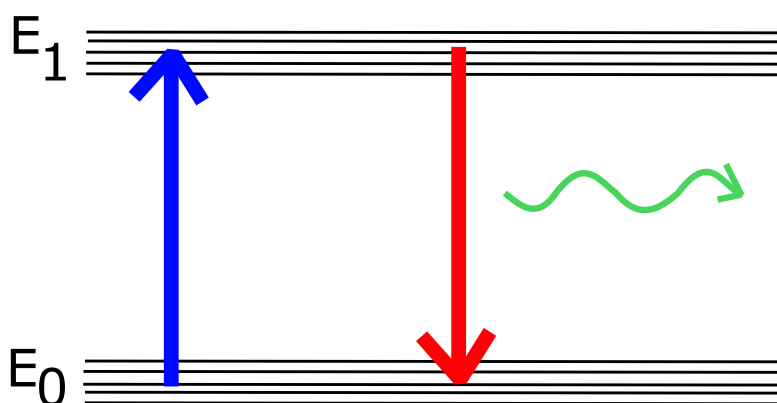


Figure 1.24: Simple Jablonski energy level diagram for a fluorescent molecule. An incoming photon excites the molecule into the excited state (blue arrow) before relaxing back to the ground state (red arrow) by emitting a photon of energy ($E_1 - E_0$) (green arrow). Example vibrational energy states are shown.

Figure 1.24 shows only one example energy level transition, but there are many different ways that a fluorescent dye molecule can be excited into a higher energy level. The absorption and emission of a molecule is therefore not just one single colour, but a spectrum over a large range of wavelengths.

The fluorescent dye molecule that will be most commonly used in this work is Alexa Fluor 647 (AF647). The absorption (dashed) and emission (solid) spectra for this dye are shown in figure 1.25.

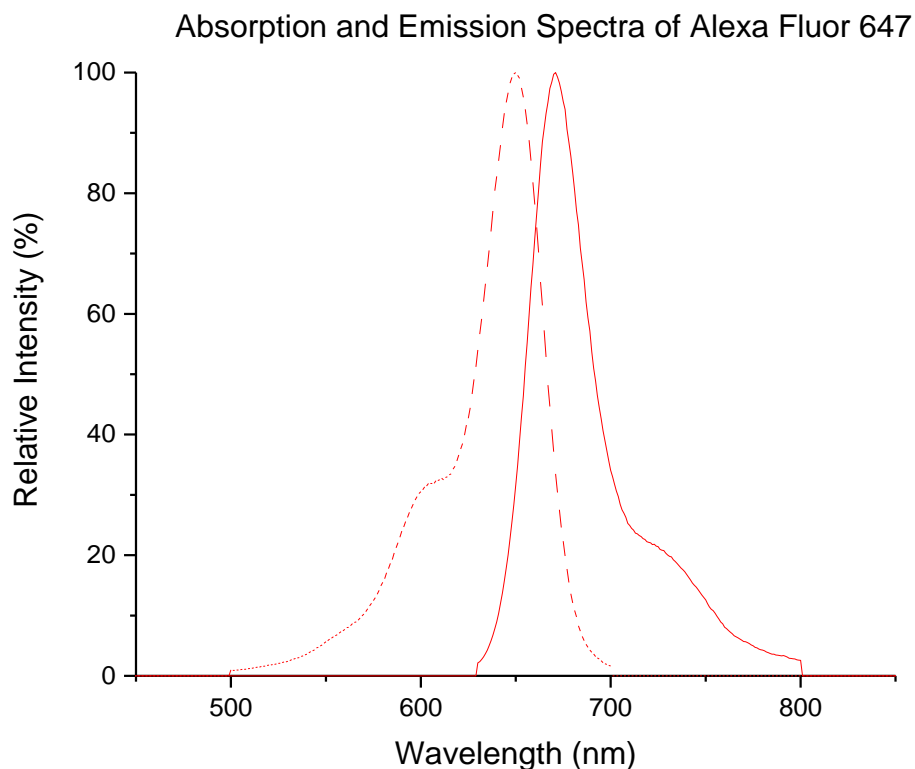


Figure 1.25: Absorption (dashed) and emission (solid) spectra of AF647 dye²⁸

The absorption and emission spectra have peaks at different wavelengths – the absorption peaks at 650nm whereas the emission peaks at 671nm. This difference in peak wavelength allows the excitation source to be separated from the emitted light such that only the emitted light is allowed through to the camera to be detected. Filters, which only allow transmission of select wavelengths of light, are used within the microscope beam path to achieve this.

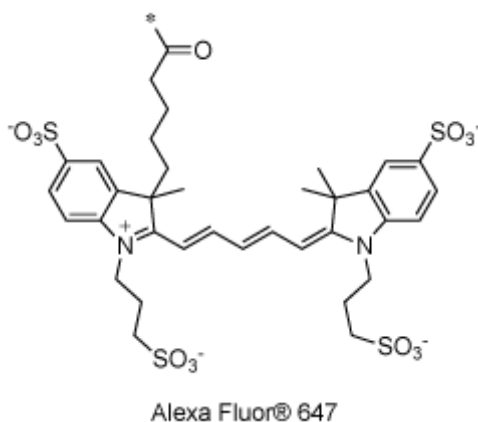


Figure 1.26: Chemical structure of Alexa Fluor 647 fluorescent dye²⁹

The chemical structure of AF 647 is shown in figure 1.26. AF 647 contains a 5-carbon polymethine bridge in the middle of the structure, which is what allows for the fluorescent abilities of the dye. The alternating single and double bonds of the bridge allow the formation of a delocalised cloud of electrons. The bridge therefore forms a quantum well in which the electrons are free to move, allowing the formation of standing waves (figure 1.27). The size of the polymethine bridge therefore dictates the colour of the emitted fluorescence.

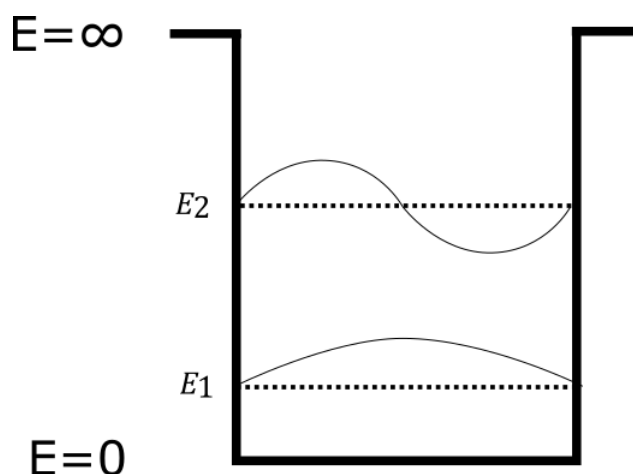


Figure 1.27: *Electrons in a quantum well form standing waves – the wavelength is determined by the width of the quantum well.*

The energy of an electron in an infinite square potential well is given by³⁰:

$$E_n = \frac{\hbar^2}{2m} \left(\frac{n\pi}{d} \right)^2 \quad (1.22)$$

Where \hbar is the reduced Planck constant, m is the mass of the electron, n is the energy level in the well and d is the width of the well.

As the energy of a photon is given by:

$$E = \frac{hc}{\lambda} \quad (1.23)$$

this means that $\lambda \propto d^2$, or the wavelength of an emitted photon is proportional to the square of the width of the quantum well. This means that the wider quantum well is, the longer the wavelength of the emitted photon. For example, AF 647 has a 5-carbon long polymethine bridge and emits in the far red - Cy3 in comparison has a polymethine bridge of only 3 carbons causing the wavelength of light emitted to be shorter: Cy3 emits in the green.

1.3.2 - Biological Labelling

When fluorescently imaging a biological sample, the protein of interest needs to be tagged with a fluorescent molecule. Most commonly, this is done either by over expression of a fluorescent protein or immunolabelling. A scale diagram of antibody labelling is shown in figure 1.28. A primary antibody which specifically targets the protein of interest is applied to the sample. A fluorescently conjugated secondary antibody which specifically attaches to the primary antibody is then applied.

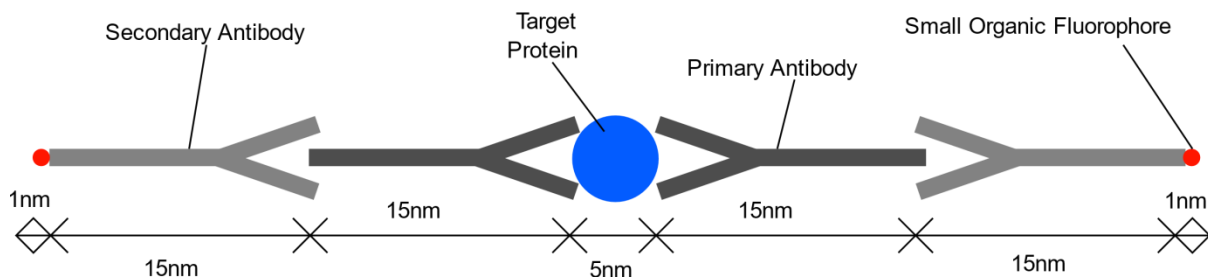


Figure 1.28: Scale diagram of immunofluorescent labelling. A primary antibody (dark grey) selectively attaches to the target protein (blue), a fluorescently conjugated secondary antibody (light grey) then selectively attaches to the primary antibody. Two labels are shown to demonstrate the potential difference in location between fluorophore (red) and target.

The average cellular protein consists of 450 amino acids, with a molecular weight of around 450 kDa³¹. From the theoretical work of Erickson (2009)³², the minimum radius of the average protein would therefore be around 2.4 nm (assuming a spherical shape). The average length of an antibody is 15 nm³³. This means that, as the fluorophore could theoretically be oriented anywhere in space about the target protein, there is a large uncertainty (± 30 nm) associated with using the location of an immunolabelled fluorophore as the location of the target protein³⁴. This makes the distance between target protein and fluorophore ten times larger than the size of the target.

This problem where the fluorophore is located a large distance away from the target protein is not an issue for regular, diffraction limited microscopy as the uncertainty is much smaller than the diffraction limit of resolution (~ 250 nm). However, it becomes more important as must be considered during superresolution imaging (discussed further in chapter 1.6) which can pinpoint the location of a single fluorophore to within ~ 25 nm³⁵.

1.3.3 - TIRF Microscopy

TIRF microscopy works via total internal reflection (TIR) – this is the case of Snell’s Law (equation 1.1) when the angle of refraction, θ_2 , is 90° or larger – i.e. the light beam is reflected from the boundary between n_1 and n_2 (figure 1.1) rather than being transmitted. When the angle of refraction equals 90° , the angle of incidence is known as the *critical angle*, θ_c . If light hits the interface between n_1 and n_2 at the critical angle or larger, the beam will be totally internally reflected. For this to occur, n_1 must be larger than n_2 .

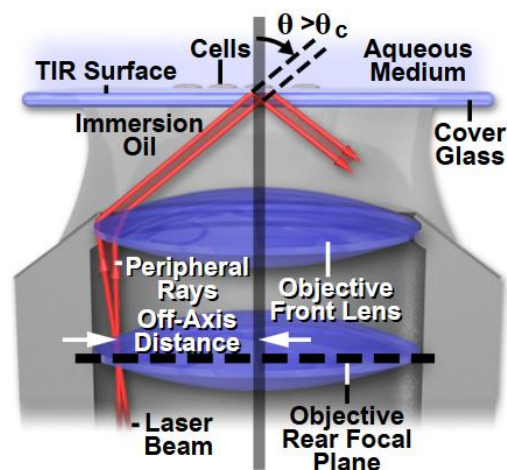


Figure 1.29: TIRF microscopy diagram³⁶

In TIRF microscopy, the excitation beam is aligned off-centre through the objective lens (figure 1.29), causing TIR at the interface between the glass coverslip and the aqueous medium the sample is surrounded with. The excitation beam therefore does not travel into the sample. However, when a beam of light is totally internally reflected, a phenomenon known as an *evanescent field* occurs at the reflection interface. This is a non-propagating electric field whose intensity falls-off exponentially with distance³⁷ and therefore only travels into the sample for a few hundred nanometres. The evanescent field only excites fluorophores located within ~ 100 nm of the glass coverslip and the emission is collected by the microscope optics as normal. This allows select excitation of only a few fluorophores, eliminating emission from out of focus molecules. TIRF microscopy is however limited to studying surface phenomenon.

1.4 – Ensemble Superresolution Imaging

Whilst the invention of the fluorescence microscope was - and still is - hugely important, scientists still spent many years working to “break” the diffraction limit: to image a sample with visible light at resolutions exceeding the diffraction limit. These techniques are termed "superresolution".

There are two main ways of overcoming the diffraction limit problem - ensemble imaging methods - such as NSOM, SIM and STED - and single molecule imaging methods, such as STORM/PALM.

1.4.1 - NSOM

In 1928, a technique now known as the Near-field Scanning Optical Microscope (NSOM/SNOM) was proposed by Synge³⁸, and again in 1956 by O’Keefe³⁹. NSOM, in a similar manner to TIRF microscopy, uses evanescent waves to selectively excite fluorophores near the surface of a sample. Unlike "normal" imaging techniques which use the far field of EM radiation to illuminate the sample, NSOM uses the near field. The near field occurs at very short - sub-wavelength - distances from the source. It is due to these short distances that NSOM is able to achieve superresolution images.

A small probe is scanned across the surface of the sample, such that the distance to the sample is less than the wavelength of light used. As the sample is very close to the detector a larger amount of the high-frequency emission can be collected (also see figure 1.14), resulting in higher resolution images. The probe can either be at a fixed distance throughout, or can change depending on the underlying sample using a feedback loop in a similar manner to Atomic Force Microscopy (AFM). There are two types of probe that can be used for NSOM – aperture and apertureless. In an aperture probe the excitation beam is shone through a small aperture in the scanning probe (figure 1.30). Apertureless NSOM is very difficult to set up, and as such is not commercially available and is not widely used.

In 1972, Ash and Nicholls⁴⁰ successfully used NSOM to break the Abbe diffraction limit for the first time, achieving resolutions of around 50nm.

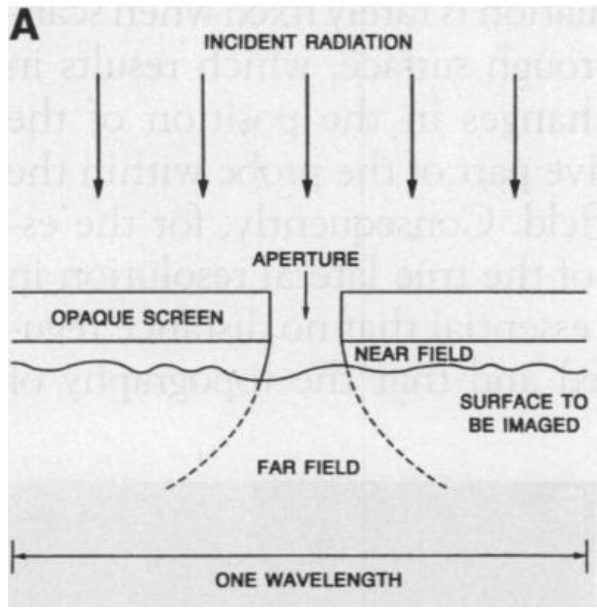


Figure 1.30: Diagram of an aperture for NSOM imaging⁴¹

1.4.2 - SIM

Structured Illumination Microscopy (SIM) was invented by Gustafsson towards the end of the 1990s⁴²⁻⁴⁴ and uses beat theory to gain a twofold improvement in resolution (demonstrated to just over 100nm)⁴². In SIM the widefield image from a microscope is treated as an unknown structure. A known structure is then overlaid, which produces moiré fringes (figure 1.31). By subtracting the unaltered moiré fringes from the unknown structures further information can be extracted. The limiting factor in SIM imaging is the spacing of the overlaid pattern - this is still diffraction limited. However, the resolution can be improved to < 50 nm when using Saturated Structured Illumination Microscopy (SSIM) which introduces "higher-frequency harmonics into the effective [moiré] pattern" by using non-linearity from saturation of the excited state⁴⁴. The excited state is considered to be saturated once the illumination source causes most fluorophores to be fluorescing. Further increasing the intensity does not "yield proportionate increases in the emission rate"⁴⁴.

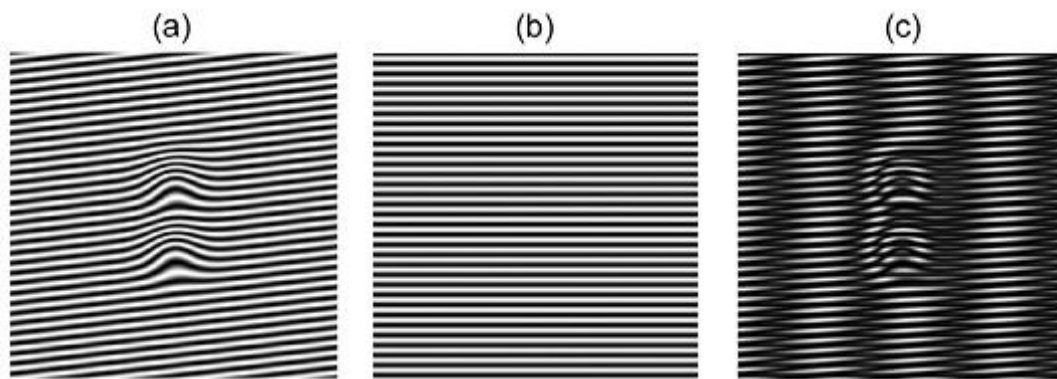


Figure 1.31: Examples of moiré patterns being used to extract more information from an unknown structure. (a) Unknown structure, (b) Known pattern to overlay, (c) Resulting moiré pattern⁴³

1.4.3 - STED

Stimulated Emission Depletion Microscopy (STED) is another ensemble technique which exploits the energy states in a fluorescent molecule to effectively reduce the size of the excitation beam such that it is smaller than the diffraction limit. It was invented by Hell in the 1990's and early 2000's⁴⁵, earning him a share of the 2014 Nobel Prize in Chemistry "for the development of super-resolved fluorescence microscopy"³⁷.

In STED the fluorophores are excited in a scanning motion, as in confocal microscopy. The excitation beam excites the molecules into the first excited energy state (S_1) (figure 1.32 A, blue and red arrows). From the excited energy level, the dye can either relax to the ground state (S_0) via emitting a photon (green arrow) or it can be stimulated using the depletion beam to drop into the higher vibrational energy states of S_0 (yellow arrow). If the molecule is 'depleted', the molecule does not fluoresce in the wavelength region for detection - it is redshifted and can therefore be ignored. If the depletion beam is shaped such that its intensity is zero in the centre and overlaid with the excitation beam, the effective PSF of the excitation beam is now much smaller⁴³ - allowing higher, "super", resolution images to be obtained, on the scale of 20 – 30 nm.

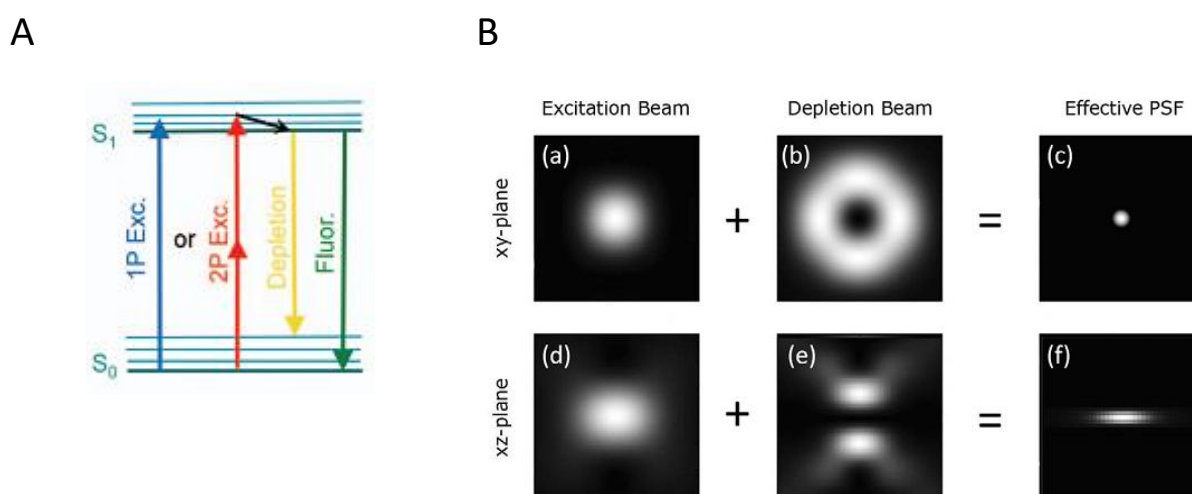


Figure 1.32: STED Microscopy. (A) Jablonski diagram for the fluorescent molecules used in STED. From the excited state S_1 , the fluorophore can either drop to the ground state, S_0 , via emitting a photon (green arrow), or can be stimulated to drop (yellow arrow). (B) Diagram showing how the excitation and depletion beam work in x,y and z planes to produce an effective PSF which is smaller than the diffraction limit⁴³

1.4.4 - Single Molecule Localisation

W. E. Moerner also won a share of the 2014 Nobel Prize in Chemistry – for the detection of single molecules. In 1989, he became the first person to observe single molecules⁴⁶ in solids. Initially this was done at very low temperatures (1.6 K) using spectroscopy, but the field advanced to fluorescent single molecule detection first at low⁴⁷ and then at room temperatures⁴⁸. In 1997, Moerner discovered light-induced switching of GFP from a semi-stable dark state to an emissive state⁴⁹ which became the basis of Single Molecule Localisation Microscopy (SMLM).

Superresolution single molecule imaging techniques such as Stochastic Optical Reconstruction Microscopy (STORM) and Photo-Activated Localisation Microscopy (PALM) work by isolating the emitted signal. The light emitted from single molecules is still diffracted, however if each individual emitter is spatially and temporally separated from the other fluorophores in the sample, the location of the single molecule can be pin-pointed accurately by fitting a Gaussian to the image of the emission. If many fluorophores in a sample are located this way, a superresolution image can be built up over time. In order to obtain single emitters, the fluorophores used in this type of imaging are capable of reversibly switching between two states - the 'on' state where emission is collected, and the 'off' state where no photons are emitted. If most of the molecules in a sample are in the 'off' state, the few molecules that remain emitting photons can be assumed to be singular, allowing data reconstruction to occur (chapter 1.5.2).

In 2006, Betzig⁵⁰ invented the PALM technique, earning him the third share of the 2014 Nobel Prize in Chemistry³⁷, which was first developed for use with fluorescent proteins⁴³. In the same year, similar techniques fPALM⁵¹ and STORM⁵² were also introduced..

The initial STORM paper, published by Rust *et al* (2006)⁵², used the dyes Cy5 and Cy3 as reporter-pairs. In this method, all molecules are sent into the dark state (a non-fluorescent, semi-stable excited state) by a strong pulse of a red (633 nm) laser. A small, sparse subset of fluorophores are then switched into an optically active emissive state with a green (532 nm) laser pulse (figure 1.33). By swapping between green and red lasers, over time many different fluorophores are excited enabling a superresolution image to be obtained – on the scale of 20 nm. A similar two-laser strategy is utilised for PALM imaging.

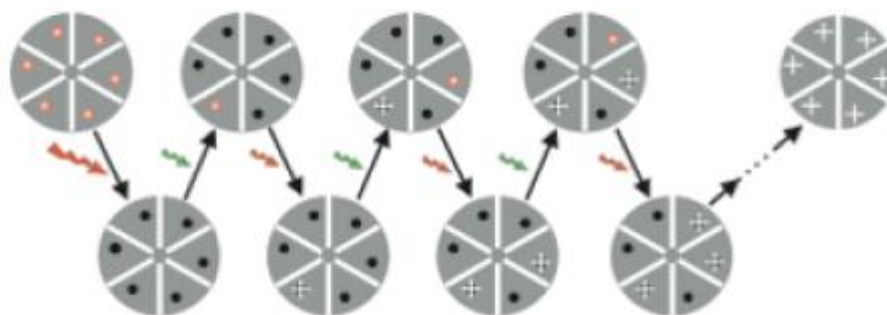


Figure 1.33: Demonstration of STORM. Fluorophores are switched into a non-emissive dark state by illumination with a red (633 nm) laser. Small, optically separate subsets of fluorophores are switched into an emissive state using a green (532 nm) laser. Over many iterations, a superresolution image can be built up⁵²

In 2008, Heilemann *et al*⁵³ proposed a technique known as direct, or dSTORM, using the dye Alexa Fluor 647 and directly activates the dye rather than using the two dye-pair system. dSTORM is, by nature of only requiring one laser, simpler to perform and as such is the method that is most often utilised by researchers. Samples are imaged in the presence of an imaging buffer containing thiol groups. These thiol groups act to stabilise the dark state of the dye, allowing the molecule to “blink” naturally

Whilst there are differences between the two techniques in how the samples are excited, once the data has been taken the reconstruction algorithms and generating a final image 'map' - are identical. “Reconstruction” is the term used for the process of fitting a 2D Gaussian to each single molecule detected. Fitting algorithms are further discussed in chapter 1.5.2.

There are many up-sides to SMLM – as it requires no specialised equipment, SML microscope set-ups are much cheaper to build and run than electron microscopy facilities. Fluorescence microscopy is well-established in the biological community and there is already a large catalogue of fluorescent probes readily available for use in samples. In comparison to the ensemble superresolution imaging methods, SMLM is able to produce higher resolution images than SIM and does not require complicated set-ups like STED and NSOM. The downside of single-molecule localisation techniques is that they are slow to produce a final image, reducing their use in live-cell imaging. The first PALM paper required imaging times of several hours⁵⁰, and the first STORM paper took 5 minutes to produce a single image⁵². These times have sped up significantly since the technique was first invented – imaging times of just seconds⁵⁴ have been reported – however it is hoped that even faster imaging speeds will one day be possible.

1.5 – Stochastic Optical Reconstruction Microscopy

STORM is a superresolution imaging technique, which means it is capable of producing images with resolutions better than the diffraction limit ($R_{\text{diffraction-limit}} \approx 250\text{nm}$).

1.5.1 – Principles of STORM

To produce super resolution images, STORM images only single fluorescent molecules. Treated as a point source, the light from each molecule is diffracted through the microscope and is viewed as an extended spot at the camera. If the single molecules are sufficiently well spaced such that the molecules do not overlap, the position of the molecule can be calculated by fitting a 2D Gaussian to the image. Over time many molecules can be located in this way in to build up a 'map' of the fluorescent molecules.

In order to image single molecules, most of the fluorophores in the sample must be non-emissive, with only a sparse few emitting light. To achieve these conditions, the dye is imaged in the presence of an imaging buffer^{55,56} containing thiol groups (Mercaptoethylamine) and an oxygen scavenging system (GLOX, consisting of Glucose Oxidase, Catalyse and Glucose).

As described in figure 1.34, the fluorescent dyes used in STORM imaging are illuminated with a laser beam to excite them into a higher energy level - the first excited singlet state, S_1 . The dye is said to be in the 'on' or 'bright' state when it is constantly moving between S_0 and S_1 , absorbing and emitting photons.

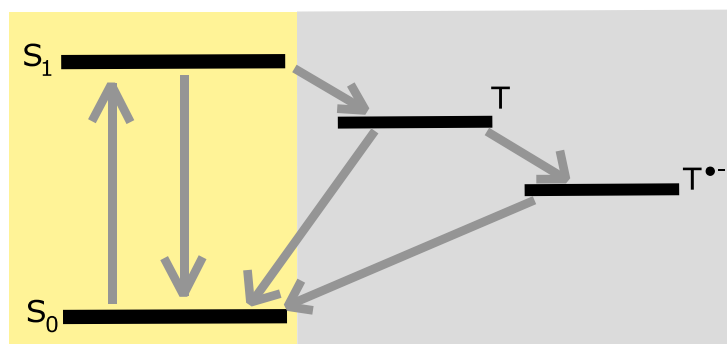


Figure 1.34: Jablonski diagram of the excited energy levels utilised in STORM imaging. S_0 is the ground state energy. The fluorophore is excited into the singlet state, S_1 , and relaxes via photon emission. From the singlet state, the dye can undergo intersystem crossing to reach the triplet state, T . The dye can once again undergo intersystem crossing to relax back to the ground state. RS^- thiolate ions in the STORM buffer can also reduce the triplet state, T , to $T^{\bullet-}$, a radical anion. The state $T^{\bullet-}$ has a very long lifetime, causing STORMing conditions to occur. From $T^{\bullet-}$, the fluorophore can be oxidised to return to S_0 .⁵⁶

Whilst the dye is in the excited singlet state, there is a small chance that the dye will drop into the 'off' or 'dark' state triplet state instead of the ground state. It is called the 'off' state because the dye transitions to the triplet state non-radiatively - without emitting a photon. The transition between the singlet and triplet states is forbidden by the *conservation of momentum*, so the probability of this transition occurring is small. In order to swap between the single and triplet states, the electrons must undergo intersystem crossing – the electrons must spin-flip such that their spins are parallel. This is a forbidden transition.

However, whilst the probability of a fluorophore dropping into the triplet state is low, the probability of the fluorophore returning to the ground state is also low as this transition also requires a change in momentum. As such, the lifetime of the triplet state is much longer than that of the singlet.

Thiol groups (R-S-H) in the imaging buffer exist as RS^- ions which are able to reduce the triplet state by forming an encounter complex⁵⁶ with the fluorophore. This forms a much more stable state with a lifetime longer than that of the triplet state – on the scale of minutes. STORMing conditions - only a few fluorophores in the bright state at any moment in time - are achieved due to the lifetime of the radical ion triplet state. Once a molecule drops into this state it will be there for a relatively long time which allows a build-up of molecules in the dark state. Molecules that fluoresce once STORMing in is process are assumed to be singular, due to the low probability that two molecules within a diffraction limited area are in the bright state at the same time point.

From the radical triplet state, the sample can either be oxidised - the RS^- ion is removed from the fluorophore - back to the ground state, or the dye can become permanently bleached where it is no longer useful for imaging.

Permanent bleaching of the dye is caused by reaction with oxygen in the system. This is why the STORM buffer contains an oxygen scavenging system, to attempt to reduce the number of dye molecules entering a permanent dark state.

1.5.2 – Reconstruction Algorithms

The intensity pattern of the fluorophore at the camera is known as the Point Spread Function (PSF). The equation for the intensity of the PSF is given by equation 1.16 which takes the form of an oscillating Bessel function (pictured in figure 1.10).

The PSF can be fitted to determine the location of the molecule. A 2D Gaussian is usually used to fit to the PSF rather than a Bessel function for computational time-saving reasons as Gaussian is a good approximation to the central maxima of the Bessel function.

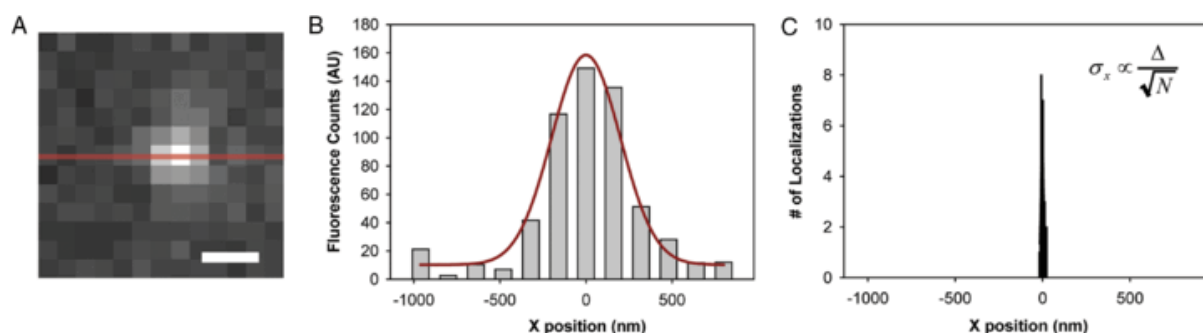


Figure 1.35: Diagram demonstrating Gaussian fitting to a single fluorescing molecule. (A) Magnified image of a single fluorescent molecule. (B) Pixel Intensity along red line in (A) (grey bars) and fitted Gaussian (red). (C) Spread of the fitted centre position for 50 localisations of the same molecule⁵⁷

Figure 1.35 shows how a Gaussian is fit to the single molecule image. The location of the molecule can be calculated as the peak of the fitted Gaussian (Figure 1.35 B). Figure 1.35 C shows the spread in the fitted centre positions for 50 fits of the same molecule. The error of this spread, σ , is known as the localisation precision (equation 1.24).

$$\sigma_x = \frac{\Delta}{\sqrt{N}} \quad (1.24)$$

where Δ is the standard deviation of the fit to the PSF and N is the number of photons detected. The localisation precision therefore improves with smaller PSF (possible by decreasing the wavelength and increasing NA - however the PSF is fixed for a given lens and wavelength) and with an increased number of detected photons⁵⁷. The localisation precision is a much smaller number than the standard deviation of the PSF, and thus forms the basis of superresolution SMLM.

The 2D Gaussian fitting function is in the form⁵⁷:

$$U(u, v) = A \exp \left[-\frac{(u - \mu_x)^2}{2\Delta^2} \right] \exp \left[-\frac{(v - \mu_y)^2}{2\Delta^2} \right] + B \quad (1.25)$$

where “(u, v) are the coordinates in the sample plane, (μ_x , μ_y) is the two-dimensional position of the molecule, A is the amplitude or peak value of the function and B is the background level”⁵⁷.

There are many open-access fitting programs currently available (for example, QuickPALM⁵⁸, ThunderSTORM⁵⁹, RapidSTORM³⁵ etc.) which fit a gaussian to every PSF in the dataset in order to ‘reconstruct’ a superresolution image of the cell. These programs work best when the data to be fitted takes the form of sparse fluorescent molecules on a dark background (figure 1.36). However, the problem with this approach is that it is very slow – in figure 1.36 there are only 23 molecules in the field of view. In order to produce a whole image many thousands of molecules must be localised. The current standard imaging time across the literature for fixed samples is around 5 – 10 minutes per image.

The main method to increase the imaging speed of STORM currently is to increase the number of fluorescent molecules visible per frame. This produces an image with overlapping PSFs which are un-reconstructable with the standard algorithms. Some groups have created reconstruction programs which are designed to extract data from overlapping PSFs⁶⁰⁻⁶² with some success – however these fitting programs are very computationally heavy taking up to days to reconstruct a single dataset.

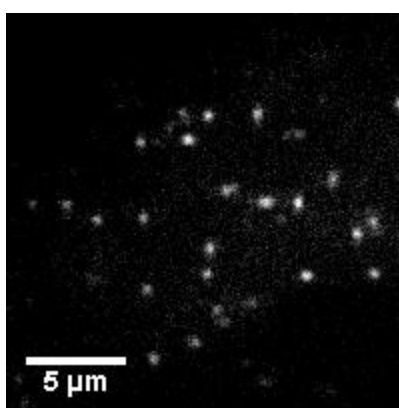


Figure 1.36: Example frame of raw STORM data. Image is of a 3T3 cell labelled with fluorescently conjugated AF 647 phalloidin, staining for f-actin

1.6 – Aims and Reasons for Project

Stochastic Optical Reconstruction Microscopy boasts resolutions far below the diffraction limit, however is a slow technique requiring many cycles of fluorophore blinks over many minutes to build up a single image. Some groups^{54,62} have demonstrated faster STORM imaging however many of these fast images were taken using fixed cells. Faster acquisition of STORM images is desirable because many processes in biology occur over very short time-scales. For example, the endocytosis of a clathrin coated pit from first appearance to scission takes on average just over two minutes⁶³. In order to image the endocytosis event in real-time, image acquisition on the scale of seconds must be possible. There are many issues to be overcome before live STORM imaging is possible – there is not only the issue of the speed of data acquisition, but there are biological concerns, and the issue of artefacts.

In order to image a live cell accurately, the cell must not be put under too much stress. Stressing the cell will cause the mechanisms and behaviours of the cell to change; which could cause the results to be incorrect. High laser powers – which are used to excite the fluorophores into the blinking behaviour – are damaging to cells, and the imaging buffer widely used for STORM (MEA plus GLOX) is toxic. Additionally, labelling the target molecule with fluorescent probes is more difficult during live imaging, as the sample cannot simply be lysed to allow entry to the probes.

Image artefacts are another problem for STORM and superresolution imaging as a whole. Due to the nature of high-resolution images, if the sample is insufficiently labelled with fluorescent dyes this will cause artefacts in the reconstructed image due to ‘holes’ where the structure is not labelled. Retaining the structural integrity of the samples is also very important – different sample preparation methods such as permeabilisation, fixatives and timings can have an effect on the underlying cell structure⁶⁴. There are also artefacts which can arise from the reconstruction. If the fitting parameters are not rigorous, the algorithms may fit false-positives to bright areas of the image which are not due to a single fluorescing molecule. Artefacts may also form due to data with labelling densities which are too high, too low, out of focus or due to a large distance between target and fluorophore⁶⁵ (also see chapter 1.3.2). Figure 1.37 shows ‘bridge’ artefacts which form between adjacent vesicles which are caused by mislocalisation of fluorophores at the edges of the vesicles⁶⁵.

All of these issues must be taken into account when imaging with STORM. However, most are outside of the scope of this work which solely concentrates on the issue of increasing the acquisition speed of STORM without the use of complicated reconstruction algorithms.

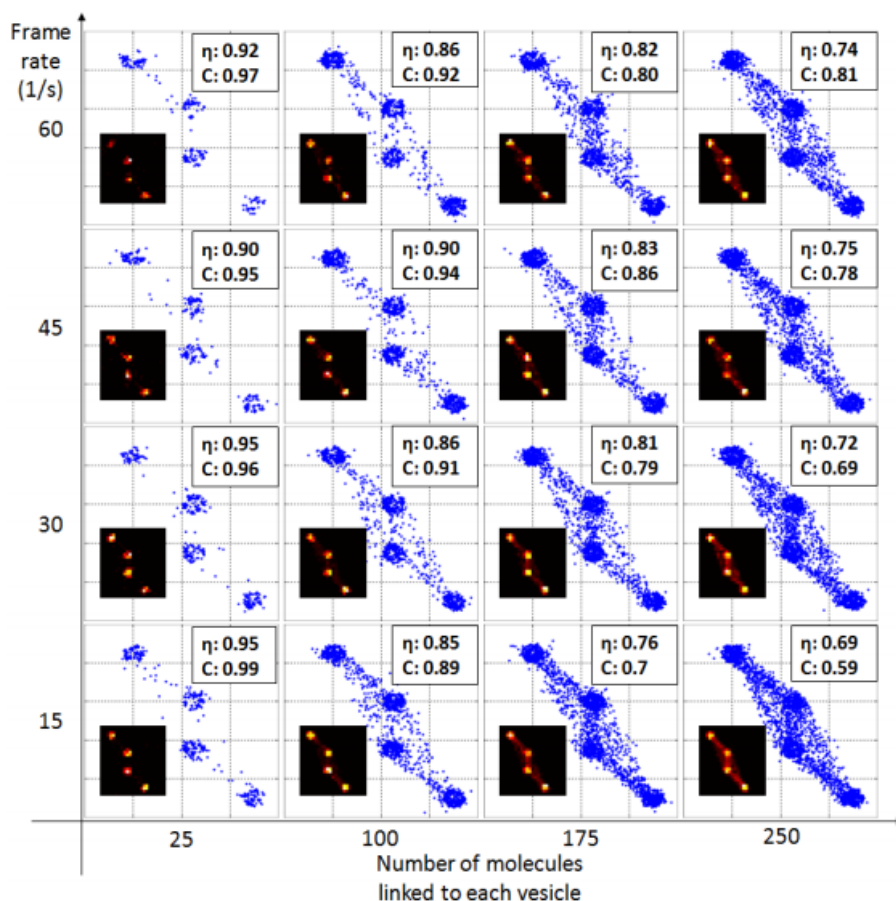


Figure 1.37: Diagram showing the formation of 'Bridge' artefacts between neighbouring vesicles (simulated data). This artefact is due to mislocalisations which stem from overlapping PSFs on adjacent vesicles⁶⁵.

Therefore, the main aims of this project are to:

- Reduce to acquisition time of STORM by:
 - Optimising the existing STORM system to take data as quickly as possible
 - Optimising the number of molecules localised per image, such that the smallest number of molecules are used
 - Increasing the amount of data that can be taken per second without increasing the density of fluorophores by imaging simultaneously in two colours

1.7 - References

- 1 Bradbury, S. & Royal Microscopical Society (Great Britain). *An introduction to the optical microscope*. (Oxford University Press (for) Royal Microscopical Society, 1984).
- 2 Hanna, H. *The Use of Magnifying Lenses in the Classical World*, Arkansas State University, (2010).
- 3 Aristophanes & Starkie, W. J. M. *The clouds of Aristophanes*. (Adolf M. Hakkert, 1966).
- 4 Seneca. Vol. 1 *Naturales Quaestiones: The Natural Questions of L. Annaeus SENECA addressed to Lucilius, Book I, [METEORS, HALO, RAINBOW, MOCK SUN, ETC.]* (432 BC).
- 5 Bradbury, S. *The evolution of the microscope*. (Pergamon, 1967).
- 6 Krotzsch, K. B. W. a. G. Geometry and dynamics in refracting systems. *European Journal of Physics* **16**, 14 (1995).
- 7 Alistair Kwan and John Dudley and Eric, L. Who really discovered Snell's law? *Physics World* **15**, 64 (2002).
- 8 Hecht, E. *Optics*. Fourth edition. Pearson new international edition. edn, (2014).
- 9 Bliven, S. *Airy Disk Spacing Near Rayleigh Criterion*,
<https://en.wikipedia.org/wiki/Angular_resolution#/media/File:Airy_disk_spacing_near_Rayleigh_criterion.png> (
- 10 Tkaczyk, T. S. *Field Guide To Microscopy*. Vol. FG13 (SPIE Press, 2010).
- 11 Hooke, R., Martyn, J. & Allestry, J. *Micrographia : or, Some physiological descriptions of minute bodies made by magnifying glasses, with observations and inquiries therupon*. (printed by Jo. Martyn, and Ja. Allestry, printers to the Royal Society, and are to be sold at their shop at the Bell in S. Paul's Church-yard, 1665).
- 12 Optics, E. *Understanding Microscopes and Objectives*,
<<https://www.edmundoptics.com/resources/application-notes/microscopy/understanding-microscopes-and-objectives/>> (
- 13 World, M. *Infinity Corrected Optics*, <https://www.microscopeworld.com/t-infinity_corrected_optics.aspx> (
- 14 Jonathan, A. K. a. M. J. a. R. Z. Comparative analysis of imaging configurations and objectives for Fourier microscopy. *J. Opt. Soc. Am. A* **32**, 2082--2092, doi:10.1364/JOSAA.32.002082 (2015).
- 15 Wikipedia. *A PN junction in thermal equilibrium with zero bias voltage applied.*, <<https://commons.wikimedia.org/wiki/File:Pn-junction-equilibrium-graphs.png>> (
- 16 Andor. *EMCCD Tutorial*, <http://www.emccd.com/what_is_emccd/emccd_tutorial/Q1_What_are_Electron_Multiplying_CCDs> (

- 17 QImaging. *Electron Multiplying (EM) Gain*,
<http://www.qimaging.com/resources/pdfs/emccd_technote.pdf> (
- 18 Andor. *Electron Multiplying CCD Cameras: The technology behind EMCCDs*,
<<http://www.andor.com/learning-academy/electron-multiplying-ccd-cameras-the-technology-behind-emccds>> (
- 19 Saumya Saurabh and Suvrajit Maji and Marcel, P. B. Evaluation of sCMOS cameras for detection and localization of single Cy5 molecules. *Opt. Express* **20**, 7338--7349, doi:10.1364/OE.20.007338 (2012).
- 20 Tadashi Maruno and Eiji Toda and Keith, B. Comparison of CMOS and EMCCD Cameras for Computational Imaging with Application to Super-resolution Localization Microscopy. *Imaging and Applied Optics Technical Papers, IM4C.3*, doi:10.1364/ISA.2012.IM4C.3 (2012).
- 21 de Broglie, L.-V. *On The Theory Of Quanta. A translation of: RECHERCHES SUR LA THÉORIE DES QUANTA*, (1925).
- 22 Davisson, C. a. G., L. H. Diffraction of Electrons by a Crystal of Nickel. *Phys. Rev.* **30**, 705--740, doi:10.1103/PhysRev.30.705 (1927).
- 23 Hayat, M. A. *Fixation for Electron Microscopy*. (Academic Press Inc, 1981).
- 24 Giesbrecht, P., Kersten, T., Maidhof, H. & Wecke, J. Staphylococcal Cell Wall: Morphogenesis and Fatal Variations in the Presence of Penicillin. *Microbiology and Molecular Biology Reviews* **62**, 1371-1414 (1998).
- 25 Stokes, G. G. On the Change of Refrangibility of Light. *Philosophical Transactions of the Royal Society of London* **142**, 463-562, doi:10.1098/rstl.1852.0022 (1852).
- 26 Shimomura, O. a. J. F. H. a. S. Y. Extraction, Purification and Properties of Aequorin, a Bioluminescent Protein from the Luminous Hydromedusan, Aequorea. *Journal of Cellular and Comparative Physiology* **59**, 223--239, doi:10.1002/jcp.1030590302 (1962).
- 27 Huang, B., Babcock, H. & Zhuang, X. Breaking the Diffraction Barrier: Super-Resolution Imaging of Cells. *Cell* **143**, 1047-1058, doi:<http://dx.doi.org/10.1016/j.cell.2010.12.002> (2010).
- 28 Scientific, T. *Fluorescence Spectraviewer*, <<http://www.thermofisher.com/uk/en/home/life-science/cell-analysis/labeling-chemistry/fluorescence-spectraviewer.html>> (
- 29 ADTBio. *Alexa® dyes*, <<http://www.atdbio.com/content/34/Alexa-dyes>> (
- 30 Harrison, P. *Quantum wells, wires and dots : theoretical and computational physics*. 3rd ed. edn, (West Sussex, England ; Hoboken, NJ : Wiley, c2009, 2009).
- 31 Milo, R. & Phillips, R. *Cell Biology by the Numbers*. (Taylor & Francis Group, 2015).
- 32 Erickson, H. P. in *Biol Proced Online* Vol. 11 32-51 (2009).

- 33 San Paulo, A. & García, R. High-resolution imaging of antibodies by tapping-mode atomic force microscopy: attractive and repulsive tip-sample interaction regimes. *Biophysical Journal* **78**, 1599-1605 (2000).
- 34 Schauen, M., Opazo, F. & Rizzoli, S. *New Labeling Tools Can Help to Realize the Full Potential of Super-Resolution Microscopy: Aptamers Enable Sensitive and Accurate Labeling of Small Subcellular Structures*, <<http://www.leica-microsystems.com/science-lab/new-labeling-tools-can-help-to-realize-the-full-potential-of-super-resolution-microscopy>> (2013).
- 35 Kamiyama, D. & Huang, B. Development in the STORM. *Developmental Cell* **23**, 1103-1110, doi:10.1016/j.devcel.2012.10.003 (2012).
- 36 **Ross, S. T., Schwartz, S., Fellers, T. J. & Davidson, M. W.** *Total Internal Reflection Fluorescence (TIRF) Microscopy*, <<https://www.microscopyu.com/techniques/fluorescence/total-internal-reflection-fluorescence-tirf-microscopy>> (
- 37 Graham-Smith, F., King, T. A., Wilkins, D. & NetLibrary Inc. x, 506 p., [508] p. of plates (J. Wiley, Chichester, England ; Hoboken, NJ, 2007).
- 38 Syngé, E. H. XXXVIII. A suggested method for extending microscopic resolution into the ultra-microscopic region. *The London, Edinburgh, and Dublin Philosophical Magazine and Journal of Science* **6**, 356-362, doi:10.1080/14786440808564615 (1928).
- 39 John Aloysius, O. K. Resolving Power of Visible Light. *J. Opt. Soc. Am.* **46**, 359--359, doi:10.1364/JOSA.46.000359 (1956).
- 40 Ash, E. A. & Nicholls, G. Super-resolution Aperture Scanning Microscope. *Nature* **237**, 510-512 (1972).
- 41 Betzig, E. a. T. J. K. Near-Field Optics: Microscopy, Spectroscopy, and Surface Modification Beyond the Diffraction Limit. *Science* **257**, 189--195, doi:10.1126/science.257.5067.189 (1992).
- 42 Gustafsson, M. G. L. Surpassing the lateral resolution limit by a factor of two using structured illumination microscopy. *Journal of Microscopy* **198**, 82--87, doi:10.1046/j.1365-2818.2000.00710.x (2000).
- 43 Leung, B. O. & Chou, K. C. Review of Super-Resolution Fluorescence Microscopy for Biology. *Applied Spectroscopy* **65**, doi:10.1366/11-06398 (2011).
- 44 Gustafsson, M. G. L. Nonlinear structured-illumination microscopy: Wide-field fluorescence imaging with theoretically unlimited resolution. *Proceedings of the National Academy of Sciences of the United States of America* **102**, 13081-13086, doi:10.1073/pnas.0406877102 (2005).

- 45 Stefan, W. H. a. J. W. Breaking the diffraction resolution limit by stimulated emission: stimulated-emission-depletion fluorescence microscopy. *Opt. Lett.* **19**, 780--782, doi:10.1364/OL.19.000780 (1994).
- 46 Moerner, W. E. & Kador, L. Optical detection and spectroscopy of single molecules in a solid. *Physical Review Letters* **62**, 2535-2538 (1989).
- 47 Orrit, M. & Bernard, J. Single pentacene molecules detected by fluorescence excitation in a p-terphenyl crystal. *Physical Review Letters* **65**, 2716-2719 (1990).
- 48 Ambrose, W. P. & Moerner, W. E. Fluorescence spectroscopy and spectral diffusion of single impurity molecules in a crystal. *Nature* **349**, 225 (1991).
- 49 Dickson, R. M., Cubitt, A. B., Tsien, R. Y. & Moerner, W. E. On/off blinking and switching behaviour of single molecules of green fluorescent protein. *Nature* **388** (1997).
- 50 Betzig, E. a. P. G. H. a. S. R. a. L. O. W. a. O. S. a. B. J. S. a. D. M. W. a. L.-S. J. a. Imaging Intracellular Fluorescent Proteins at Nanometer Resolution. *Science* **313**, 1642--1645, doi:10.1126/science.1127344 (2006).
- 51 Hess, S. T., Girirajan, T. P. K. & Mason, M. D. Ultra-high resolution imaging by fluorescence photoactivation localization microscopy. *Biophysical journal* **91**, 4258-4272 (2006).
- 52 Rust, M. J., Bates, M. & Zhuang, X. Sub-diffraction-limit imaging by stochastic optical reconstruction microscopy (STORM). *Nature Methods* **3**, doi:10.1038/nmeth929 (2006).
- 53 Heilemann, M. *et al.* Subdiffraction-resolution fluorescence imaging with conventional fluorescent probes. *Angewandte Chemie-International Edition* **47**, 6172-6176, doi:10.1002/anie.200802376 (2008).
- 54 Jones, S. A., Shim, S.-H., He, J. & Zhuang, X. Fast, three-dimensional super-resolution imaging of live cells. *Nature Methods* **8**, doi:10.1038/nmeth.1605 (2011).
- 55 Dempsey, G. T., Vaughan, J. C., Chen, K. H., Bates, M. & Zhuang, X. W. Evaluation of fluorophores for optimal performance in localization-based super-resolution imaging. *Nature Methods* **8**, 1027+, doi:10.1038/nmeth.1768 (2011).
- 56 Heilemann, M., van de Linde, S., Mukherjee, A. & Sauer, M. Super-Resolution Imaging with Small Organic Fluorophores. *Angewandte Chemie-International Edition* **48**, doi:10.1002/anie.200902073 (2009).
- 57 Moerner, W. E. Microscopy beyond the diffraction limit using actively controlled single molecules. *Journal of Microscopy* **246**, 213--220, doi:10.1111/j.1365-2818.2012.03600.x (2012).
- 58 Henriques, R. *et al.* QuickPALM: 3D real-time photoactivation nanoscopy image processing in ImageJ. *Nature Methods* **7**, doi:10.1038/nmeth0510-339 (2010).

- 59 Ovesný, M., Křížek, P., Borkovec, J., Švindrych, Z. & Hagen, G. M. ThunderSTORM: a comprehensive ImageJ plug-in for PALM and STORM data analysis and super-resolution imaging. *Bioinformatics* **30**, 2389-2390, doi:10.1093/bioinformatics/btu202 (2014).
- 60 Min, J. *et al.* FALCON: fast and unbiased reconstruction of high-density super-resolution microscopy data. *Scientific reports* **4** (2014).
- 61 Holden, S. J., Uphoff, S. & Kapanidis, A. N. DAOSTORM: an algorithm for high-density super-resolution microscopy. *Nature Methods* **8**, doi:10.1038/nmeth0411-279 (2011).
- 62 Cox, S. *et al.* Bayesian localization microscopy reveals nanoscale podosome dynamics. *Nature Methods* **9**, doi:10.1038/nmeth.1812 (2012).
- 63 Merrifield, C. J., Perrais, D. & Zenisek, D. Coupling between Clathrin-Coated-Pit Invagination, Cortactin Recruitment, and Membrane Scission Observed in Live Cells. *Cell* **121**, 593-606, doi:http://dx.doi.org/10.1016/j.cell.2005.03.015 (2005).
- 64 Whelan, D. R. & Bell, T. D. M. Image artifacts in Single Molecule Localization Microscopy: why optimization of sample preparation protocols matters. *Scientific Reports* **5**, 7924, doi:10.1038/srep07924 (2015).
- 65 Sinkó, J. *et al.* TestSTORM: Simulator for optimizing sample labeling and image acquisition in localization based super-resolution microscopy. *Biomedical optics express* **5**, 778-787 (2014).

2 – Materials and Methods

Contents

| | |
|---|----|
| 2.1- Cell-Line Culture..... | 52 |
| 2.1.1 - NIH3T3-GL Culture | 52 |
| 2.1.2 - <i>Staphylococcus Aureus</i> Culture..... | 52 |
| 2.2 - Primary Culture..... | 52 |
| 2.2.1 - Animals | 52 |
| 2.2.2 - Dorsal Root Ganglion Dissection..... | 52 |
| 2.2.3 - DRG Culture | 53 |
| 2.3 - Preparation of Cover slips..... | 53 |
| 2.3.1 - Cover Slips for Cell Line Culture..... | 53 |
| 2.3.2 - Cover Slips for Primary Culture..... | 53 |
| 2.4 - Fluorescent Labelling..... | 53 |
| 2.4.1 - Mammalian Cell Labelling..... | 53 |
| 2.4.2 - Bacterial Cell Labelling | 54 |
| 2.5 - Mounting Cover Slips..... | 55 |
| 2.6 - Microscopy..... | 55 |
| 2.6.1 - Wide Field Microscopy..... | 55 |
| 2.6.1 - STORM | 55 |
| 2.6.2 - STORM Reconstruction Algorithm | 55 |
| 2.7 - Tables of Reagents..... | 58 |
| 2.7.1 - Mammalian Cell Culture Media | 58 |
| 2.7.2 - List of Buffers and Fixatives for Mammalian Culture | 59 |
| 2.7.3 - List of Buffers and Fixatives for Bacterial Culture..... | 60 |
| 2.7.4 - STORM Buffer | 61 |
| 2.7.5 - List of Fluorescently Conjugated Labels..... | 61 |
| 2.8 - References | 62 |

2.1- Cell-Line Culture

2.1.1 - NIH3T3-GL Culture

NIH3T3-GL (3T3) cells (obtained from Dr. Frederic Charron, Montreal, Canada) were cultured in Dulbecco's modified eagle's medium (DMEM, GIBCO), supplemented with 10% Fetal Bovine Serum (FBS, GIBCO), 1% Glutamine (GIBCO) and 1% Penicillin-Streptomycin (GIBCO) at 37°C, 5% CO₂. Cells were seeded at 1x10⁴ cells/well on cover slips (as described in section 3.2) and left overnight in the incubator to grow before use.

2.1.2 - *Staphylococcus Aureus* Culture

An overnight culture of *Staphylococcus aureus* (SH1000) containing 1 colony in 10 ml Brain Heart Infusion (BHI), 37 g/l, sterilised by autoclaving for 20 mins at 121°C, 103 kPa) was prepared and grown at 37°C, 250 rpm shaking for 18 hours. This was recultured to an OD₆₀₀ of 0.05 into 50 ml BHI in a 250ml conical flask (same growth conditions as overnight) & left to grow for 90 mins for cells to reach mid exponential phase (OD₆₀₀ ~ 0.3).

2.2 - Primary Culture

2.2.1 - Animals

All mice were maintained on a C57/BL6 strain background (≥10 generation backcross). All mice were bred and maintained at the University of Sheffield animal facility, and all experiments performed, in accordance with UK Home Office regulations. All Experiments were performed at Embryonic day 13 (E13).

2.2.2 - Dorsal Root Ganglion Dissection

All animals were sacrificed at E13 via an overdose of the inhaled anaesthetic isofluorane (Isocare) prior to cervical dislocation. Embryos were removed and placed into 4°C Leibovitz's L-15 Medium (L-15, GIBCO) on ice until use.

Dissection of DRG was done in L-15 media under a dissection microscope and Dorsal Root Ganglia (DRG) were placed in L-15 media on ice until dissection was complete. To dissect DRG, the head and organs of the embryo were removed, and the backbone was cut open to reveal the spinal cord. DRG were removed by gently pulling the spinal cord until the DRG came free, still attached to the spinal cord. Singular DRG were cut from the spinal cord and dangling axons were removed before plating (~4 DRG per well) on cover slips. It was important to ensure DRG were touching the cover slip to ensure attachment of neural outgrowth.

2.2.3 - DRG Culture

Primary DRG were cultured in OPTI-MEM (GIBCO) with 0.1% Nerve Growth Factor (Sigma) supplemented with 1% Glutamine and 1% Penicillin-Streptomycin for 48+ hours in a 37°C, 5% CO₂ incubator.

2.3 - Preparation of Cover slips

Glass cover slips (13 mm ϕ) were heat-sterilised and placed into 4-well culture dishes. Coating solutions were made up in filter-sterilised distilled water.

2.3.1 - Cover Slips for Cell Line Culture

0.5mg/ml Poly-D-Lysine (PDL)(Sigma Aldrich) was added to cover slips overnight at 37°C. Cover slips were washed 3x in distilled water. Once cover slips were made up, they were left in distilled water at 4°C and used within one month.

2.3.2 - Cover Slips for Primary Culture

Cover slips were made either the day before or day of dissection. 100 μ g/ml Poly-L-Lysine (PLL)(Sigma Aldrich) was added to the cover slips and incubated for 1 hour at 37°C. Laminin (Sigma Aldrich) at 20 μ g/ml was then added to the cover slips either for 3 hours at room temperature or overnight at 4°C. Cover slips were washed 3x in PBS and left in OPTI-MEM on ice until use.

2.4 - Fluorescent Labelling

2.4.1 - Mammalian Cell Labelling

All mammalian cells were fixed in 4% paraformaldehyde (PFA) for 30 minutes. Reagents were either added to cells by running them down the side of each well or by inverting cover slips in drops of reagent for delicate samples. This was to avoid losing fragile explants during staining. To do this, a sheet of parafilm was adhered to the desk using a small amount of water. The reagent drops (~20 μ l) were placed on the parafilm and cover slips were inverted onto these. To ensure cover slips did not dry out, a polystyrene box lined with damp paper towels was placed over the samples throughout.

Cells were permeabilized by washing 3x 10 minutes with 0.05% Triton-X in Phosphate Buffered Saline (PBS).

For actin staining, samples were blocked in 0.5% Fish Skin Gelatin (FSG) for 20 minutes. Fluorescently conjugated phalloidin stock at 6.6 μ M in methanol was diluted 1:200 in 0.05% Triton-X in PBS and

added to each well for 30 minutes to 1 hour at room temperature. Cells were kept in the dark after fluorophores were added.

For antibody staining, samples were blocked in 3% Heat-Inactivated Donkey Serum (HIDS) in PBS for 20 minutes. The primary antibody was added with 3% HIDS in 0.05% TX-100 PBS overnight at 4°C, or on a shaker at room temperature for 1 hour. The samples were washed 3x 10 minutes in 0.05% TX-100 PBS before addition of the secondary antibody (with 3% HIDS in 0.05% TX-100 PBS) for 30 minutes at room temperature.

For a pulse-chase uptake of fluorescently conjugated transferrin (TF), samples were chilled on ice for 30 minutes before starting. TF was added to the samples for 30 minutes (on ice) to a concentration of 0.025mg/ml (TF). Cells were washed 3x 10 minutes in cold culture media to remove unattached dye before being placed in the incubator for between 1 - 10 minutes. Cells were once again placed on ice to stop further movement of TF within the cell before being fixed.

Membrane staining using Dil required incubating the sample at 37°C for 10 minutes with a concentration of Dil to 10 µM.

After staining cells were washed 3x 10 minutes in 0.05% Triton-X in PBS. Samples were mounted as described in section 2.5.

2.4.2 - Bacterial Cell Labelling

To label 5 minutes of cell wall growth ADA (Azido-D-Alanine, Iris Biotech) was added (5µl of 100mM stock to 1 ml culture) and cells were incubated on a rotator at 37°C for 5 minutes. Sample was spun down for 5 minutes at 13.4 rpm and the supernatant was removed.

The sample was fixed for 30 minutes in 16% (w/v) paraformaldehyde . Cells were resuspended in 0.5ml dH₂O and 0.5ml fixative.

Once fixed, the sample was again spun down for 5 minutes at 13.4 rpm and resuspended in 440 µl Click-iT Buffer (Invitrogen), 50 µl Click-iT additive (Invitrogen), 10 µl CuSO₄ & 5 µl 5µg/ml Alexa Fluor 647 (Alkyene)(Invitrogen) in DMSO on a rotator for 30 minutes. Sample was washed in PBS and diluted to an appropriate concentration for microscopy (~100 µl) before mounting

2.5 - Mounting Cover Slips

Mammalian cell cover slips were mounted on glass microscope slides using either STORM buffer or VECTASHIELD with DAPI (H-1200, Vector) as mounting media. Microscope slides were cleaned in ethanol prior to use. Cover slips were secured to slides with nail varnish.

To mount *Staphylococcus* samples, 5µl of cell suspension was placed in the centre of a microscope slide. Cells were dried using a nitrogen gas line. Excess cells were washed off using distilled water, and the slide was dried using nitrogen gas. STORM buffer was dropped onto the cells and a cover slip carefully lowered on top, ensuring no air bubbles. The cover slip was then secured using nail varnish.

2.6 - Microscopy

2.6.1 - Wide Field Microscopy

Wide field fluorescence microscopy was performed on a Motorised Olympus BX61 using a 60x UplanApo (NA 1.4) objective lens. Images were captured using a Hamamatsu Orca ER CCD on Volocity imaging software.

2.6.1 - STORM

All STORM images were acquired on a bespoke system. Images were captured using a 60x Olympus oil objective lens on a Andor 4.3 Zyla sCMOS camera. Images were captured using Andor SOLIS (4.28.30026.0) software using 540 MHz pixel read out rate in rolling shutter mode with 12 bit sensitivity/dynamic range. Laser power was measured using a power meter (Thorlabs) placed as close to the microscope base as possible, the laser spot size was measured from the camera.

Before images were recorded, the samples were allowed time to bleach out and reach "blinking" behaviour: when the laser is initially turned on, all molecules start to fluoresce and it takes time for the majority of molecules to drop into the dark state. This time was not fixed but depended on the sample - images were only recorded after this process had taken place. Raw data was saved as a series of .tiff images, known as an image stack.

2.6.2 - STORM Reconstruction Algorithm

All STORM data was analysed by the same fitting algorithm, written by a previous group member (Robert Turner, 2013). A flow diagram of the algorithm stages is shown in Figure 2.1.

For each image in the stack, the background was subtracted using a tophat filter. A user-inputted threshold was then applied to the image, below which points were discarded. The remaining points were sorted into a list in descending order. The brightest points in the image were assumed to be

due to fluorescing molecules, and a list of potential candidates was obtained by subtracting all of the points on the list in the surrounding area of each bright point. This was to avoid selecting the same molecule multiple times. The brightest pixel in the area was assumed to be the centre point. Areas surrounding the candidate pixels were then cut out of the image for fitting. The size of the ROI was a square of length $(2S + 1)$ where S was the size of the required separation between molecules (typically $S = 4$ or 5 pixels). Fitting was done using a non linear least squares algorithm to a 2D gaussian of the form:

$$F = a * \exp \left[- \left(\frac{x - b}{c} \right)^2 - \left(\frac{y - d}{e} \right)^2 \right] + f \quad (2.1)$$

where a is related to the pixel intensity/number of photons emitted by the molecule, b and d are the sub-pixel molecular coordinates, c and e are related to the size of the molecule and f is the background signal level¹. Typically, $\frac{3}{4}$ of the maximum pixel intensity in the image was used as a , and the mean pixel intensity over the whole image was used as f .

Once the fitting process was complete for all images in the stack, the table of fits was collated. This data was then filtered on width of molecule in x and y to remove fits based on single pixel noise or that which were too large to be a single molecule, the range of widths obtained before filtering can be seen in figure 2.2. Usually, the widths were filtered between 1 - 3 pixels. It was also possible to filter on the normalised residual of fit. Filtering also discarded multiple points (localised molecules which were found within a user-defined Δx , Δy and Δt of each other and therefore counted as the same molecule). The data points were then ready to be rendered into the final image.

Additionally, QUICKpalm² and ThunderSTORM¹ were also used to fit and render STORM images.

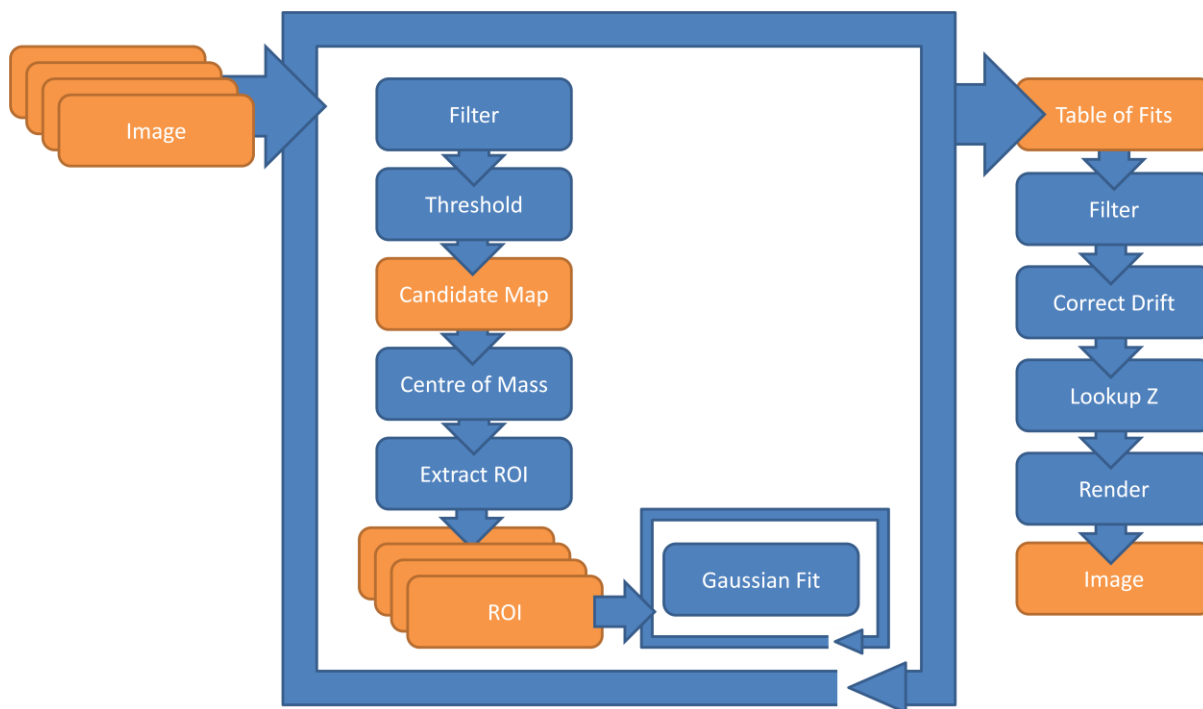


Figure 2.1: Flow Diagram for STORM image Reconstruction Algorithm (Robert Turner, 2013)

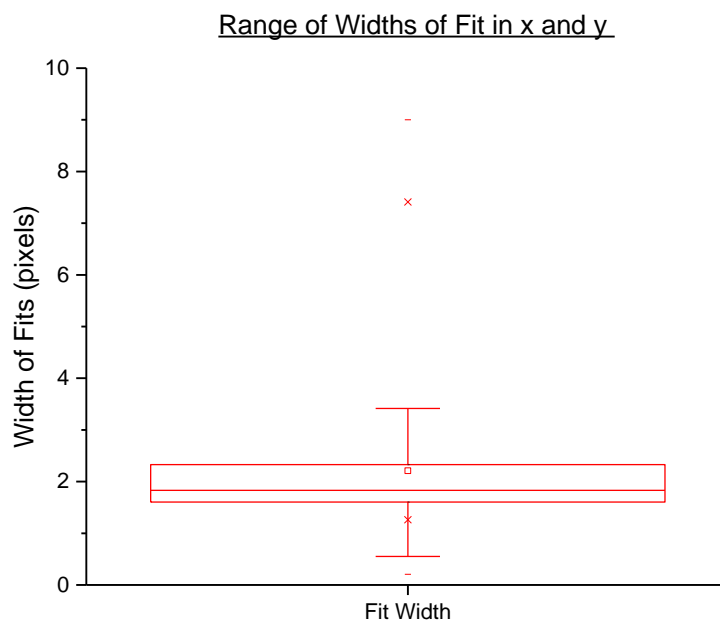


Figure 2.2: Range of fit widths in x and y obtained from fitting algorithm

2.7 - Tables of Reagents

2.7.1 - Mammalian Cell Culture Media

| Reagent | Catalogue Number | Supplier |
|--|------------------|-------------------|
| DMEM, high glucose, Pyruvate, no glutamine | 21969-035 | Gibco, Invitrogen |
| FBS-Fetal Bovine Serum | 10270 | Gibco, Invitrogen |
| 0.25% Trypsin-EDTA (1x), Phenol Red | 25200-056 | Gibco, Invitrogen |
| L-Glutamine 200mM solution | 25030 | Gibco, Invitrogen |
| Penicillin-Streptomycin | 15140 | Gibco, Invitrogen |
| Leibovitz's L-15 | 11415-049 | Gibco, Invitrogen |
| Opti-MEM | 31985 | Gibco, Invitrogen |

2.7.2 - List of Buffers and Fixatives for Mammalian Culture

| Buffer/Fixative | Formula | Amount/Volume |
|----------------------------------|--|---------------|
| 4% PFA, 1 liter | 1. Paraformaldehyde (PFA) | 40 g |
| | 2. dH ₂ O | 500 ml |
| | Add NaOH dropwise and warm on a hotplate with stirrer bar until completely dissolved. Adjust the pH to 7.2 | |
| | 3. 0.2M PB buffer, pH 7.2 | 500 ml |
| | Filter and make aliquots and store at -20°C | |
| 0.2M PB buffer (pH 7.2), 1 liter | 1. Na ₂ HPO ₄ | 21.8 g |
| | 2. NaH ₂ PO ₄ | 6.4 g |
| | 3. dH ₂ O | 900 ml |
| | Use stirrer bar until completely dissolved. Adjust pH to 7.2 with conc. HCl. Adjust volume to 1 litre with dH ₂ O | |
| 10x PBS, 1 liter | 1. NaCl | 80 g |
| | 2. KCl | 2.0 g |
| | 3. Na ₂ HPO ₄ | 14.4 g |
| | 4. KH ₂ PO ₄ | 2.4 g |

2.7.3 - List of Buffers and Fixatives for Bacterial Culture

| Buffer/Fixative | Formula | Amount/Volume |
|-------------------------------|---|---------------|
| BHI (pH 7.4), 1 litre | Oxoid Nutrient Agar was added at 1% (w/v) for BHI Agar. | |
| | 1. NaCl | 8.0 g |
| | 2. Na ₂ HPO ₄ | 1.4 g |
| | 3. KCl | 0.2 g |
| | 4. KH ₂ PO ₄ | 0.2 g |
| | Solution made up to 1 litre in PBS and then pH adjusted to 7.4 with NaOH | |
| 16% (w/v) Paraformaldehyde | 1. 100 mM Sodium Phosphate Buffer (pH 7.0) | 50 ml |
| | 2. Paraformaldehyde | 8.0 g |
| | Solution was heated to 60°C with stirring for 20mins, Maintaining heat and agitation. NaOH (≥ 5M) solution was added drop wise until the solution cleared. The solution was stored at 4°C for up to 3 months. | |
| Staphylococcus Fixative | 1. Paraformaldehyde, 16% (w/v) | 0.5 ml |
| | 2. PBS | 2 ml |

2.7.4 - STORM Buffer

| Buffer/Fixative | Formula | Amount/Volume |
|--------------------|---|--------------------------------|
| STORM Buffer, 1 ml | 1. PBS | 990 μ l |
| | 2. MEA (100 mM) | 10 μ l of 1M Stock |
| | MEA aliquots were made under nitrogen and stored at 4°C. Once opened aliquots were used within two weeks as MEA is hygroscopic. | |
| | 3. Glucose (10% W/V) | 0.1 g |
| | 4. Catalase (40 μ g/ml) | 11.2 μ l of 4 mg/ml Stock |
| | 5. Glucose Oxidase (0.5 mg/ml) | 111.1 μ l of 5 mg/ml Stock |
| | STORM buffer was made up fresh for every use, stocks of Catalase and Glucose Oxidase were kept for two weeks at 4°C. | |

2.7.5 - List of Fluorescently Conjugated Labels

| Reagent | Catalogue Number | Supplier |
|-----------------------------|------------------|-------------------------|
| Alexa Fluor 647 Phalloidin | A22287 | Thermofisher Scientific |
| Alexa Fluor 532 Phalloidin | A22282 | Thermofisher Scientific |
| Alexa Fluor 488 Phalloidin | A12379 | Thermofisher Scientific |
| Atto 550 Phalloidin | 19083 | Sigma Aldrich |
| Alexa Fluor 647 Transferrin | T23366 | Thermofisher Scientific |
| Dil | D3911 | Thermofisher Scientific |
| Alexa Fluor 647 Alkyne | A10278 | Thermofisher Scientific |

2.8 - References

- 1 Ovesný, M., Křížek, P., Borkovec, J., Švindrych, Z. & Hagen, G. M. ThunderSTORM: a comprehensive ImageJ plug-in for PALM and STORM data analysis and super-resolution imaging. *Bioinformatics* **30**, 2389-2390, doi:10.1093/bioinformatics/btu202 (2014).
- 2 Henriques, R. *et al.* QuickPALM: 3D real-time photoactivation nanoscopy image processing in ImageJ. *Nature Methods* **7**, doi:10.1038/nmeth0510-339 (2010).

3 – Building and Optimisation

Contents

| | |
|--|----|
| 3.1 - Introduction | 64 |
| 3.2 – Results | 69 |
| 3.2.1 – Measuring the Point Spread Function | 70 |
| 3.2.2 – Optimisation of Readout Laser Power | 71 |
| 3.2.3 - Optimisation of Frame Rate..... | 81 |
| 3.2.4 - Effect of changing the STORM buffer concentrations | 85 |
| 3.3 - Conclusions | 89 |
| 3.4 - References | 91 |

3.1 - Introduction

To increase the imaging speed of STORM, first the microscope was optimised - this was to determine the speed constraints of the system before attempting to image more quickly using other methods.

The STORM microscope used throughout this work was a bespoke system, initially developed for single colour, two dimensional imaging. In order to maximise the imaging speed, the microscope was first optimised to collect the maximum number of data points at the highest Signal-to-Noise Ratio (SNR) possible (equation 3.1). This also ensured the system was working at maximum efficiency throughout the project and that imaging protocols were standardised throughout.

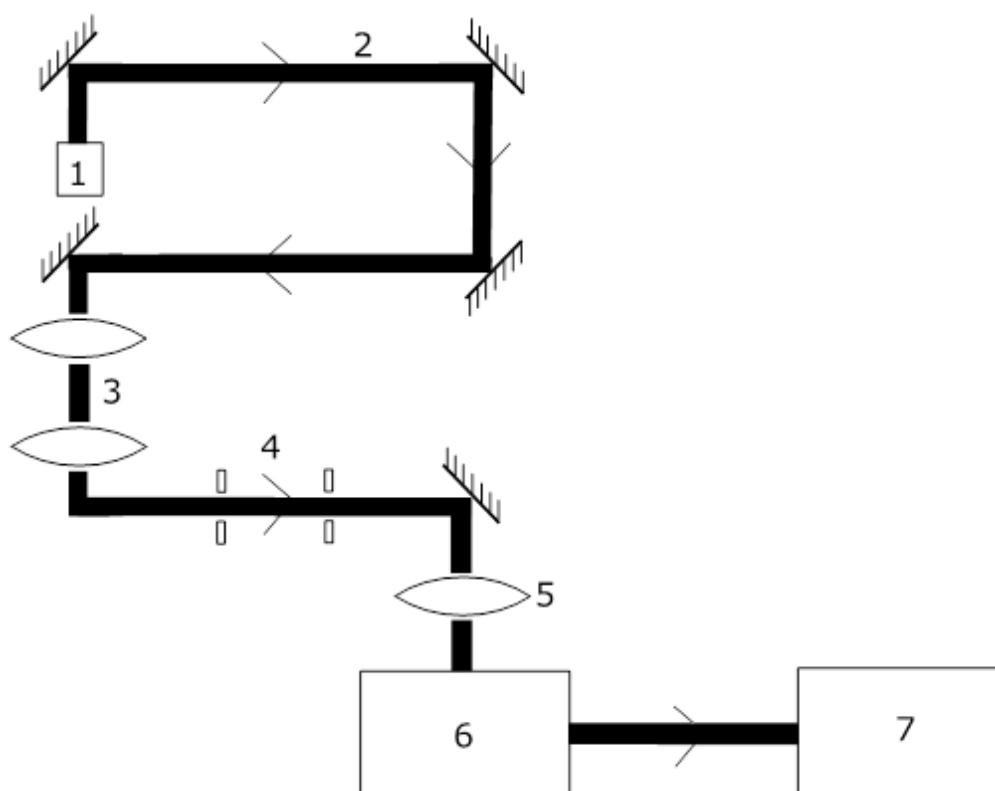


Figure 3.1: Schematic of the STORM microscope system. 1. Laser Source, 2. Laser Light Path, 3. Beam Expander, 4. Pinhole apertures, 5. Lens, 6. Microscope base, 7. sCMOS Camera

The optical setup of the STORM system is shown in figure 3.1. It was built on a passively damped optical table (Thorlabs) and consisted of a Nikon Ti base with a 60x Olympus objective lens, an Andor 4.3 Zyla sCMOS camera with illumination provided by laser lines at 647nm, 532nm and 405nm. All lasers were coupled to the microscope in free space after being expanded and focused on to the backplane of the objective. The image from the microscope side port was relayed to the camera using a 1:1 4f imaging system. The pinholes (figure 3.1 - 4) were used as an alignment tool, and the final lens before the microscope base (figure 3.1 - 5) was used to illuminate the samples with a beam, rather than a focused point. There are no notch filters within the system. This general layout

is very common in STORM imaging. Unless otherwise stated, all experiments were performed as epifluorescence.

Raw STORM data was saved as a series of .tif images, generally with around 10,000-15,000 images per stack. The images were subsequently run through a custom reconstruction program in MATLAB to obtain the final STORM image (written by previous group members). Each raw data frame took the form of a noisy background dotted with spatially-separated bright blinks where each blink is assumed to be the emission from a single molecule - a sample frame can be seen in figure 3.2. The reconstruction program locates the blinks and fits them to a Gaussian profile in order to pin-point the location of each molecule. This is described in more detail in Chapter 1.5.2.

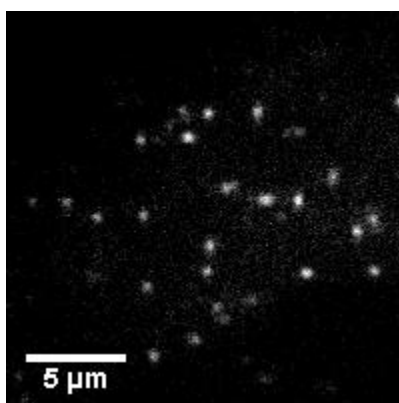


Figure 3.2: *Example frame of raw STORM data. Image is of a 3T3 cell labelled with fluorescently conjugated AF 647 phalloidin, staining for f-actin*

In order for the program to reconstruct an accurate image it is important that:

- 3.A The background noise is kept to a minimum
- 3.B The blinks are as bright as possible
- 3.C The blinks are well separated in space (the blink density is not high)

Minimising the background (3.A) and maximising the blink intensity (3.B) is equivalent to maximising the Signal-to-Noise Ratio (SNR), as defined by:

$$SNR = \frac{\mu_{Signal} - \mu_{BG}}{\sigma_{BG}} \quad (3.1)$$

Where μ is the intensity of the signal or background (BG) and σ is the standard deviation.

Maximising the SNR is important for two reasons. Firstly, it ensures that each blink can be more easily localised by the reconstruction algorithm, so more molecules can be localised overall. The algorithm searches for bright points within each .tif image and will therefore not locate events where the SNR is too low (i.e. when the signal is obscured by the noise) or events which are too small (i.e. those which are found over only one or two pixels and therefore likely to be caused by thermal noise). A high SNR ensures a more accurate localisation precision¹, and therefore a better overall image resolution. The localisation precision is a measure of how accurately the location of each fluorescing molecule can be calculated. The molecules are localised in space by fitting a Gaussian to each event. The higher the signal is compared to the background, the more accurate the fit will be.

Background noise is unavoidable to a certain extent. Background noise comes in two forms - noise from the imaging system and noise from the sample.

Noise from the imaging system mainly consists of read noise, shot noise and thermal noise. Read noise originates from the work done by the camera to 'read out' the number of electrons in each pixel and convert them into a digital signal that can be read by a computer. Read noise is inherent in every frame taken and cannot be removed as it takes work to measure the signal. Read-out noise becomes more important as the frame rate increases - if the exposure time is very short, the number of photons incident will be lower and therefore the read noise becomes a larger proportion of the pixel intensity. The root mean square (RMS) of the read-out noise increases with increasing sampling frequency i.e. with increased frame rate¹².

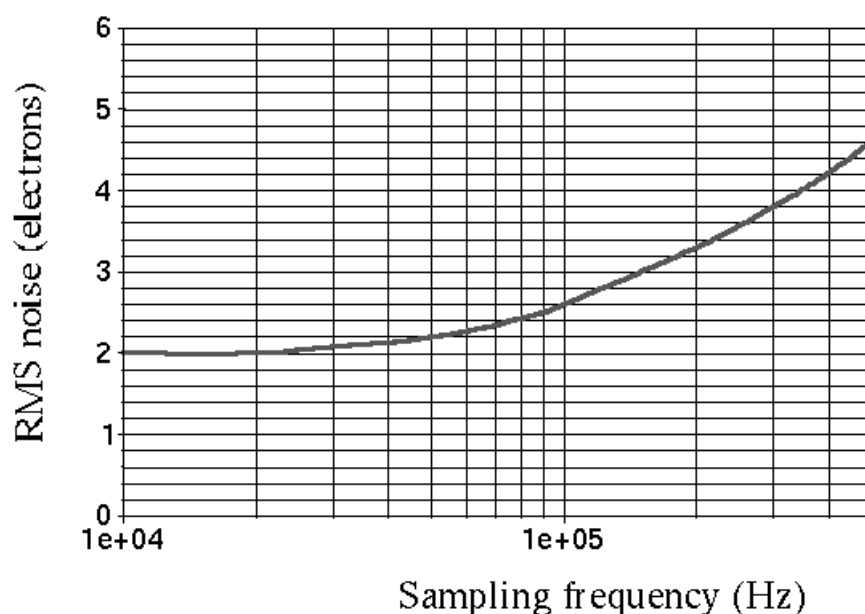


Figure 3.3: RMS of read-out noise increases with increasing sampling frequency or frame rate¹².

Shot noise comes from statistical fluctuations in the number of photons that are converted into electrons per unit time. The photons incident on the sample are emitted at random from the laser source. Over large amounts of time the differences in intensity are negligible, however at very low light levels these variances become more important. Shot noise takes the form of a Poisson distribution. Since very low light level conditions are not present in this work, shot noise is not a factor.

Thermal noise is time dependent and is caused by excited thermal electrons present in the camera array accumulating within pixels, generating false signal. As time passes more and more electrons will become excited due to thermal energy rather than incoming photons, increasing the thermal noise. Cooling the camera can help overcome this issue - the camera used throughout this work was air cooled to stay at 0 °C.

More details on camera noise can be found in chapter 1.1.4.

Noise from the sample is due to photons which are incident on the camera but which do not originate from the area of interest in the sample. These photons can be caused by excessive laser intensity and light scatter, autofluorescence of the sample, out of focus light from thick samples, breakdown of filters, and floating fluorophores which are unattached to the area of interest in the cell.

Careful sample preparation is key when attempting to minimise noise due to unattached fluorophores, by optimising the concentration of dye used to label the sample, and utilising multiple washing steps to remove excess dye from the sample (see Chapter 2.4).

It is possible to photobleach a cell's natural autofluorescence by exposing the sample to large amounts of UV radiation before the fluorophore of interest is added. However, this was not attempted during this work.

The blinks should be well separated in space (3.C), again to ensure a more accurate reconstruction. If the fluorophores are too close together their signals start to overlap, causing uncertainty in the precision of the gaussian fit. The reconstruction algorithm rejects any molecules that are localised within a certain number of pixels of each other (generally set to 4 pixels which is approximately equal to the FWHM of the average PSF, figure 3.4) in order to maintain a high localisation precision. Whilst there are methods which allow multipoint fitting, for example DAOSTORM² and 3B³, these take a large amount of computing power and time - taking several hours to reconstruct a single image - and are difficult to optimise. Optimisation for multipoint fitting requires carefully controlling the labelling density in order to overlap the correct amount of fluorophores per frame. Too few

fluorophores per frame means the multipoint fitting programs are not working optimally; too many fluorophores and the programs cannot reconstruct the image. For these reasons, multipoint fitting was not utilised in this work.

Overall, it is a balancing act between obtaining high SNRs whilst maximising the number of fluorescing molecules per frame in order to obtain a STORM image in the shortest time possible.

Another consideration in the optimisation process is the reconstruction algorithm used to analyse the data. A home written code (see chapter 2.6.2) was used for all of the analysis used within this chapter. This is a basic algorithm with several flaws - the main being the detection of "molecules" within the image which are not real molecules. The algorithm picks out bright points within the image and runs the analysis on these points. Once the points have all been fitted, there is a filtering process to get rid of these extra localisations, however it is often difficult to discern whether a localisation is due to a real molecule or due to noise. It is therefore also important to study the raw data by eye to determine whether the analysis can be trusted to accurately represent the underlying labelled structure or not (i.e. whether the reconstruction algorithm can accurately localise molecules rather than noise).

3.2 – Results

The dye *Alexa Fluor 647* (AF 647)(ThermoFisher Scientific), which emits in the far-red spectrum, was chosen for use with the STORM system. This was mainly based on the work of several groups⁴⁻⁷ at the time who had shown promising results using the AF 647 dye. Additionally, Dempsey *et al*⁸ conducted a study on the best dyes for STORM imaging, comparing performance in several areas such as the number of photons emitted, duty cycle, survival fraction and number of switching cycles. The number of photons emitted whilst in the on state should be large, so fluorescing molecules can be easily localised against the background. The duty cycle refers to the fraction of time the molecule spends in the fluorescent state compared to the length of time spent in the dark state – this should be low for STORM imaging, meaning the dye spends much longer in the off state than it does fluorescing. The survival fraction represents the number of non-photobleached molecules left in the sample. The number of switching cycles refers to the number of times a fluorophore is able to swap between the on and off states before becoming permanently photobleached. This value needs to be high enough to enable the sample to reach STORMing conditions (i.e. the conditions required to perform STORM) without becoming photobleached. If imaging a static sample, then it is advantageous for the fluorophores to be in the on state only once during data collection⁹. However, if imaging live samples, the number of switching cycles should be high to enable the position of the molecule to be imaged over time. For PALM imaging, molecules are usually only excited once before photobleaching occurs, which ensures each fluorophore is only localised once per reconstructed image. New evidence¹⁰ has emerged that this photobleaching may not be permanent and the possibility of double counting molecules must also be taken into account for PALM imaging.

AF 647 was shown to be the best performing dye tested in the study⁸ in and therefore it is the dye concentrated on in this chapter.

3.2.1 - Measuring the Point Spread Function

In STORM, the fluorophore blinks seen at the camera are assumed to be from singular dye molecules and are therefore considered point sources of light. However, due to diffraction these point sources are imaged at the camera as having a finite size. The Point Spread Function (PSF) describes their shape at the camera. In order to characterise the imaging system, the PSF was measured.

To measure the PSF, a reconstruction of a STORM image was run through a MATLAB script (Appendix 8) which selected 9x9 pixel areas, centred on the brightest pixel found in each fit from the reconstruction algorithm. Approximately 51,000 fluorophore PSFs were averaged using ImageJ's 'z-stack projection' tool set to 'average intensity'. Figure 3.4 shows the average image projection of the PSF, which gives a value of 4 pixels or ~432 nm for average molecular FWHM (1 pixel \approx 100nm).

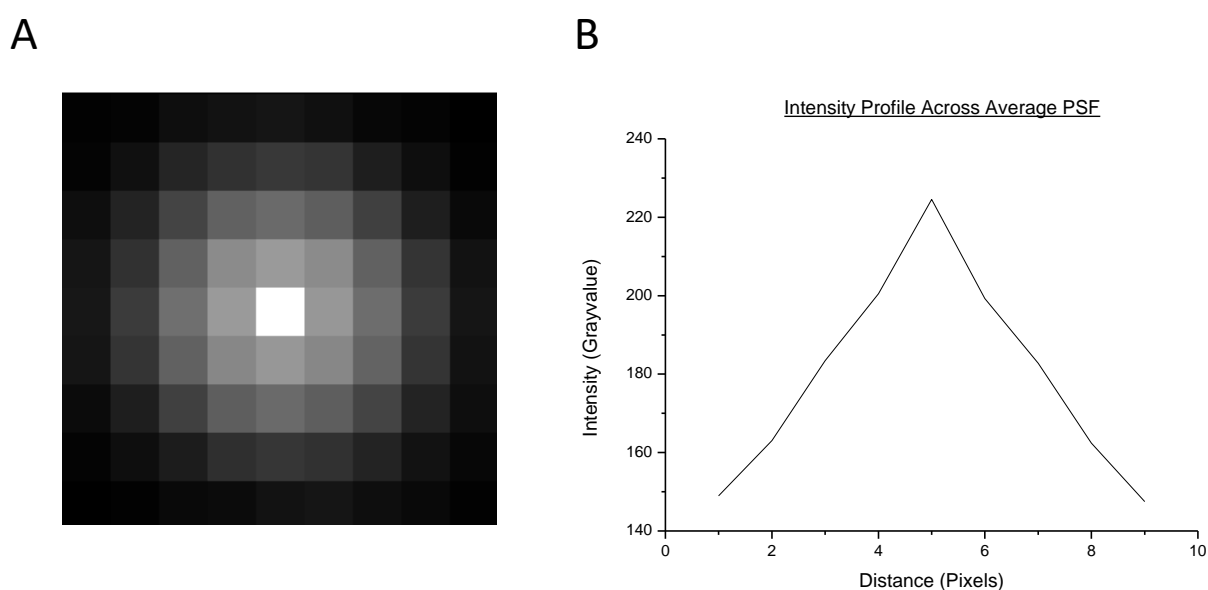


Figure 3.4: PSF of custom STORM system, (A) Enlarged image of average PSF, made from ~51,000 averaged fluorophore PSFs. (B) Intensity profile across the average PSF

The expected PSF value, (using equation 1.19) is 264nm or around 2.5 pixels, calculated using a wavelength of 647 nm and a NA of 1.49. The measured value is around twice the size of the calculated value - both because the system is not perfect, and because the measured value is an imperfect average of many fluorophores. The average PSF image is made from many images which were not aligned - the 'brightest pixel' of each single image gives only a rough estimate of the centre of each localised point. This will increase the size of the measured PSF. Using this approach limits the PSF measured, as there is no sub-pixel information. A better way to calculate this would be to use the sub-pixel information from the fitted Gaussians in the reconstruction. However, this approximate value of the average PSF size was used as a rough guide to filter reconstructed data for fits either too large or too small to be signal from fluorophores.

3.2.2 – Optimisation of Readout Laser Power

The readout laser is defined as that which produces a signal to 'read out' to the camera. The readout laser controls the amount of signal-photons given out by the sample. In the case of AF647 dye, a 140 mW 647nm laser (Coherent Obis) was used for this purpose.

The basic principles of STORM imaging are described in chapter 1.5.1. The readout laser causes the dye to fluoresce - when this is occurring the dye is said to be turned 'on'. In order to obtain so-called "STORMing conditions", the majority of the dye molecules needs to enter into a long-lived 'dark state', T, referred to as being 'off' - figure 3.5.

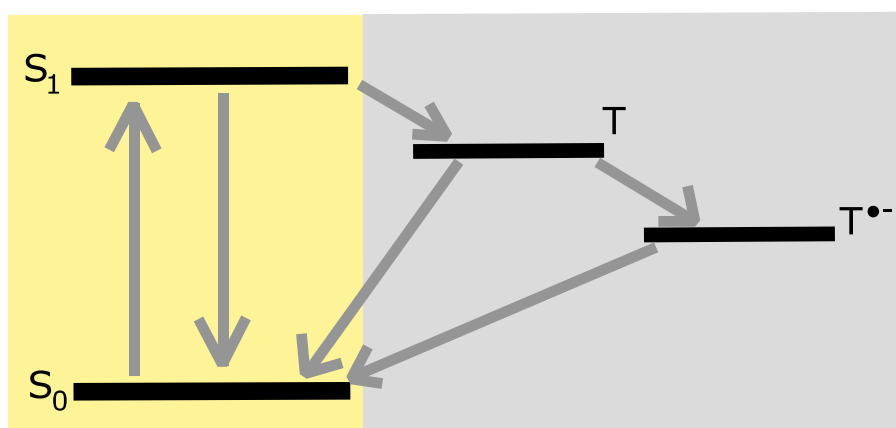


Figure 3.5: Jablonski Diagram for STORM dyes. S_1 is the bright, emissive 'on' state whereas T and T^* form the dark, non-emissive 'off' state. See chapter 1.5.1 for more information.

The long-lived dark state takes the form of a triplet state. The transition between the emissive bright state and the triplet state is quantum mechanically forbidden and so the probability that the dye falls into the dark state instead of the ground state is low. However, as the lifetime of the dark state is very much longer than the time spent in any other state, STORMing conditions will be reached after several seconds - that is, most of the dye molecules in the sample will be in the dark state, with only a small sparse subset of molecules emitting at any time. The time taken for the dye to fall into the dark state from the bright state corresponds to the length of time the fluorescent blinks are seen at the camera.

For every photon that is absorbed by the fluorophore, one photon is emitted. Until the fluorophore enters into the dark state, it will continuously move between the ground and the excited state as photons are absorbed and emitted. As the readout laser power density is increased, more readout-photons will be incident on the sample causing it to emit more photons. This results in a larger signal at the camera. Eventually, excitation of the dye molecules cannot occur any faster and a peak signal emission will be reached.

The excited state lifetime of a AF647 dye molecule is on the order of 1ns^{13} . Hence, the fastest any single dye molecule can be excited is once every nanosecond, or 1×10^9 times per second. The maximum laser power density required to achieve the maximum number of signal photons can therefore be calculated.

Assume the laser is incident on the sample over a $30\ \mu\text{m}$ square. Assume that each dye molecule is $10\ \text{nm} \times 10\ \text{nm}$ in size. Therefore:

$$Area_{laser} = 30\mu\text{m} .30\mu\text{m} = 9 \times 10^{-10} \text{ m}^2 \quad (3.2)$$

$$Area_{molecules} = 10\text{nm} .10\text{nm} = 1 \times 10^{-16} \text{ m}^2 \quad (3.3)$$

$$N_{molecules} = \frac{Area_{laser}}{Area_{molecules}} = 9 \times 10^6 \quad (3.4)$$

If the maximum number of incident photons a dye molecule can absorb is 1×10^9 per second, then

$$N_{photons} = N_{molecules} \cdot 1 \times 10^9 = 9 \times 10^{15} \quad (3.5)$$

An incoming $647\ \text{nm}$ photon has energy:

$$E = hf = \frac{hc}{\lambda} \approx 3 \times 10^{-19} \text{ J} \quad (3.6)$$

where E = energy, h = Planck's Constant, f = frequency of incident light, c = speed of light in a vacuum and λ = wavelength of incident light.

The power of the laser, P , is defined as the energy incident per second, where N = number of incident photons and t = time.

$$P = \frac{NE}{t} \quad (3.7)$$

Therefore:

$$P_{max} = \frac{N_{photons} \cdot E}{1} \approx 3 \text{ mW} \quad (3.8)$$

To convert power into power density, equation (3.9) is used:

$$\rho = \frac{P}{A} \quad (3.9)$$

This gives a theoretical value of laser power density at which the dye intensity is at a maximum of 3 mW, or 400 W/cm² over a 30 μm diameter laser spot.

Assuming that the molecule has a size of 10x10 nm is an over estimate. If the molecule size is dropped to 1x1 nm, the laser power density required jumps to 300mW or 40,000 W/cm². A more realistic cross section taken during STED experiments¹¹ is approximately 1x10⁻¹⁶ cm². This is 100 times smaller than the 1x1 nm estimate, taking the required laser power density to 4x10⁶ W/cm². This is far higher than the laser power used within these experiments.

Above the maximum laser power density the amount of photons incident on the sample is larger than the amount it can absorb : once a dye molecule is in the excited state, it cannot absorb another until it relaxes. The saturation value will likely be closer to 40,000 W/cm², therefore it is unlikely that the molecules will be saturated during these works.

In addition to increasing the number of emitted photons, increasing the laser power also increases the amount of background noise in the sample. The background noise should initially increase linearly with readout laser power. However, as the laser power increases, non-linear second- and third-order effects such as two-photon absorption start to become more important. Two-photon absorption, for example, is when the fluorophore simultaneously absorbs two photons to reach a higher energy level than normal. The transition rate to the higher energy level due to two-photon absorption is proportional to the intensity of the readout laser squared and therefore dominates over linear absorption at high intensities. The laser power density required to start detecting two photon absorption¹² is in the range of 100 GW/cm² - significantly higher than those used within this work.

This means that theoretically the SNR should have a peak value when the dye molecules are emitting the maximum number of photons possible above the background noise. Above this laser power density, the background noise will increase at a faster rate than the signal intensity, causing a drop in SNR.

Biological samples were used to study the effect of readout laser power on the SNR: a standard preparation of NIH 3T3 cells were stained with fluorescent phalloidin, which binds to f-actin. Actin monomers join together to form long thin filaments known as f-actin. The samples were imaged at a constant frame rate of 20fps and the power of the readout laser was increased in increments of approximately 10mW. The laser-spot size incident on the sample measured approximately 30μm in diameter meaning that the power density throughout the experiment ranged between 1000 and 4500 W/cm².

Figure 3.6 (A) shows how the average signal changes as the power density was increased. The average signal stays approximately constant before sharply rising after 3500 W/cm². A similar pattern can be seen in figure 3.6 (B), showing how the background noise changes with power density.

The average signal was calculated through the reconstruction program in MATLAB (Appendix 14) - each fitted localisation corresponded to a 'brightest pixel' in the raw image - the intensity values of the brightest pixels were found and averaged for the whole dataset.

Two different methods for calculating the background noise were used. For the ImageJ method, a line was drawn on the raw data, making sure the line was inside the cell but did not go over any fluorescing molecules and was at least 100 pixels long. The pixel values were then averaged. For the histogram method, the intensities of each pixel in the entire raw dataset were made into a histogram. Assuming the number of fluorescing molecules per image frame was small, the number of 'background' pixels \gg the number of 'signal' pixels, allowing a Gaussian to be fitted to the histogram as the noise dominates the histogram. The average background noise was then set as the upper value of the FWHM, i.e. as the mean plus the standard deviation. The percentage difference (equation 3.10) between the two methods was calculated to be $(7.1 \pm 7.7)\%$ meaning the two methods are comparable. Figure 3.7 shows the relative frequency of the signal and noise intensities. Also plotted in figure 3.6 B is the change in background noise outside of the cell (blue). The background noise outside of the cell is slightly lower than that within the cell, but follows the same general pattern.

$$\% \text{ Difference} = \frac{|\text{difference}|}{\text{average}} = \frac{\sqrt{(x - y)^2}}{\frac{1}{2}(x + y)} \quad (3.10)$$

The intensity does not vary with Laser Power Density as expected - the intensity does not peak and then plateau. This is likely to be because the molecules have not reached saturation. The sharp rise in signal and noise intensity after 3500 W/cm² could be due to the photophysics of the system changing, allowing dye molecules to emit more photons whilst in the dye state. Alternatively, this could be due to problems with the reconstruction algorithm accepting false localisations which may skew the brightest pixel metric. The increase is not due to the built-in gain settings of the camera, as these do not change over the range of values tested. Figure 3.6 C shows the correlation between the average signal and average noise. There is a linear relation between these two variables ($R^2 = 0.9092$) which suggests that the changes in signal and noise are due to the laser power.

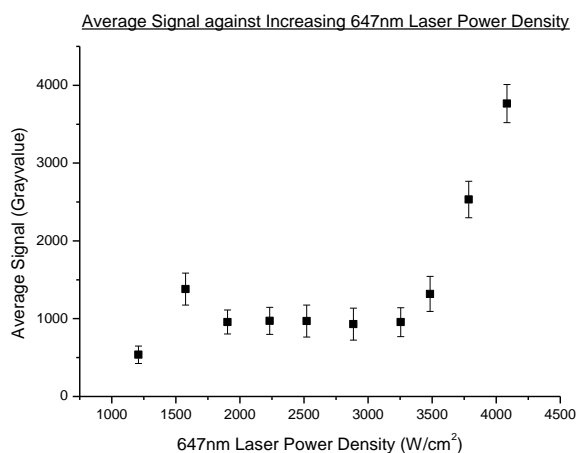
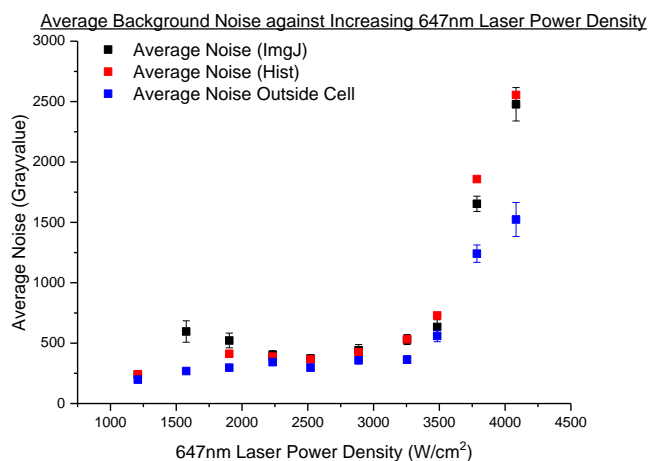
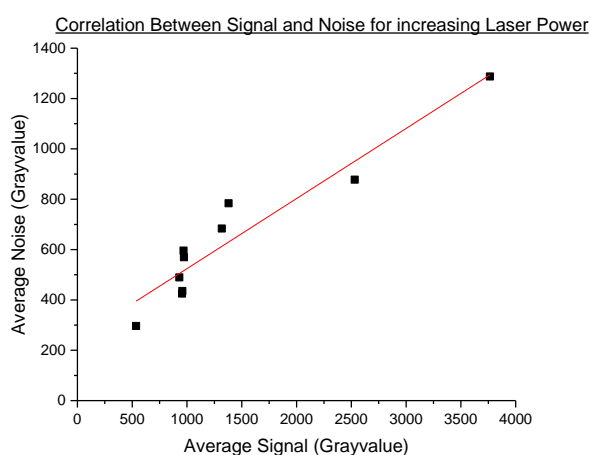
A**B****C**

Figure 3.6: 647 nm Laser Power Density Increase against (A) Average Signal Intensity (~70,000 localisations per data point) and (B) Average Noise Intensity. Average Noise calculated either from ImageJ (black) or from a Gaussian fit to the histogram of image intensity (red). Also shown is average noise taken from outside the cell (blue). Noise averaged over ~150 pixels (C) Correlation between Average Noise and Average Signal (black) with linear fit (red). Error bars represent the standard deviation of the data.

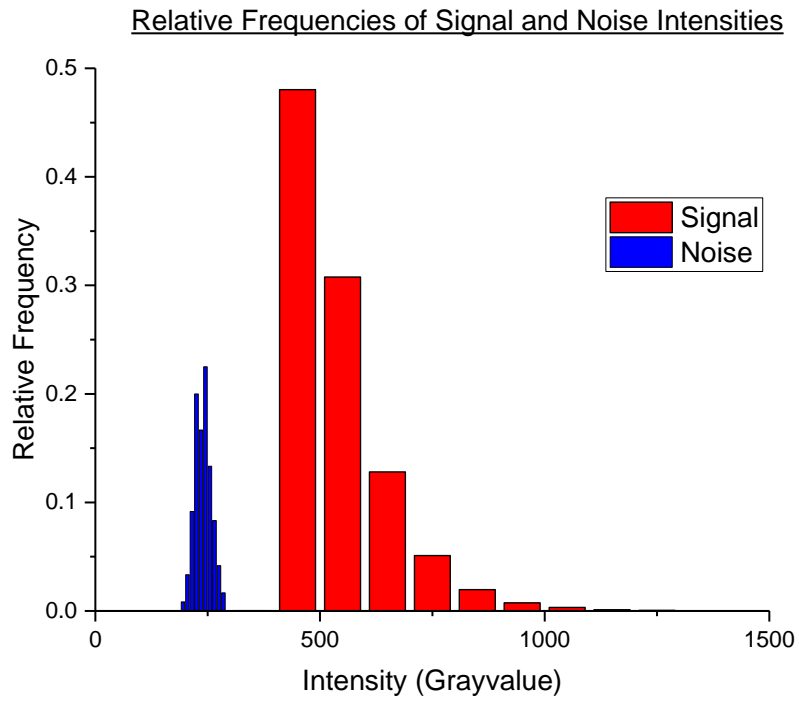


Figure 3.7: Histogram showing the relative frequencies of Signal and Noise intensities

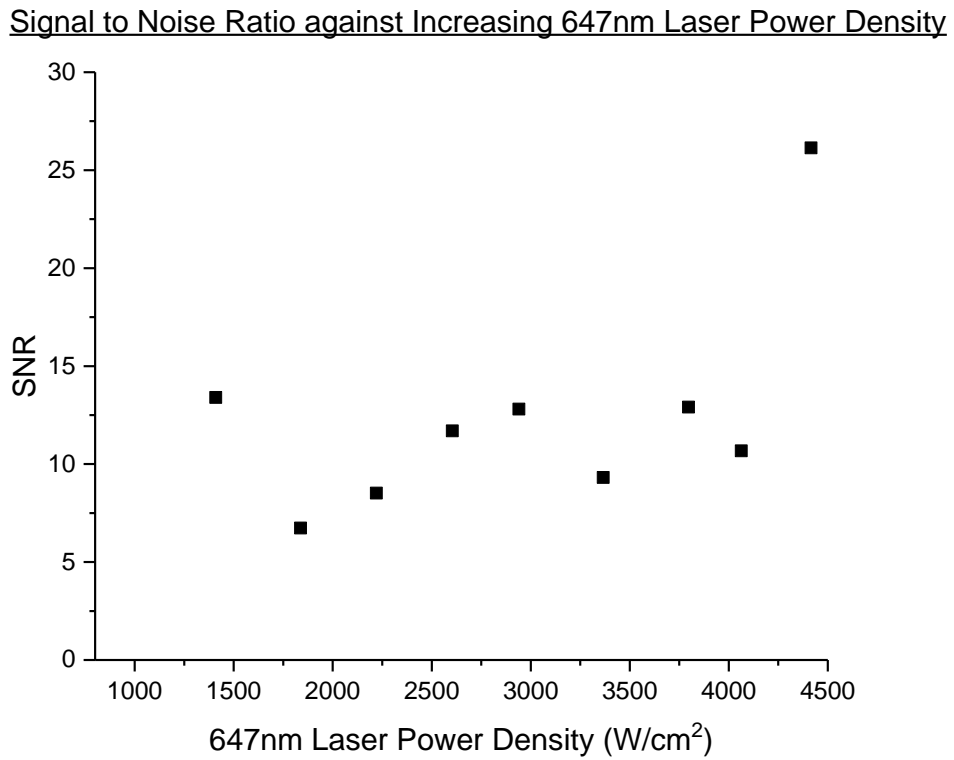


Figure 3.8: 647 nm Laser Power Density Increase against Signal-to-Noise Ratio.

The SNR is approximately constant (~ 10) throughout the increase in laser power density experiment. This suggests that the laser power density used to image the sample has no effect on the resulting STORM image. Therefore in order to image faster the highest laser power available should be used.

Another consideration for the readout laser is how it affects the number of localisations found per second - or how many molecules, on average, are in the bright state per second (figure 3.10). Increasing the laser power changes the duty cycle of the fluorophore. This is because the stability of the excited states is affected by the electric field of the laser, allowing molecules to cycle between bright and dark states more quickly at higher powers. A STORM image will be built up more quickly if more molecules are localised per second .

In order to be able to fairly compare the number of localisations found per second, firstly the localisations were filtered for multiples. Multiples occur when the fluorophore emits light over more than a single frame and as such appears in multiple frames (two or more) in the same area and is counted more than once. The filtering program (written by previous group members) removes localisations found within a specified Δx , Δy , Δz and Δt . Δx , Δy , Δz were each set at 2 pixels - half the FWHM of the average blink profile (figure 3.4) - so as to only remove localisations suspected of being from the same molecule.

Δt was set to be 10% of number of frames captured in one second (e.g. at 50 fps this would be 5 frames). This is because at faster frame rates the signal from a fluorescing molecule will be spread out over more frames - therefore the number of frames that multiples need to be considered over increases with frame rate (figure 3.9).

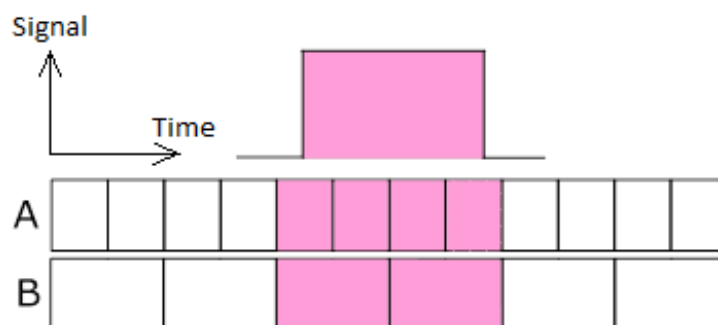


Figure 3.9: When imaging at faster frame rates, the signal from a fluorophore is spread out over a larger number of frames - (A) is sampling data twice as fast as (B) and therefore the event is spread out over double the number of frames in (A) as in (B).

Secondly, the area of the image covered by 3T3 cells was calculated for each dataset. This was calculated because each dataset was imaged in a different location to avoid imaging bleached fluorophores. This meant each dataset was covered by a different amount of cell. To do this, the entire dataset was flattened using ImageJ's 'z-stack projection' tool set to 'maximum intensity'. This makes a Maximum Intensity Projection (MIP) image where each pixel takes the maximum intensity value for that pixel location throughout the image stack. The MIP was then thresholded into a binary image using a custom MATLAB script (Appendix 10) and the cell area was found by summing the binary image. The fraction of each dataset covered by cell was then calculated and used to adjust the number of localisations per dataset.

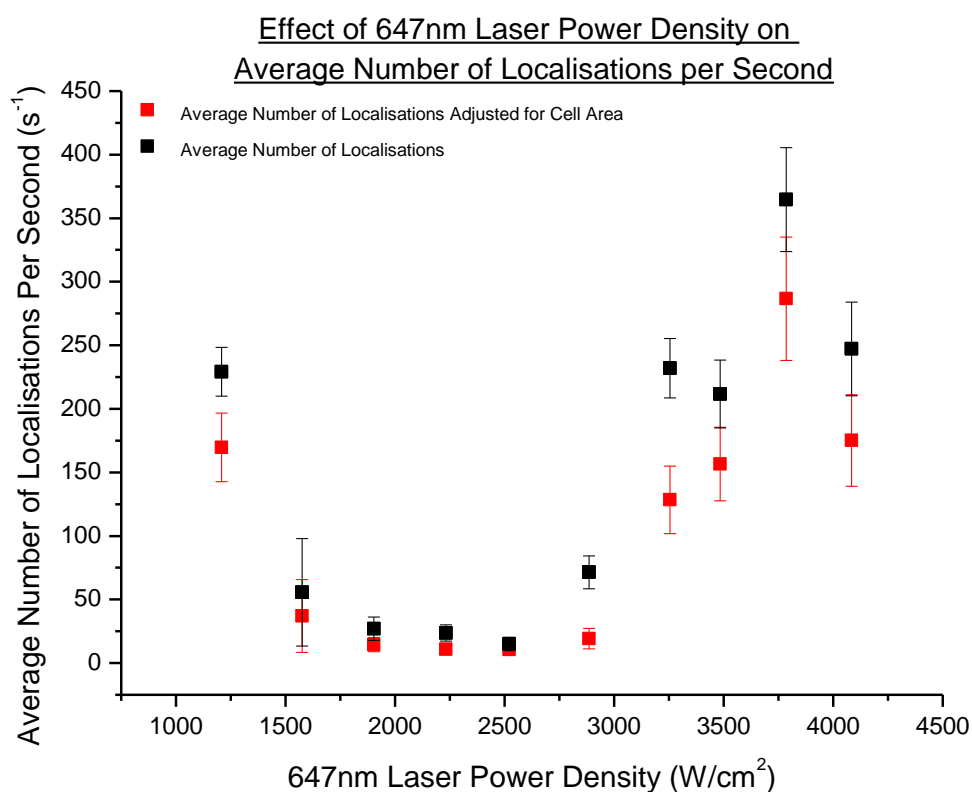


Figure 3.10: The average number of localisations found per second ($n = 500$) against increase in Laser Power Density. Data all taken at a constant frame rate (20 fps) in NIH 3T3 cells labelled with AF 647 phalloidin. (Black) Raw average number of localisations found per second, (Red) Data adjusted for area of cell covering the field of view. Error bars represent the standard deviation of the data.

The number of localisations found per second increases sharply after around 3000 W/cm² (figure 3.10). The raw data taken from laser power densities above 3000 W/cm² have a very high background (figure 3.6 B, figure 3.11 C) and the density of fluorescing molecules is very high. This makes reconstruction of the data difficult and whilst the number of localisations found per second on average is high this possibly has a detrimental effect on the quality and reliability of the reconstruction.

At laser power densities below 3000 W/cm^2 fluorophore PSFs are more distinguishable from the background noise: fitting the data is therefore more reliable, even though the overall number of molecules localised per second is smaller. The data taken at 1200 W/cm^2 (figure 3.11 A) has very sparse blinks in comparison to the dataset taken at the next laser power density, 1600 W/cm^2 (figure 3.11 B), and has a lower background noise. The reason why the number of molecules localised for this data point is so much higher than the rest of the data before the jump at 3000 W/cm^2 , despite the signal in this dataset also being lower, is possibly because less molecules are rejected due to overlapping in the initial reconstruction.

In order to image quickly, the laser power density should therefore be as high as possible as this produces the largest number of localised molecules per second at no cost to the SNR. However, care must be taken that the reconstructions are accurately localising molecules rather than noise, which may then require imaging using a lower laser power density (i.e. under 3000 W/cm^2).

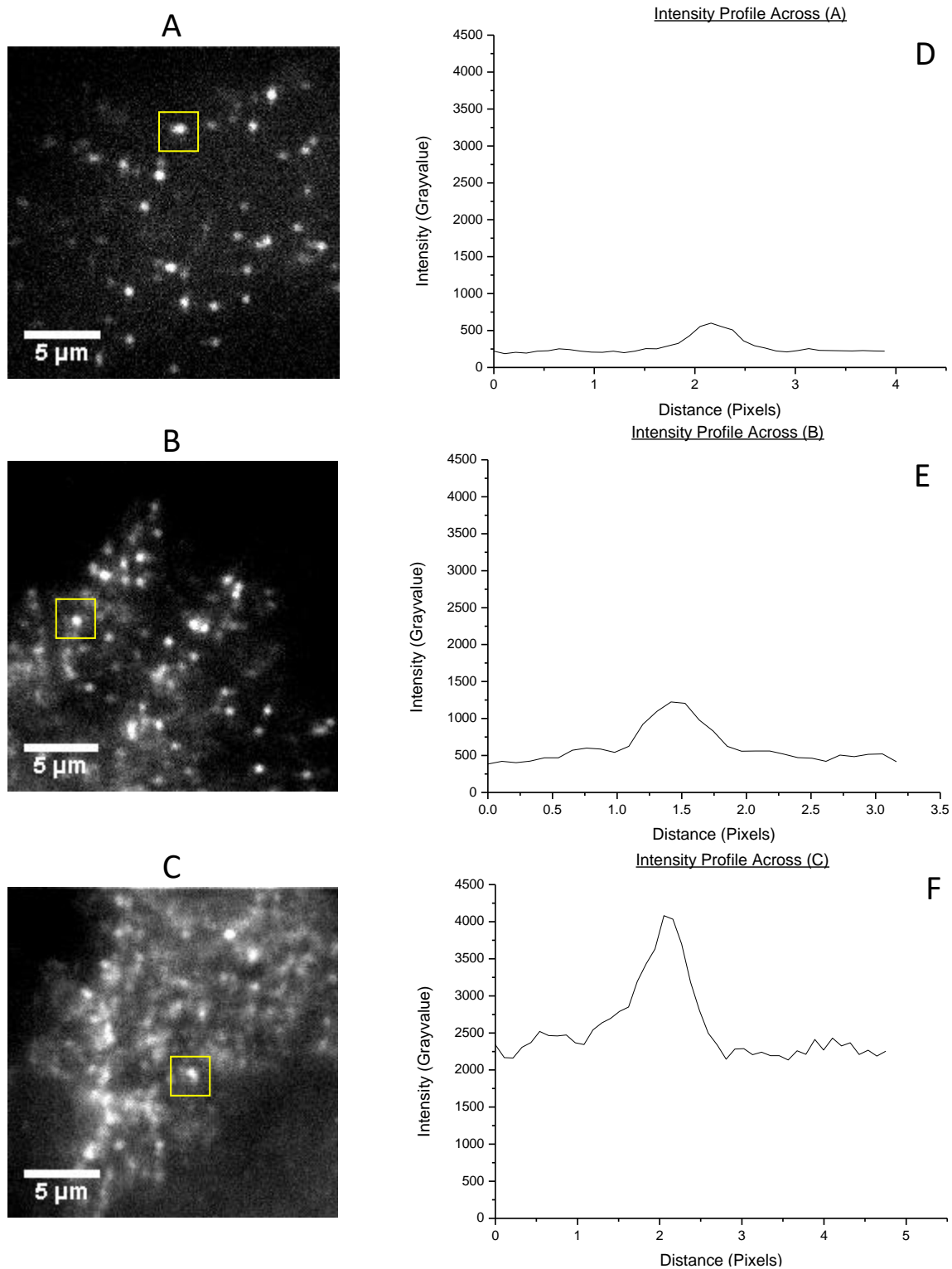


Figure 3.11: 3T3 NIH Cells labelled with fluorescently conjugated AF 647 Phalloidin. Example frames from datasets taken at the same frame rate (20 fps) and at a laser power density of (A) 1200 W/cm^2 , (B) 1600 W/cm^2 , (C) 4000 W/cm^2 . (D-F) Show line profiles across the blink outlined in yellow on each image, at (D) 1200 W/cm^2 , (E) 1600 W/cm^2 , (F) 4000 W/cm^2 . Intensity axes are shown to the same scale for comparison.

3.2.3 - Optimisation of Frame Rate

The frame rate of imaging is a very important consideration when attempting to maximise the SNR.

As the fluorophores are under constant illumination until they drop into the long-lived dark state they are effectively continuously emitting photons. However, a 'frame' occurs over a finite amount of time which corresponds to the amount of time the camera is collecting data for. Therefore in order to maximise the fluorophore signal per frame, the frame rate should allow as many photons as possible to be collected by matching the frame rate to the time the fluorophores spend in the bright state.

When the frame rate is slow, the signal will be high as all photons emitted by a single fluorophore before it drops into the dark state will be collected in one frame - if the frame rate is too slow this may increase the density of fluorophores too much, such that they start overlapping. However, as the frame rate increases, the number of signal-photons emitted will remain the same for a constant readout power and the signal will start to get 'spread out' over multiple frames (figure 3.9). This will reduce the fluorophore signal per frame, and also causes multiples. As data is filtered for multiples, allowing the fluorophore to emit over many frames results in much of the signal emitted being lost.

As previously, samples of NIH 3T3 cells stained for f-actin using fluorescently conjugated AF 647 phalloidin were tested. A constant readout laser power density of 4000 W/cm^2 was used throughout and the frame rate was increased from 20 - 200 fps. This high laser power density was used to ensure that fluorophores were visible even at high frame rates, at the expense of decreasing SNR.

Figure 3.12 shows there is no change in the SNR when increasing the frame rate. As the data was taken at a constant laser power density, the average number of photons emitted from the sample per unit time (the average signal) should be the same throughout. Any variations in the signal and noise should therefore only arise from the changes in frame rate and will increase/decrease by the same amount for each imaging speed tested: any signal/background noise will also become 'spread out' over the same number of frames.

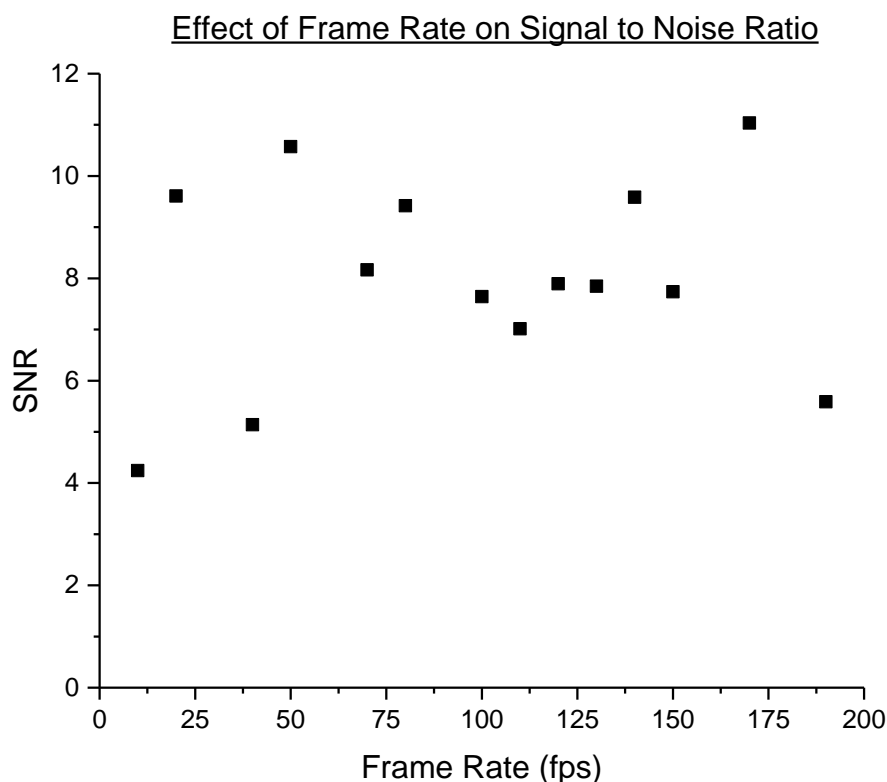


Figure 3.12: *Effect of Frame rate on Signal-to-Noise Ratio. Data all taken at a constant laser power density (4000 W/cm^2) in NIH 3T3 cells labelled with AF 647 phalloidin. Each signal value was an average of $\sim 70,000$ localisations. Each noise value was an average of ~ 120 pixels.*

If camera read noise was significant, as the frame rate is increased the SNR would drop. At higher frame rates the signal intensity drops - as the camera read noise is constant, this could cause the signal intensity to drop below the noise due to the camera. However, this does not happen: the read noise is insignificant in comparison to other noise sources. This therefore shows that all the background noise in the image is due to the sample (cell autofluorescence, loose dye, out-of-focus light etc.) rather than due to the camera read noise. Camera read noise is fixed for the camera and cannot be removed (see Chapter 1.1.4). However, figure 3.11 shows that the camera read noise is insignificant to the SNR and therefore not a concern when imaging.

Figure 3.13 shows the relationship between the number of localisations found per second and frame rate. Multiples have been removed and results have been adjusted for cell area (red data points). There is a clear increase in number of localisations between 100-150 fps. Therefore, to image as fast as possible - by imaging as many fluorophores as possible per second - data should be taken in this frame rate range.

At slower frame rates, the number of localisations found per second is also lower than at the peak of 100-150 fps. This could be due to losing information from short-lifetime blinks. If a molecule is only

in the bright state for a very short amount of time, the signal from that molecule may be indistinguishable from the background noise at slower frame rates because the contribution from noise is larger.

The number of localisations found per second decreases at high frame rates due to thresholding. When reconstructing the datasets only pixels above the threshold value are considered for fitting - therefore at faster frame rates when the fluorophore intensity is split over many frames the signal is often lower than the threshold, causing fewer molecules to be localised.

Figure 3.13 shows example frames taken from 20, 120 and 190 fps. Although the SNR is constant throughout, the frame from the sample taken at 190 fps (figure 3.14 C) is less distinct than that taken at 20 fps (figure 3.14 A). This is also shown in figures 3.14 D-F which show the relative frequency of intensity for each example frame rate. Data taken at the slower frame rates (figure 3.14 A) also have less dense fluorophore distributions. Together this means that reconstructions at higher frame rates will be less reliable.

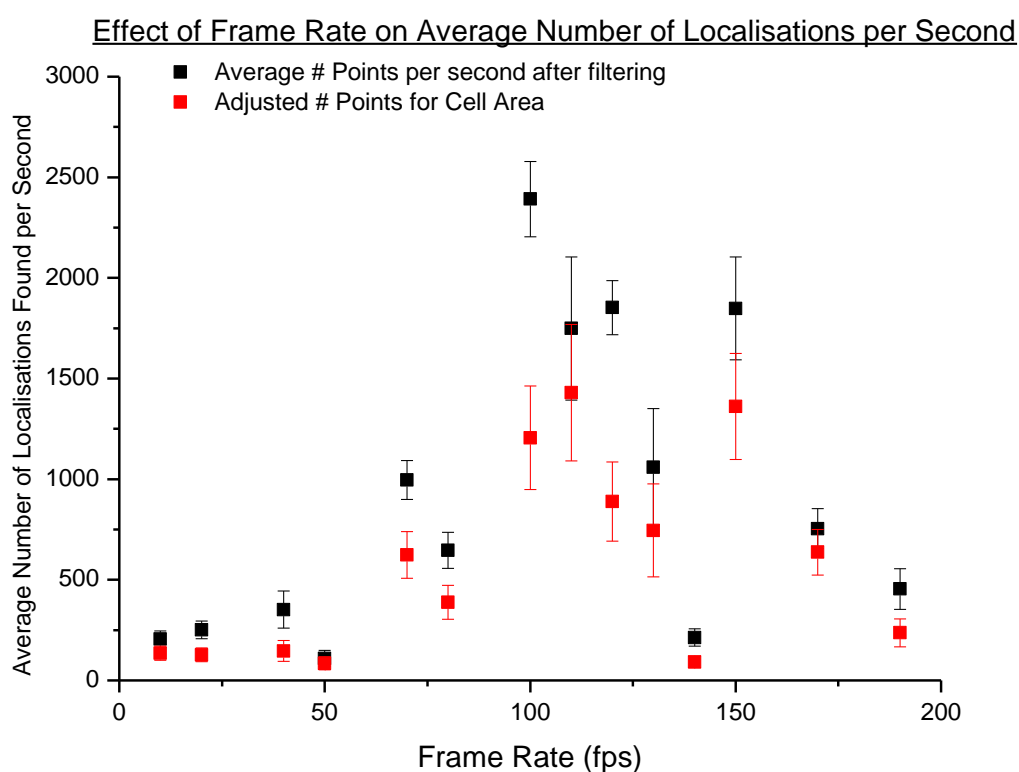


Figure 3.13: *Effect of Frame rate on average number of molecules localised per second. Data all taken at a constant laser power density (4000 W/cm^2) in NIH 3T3 cells labelled with AF 647 phalloidin. (Black) Raw average number of localisations found per second, (Red) Data adjusted for area of cell covering the field of view. Error bars represent the standard deviation of the data. For each point, $n \approx 100$.*

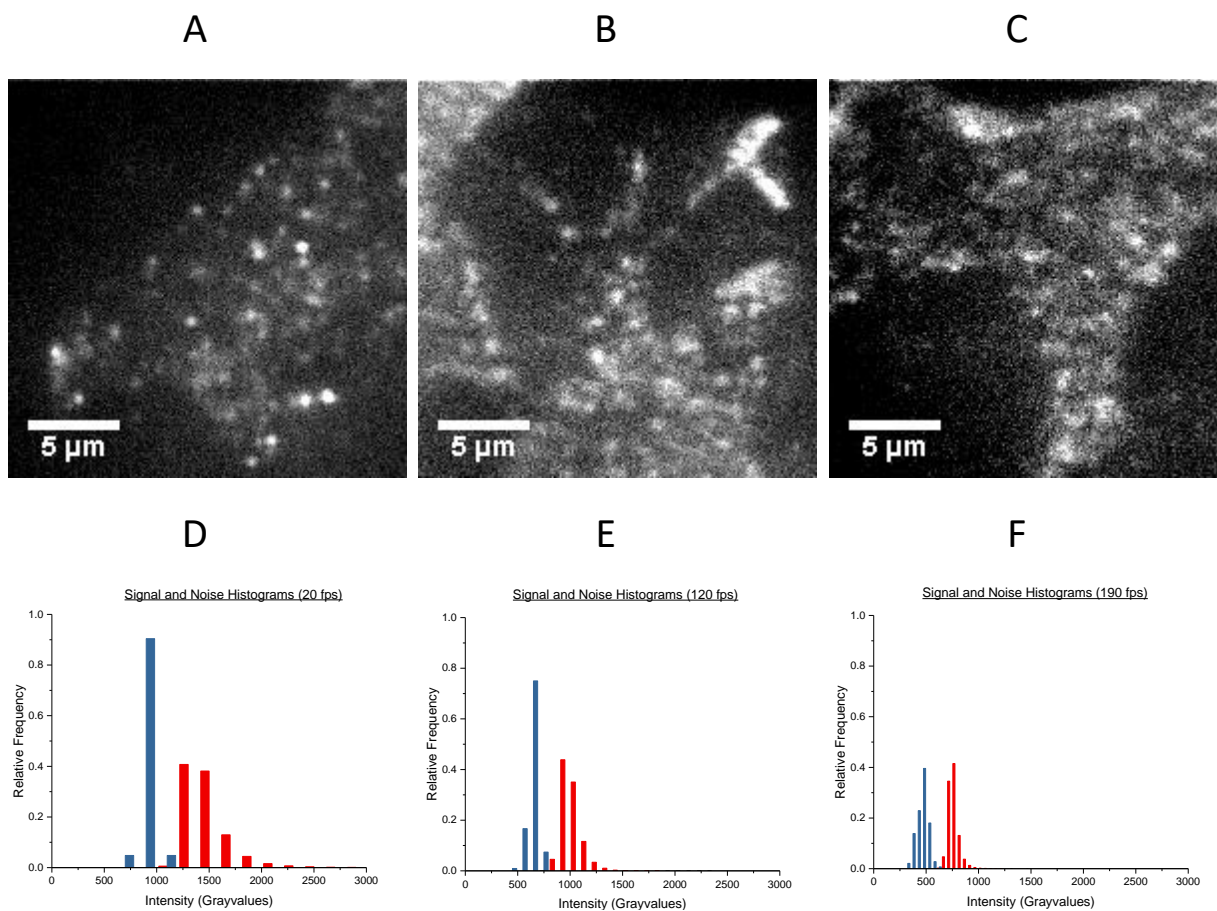


Figure 3.14: 3T3 NIH Cells labelled with fluorescently conjugated AF 647 Phalloidin. Example frames from datasets taken at the same Laser Power Density (4000 W/cm^2) and at a frame rate of (A) 20 fps, (B) 120 fps, (C) 190 fps. Histograms show the relative frequencies of noise (blue) and signal (red) for the example datasets at (D) 20 fps, (E) 120 fps, (F) 190 fps.

3.2.4 - Effect of changing the STORM buffer concentrations

In order to obtain STORM conditions, the sample must be imaged in STORM buffer, which consists of two parts - a reducing agent and an anti-oxidising agent. The reducing agent works to stabilise the fluorophore whilst in the dark state in order to extend its lifetime⁷, while the anti-oxidising agent reduces the amount of permanent bleaching¹³ in the sample.

Following the method described in Dempsey *et al* (2011)⁸, the STORM buffer used consisted of 10 mM β -mercaptoethylamine (MEA), 5 mg/ml Glucose Oxidase, 4 μ g/ml Catalyse and 10% w/v Glucose in PBS in TN buffer. However it is unclear precisely how these chemicals effect the rate of blinking of the dyes.

Again, biological samples (NIH 3T3 cells stained for f-actin using fluorescently conjugated AF 647 Phalloidin) were tested. A constant readout laser power of 900 W/cm² was used throughout at a frame rate of either 100 or 200fps. Both frame rates were used, as samples have a large amount of variability. The frame rate was changed on a sample-by-sample basis to obtain the best blink density possible, determined by eye whilst imaging.

The concentration of MEA was changed from 0 to 350mM - all other chemicals were kept at the same concentrations throughout. A sample mounted in 'VECTASHIELD with DAPI' (Vector Labs), a standard mounting medium used for biological samples, was also tested (red data points), as samples mounted with VECTASHIELD have been shown to reach STORMing conditions¹⁴.

Figure 3.15 shows how the average number of localisations found per second varies with concentration of MEA. The number of localisations found was very high at low concentrations, including 0 mM MEA. The number of localisations found per second hits a minimum at around 50 mM MEA concentration, before rising to an approximately constant value after 100 mM. Figures 3.15 B, C and D show example frames at MEA concentrations of 10, 100 and 350 mM respectively. Samples with very low amounts of MEA do not show STORMing conditions (Figure 3.16 B) - there is not enough thiolate ions in the system to ensure the majority of dye molecules are in the dark state at any moment in time. This results in an overly large number of molecules localised, as the reconstruction software cannot separate the real PSFs from the noise. This is demonstrated in figure 3.17, which shows example frames with the STORM reconstruction points overlaid at (A) 10 mM and (B) 200 mM concentration of MEA. As the reconstruction algorithm accepts any small, clustered bright area of the image as a molecule if the molecules are too close together or the background is too high, the algorithm is not reliable at picking out only the fluorescing molecules. This shows that the high counts for number of molecules localised per second at low MEA concentrations are due to artefacts.

As the concentration of MEA increases, eventually the number of molecules obtained reaches a constant value - this is from around 100 mM concentrations and higher. VECTASHIELD produces a similar number of localisations per second to samples at 100 mM concentrations and higher.

Figure 3.18 shows how the SNR rate changes with increasing concentrations of MEA. The SNR is unchanged as the concentration of MEA increases. The sample imaged in VECTASHIELD has a similar SNR to those imaged in STORM buffer.

From these results, 100 mM MEA concentration should be used for STORM imaging, and was used throughout.

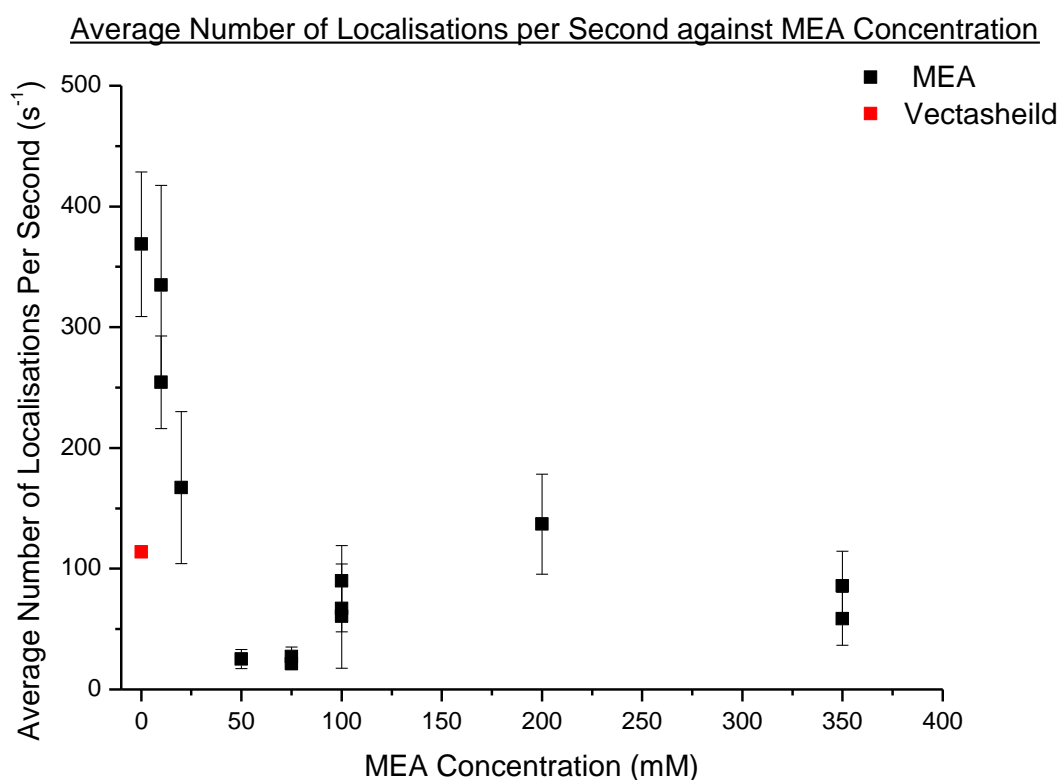


Figure 3.15: Effect of Buffer MEA Concentration on the average number of localisations per second ($n = 100$), adjusted for cell area. Data taken at a constant laser power density (980 W/cm^2) and frame rate (either 100fps or 200 fps) in NIH 3T3 cells labelled with AF 647 phalloidin. (Black) Sample imaged in MEA, (Red) Sample imaged in VECTASHIELD. Error bars represent the standard deviation of the data.

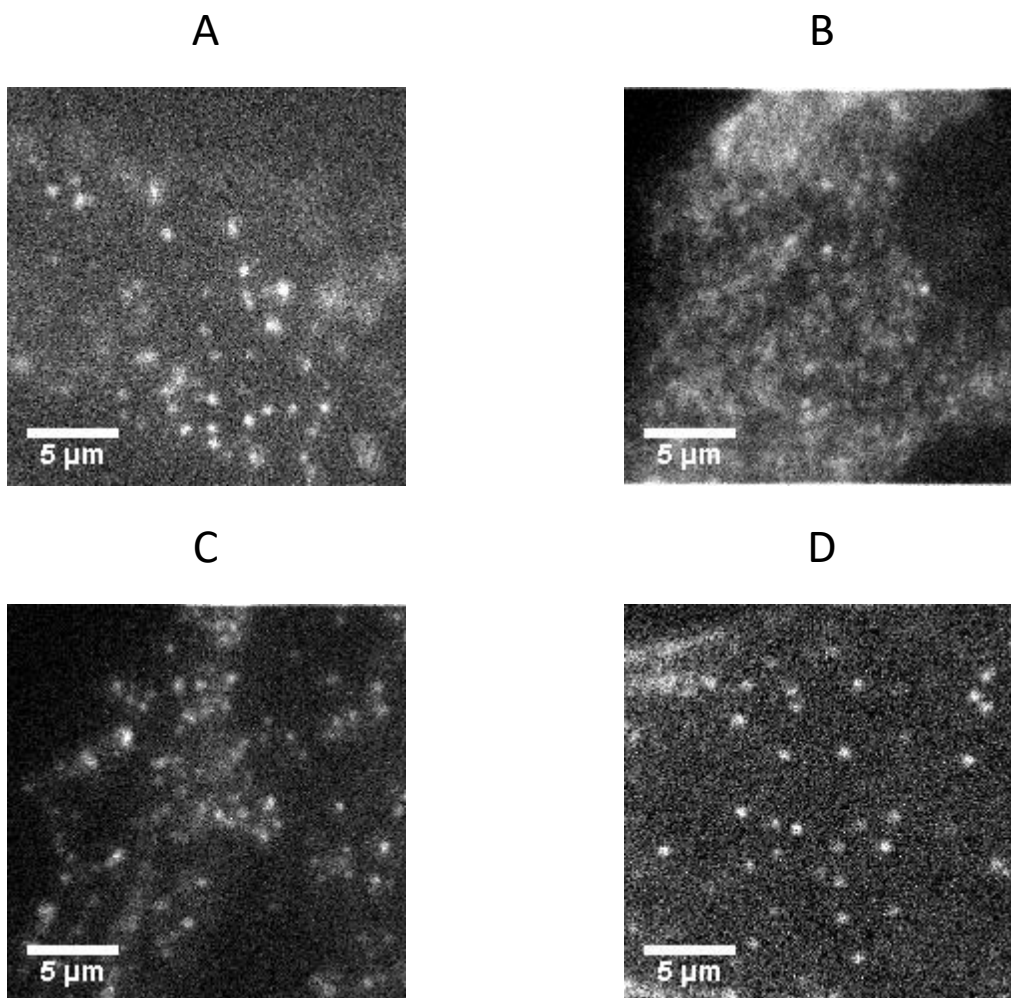


Figure 3.16: 3T3 NIH Cells labelled with fluorescently conjugated AF 647 Phalloidin. Example frames from datasets taken at the same Laser Power Density (980 W/cm^2) and frame rate of 100fps (A,C) or 200 fps (B, D) in imaging buffer consisting of (A) VECTASHIELD, (B) 10 mM MEA, (C) 100 mM MEA, (D) 350 mM MEA

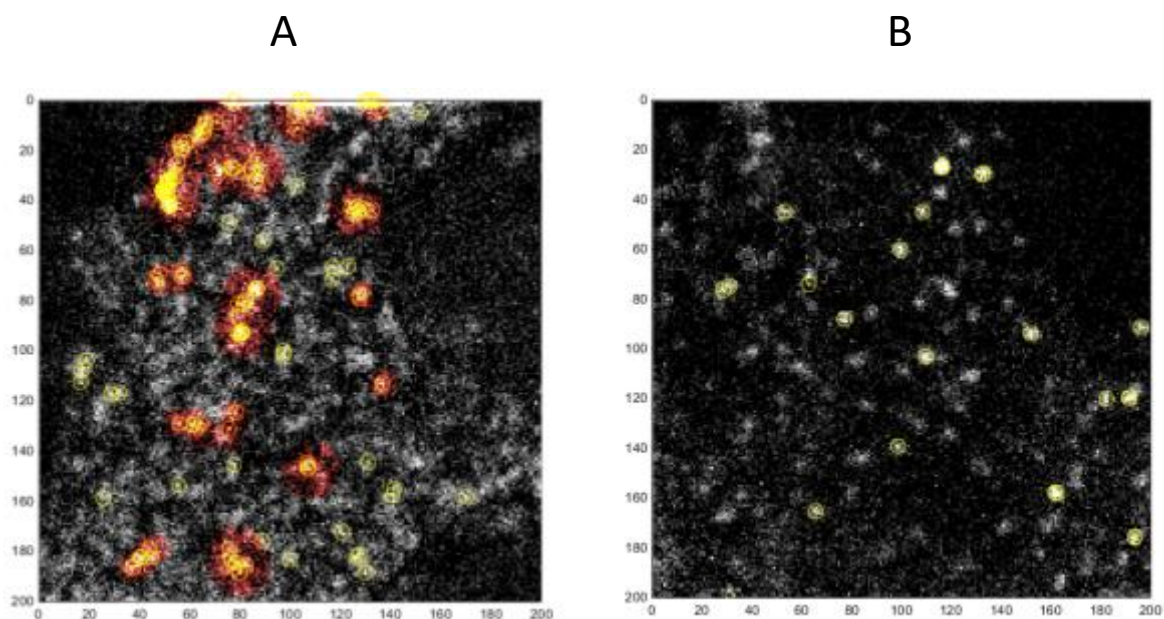


Figure 3.17: Example images highlighting localised molecules from STORM reconstruction for (A) 10 mM MEA and (B) 200 mM MEA. Areas where the algorithm appears to be failing are marked in red.

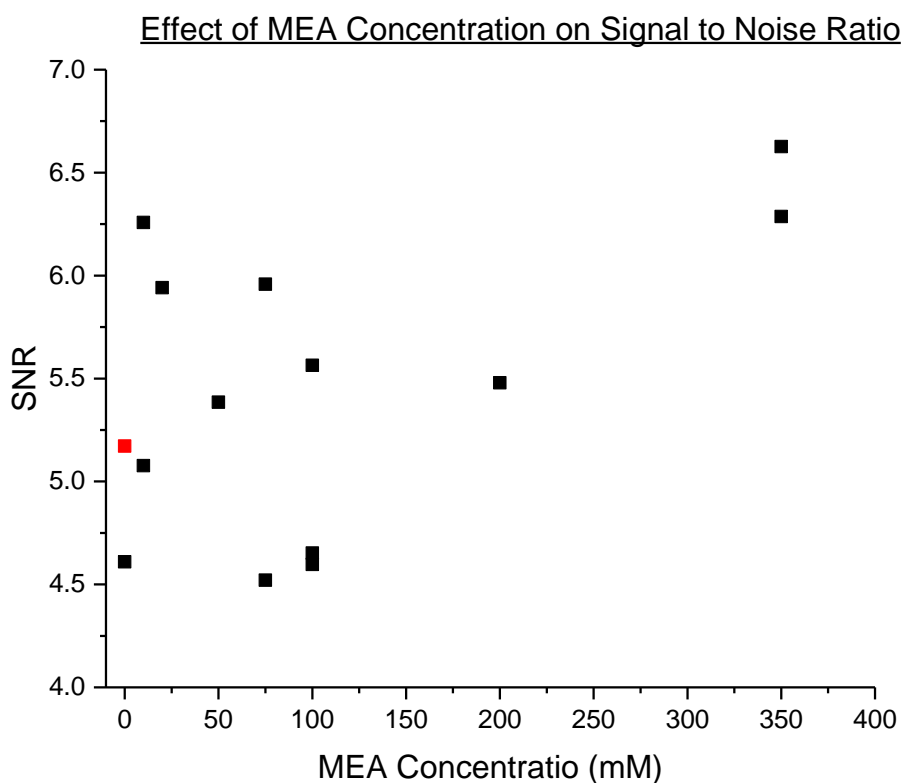


Figure 3.18: Effect of Buffer MEA Concentration on the SNR. Data taken at a constant laser power density (980 W/cm^2) and frame rate (either 100fps or 200 fps) in NIH 3T3 cells labelled with AF 647 phalloidin. (Black) Sample imaged in MEA, (Red) Sample imaged in VECTASHIELD. Signal averaged over $\sim 70,000$ localisations, noise averaged over ~ 120 pixels.

3.3 - Conclusions

In order to produce a STORM image quickly, it is necessary to maximise both the SNR and the number of molecules localised per frame. In this chapter, how three imaging parameters - readout laser power density, frame rate and MEA concentration in imaging buffer - effected both the SNR and the number of localised molecules were studied in order to define the best imaging parameters for imaging at speed.

Changing the readout laser power density does not change the SNR (figure 3.8). This is because signal and noise are linearly correlated (figure 3.6 C) which shows that these two parameters increase mainly due to the the effect of the laser rather than any other physical effects. The number of molecules localised per second increases with the readout power density (figure 3.10) however, this comes at the cost of well-separated PSFs which may cause difficulties in reconstruction (figure 3.11 C). This suggests that the readout laser power used should be the highest possible to obtain STORMing conditions as increasing the power does not produce any increase in the SNR. From the behaviour of the number of localisations per second with increasing laser power density, the power density used for STORM imaging should be high as this increases the number of molecules localised per second. However, in practice it should not go higher than 3000 W/cm^2 due to the presence of overlapping PSFs at power densities higher than this causing issues in reconstruction.

The SNR does not change for different frame rates (figure 3.12), as the signal and noise are spread out over the same number of multiple frames. The number of molecules localised per second peaks at around 100 - 150 fps (figure 3.13), which may be due to losing short-lifetime fluorophores at slow frame rates and thresholding out dimmer fluorophores at high frame rates.

The imaging buffer contains MEA which stabilises the dark state of the fluorophores and therefore allows STORMing conditions to occur. Changing the concentration of MEA does not affect the SNR (figure 3.18). Samples with low concentrations of MEA appear to not reach adequate STORMing conditions (figure 3.16 B). These samples with low MEA concentrations have overlapped PSFs and high background causing difficulty in reconstruction (figure 3.17), and also causing the artificially high number of molecules localised over time (figure 3.15). The optimum concentration was found to be 100 mM, as the number of molecules localised per second plateaus at concentrations higher than this.

Overall, this chapter concludes that the optimum imaging conditions for imaging at speed are to use an imaging buffer containing 100 mM MEA, to image between 100 - 150 fps and to use a readout laser power density which is only just high enough to produce an image where the PSFs are well separated.

These imaging conditions are aimed at obtaining STORM images as quickly as possible. Whilst the optimum imaging conditions found are correct in general - on a sample-by-sample basis, variability is large. Samples may vary due to temperature, sample preparation, labelling efficiency or age of STORM buffer. It is therefore very difficult to pin down precise imaging conditions for every sample. We therefore conclude that the parameters found in this chapter are a good 'starting point', but that all parameters should be tweaked depending on the sample in order to obtain the best images.

Additionally, what has not been considered is what the reconstructed images look like, or the reconstruction quality. Data in this chapter was not taken for long enough to build up accurate images for every dataset, and the accuracy of a STORM reconstruction is difficult to quantify. The aim of this chapter was to find conditions suitable for obtaining data as quickly as possible - however as can be seen from the raw data (figures 3.11, 3.14, 3.16), conditions that maximise the number of molecules found per second no longer have sparse, well separated PSFs. This is why increasing the imaging speed is often detrimental to the resolution obtainable .

3.4 - References

- 1 Thompson, R. E., Larson, D. R. & Webb, W. W. Precise nanometer localization analysis for individual fluorescent probes. *Biophysical Journal* **82**, 2775-2783 (2002).
- 2 Holden, S. J., Uphoff, S. & Kapanidis, A. N. DAOSTORM: an algorithm for high-density super-resolution microscopy. *Nature Methods* **8**, doi:10.1038/nmeth0411-279 (2011).
- 3 Cox, S. *et al.* Bayesian localization microscopy reveals nanoscale podosome dynamics. *Nature Methods* **9**, doi:10.1038/nmeth.1812 (2012).
- 4 Rust, M. J., Bates, M. & Zhuang, X. Sub-diffraction-limit imaging by stochastic optical reconstruction microscopy (STORM). *Nature Methods* **3**, doi:10.1038/nmeth929 (2006).
- 5 Huang, B., Wang, W., Bates, M. & Zhuang, X. Three-dimensional super-resolution imaging by stochastic optical reconstruction microscopy. *Science* **319**, doi:10.1126/science.1153529 (2008).
- 6 Jones, S. A., Shim, S.-H., He, J. & Zhuang, X. Fast, three-dimensional super-resolution imaging of live cells. *Nature Methods* **8**, doi:10.1038/nmeth.1605 (2011).
- 7 Heilemann, M. *et al.* Subdiffraction-resolution fluorescence imaging with conventional fluorescent probes. *Angewandte Chemie-International Edition* **47**, 6172-6176, doi:10.1002/anie.200802376 (2008).
- 8 Dempsey, G. T., Vaughan, J. C., Chen, K. H., Bates, M. & Zhuang, X. W. Evaluation of fluorophores for optimal performance in localization-based super-resolution imaging. *Nature Methods* **8**, 1027-+, doi:10.1038/nmeth.1768 (2011).
- 9 Wang, S. a. M. J. R. a. D. G. T. a. X. X. S. a. Z. X. Characterization and development of photoactivatable fluorescent proteins for single-molecule-based superresolution imaging. *Proceedings of the National Academy of Sciences* **111**, 8452-8457, doi:10.1073/pnas.1406593111 (2014).
- 10 Annibale, P., Vanni, S., Scarselli, M., Rothlisberger, U. & Radenovic, A. Quantitative Photo Activated Localization Microscopy: Unraveling the Effects of Photoblinking. *PLOS ONE* **6**, e22678, doi:10.1371/journal.pone.0022678 (2011).
- 11 Kastrup, L. & Hell, S. W. Absolute optical cross section of individual fluorescent molecules. *Angewandte Chemie-International Edition* **43**, 6646-6649, doi:10.1002/anie.200461337 (2004).
- 12 Bestvater, F. *et al.* Two-photon fluorescence absorption and emission spectra of dyes relevant for cell imaging. *Journal of microscopy* **208**, 108-115 (2002).
- 13 Heilemann, M., van de Linde, S., Mukherjee, A. & Sauer, M. Super-Resolution Imaging with Small Organic Fluorophores. *Angewandte Chemie-International Edition* **48**, doi:10.1002/anie.200902073 (2009).
- 14 Nicolas Olivier and Debora Keller and Vinoth Sundar Rajan and Pierre, G. n. a. S. M. Simple buffers for 3D STORM microscopy. *Biomed. Opt. Express* **4**, 885--899, doi:10.1364/BOE.4.000885 (2013).

4 - Reconstruction Density Limit

Contents

| | |
|--|-----|
| 4.1 - Introduction | 93 |
| 4.2 – Results | 101 |
| 4.2.1 - Simple Image Quality Analysis (small section analysis) | 101 |
| 4.2.2 - Image Quality Analysis: Radial Distances Histograms | 106 |
| 4.2.3 - Image Quality Analysis: Actin Cables | 111 |
| 4.2.4 - Cut-off Point Analysis in Staphylococcus Cells..... | 115 |
| 4.2.5 - Cut-off Point Analysis in Actin..... | 122 |
| 4.2.7 - Dependence of Cut Off Density with Laser Power | 124 |
| 4.3 - Conclusions | 128 |
| 4. 4 - References | 131 |

4.1 - Introduction

The motivation behind this project was to increase the imaging speed of STORM, with the eventual aim being the ability to image cell dynamics in real time. In addition to the problem of acquiring STORM images more quickly, there are other concerns regarding the viability of live cell STORM imaging. STORM and other superresolution imaging techniques often require very high laser powers which can damage and stress the cells (phototoxicity) which changes the structure of the cell causing images to be unreliable¹. STORM imaging requires an imaging buffer to assist the fluorophores in entering into single molecule blinking behaviour, however the standard buffer used² is toxic to cells. The fluorophores used for STORM are generally non-genetically coded and require antibodies to target the fluorescent molecule to specific proteins of interest. This method of cell labelling is not compatible with live cell imaging as antibodies are not membrane permeable³. These issues must be resolved before live cell STORM imaging can occur, however only the issue of increasing imaging acquisition will be studied in this work.

Several groups have published 'high speed' STORM images^{4,5}, generally requiring only a few seconds to obtain a STORM image. To obtain images faster the current method is to increase the number of molecules localised per unit time. Often, this requires very slow and complicated reconstruction programs which attempt to form images from overlapping PSFs^{5,6}.

In this chapter we turn this approach for increasing the imaging speed on its head: rather than attempting to image an increased number of molecules, we will instead be looking at how many molecules are required to form an image. STORM images are made up of a series of localised dots - but just how many of these dots are necessary in order to build up a superresolution image? A superresolution image is defined as having a resolution better than that achievable by standard light microscopy methods (~250 nm) but how do we define resolution in a STORM image? How many molecules must be localised before this "super" resolution is obtained?

Image resolution is a general measure of how much detail is visible in an image. It can therefore be thought of as a measure of "how good" the image is, or the quality of the reconstruction. However, it is important to note that resolution is not a measure of how accurately an image reflects the ground truth of the underlying object. Simply because details on a shorter length-scale are visible does not necessarily mean that the image is "accurate". We can instead define the image quality as how accurately an image represents the object. Image quality depends on many factors, including⁷:

- Imaging conditions - i.e. Signal-to-Noise Ratio
- Overall number of molecules localised

- Sample Drift
- Labelling density of the sample
- The quality of labelling in the sample (i.e. uniform labelling)

Nevertheless an image resolution stating the smallest visible length-scale in an image is an important quantity for image analysis. It is this value that determines how well details in the image can be seen and therefore how much information can be inferred from the image. Unfortunately for STORM, calculating the image resolution is not straightforward. This is because a STORM image is not a true image, but a reconstruction: a computer generated "map" of the location of molecules within the sample.

Currently the field of superresolution microscopy does not have a consensus on how to measure the image resolution. The initial papers published in STORM/PALM^{8,9} tended to quote values of localisation precision in x, y and z as their image resolution. The localisation precision is a measure of how accurately a molecule can be localised in space: it is therefore generally taken to be the error of the fit of the PSF (i.e. the fit to the single fluorescent molecules) and typically has values of 20-30 nm in x and y, and 50-60 nm in z¹⁰. However, this does not actually describe the resolution of the reconstructed image since 'resolution' in this case is defined as the amount of detail that can be resolved in the image: the localisation precision does not contain enough information to describe this. Whilst single molecules in the raw STORM data can be easily resolved in space to an accuracy of 20 nm this is not the same as the resolution in the reconstructed image.

For example, a STORM image with only a few very precisely localised molecules is not particularly useful for further study as it does not provide any knowledge of the *relationship* between the location of the molecules - there is no way to determine the underlying structure unless more molecules are localised (figure 4.2 A).

The resolution of a standard optical microscope is typically defined using the *Rayleigh Criterion* (chapter 1.1.2) which is determined by the physical constraints of the microscope (Numerical Aperture (NA) of lens) and the wavelength of light used (λ) (equation 1.19). The Rayleigh Criterion is the minimum separation between two objects such that they can be viewed as two objects. Once the separation becomes smaller than the Rayleigh Criterion, the PSFs of the objects merge into one and are considered unresolvable. Typically, standard optical microscopes use the Rayleigh Criterion as a guide to the best possible resolutions obtainable. Raw STORM data is still subject to diffraction and the Rayleigh Criterion. However, because the molecules imaged are singular and then reconstructed this definition no longer applies to the final image.

Some groups¹¹ therefore define the STORM image resolution as the smallest resolvable distance between two known objects in a reconstructed image, for example, the smallest gap that can be seen between two intersecting actin filaments. Measuring this distance is essentially finding the Rayleigh Criterion - finding the minimum distance such that two objects are visibly separate. Measuring the width of a single actin filament is also used to measure the accuracy of an image. As the width of actin filaments is known through EM ($\sim 10 \text{ nm}^{12}$), this allows the resolution to be determined from the image.

In 2013, Nieuwenhuizen *et al*¹³ published a method of analysing superresolution images using Fourier Ring Correlation (FRC), a technique commonly used to analyse EM images¹⁴. FRC analysis splits the data set into two images ($f_1(r)$ and $f_2(r)$), takes the Fourier transform of the two datasets, and then calculates the statistical correlation between the two over pixels at the edge of a circle of constant spatial frequency (q). Formally, the FRC curve equation is given by:

$$FRC(q) = \frac{\sum_{\vec{q} \in \text{circle}} \hat{f}_1(\vec{q}) \hat{f}_2(\vec{q})^*}{\sqrt{\sum_{\vec{q} \in \text{circle}} |\hat{f}_1(\vec{q})|^2} \sqrt{\sum_{\vec{q} \in \text{circle}} |\hat{f}_2(\vec{q})|^2}} \quad (4.1)^{13}$$

Figure 4.1 B demonstrates the FRC curve. At low frequencies the correlation is high (~ 1), and this drops off at higher frequencies until noise dominates the system and there is no correlation (0) (figure 4.1 B). That is, at low resolutions the images match or correlate almost perfectly. The correlation between the two images decays to 0 at higher resolutions/smaller length scales, i.e. details in the image become blurred and are no longer distinguishable from the background.

Spatial frequency is the inverse of distance, therefore Nieuwenhuizen *et al* defined the resolution of the image to be when the correlation drops below a certain threshold - this threshold represents the point at which small details become blurred with noise and are no longer visible or resolvable. The threshold was found to be $\frac{1}{7} \approx 0.143$, determined using simulated data (blue line, figure 4.1 B).

In contrast to other methods for determining the image resolution, the FRC method analyses the entire image once it is reconstructed - not just a part of it like the smallest-distance method. The FRC method therefore gives the "length scale at which details are resolved *on average* rather than *with certainty*"¹³.

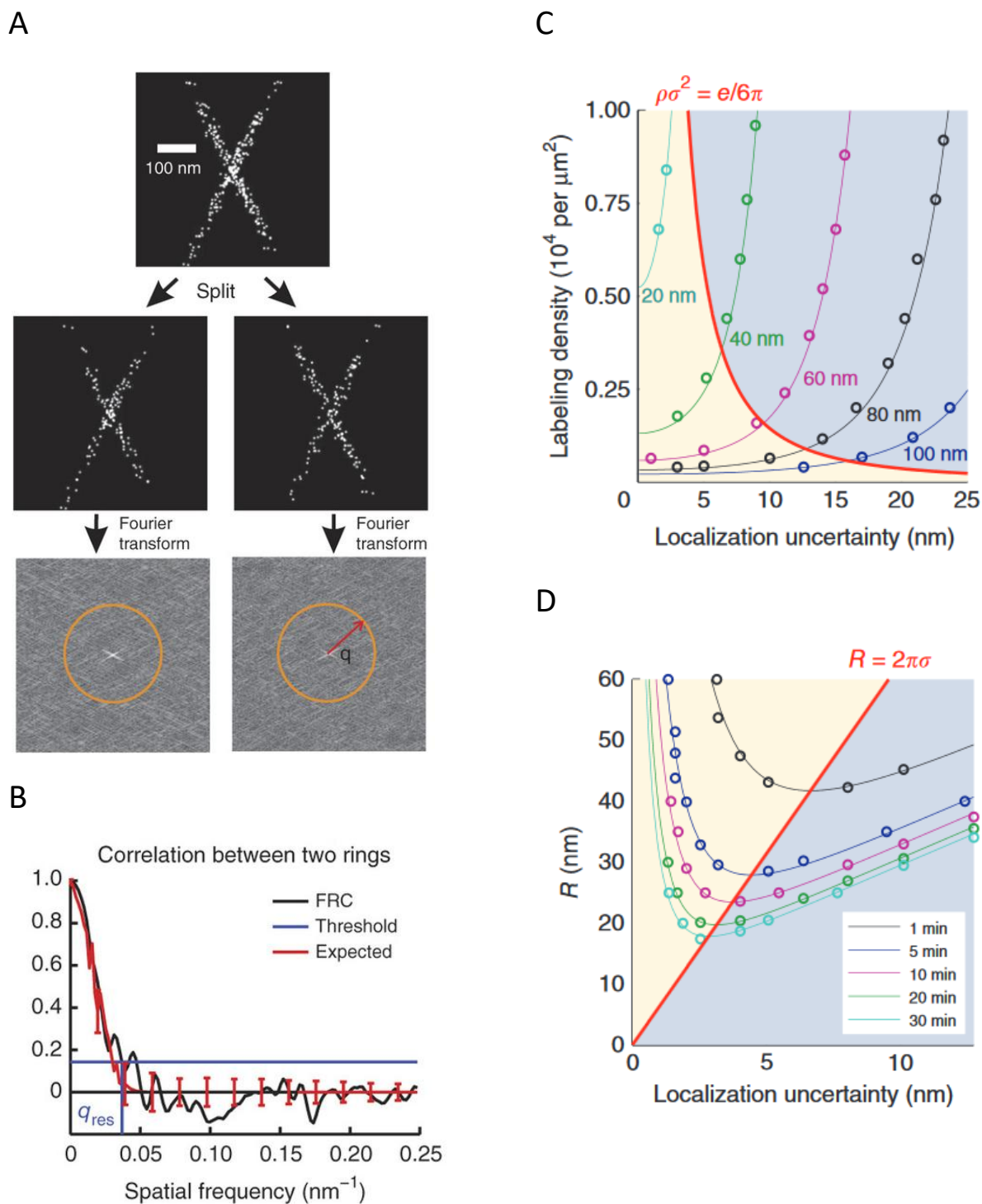
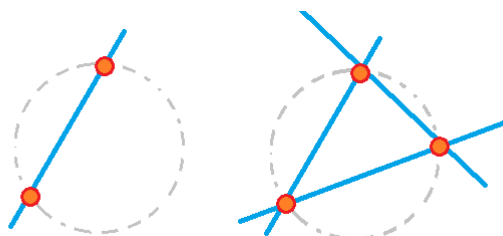


Figure 4.1: Demonstration of using FRC to analyse STORM images, reproduced from¹³ (A) The dataset is split into two and Fourier transformed. Correlation analysis is performed over rings of constant frequency¹³¹³ (q). (B) The correlation between the two data sets changing with increasing spatial frequency. (C) Lines of constant FRC resolution as labelling density and localisation uncertainty changes, from simulated data. Yellow area represents density limited, blue represents localisation uncertainty limited imaging. (D) Change in image resolution for different localisation uncertainties over different time periods. The minima falls between the two regimes (yellow localisation limited, blue density limited).

Using the FRC method, Nieuwenhuizen *et al*¹³ (2013) suggested that maximum resolution achievable in a STORM image occurs at a trade-off between two regimes - either the resolution is limited by the number of molecules present in the reconstruction (density-limited) or it is limited by the precision at which molecules can be located (localisation-limited). This idea is demonstrated in figure 4.2. Each molecule that is located has an uncertainty associated with it (the localisation precision, σ , which can be visualised as a circle centred on the molecule, with radius = σ). A STORM image is built up of many of these circles. When the circles are spread out, the image is density-limited; when the circles overlap the sample is localisation-limited. If the image is density-limited, the underlying structure of the sample cannot be known for certain. For example, figure 4.2 shows the building up of a circular structure from $r = \sigma$ circles. Figure 4.2 A shows a density-limited image - there are not enough molecules to accurately depict the underlying circular shape, and it is also impossible to know whether the structure is continuous or made up of discrete points. As more molecules are localised (figure 4.2 B) the circles begin to overlap. At this point the image begins to be localisation-limited. Imaging further overlapping molecules will not increase the information in the image and is therefore unnecessary. Hence, once the sample reaches the crossover point between the two regimes there is no need to continue imaging - the achievable resolution is at a maximum. This trade-off value gives a "time limit" or "cut off point" for when imaging.

A



B

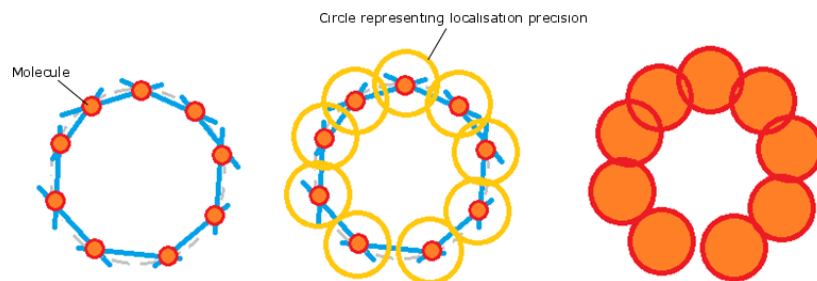


Figure 4.2: Diagram demonstrating the trade-off between localisation precision and localisation density. (A) Localisation density limited regime – there are not enough molecules localised to accurately build up an image. (B) Localisation precision limited regime – additional molecules will not increase the image resolution

To calculate the trade off, Nieuwenhuizen *et al* (2013)¹³ calculated the explicit resolution of simulated STORM data using the average FRC curve set to $\frac{1}{7}$, the threshold for the cut-off limit. The statistical average of the FRC curve is:

$$\langle FRC \rangle = \frac{(Q + NS(q))e^{(-4\pi^2\sigma^2\rho^2)}}{2 + (Q + NS(q))e^{(-4\pi^2\sigma^2\rho^2)}} \quad (4.2)$$

Where Q represents the average number of activation cycles per molecule (i.e. Q accounts for the possibility that a fluorophore will emit more than once per image. This is set to 0 as we are assuming each fluorophore emits only once), N is the total number of molecules localised ($N \gg 1$) and S(q) is the image resolution at the cut-off limit.

Setting equation 4.2 to $\frac{1}{7}$ produces:

$$NS(q)e^{(-4\pi^2\sigma^2q^2)} = \frac{1}{3} \quad (4.3)$$

which can then be used to produce an explicit expression for the FRC resolution.

The simulated data consisted of two parallel lines with a cosine crosssection and an average localisation density of ρ . If the data takes the form of a periodic structure with $M \geq 1$ periods with period length d and length L and assuming L is sufficiently large, then S(q) evaluated at $q = 1/d$ is:

$$S(q) = \frac{d}{4\pi L} \quad (4.4)$$

If the grating can just be resolved, then the resolution, $R = d$. Therefore combining equations 4.3 and 4.4 gives the resolution of the simulated image as:

$$R = \frac{2\pi\sigma}{\sqrt{W(6\pi\rho\sigma^2)}} \quad (4.5)$$

where W(x) is the Lambert W function.

The trade off between the two regimes - localisation and density limit - occurs when the "relative gains in resolution due to changes in either ρ or σ are equally large". That is, when

$$\frac{\sigma^2}{R} \frac{\partial R}{\partial \sigma^2} = -\frac{\rho}{R} \frac{\partial R}{\partial \rho} \quad (4.6)$$

Evaluating the derivatives gives the result:

$$R = 2\pi\sigma \quad (4.7)$$

and that the trade off occurs at:

$$\rho\sigma^2 = \frac{e}{6\pi} \approx 0.143 \quad (4.8)$$

for two parallel lines where ρ = localisation density and σ = localisation precision.

The localisation precision, σ , is a measure of how accurately the centre point of a diffraction-limited point can be determined. The centre can be localised "arbitrarily precisely, given a sufficient number of photons (N)"¹⁵. This means the localisation precision is different for each molecule that is localised, and depends on the intensity of each molecule. Thompson *et al* (2002)¹⁵ define the localisation precision for each dimension (in 2D) to be:

$$\langle(\Delta x)^2\rangle = \frac{s^2 + a^2/12}{N} + \frac{8\pi s^4 b^2}{a^2 N^2} \quad (4.9)$$

where Δx is the error in localisation, s is the standard deviation of the point spread function, a is the pixel size, N is the number of photons detected and b is the background noise.

The localisation precision can be measured experimentally using non-blinking fluorescent beads such as Tetraspecks (Thermofisher) or gold nanoparticles. The beads are imaged over several frames and reconstructed as normal; the standard deviation of the central position was used to determine the localisation precision (see chapter 1.5.2). This calculation was done regularly by previous group members and was, on average, taken to be 20 nm.

Using this value for σ gives a value for the cut off limit as being:

$$\rho(t) = \frac{e}{6\pi\sigma^2} = 3.16 \times 10^{-4} nm^{-2} \quad (4.10)$$

In units of localisations per pixel, this gives a cut-off limit of ~ 3.16 (using the approximate conversion of 1 pixel = 100 nm x 100 nm).

This cut-off limit is interesting because it gives a solid test to determine the number of frames required to make a 'movie still' (i.e. a single reconstruction in a stack of reconstructions which is part of a superresolution movie) and also because it determines a minimum time that a STORM image takes to be created. Therefore this gives a novel approach to fast imaging, as no extraneous molecules/frames are allowed in each image. This gives the fastest possible reconstructions which are suitably molecularly dense. The proposed theory is a post-processing technique, designed to be applied to large datasets which are split up into movie stills after the whole set has been collected.

In this chapter the localisation density changes will be investigated and where the cut-off limit is for real samples. It will be considered whether the images produced from the cut-off limit are "good" images and if they reflect the underlying biology.

4.2 – Results

Staphylococcus aureus and NIH 3T3 cells stained with AF 647 were used throughout this chapter, prepared as described in chapter 2.4. These cells were chosen due to the regular shapes formed making analysis easier – actin in cells forms long thin filaments and 5 minutes of cell wall growth in *Staphylococcus* data forms either a circle or an elliptical 'Φ' shape depending on the spatial orientation of the septum and where in the life-cycle the cell was at upon fixation.

4.2.1 - Simple Image Quality Analysis (small section analysis)

Following the Nieuwenhuizen *et al*¹³ (2013) paper, a simple analysis was done on *Staphylococcus* data to determine how the theoretical cut-off limit translates to real data. The data taken for this analysis was imaged at 20 fps.

A custom MATLAB code was used to select circular areas of the *Staphylococcus* cell (appendix 7) and calculate the localisation density as a function of time:

$$\text{Localisation Density} = \frac{\# \text{ Localisations Found}}{\text{Area}} \quad (4.11)$$

The MATLAB code was given a random point (x_1, y_1) within the cell, and the distance of all points (x, y) from this location (d) was calculated using Pythagoras' theorem in the form:

$$d = \sqrt{(x - x_1)^2 + (y - y_1)^2} \quad (4.12)$$

The number of localisations found in each frame within a certain distance of the chosen point (x_1, y_1) were then selected for analysis.

The areas chosen were centred on the growing septum, with a chosen radius of 2 pixels corresponding to 216 nm. From EM studies the cell wall of *Staphylococcus* cells has been shown to be ~20-30nm in width¹⁶. However, from reconstructed images on average the cell wall was measured to be ~ 200 nm, meaning the circles selected covered the whole cell wall.

Figure 4.3 shows the increase in localisation density over time. The horizontal black line at 3.16 localisations/pixel represents the cut-off limit as specified by equation 4.10. The maximum time taken to reach the cut-off limit was ~300 s, suggesting this is the maximum time required to build up a STORM image for the settings used with this sample.

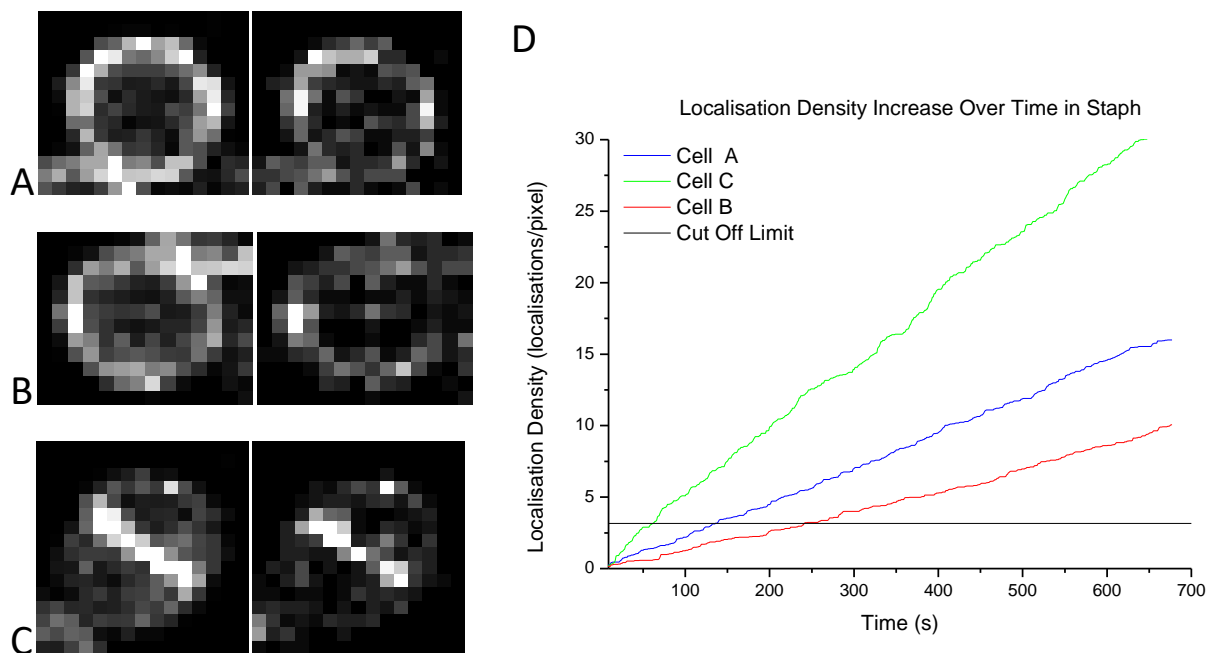
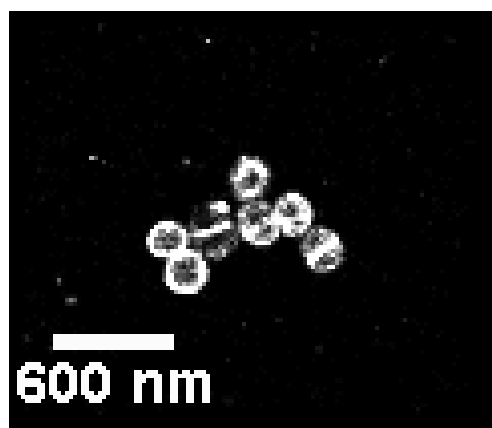


Figure 4.3: (A) Average increase in Localisation Density over time for three different cells in the same image. Black line represents the cut off density limit. (B) Cell 'A' (blue), (C) Cell 'B' (red), (D) Cell 'C' (green). Left hand images show reconstructions made from all frames, right hand images show reconstructions at the cut off limit.

The density of localisations increases linearly over time for all areas studied, taking between 20 and 150 seconds to localise one molecule per pixel², taking 64 seconds on average. As the density increase over time is linear, the time taken to reach the cut off limit density and therefore the time a sample must be imaged for should be predictable.

The data was then reconstructed to compare the final images - this was done to check the concept of the cut-off limit. Whilst theoretically there is no need to continue adding molecules to the reconstruction once the image is localisation-limited, does this translate to the real images? How does the "quality" of the image made from either all the data (~ 10 minutes) compare to that reconstructed from ~200 s worth of data? That is, when imaging quickly can the reconstruction be trusted to represent the underlying structure?

A



B

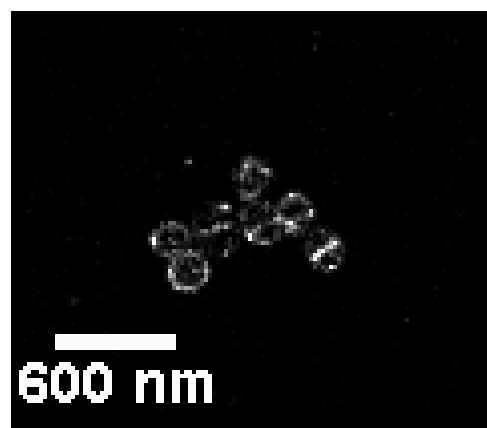


Figure 4.4: *Staphylococcus* cells imaged for ~10 minutes at 20 fps. Images are set to the same brightness/contrast scale (1-50). (A) All frames. (B) Image at the cut off limit

Example images can be seen in figure 4.4. Figure 4.4 A shows example reconstructions with 10 minutes of data, figure 4.4 B shows the reconstruction of the same data set only with the stack cut at the cut-off limit. The average cell wall width measured from figure 4.4 A was 52.4 nm, and the average cell wall width from figure 4.4 B was 43.2 nm. In comparison, the size of the cell wall as measured by EM is around 20-30nm¹⁶.

Whilst the value for the average cell wall width is smaller in the image with fewer localisations and therefore closer to the "true" value, this does not automatically make it a better image. The width of cell walls in the 'all frames' image could be larger due to drift as it is imaged over a longer period of time. However, it could also be that by stopping sooner important molecules are missed, giving an inaccurate assessment of the capabilities of the imaging system.

A rudimentary attempt to compare the differences between the two images is to see how continuous the cell wall of the data is at the cut-off point as theoretically the septum should be continuous (figure 4.5). The pixel intensities around the cell shown in the inset (figure 4.5 A and B) were measured using the ImgJ plugin "Oval"¹⁷, set to take 100 values.

As can be seen in figure 4.5 C, the intensity at the cut-off limit, whilst being lower than that from 'all frames' is still approximately the same shape, showing 'flaws' in the same areas. This trend is easier to see in the normalised graph, figure 4.5 D.

Equation 4.13 was used to normalise the data:

$$z_i = \frac{x_i - \min(x)}{\max(x) - \min(x)} \quad (4.13)$$

The intensity values around the cell wall are, on average, different by $(154.4 \pm 21.7)\%$. The % difference between the number of frames at the cut-off and the whole dataset is 148.6%, showing that the reconstructed intensity increases linearly with number of frames. This is expected as the density increases linearly.

The percentage difference between two values, x and x' is calculated using equation 4.14.

$$\% \text{ Difference} = \frac{x - x'}{\left| \frac{(x + x')}{2} \right|} * 100 \quad (4.14)$$

From the images in figure 4.4, it can be difficult to determine by eye whether the images obtained from the cut-off limit do contain as much information or if they are able to represent the underlying cell as accurately as images taken over longer time-scales. From figure 4.5 D it can be concluded that cells at the cut-off limit do seem to accurately represent cells at the final frame count, only at a lower intensity.

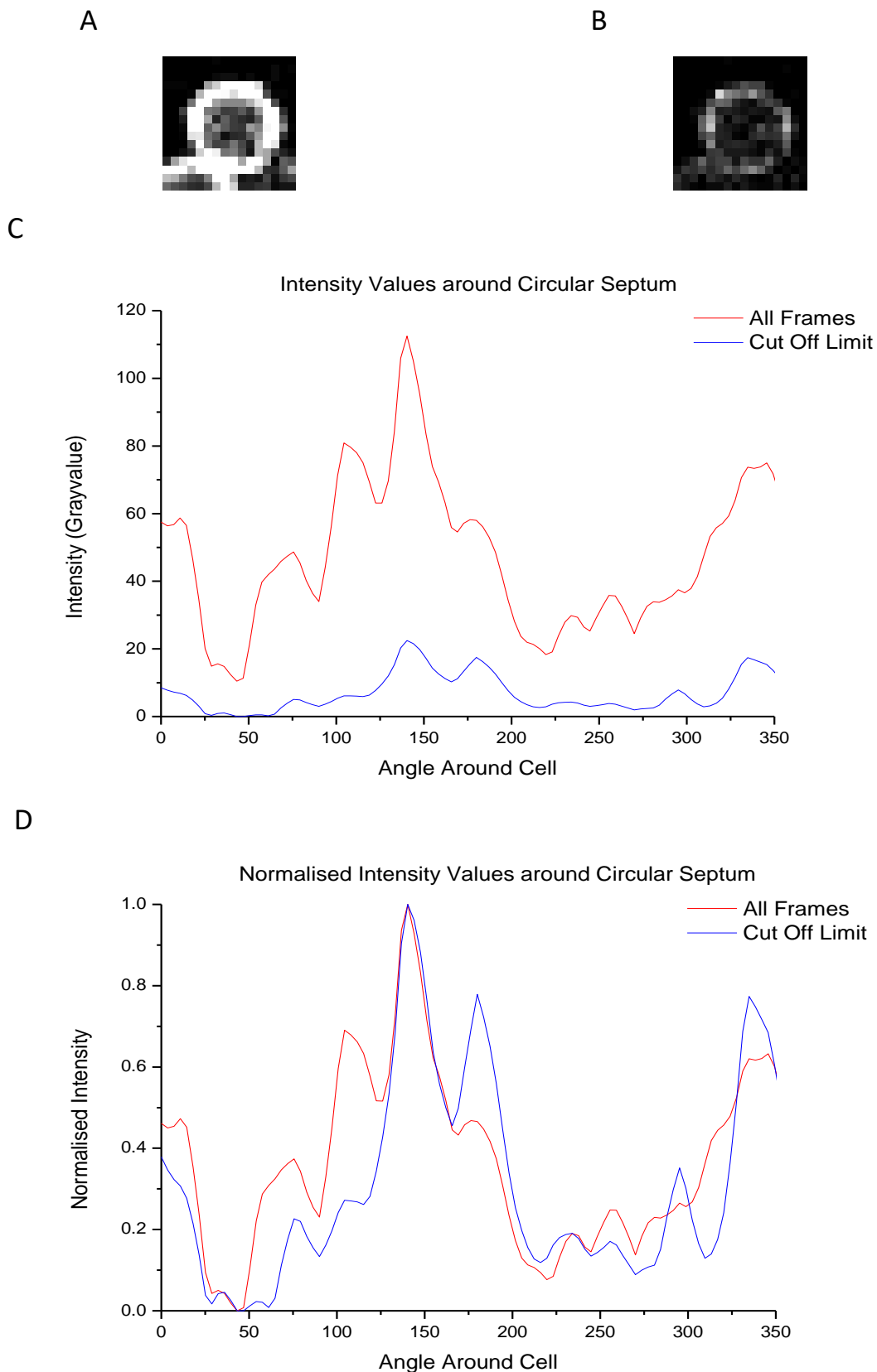


Figure 4.5: *Measuring the Signal Intensity around the cell shown in (A) and (B). (A) Image made from ~10 minutes worth of data, (B) Image at the cut off density limit, ~3 minutes. (C) shows how the intensity varies with angle around the cell. (D) Normalised intensities around the cell.*

4.2.2 - Image Quality Analysis: Radial Distances Histograms

It is difficult to judge using simple by-eye observations of the images in figure 4.4 whether there is enough information in the cut-off limit image. When is an appropriate time to stop imaging? Clearly this is sample and experiment dependent – the stop time will change depending on what precisely is being imaged. For the purposes of this experiment, Staphylococcus bacteria cells stained for 5 minutes of cell wall growth will be analysed under the following criteria:

1. Is the cell wall visible above the background?
2. Is the cell wall continuous?
3. If there is a 'gap' in the cell wall, how does this affect analysis?

To analyse the cells, a custom MATLAB code (appendix 9) was written to find the distance of all molecules from the centre of a cell, when the septum was oriented such that the image made a circle. Similarly to the first analysis method (chapter 4.2.1), the MATLAB code in appendix 9 uses Pythagoras' theorem (equation 4.12) to calculate the distance of all points from a selected central point (figure 4.7 A).

The approximate centre of the cells was found by eye (figure 4.6 A), and then roughly optimised using k-means clustering on the radial distance values. MATLAB has an inbuilt K-means function. K-means is a grouping algorithm which sorts data into given k groups by minimising the distances between mean values¹⁸.

When k-means clustering performed on the radial distance values, the resulting groups are in the form of concentric rings around the central point used to calculate the radial values. The centre value was refined until the k-means groups were visibly concentric with the cell. This is demonstrated in figure 4.6 A and B - in A an approximate central value is given resulting in the circled region clearly showing the groups are not centralised to the cell - there are less members in the green group in the circled side of the cell. In B a more accurate central value has been found: the circled region now matches the rest of the cell.

Another method for finding the cell centre is the Circular Hough Transform, a basic circle detecting algorithm also included in the MATLAB package. Difficulty arose when using this however as it could not be used directly on the data points reconstructed from MATLAB and instead needed to be used on the rendered final image. This caused a mismatch in cell centre location as the rendered image was at a different magnification (figure 4.6 D - the central value used is clearly not within the cell). For ease of use, the k-means clustering method was used over the Circular Hough Transform method.

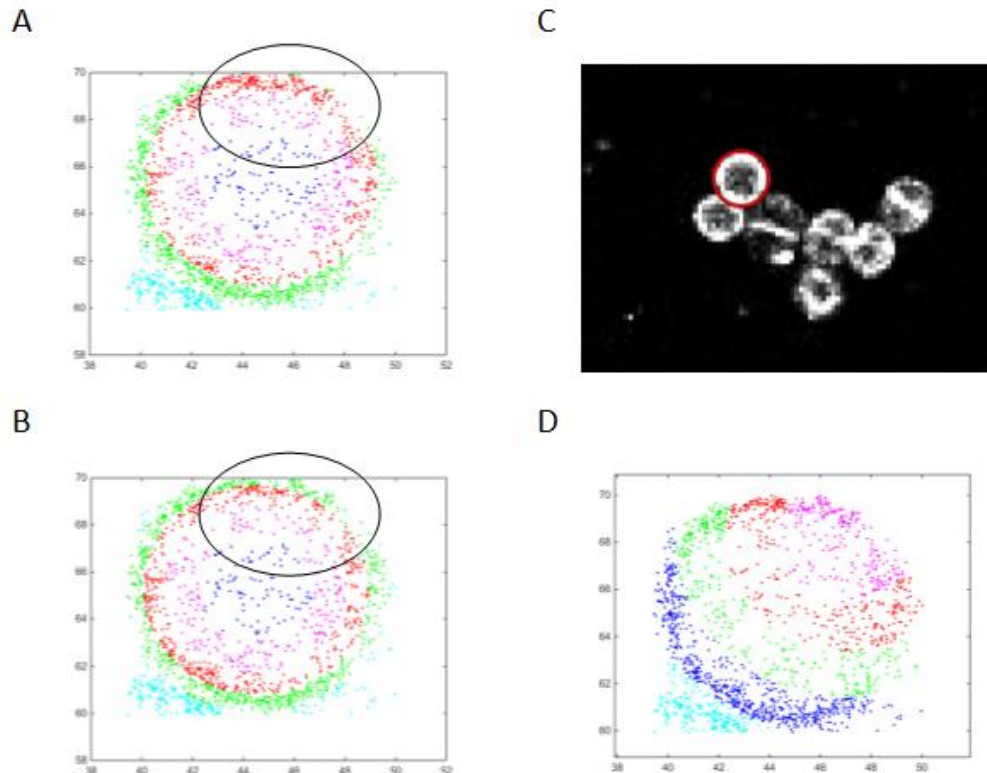
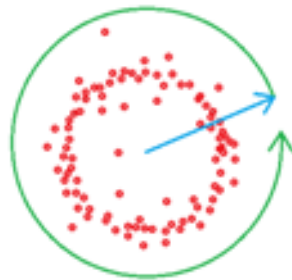


Figure 4.6: *Determining the centre coordinates of a Staph cell. Scales in pixels. (A) Initial K-means clustering, with estimated centre location. (B) Centre value was found once the K-means groups were in the form of concentric circles. Areas circled in A and B show how the K-means groups become concentric in B (the green circle becomes clearly uniform). (C) Hough Circular Transform performed on a rendered image. (D) K-means clustering performed on the cell using values obtained from the Circular Hough Transform*

Once the cell centre had been found, histograms of the radial distances were plotted. The figures start at distance = 0, the cell centre, where there are few localisations (figure 4.7 B). As the distance away from the centre increases the peak in the histograms corresponds to the cell wall. From these peaks, the average cell wall width can be calculated. This was done by fitting a Gaussian to the histograms, using the FWHM as the cell wall value. The average width obtained for cells using all frames was 152.4 nm, and for cells at the cut off point the average width was 181.3 nm. The FWHM for cells at the cut-off point is larger than for those using all frames due to noise and the reduced intensity.

A



B

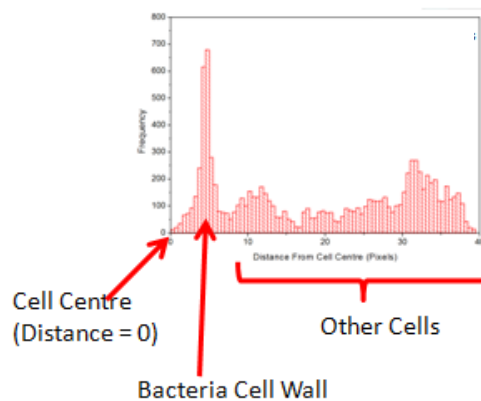


Figure 4.7: Diagram demonstrating localisation distance histograms. (A) The distance of all molecules from a central location was calculated. (B) Example histogram

Histograms were plotted for four different amounts of frames - all frames, at the cut-off limit (determined individually for each cell from the graph in figure 4.3), double the cut-off limit time and half the cut-off limit time. The inset images for each histogram show the cell which it represents. Inset images are all plotted at the same brightness/contrast settings (0-50) to allow direct comparisons to be made.

It is statistically difficult to quantify the histograms, for example to determine when the cell wall peak is no longer distinguishable, especially if the underlying structure is not known. The cell in figure 4.8 D has a clear break in the cell wall which is not visible from the histogram.

However, although images made up of less frames instinctively look to be worse to the eye, these images may contain similar amounts of information to reconstructions taken over a larger amount of time. From the images in figure 4.8 A-D, the idea of the cut-off limit seems to hold. Visually, the images at the cut off point seem to be at a threshold of whether the circular cells can be confirmed to be visible above the background and whole. This implies that the cut off limit method of analysis is valid.

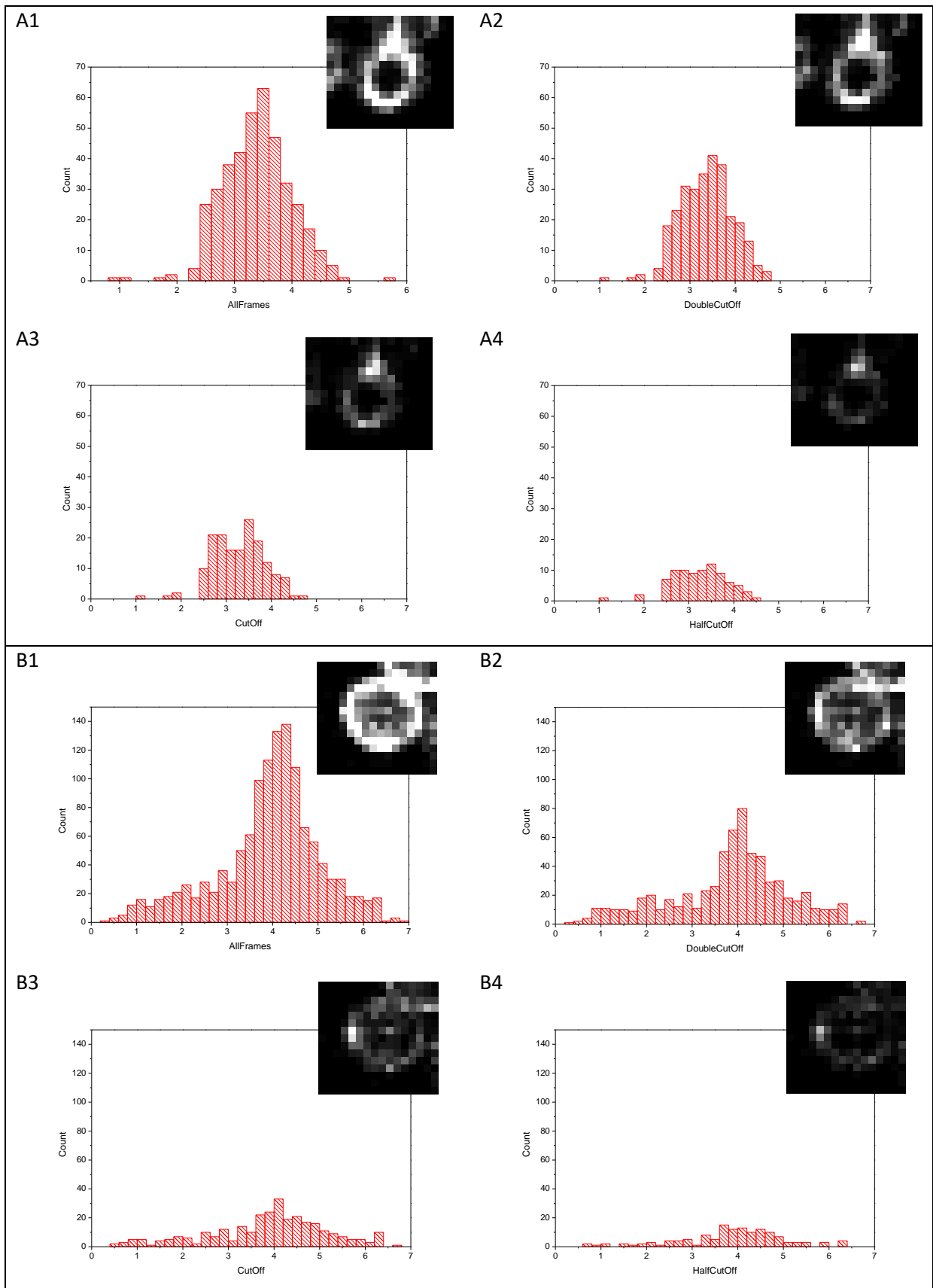


Figure 4.8: Histograms showing the number of localisations found with increasing distance from the centre of a circularly oriented *Staphylococcus*. cell. Scale is in pixels (A-D) show four different cells at four different time

points. (1) All frames, (2) $t = 2t_{cutoff}$, (3) $t = t_{cutoff}$, (4) $t = \frac{t_{cutoff}}{2}$

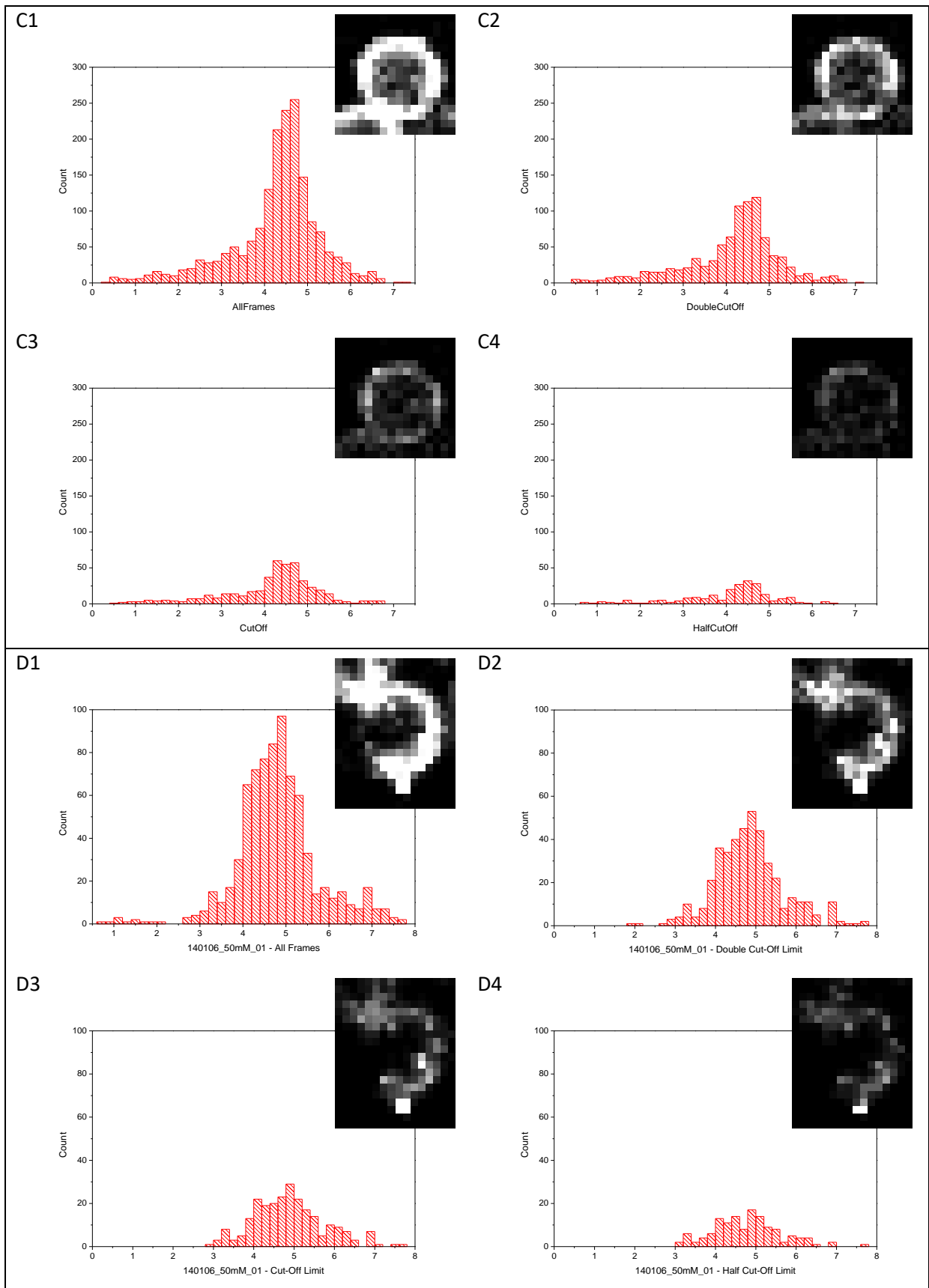


Figure 4.8: *Continued*

4.2.3 - Image Quality Analysis: Actin Cables

Section 4.2.2 was completed solely on specifically oriented Staphylococcus cells, which form circles. In order to verify the FRC cut-off analysis on another type of sample, NIH 3T3 cells with fluorescently labelled F-actin was imaged (figure 4.9).

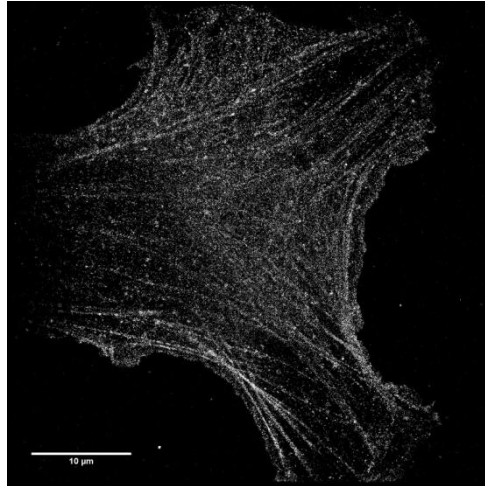


Figure 4.9: Reconstructed STORM image of actin cables in a NIH 3T3 cell, labelled with AF 647 phalloidin.

Actin is a small monomer which links together with itself to form long, thin polymer chains which are ~ 10 nm wide in diameter¹² as measured by EM. These actin cables are easily imaged and also form a simple, regular structure upon which to perform the FRC analysis.

To select the actin cables for analysis, a custom MATLAB code was written (appendix 5). This code was given 4 points (figure 4.10) around the cable such that:

$$\begin{array}{ll} x_4 < x_1 < x_2 & y_1 > y_2 > y_3 \\ x_4 < x_3 < x_2 & y_1 > y_4 > y_3 \end{array}$$

The MATLAB code (appendix 5) rotates the points within the selected area to be parallel with the vertical and then counts the number of localisations within. To calculate the vertical, the midpoint between points 1-4 and 2-3 (Figure 4.10 green circles) were found and a line was drawn between the two (green line). This line was then rotated to the vertical and the new positions of the rotated localisations were calculated.

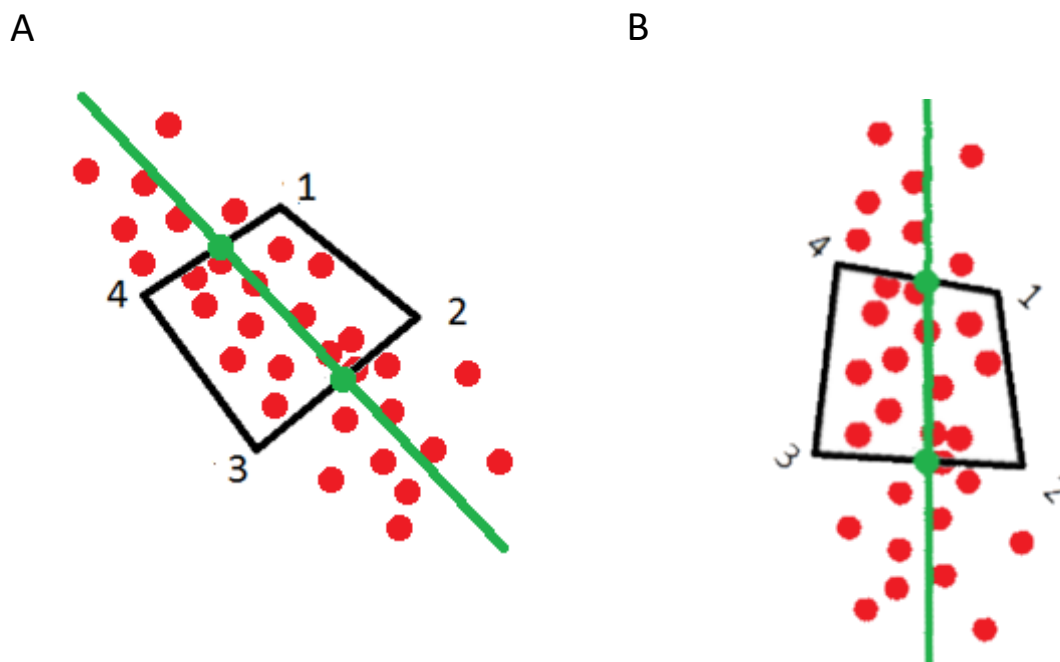


Figure 4.10: Diagram showing how actin cables were selected - four points (1-4) forming a quadrilateral around the cable. (A) Points selected around actin cable, midpoints shown in green. (B) Midpoint line rotated to the vertical.

To determine the precise area of the actin cable, the number of localisations were summed down the length of the cable. Figure 4.11. shows an example of the resulting width of actin cable graph. To determine the width of the actin cable, the turning points of the graph were calculated - in this case the width was calculated as 172.8nm (or 44 nm using the FWHM). The area of the cable was then determined using the calculated width and the length of the selected area.

As in section 4.1, the increase of localisations over time was found per cable in order to plot the density increase as a function of time. This can be seen in figure 4.12. The horizontal black line represents the FRC cut-off density.

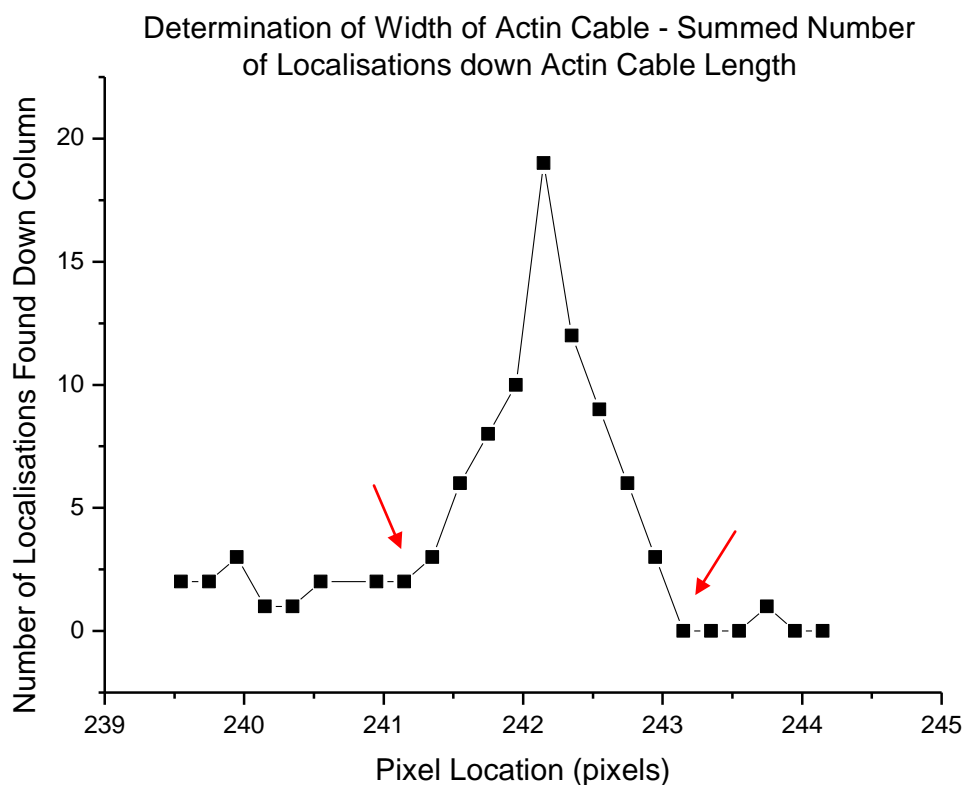
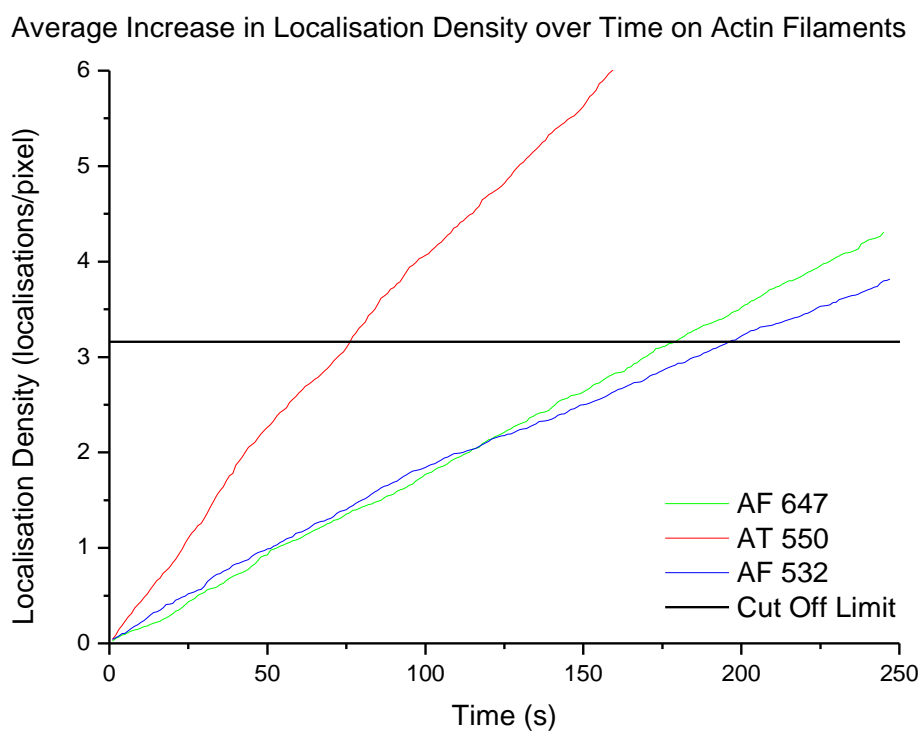


Figure 4.11: Example graph demonstrating the method used to calculate the area of an actin cable from a STORM reconstruction. The width of the cable was taken to be from the turning points of the graph (labelled with red arrows). In this example, the width is 1.6 pixels or 172.8 nm. The FWHM is ~ 0.4 pixels or 44 nm.

Figure 4.12 shows the average density increase over time for three different dyes - AF 647, AF 532 and AT 550. The density increases linearly with time, similarly to in *Staphylococcus* cells (figure 4.4), averaging 180s for AF647, 197s for AF 532 and 77s for AT 550 to reach the cut off density. To compare these values more easily, a box plot has been drawn (figure 4.12 B). AF 532 and AF747 increase at a very similar rate, whereas AT 550 is much quicker.

A



B

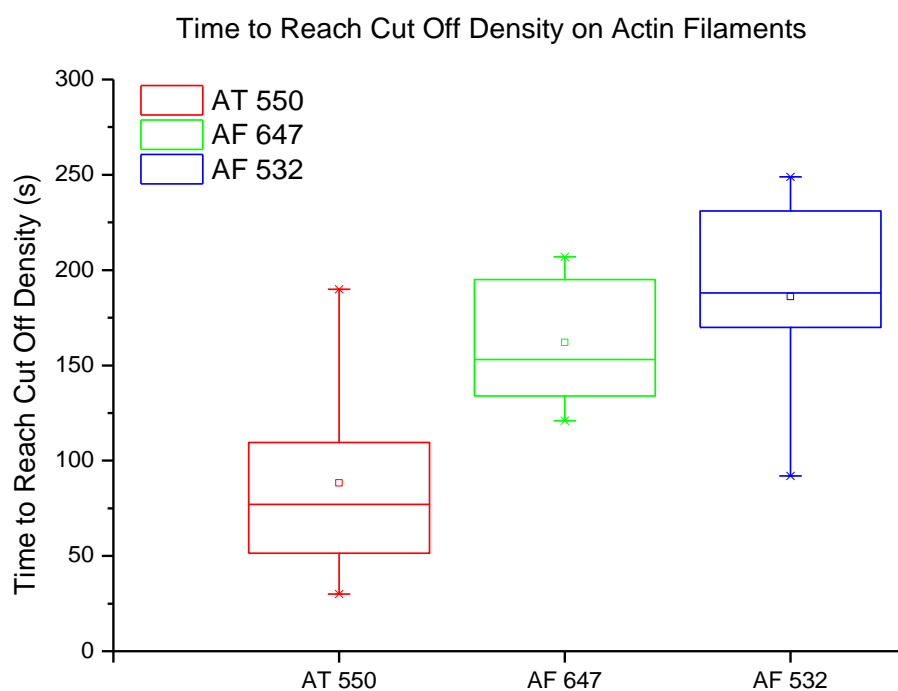


Figure 4.12: (A) Average increase in localisation density over time for actin filaments with three different dyes - AF 647 (green), AF 532 (blue) and AT 550 (red). The cut off limit is shown by a black line. (B) Box Plots showing the time taken to reach the cut off density limit

4.2.4 - Cut-off Point Analysis in Staphylococcus Cells

Not all areas of an image reach the FRC cut-off limit at the same time (or within a short time distribution) , which could be reasonably expected from a uniformly labelled sample. Figure 4.3 shows over a 200s difference in the time taken for various areas of an image to reach the cut-off density. This can cause problems when trying to image quickly - if some areas of the cell trail behind due to lack of blinks in that area, it will only be possible to image the whole cell as fast as the slowest part. Alternatively, depending on the area of interest, it should be possible to build up an image at the speed of that area, regardless of what is happening elsewhere in the sample.

To this regard, the previous data analysis technique - studying the increase in density over time in a very small area - could be misleading. It tells nothing of how a whole area, e.g. a whole bacterium, is built up over time. As can be seen in the figure 4.8 D, the cell reaches the cut-off limit(/passes the 'histogram test') despite clearly not being "whole". It was therefore decided to set a 'confidence limit' to the area of interest.

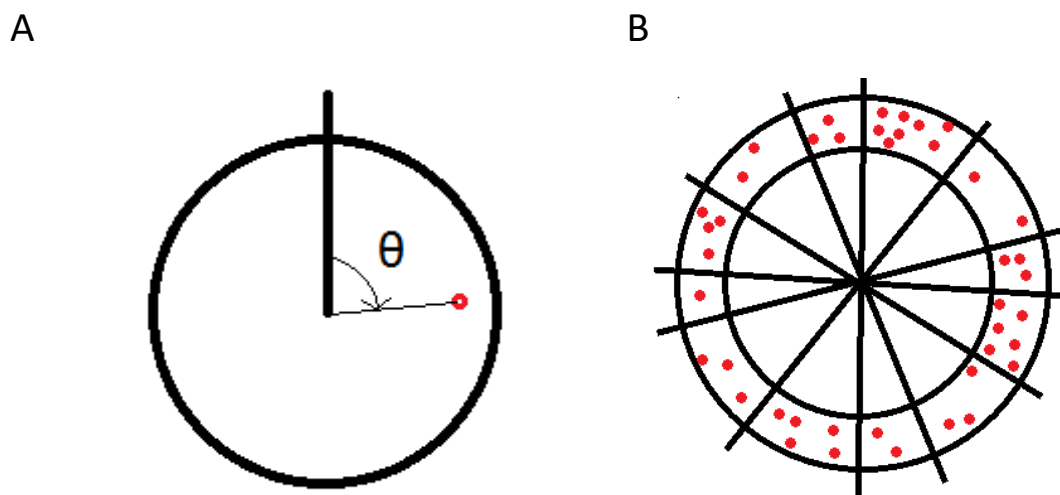


Figure 4.13: Diagrams demonstrating how cells were analysed for the confidence limit analysis (A) The angle to the vertical, θ , was calculated for each localisation. (B) Cells were split into groups based on angle

A diagram of how this confidence test was achieved can be seen in figure 4.13. As the Staphylococcus cells formed mostly-regular circles, each cell was split up into angular groups. To do this the custom MATLAB code (Appendix 9) was edited to calculate the angle from the vertical, θ , for each localisation as well as its distance from the central point. The area of each group was calculated using the maximum radial distance value once the cell had been specifically selected using k-means grouping (i.e. so there were no extra spurious locations outside the cell increasing the cell area). The area was estimated to be a whole sector rather than an annulus as the "inside" radius of the cell wall

was often difficult to calculate due to noise within the centre. This causes a slight overestimate in the cell wall area.

Figure 4.14 A shows the percentage of groups in the cell that are above the cut-off limit over time. Blue lines represents datasets taken at 20fps, green at ~30fps and red at ~100fps.

It is interesting to note that datasets taken at higher frame rates seem to reach confidence more quickly (figure 4.17 B). This would confirm the results from chapter 3.2.3 which show the number of localisations found per second peaks between 100 - 150 fps. Whilst the pattern cannot be completely confirmed, as nearly 60% of the cells tested did not reach the minimum requirements (90% of cells at or above the cut off density), the time the cells would have reached confidence can be estimated by linearly fitting each dataset.

Figure 4.14 B shows the range of R^2 values for the fits at each speed. The higher the R^2 value, the better the 'goodness of fit' to the dataset. Whilst there is a larger amount of variability in the R^2 for the 20 fps data, all R^2 values are close to 1 indicating a high degree of confidence in the fit.

Not only do the datasets taken at higher (100 fps) frame rates reach confidence sooner than the slower (20 and 30 fps) datasets, there also seems to be less 'horizontal' graph sections for the faster datasets. These horizontal sections indicate a 'time lag' between successive groups filling, which implies that data taken at slower frame rates is not simply slower to reach confidence due to the reduction in frame rate. This could be due to fluorophores in the area of interest bleaching over time. Figures 4.14 C and D show the datasets re-plotted separately to demonstrate the horizontal sections do not appear as a scaling issue.

To test confirm these results - whether the increase in percentage number of groups at or above the cut off limit is a random process - data was simulated. To do this, a custom MATLAB code was written (appendix 11). This code takes 20 groups and used a uniformly distributed random integer generator (included in MATLAB package) to randomly assign a 'molecule' to a group each iteration. A uniform distribution random number generator was used in order to simulate a molecule being equally likely to be added to all groups. The cut off density value given was 10 molecules/pixel (figure 4.15 A). The code was then modified so that 20% of the time it would randomly not assign a molecule to any group (appendix 12) in order to simulate bleached molecules (figure 4.15 B). A third code was written to make 5 groups more likely to be chosen (appendix 13) to simulate areas of the cell with a higher fluorophore density (figure 4.15 C), or alternatively areas which have been bleached and are therefore less likely to fluoresce.

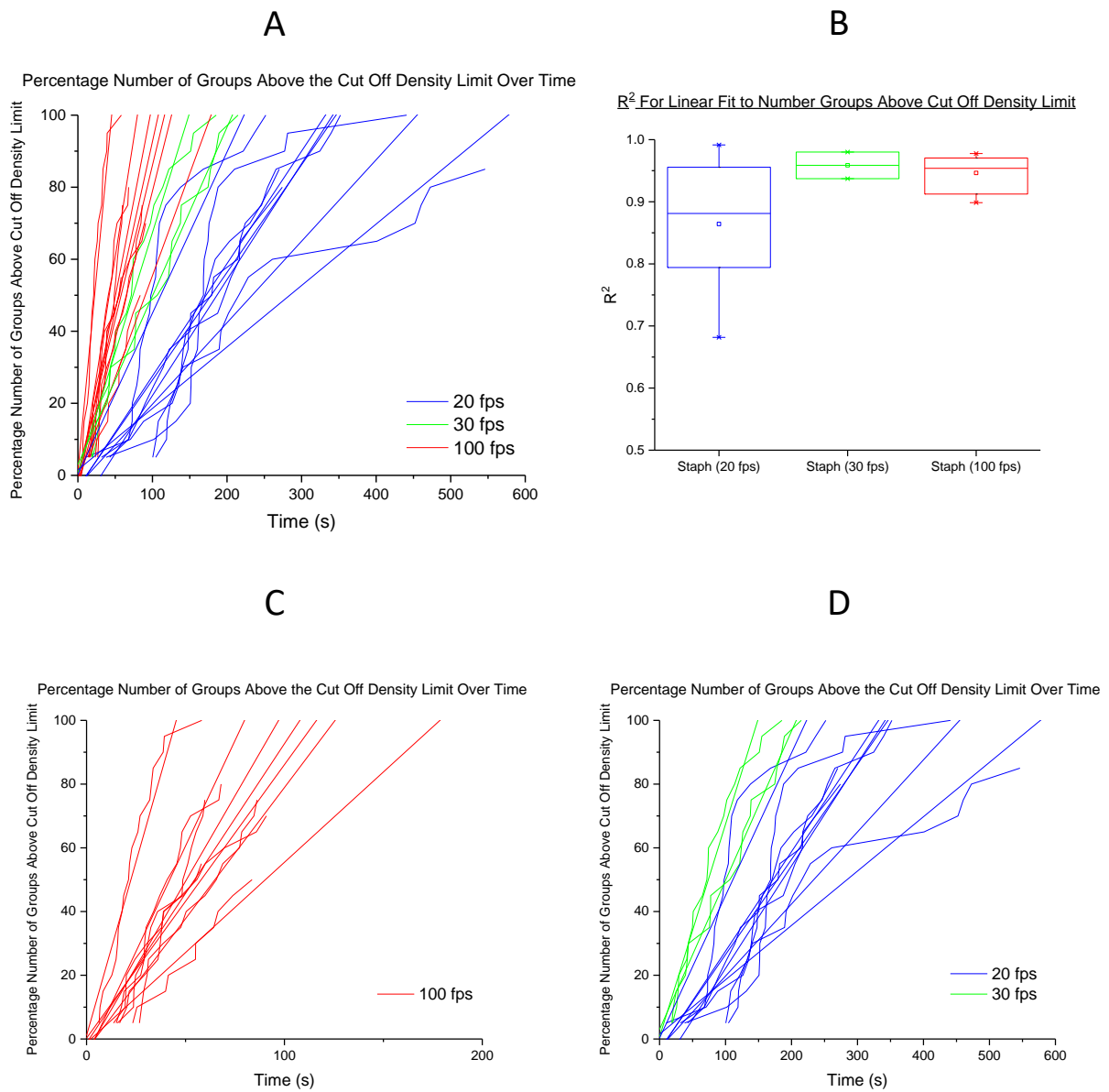
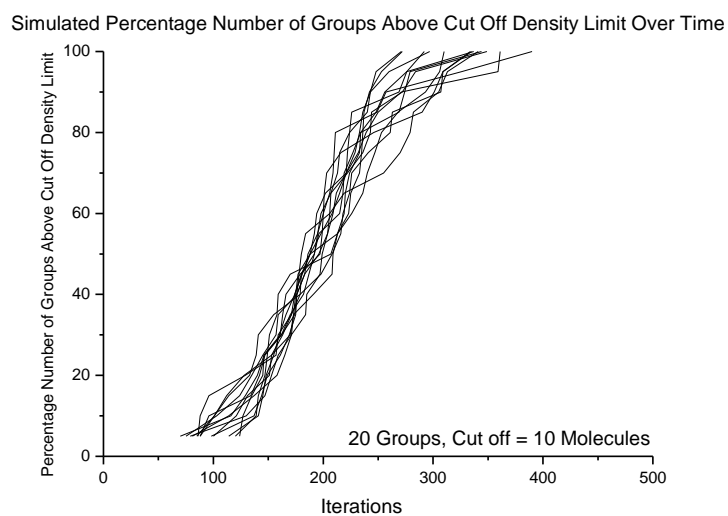
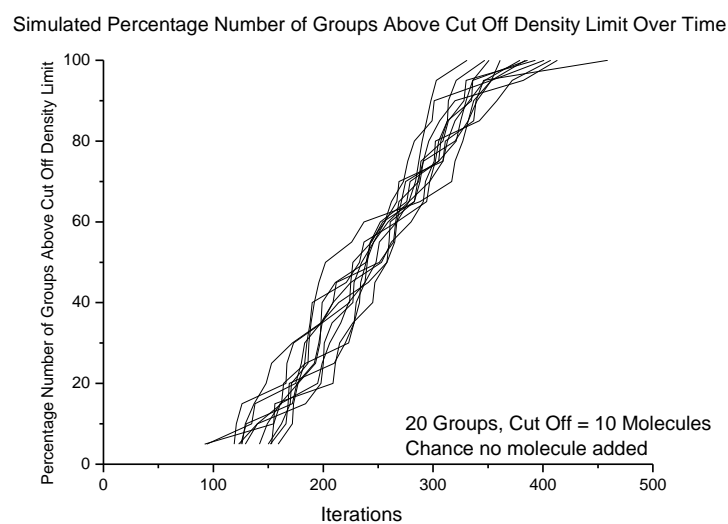


Figure 4.14: (A) How the number of groups which have a localisation density at or larger than the cut off limit increases over time. Each dataset has been linearly fitted and plotted alongside. (C and D) Datasets separated by frame rate. (B) Box plot of the R^2 values showing how the goodness of fit varies with frame rate.

A



B



C

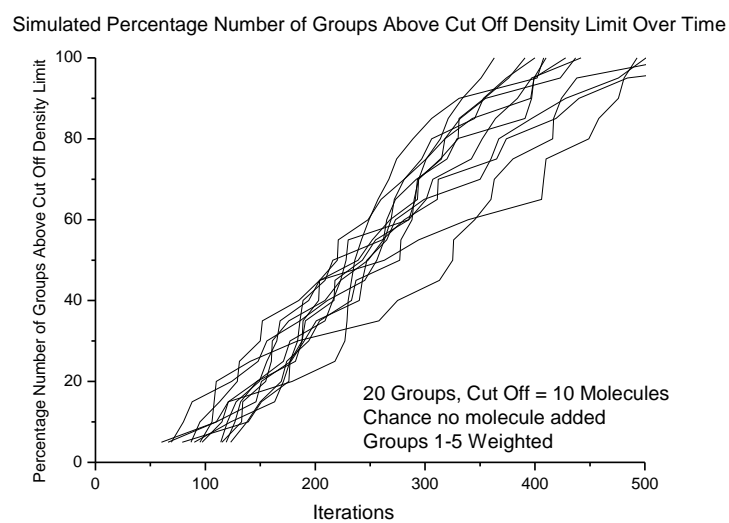
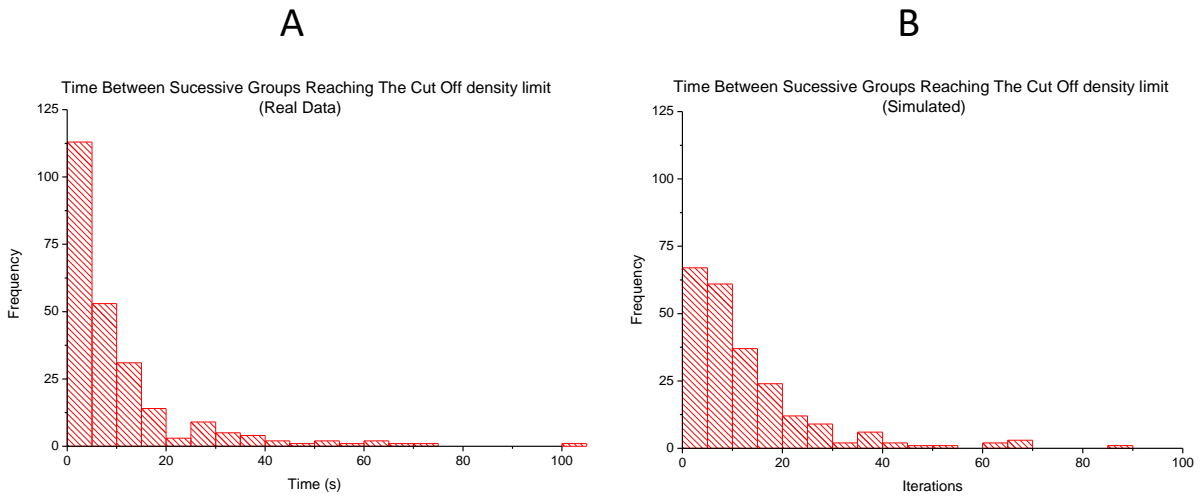


Figure 4.15: Simulated data showing the percentage number of groups above or at the cut off density limit. (A) 20 groups, cut off density = 10. (B) 20 groups, cut off density = 10 , 20% chance to not add a molecule to a group each iteration. (C) 20 groups, cut off density = 10 molecules, 16.7% chance to not add a molecule to a group, groups 1-5 weighted double with respect to groups 6-20

For the simulated data, the time taken to start reaching the cut-off point varies depending on the parameters given. However, once the groups start reaching the cut-off limit, the number of groups reaching the limit from that point tends to increase linearly over time. To compare the simulated data to the real data, the amount of time between each consecutive group reaching the cut-off limit was plotted as a histogram in figure 4.16. Although 'iterations of code' and 'time' are difficult to match up perfectly, the histogram from the simulated data appears to match up with the histogram from the real data; the shape is similar (figure 4.16 C). This shows that the process of groups filling with localised molecules is a random process.

Entire cells, on average, take longer to become 90% confident than the time taken for small selected areas of a cell take to reach the cut off limit density. Figure 4.17 shows box plots of the times taken to reach 90% confidence for different systems - actin analysis in AF 532 (red), AT 550 (green) and AF 647 (cyan) and AF 647 Staphylococcus analysis in both small areas (blue) and through the 90% confidence method (magenta). The average time (from fitted data) to reach 90% confidence in all cells was 203.31 s, compared to the 196.96 s on average from the small-area density increase analysis. Whilst these values appear to be in agreement, the small-area density value came solely from cells imaged at 20fps. In comparison, the average time to reach confidence for 20fps samples only was 342.17s: over 100s slower. Figure 4.17 C shows the number of molecules rejected during the reconstruction process for datasets taken at 20 fps and 100 fps. There is a very large variability in the number of molecules rejected between datasets yet overall there is no difference between the average number rejected for both frame rates. Therefore the number of molecules rejected from each dataset should not have an effect on the time to reach confidence.



C

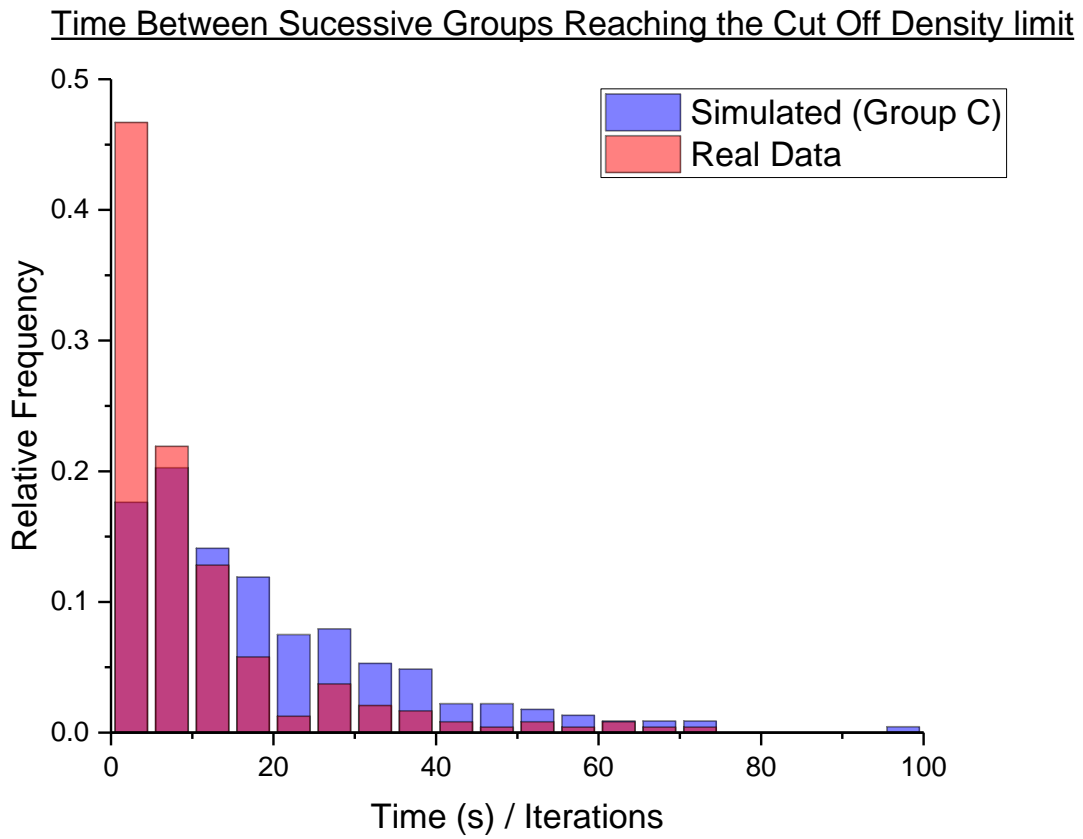
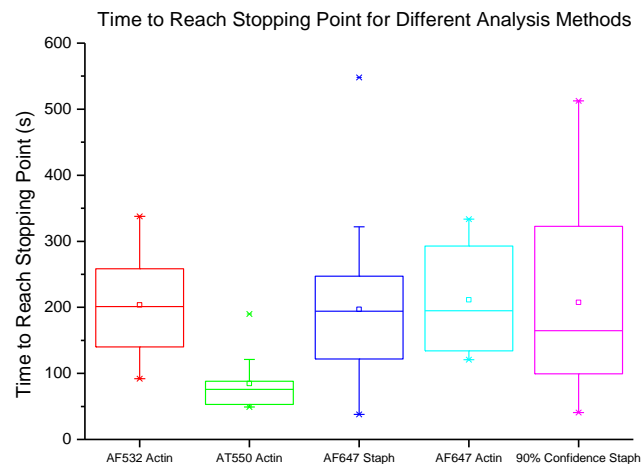
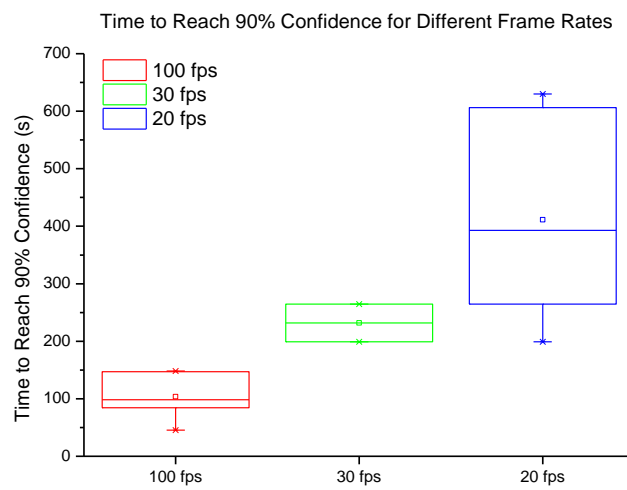


Figure 4.16: Histograms showing the time between successive groups reaching the cut off density limit. (A) Real data, (B) simulated data. Histograms made up from the same number of data points. (C) Merged graph of real (red) and simulated (blue) data.

A



B



C

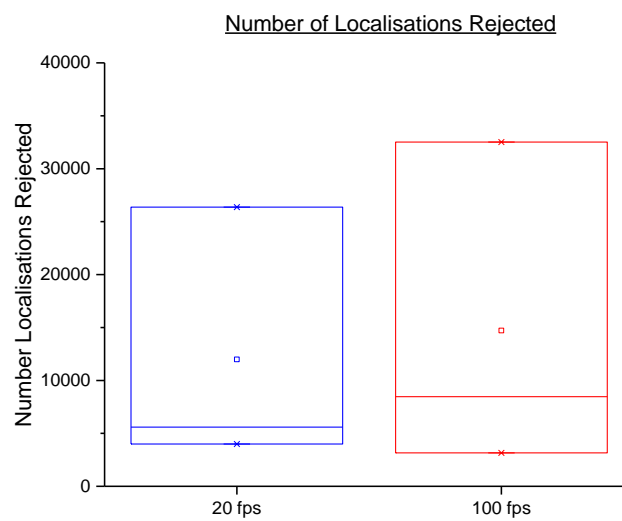


Figure 4.17: (A) Box plots comparing the amount of time required to reach the stopping point - either the cut off density or 90% confidence - in different systems and with different fluorophores. (B) Comparison of time to reach 90% confidence for different frame rates. (C) Number of localisations rejected in the reconstruction process per frame rate.

4.2.5 - Cut-off Point Analysis in Actin

To check the 90% confidence analysis on a different system, actin cables were analysed.

During the previous analysis (section 4.2.3), each actin cable selected was split up into a grid in order to find the width of the cable. In order to analyse sections of the cable, each cable was then further split into groups and the same analysis was carried out.

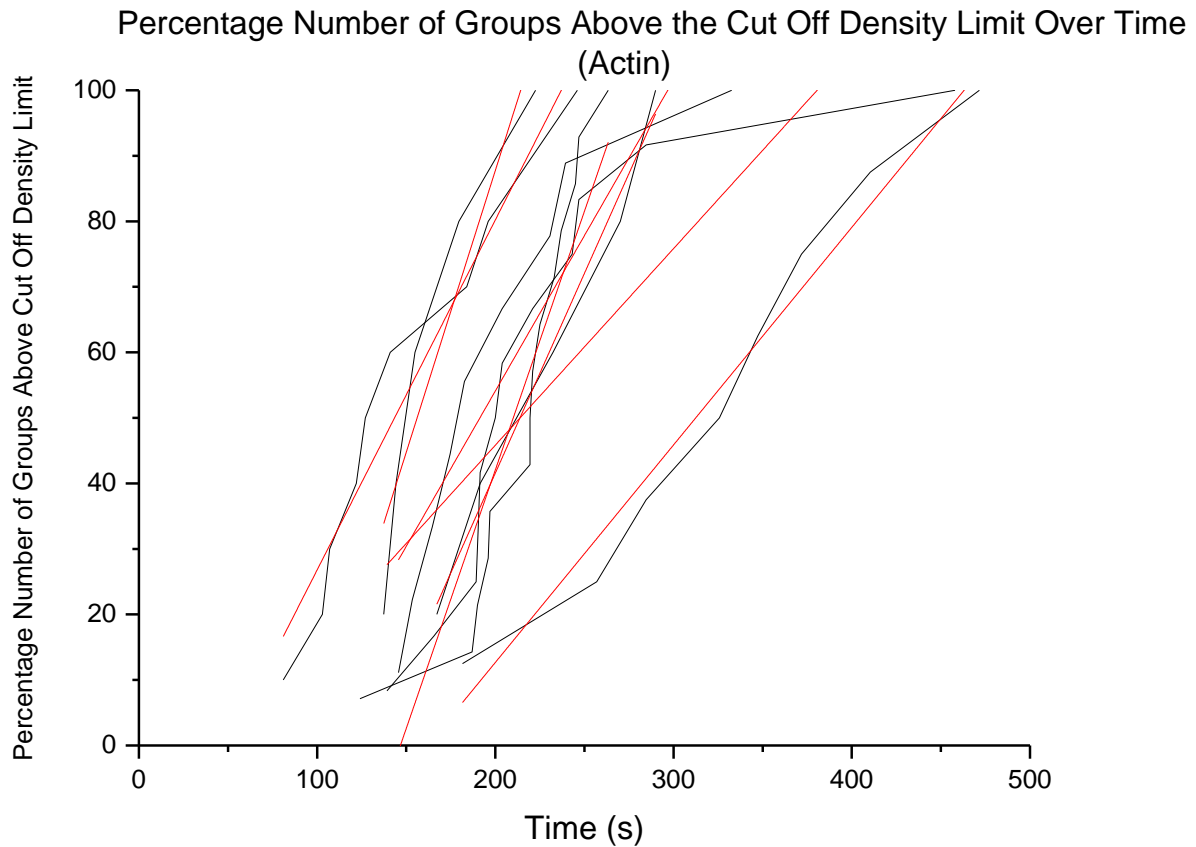


Figure 4.18: *The increase in percentage number of groups at or above the cut off density limit over time in actin. Raw data (black), linear fit (red).*

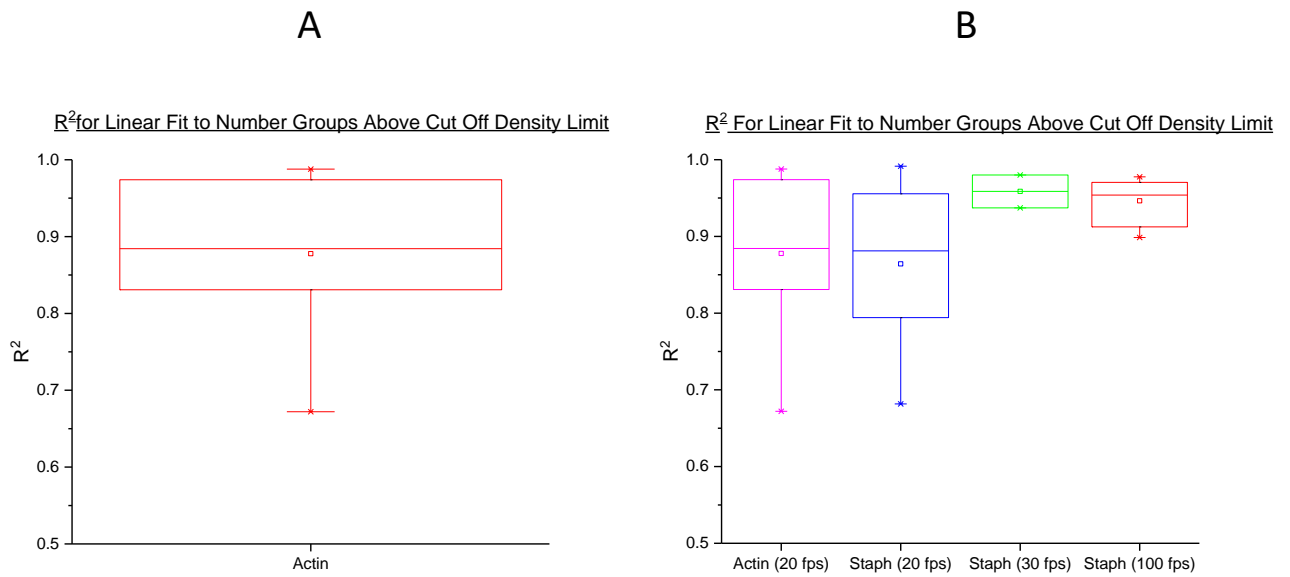


Figure 4.19: *The increase in percentage number of groups at or above the cut off density limit over time in actin. Raw data (black), linear fits (red).*

Figure 4.18 shows how the percentage number of groups at or above the cut off limit increases with time in actin. As for Staphylococcus and the simulated data, the percentage number of groups increases linearly with time once the first group has reached the cut off density. This again agrees with the Staphylococcus data.

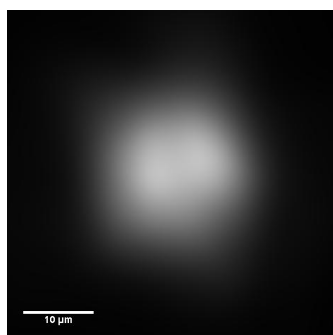
Figure 4.19 A shows the range of R^2 values for the fits to the increase in percentage of groups over the cut off limit for actin cables. This is then compared to the R^2 values for the Staphylococcus data in figure 4.19 B, to demonstrate the actin data is of a similar quality.

4.2.7 - Dependence of Cut Off Density with Laser Power

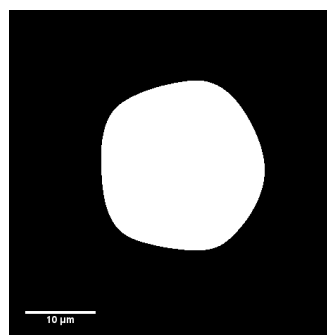
The FRC limit varies across an image (most clearly shown in figure 4.4 A), but is this something that happens randomly or does it depend on any controllable quantities?

As discussed in chapter 3, the blinking of a dye depends on the buffer concentration and the laser power. Chapter 3 discusses the *overall* effects of these on the blinking of a dye but it did not look at how these varied across a sample.

A



B



C

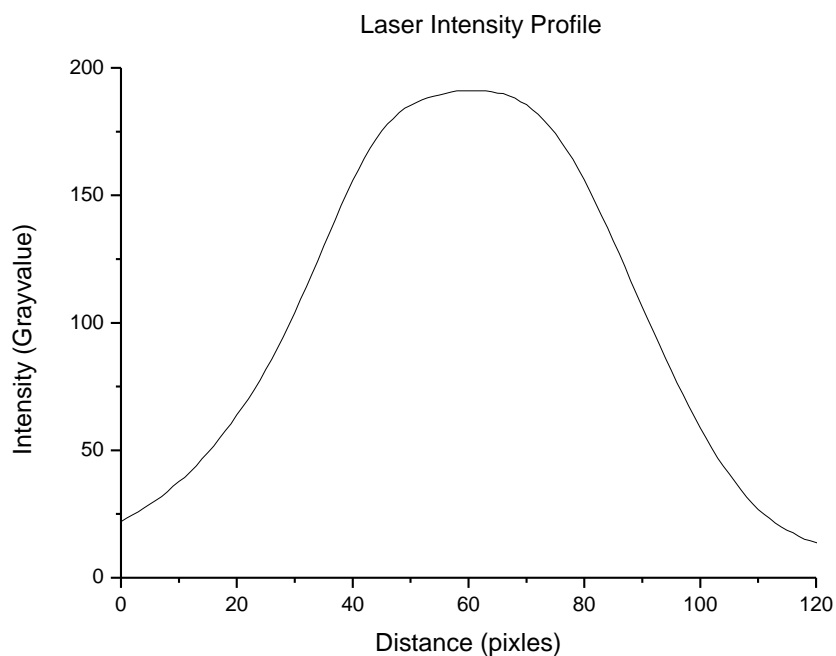


Figure 4.20: Intensity profile of 647 nm laser used throughout STORM experiments. (A) Created from a 'z-projection' of many frames with a gaussian blur, $\sigma = 20$ nm (using ImageJ). (B) Binary image of (A) as calculated by MATLAB program (Appendix 10). (C) Line profile across (A)

Figure 4.21 shows how the number of molecules localised over an entire sample varies with 647nm laser power density. This was analysed using the small-area analysis method used in chapters 4.2.1 and 4.2.3. It was shown in figure 3.6 that the number of molecules localised per second stays mostly constant before dramatically increasing after $\sim 3000 \text{ W/cm}^2$. It was therefore predicted that the laser should not have an effect on the blinking rate of the sample across the image.

In order to find the profile of the laser, bright cells were imaged at a low frame rate and high laser power over the full screen of the camera. The cells were moved around such that the whole of the illuminated area was covered over the course of the recording. This meant that all areas illuminated by the laser were covered. The resulting stack was flattened into a single image using the 'z-Stack - average' feature of ImageJ and a Gaussian blur ($\sigma = 20\text{nm}$) was added to the image. An example laser intensity image obtained via this method can be seen in figure 4.20 A. This image shows a non homogeneous laser profile however, this is not a true reflection of the laser beam profile but is a symptom of using a convolution of cells as a stand-in for the laser beam profile. Overall, the laser profile was approximately Gaussian (figure 4.20 C).

Rather than measuring the intensity of the laser at all points in the image, cut-off density was looked at with regards to the distance of the area from the centre of the laser spot. This was for ease of computation - the laser intensity varies with distance across the camera sensor and as the beam profile is approximately Gaussian, the distance from the beam centre is proportional to the laser intensity.

In order to calculate the centre of the laser spot a custom MATLAB script (appendix 10) was written to turn the z-averaged laser intensity image into a binary image. To do this, the laser image was imported into MATLAB as a matrix. If the intensity value in any cell was larger than a certain user-decided threshold, the MATLAB function set the cell value to 1. Otherwise the cell value was set to 0. This code allowed a more accurate determination of the size of the laser spot – the inbuilt MATLAB code, 'im2BW', calculates the binary cut-off depending on a threshold value between 0 – 1 which did not directly relate back to the intensity values displayed in the matrix. A Circular Hough Transform was then used to calculate the centre value and radius of the laser spot.

Figure 4.21 shows how the cut-off limit time changes with distance from the laser spot centre. As can be seen from both the actin trace (blue) and the Staphylococcus trace (red), the time to hit cut-off is generally constant across the sample. However, what this image does not show is how the sample structure effects the cut-off time. Figure 4.21 is mostly structure independent, as small areas which reached the cut off limit were chosen for the analysis. These areas which reach the cut off density limit did do at approximately the same rate regardless of distance from the laser centre.

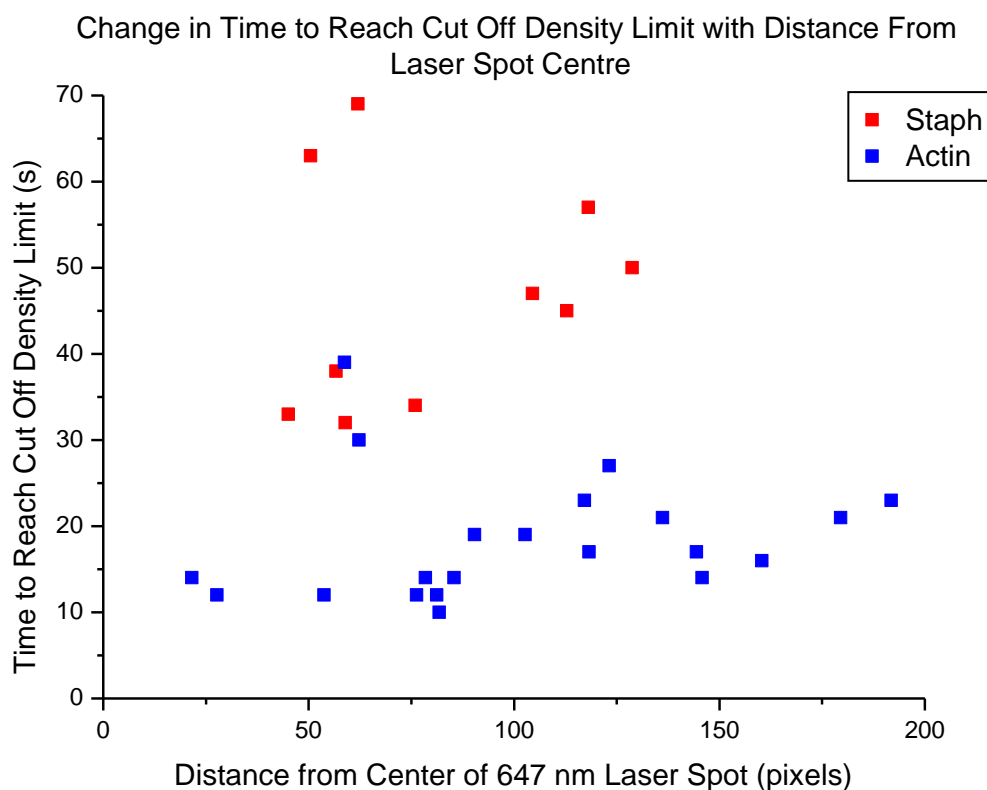


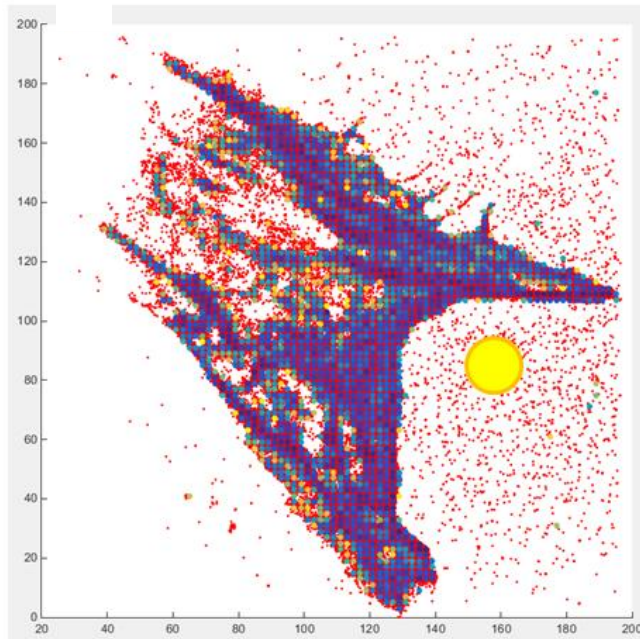
Figure 4.21: Change in time taken to reach the cut off density limit with distance from the centre of the laser spot. (Red) *Staphylococcus*, (Blue) *Actin*

To demonstrate further that it is the sample structure not the laser power that determines when an area will reach cut-off density, figures 4.22 A and B were made. These are raw STORM localisation plots – each (red) dot represents a molecule that has been localised. A custom MATLAB code (appendix 1) was written to split the image into small user-chosen bins, and then calculate the time each bin took to reach the cut-off limit. The bins were then plotted over the top of the STORM data points and are colour-coded. Darker blue circles represent a shorter time to reach the cut-off limit, with bright yellow circles taking longer times. If there is no circle (i.e. red molecules are visible) then the area did not reach the cut-off limit. The large yellow circles represent the laser spot centre.

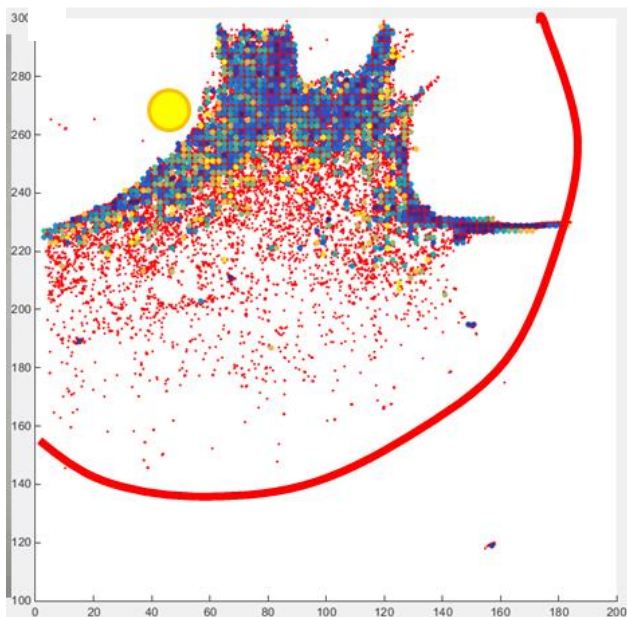
In figure 4.22 A & B the darkest blue areas (areas to reach cut-off the fastest) have no relation to distance to the laser and only depend on the structure of the cell.

The only dependence the laser profile has on the data is that molecules which are too far out from the centre do not have enough energy to blink on and off resulting in little or unusable data.

A



B



C



Figure 4.22: Images showing how the cut off limit varies across a sample. Images show 3T3 cells labelled with AF647 phalloidin.(A&B) Coloured circles (blue - yellow in colour) represent the amount of time taken to reach the cut off density in each binned area section. Red localisations represent the localisations found in areas which did not reach the cut off limit. Large yellow circles represent the laser spot centre. (C) Scale. Bluer coloured circles represent areas of the cell which reached the cut off density more quickly, yellow represents slower areas of the cell

4.3 - Conclusions

Nieuwenhuizen *et al* (2013)¹³ proposed that the resolution of a STORM image is either localisation- or density-limited. That is, the resolution is either hindered by too few localized molecules, or the localisation precision prevents obtaining a higher resolution. This trade off between regimes points towards a maximum time required to image STORM samples in order to obtain the highest possible resolution. The fastest imaging time possible will be to stop imaging once the sample has reached a certain localisation density. This analysis technique could be used to split live STORM images into 'movie stills' (i.e. a single reconstruction in a stack of reconstructions) and would ensure the fastest image acquisition rate for the system.

From figure 4.3, it can be seen that the localisation density (the number of molecules localised per area) increases linearly over time in small areas. However, the rate at which the density increases varies by a large amount even over a single image. This means that the imaging time mostly depends on which area of the sample is of interest - if the area of interest's localisation density increases at a slow rate, this will constrain the image acquisition time.

To test whether the 'cut off localisation density' limit held for real data, the ImageJ plugin 'Oval' was used to measure the intensity around the cell wall of a *Staphylococcus* cell. Although at a much lower intensity the image at the cut off limit followed the same shape as the image made from 10 minutes worth of data (figure 4.5). This suggests that although the image that took longer to produce and is more "aesthetically pleasing" to the eye it does not actually contain more information. This means that using the cut off density to determine when to stop adding more molecules to a STORM image is likely to be valid.

Images of *Staphylococcus* cells were produced using 10 minutes worth of data ("All Frames"), images at the time taken to reach the cut off limit, double the cut off limit and half the cut off limit (figure 4.8). The distances of all localisations from the cell centre were plotted in histograms, where the peak represents the cell wall. Analysis of the histograms to confirm the cut off limit proved statistically difficult, however visually the cut off limit again appears to be valid - cells at the cut off limit are on the edge of being considered a whole cell.

As well as *Staphylococcus* cells, actin cables in 3T3 cells were analysed to confirm that the results were not sample dependent. Figure 4.12 shows the average density increase in actin cables for three different fluorophores. The density increase over time is again linear with a large range of rates across a sample (Figure 4.12 B). Interestingly, the rate of increase in localisation density over time for the dye AT 550 is much higher than that for either of the Alexa Fluor dyes tested.

Analysing small areas of a sample can only give a measure of how quickly that area is built up, and does not give any indication of how quickly a larger area can be imaged. In order to image an entire staphylococcus bacterium over time, the cell was split up into groups depending on angle from the vertical and the percentage of groups at or above the cut off density was plotted against time (figure 4.14). The cell takes a certain amount of time before it becomes 'filled' with enough localisations that the cut off density is reached, however after this point the number of groups at or above the cut off limit increases mostly linearly. Data taken at a faster frame rate reaches the cut off density limit faster - this agrees with the results from chapter 3.2.3 which showed that the number of localisations obtained peaks for frame rates between 100-150 fps. Reasons why data taken at slower frame rates reaches 90% confidence more slowly could be due to bleaching of fluorophores in the region of interest.

Data was simulated to test whether increase in the percentage number of groups at or above the cut off density limit was an entirely random process (figure 4.15). In order to compare real and simulated data, the amount of time between subsequent groups reaching the cut off was plotted in a histogram (figure 4.16). As these two histograms are very similar in shape, this shows that the blinking process is mostly random.

Overall, the amount of time required to image an entire cell is larger than that for a small area of the sample (figure 4.17 B and 4.3 A). This is consistent with the finding that localisation density does not increase at the same rate through the sample.

Actin filaments were analysed in a similar manner to Staphylococcus to test another sample type with the 90% confidence analysis. Figure 4.18, the percentage increase of groups at or above the cut off density limit over time, is very similar to the simulated and Staphylococcus data.

One reason for why some areas of the sample reach the cut off density faster than others could be due to laser intensity. Chapter 3.2.2 showed that for the laser power densities utilised throughout this project, laser power density does not affect the number of localisations found per second. Therefore it was expected for the time to reach the cut off limit to be independent of the laser intensity, or distance from the centre of the laser beam. Figure 4.21 confirms in both actin and Staphylococcus samples that the time taken to reach cut off is constant over an increasing distance from the centre of the laser beam. Figures 4.22 show an entire image of a 3T3 cell labelled for f-actin. The colour of the dots (blue - yellow) represent the time taken to reach the cut off density, with bluer dots reaching the limit more quickly. From these images, it can be seen that the cut off limit depends mainly on cell structure (i.e. the labelling density) and does not depend on the laser power density. There is a linear dependence on density, chapter 3 showed there is a weak

dependency on laser power density and MEA concentration so therefore it is expected that the density dependence will dominate.

Another reason for some areas of the sample reach the density limit faster than others could be due to non uniform labelling density across the sample.

The Nieuwenhuizen *et al* (2013) paper includes an ImageJ plugin called 'Fire', which takes the final STORM reconstruction and using FRC analysis to calculate the average resolution across the entire image. This is a very useful tool for the wider community as it is quick and easy to install and use. Through testing in this chapter FRC analysis seems to be a reliable way of calculating the resolution in a STORM image. However, the FRC method does only give an average resolution and does not take into account the time taken to reach each resolution.

In practice, this method of determining when to stop imaging is useful as a post-processing analysis technique - especially useful for compiling superresolution movies. Culley *et al* (2017)¹⁹ have recently published a piece of software called SQUIRREL which analyses superresolution imaging artefacts by comparing the superresolution image to the wide field image using FRC analysis. Similarly, a potential idea for future exploration could be using the intensity values from a wide field image to predict the cut-off limit.

4. 4 - References

- 1 Wäldchen, S., Lehmann, J., Klein, T., van de Linde, S. & Sauer, M. Light-induced cell damage in live-cell super-resolution microscopy. *5*, 15348, doi:10.1038/srep15348
<https://www.nature.com/articles/srep15348#supplementary-information> (2015).
- 2 Dempsey, G. T., Vaughan, J. C., Chen, K. H., Bates, M. & Zhuang, X. W. Evaluation of fluorophores for optimal performance in localization-based super-resolution imaging. *Nature Methods* **8**, 1027+, doi:10.1038/nmeth.1768 (2011).
- 3 Fernández-suárez, M. & Ting, A. Y. Fluorescent probes for super-resolution imaging in living cells. *Nature Reviews. Molecular Cell Biology* **9**, 929-943, doi:http://dx.doi.org/10.1038/nrm2531 (2008).
- 4 Jones, S. A., Shim, S.-H., He, J. & Zhuang, X. Fast, three-dimensional super-resolution imaging of live cells. *Nature Methods* **8**, doi:10.1038/nmeth.1605 (2011).
- 5 Cox, S. *et al.* Bayesian localization microscopy reveals nanoscale podosome dynamics. *Nature Methods* **9**, doi:10.1038/nmeth.1812 (2012).
- 6 Holden, S. J., Uphoff, S. & Kapanidis, A. N. DAOSTORM: an algorithm for high-density super-resolution microscopy. *Nature Methods* **8**, doi:10.1038/nmeth0411-279 (2011).
- 7 Huang, B., Babcock, H. & Zhuang, X. Breaking the Diffraction Barrier: Super-Resolution Imaging of Cells. *Cell* **143**, 1047-1058, doi:http://dx.doi.org/10.1016/j.cell.2010.12.002 (2010).
- 8 Rust, M. J., Bates, M. & Zhuang, X. Sub-diffraction-limit imaging by stochastic optical reconstruction microscopy (STORM). *Nature Methods* **3**, doi:10.1038/nmeth929 (2006).
- 9 Betzig, E. a. P. G. H. a. S. R. a. L. O. W. a. O. S. a. B. J. S. a. D. M. W. a. L.-S. J. a. Imaging Intracellular Fluorescent Proteins at Nanometer Resolution. *Science* **313**, 1642--1645, doi:10.1126/science.1127344 (2006).
- 10 Huang, B., Wang, W., Bates, M. & Zhuang, X. Three-dimensional super-resolution imaging by stochastic optical reconstruction microscopy. *Science* **319**, doi:10.1126/science.1153529 (2008).
- 11 Gustafsson, N. *et al.* Fast live-cell conventional fluorophore nanoscopy with ImageJ through super-resolution radial fluctuations. *Nature Communications* **7**, 12471, doi:10.1038/ncomms12471, <http://www.nature.com/articles/ncomms12471#supplementary-information> (2016).
- 12 Niederman, R. a. A. P. C. a. H. J. Three-dimensional structure of actin filaments and of an actin gel made with actin-binding protein. *The Journal of Cell Biology* **96**, 1400--1413, doi:10.1083/jcb.96.5.1400 (1983).

- 13 Nieuwenhuizen, R. P. J. *et al.* Measuring image resolution in optical nanoscopy. *Nature Methods* **10**, 557-+, doi:10.1038/nmeth.2448 (2013).
- 14 Penczek, P. A. Resolution measures in molecular electron microscopy. *Methods Enzymol* **482**, 73-100, doi:10.1016/s0076-6879(10)82003-8 (2010).
- 15 Thompson, R. E., Larson, D. R. & Webb, W. W. Precise nanometer localization analysis for individual fluorescent probes. *Biophysical Journal* **82**, 2775-2783 (2002).
- 16 Cui, L. *et al.* Cell wall thickening is a common feature of vancomycin resistance in *Staphylococcus aureus*. *Journal of Clinical Microbiology* **41**, 5-14, doi:10.1128/jcm.41.1.5-14.2003 (2003).
- 17 ImageJ Plugin: Oval Profile Plot.
- 18 Lloyd, S. Least squares quantization in PCM. *IEEE Transactions on Information Theory* **28**, 129-137, doi:10.1109/TIT.1982.1056489 (1982).
- 19 Culley, S. *et al.* NanoJ-SQUIRREL: quantitative mapping and minimisation of super-resolution optical imaging artefacts. *bioRxiv* (2017).

5 – Imaging with Dual Labelled Samples

Contents

| | |
|--|-----|
| 5.1 – Introduction | 134 |
| 5.2 – Results | 138 |
| 5.2.1 - Selection of Secondary Fluorophore | 139 |
| 5.2.2 - Testing the Increase in Imaging Speed | 142 |
| 5.2.3 - Investigation of Dual Labelled Blinking Dynamics | 146 |
| 5.3 – Conclusions | 148 |
| 5.4 - References | 150 |

5.1 – Introduction

The microscope is a widely used tool in the biological sciences; one of the most common techniques is multicolour fluorescence imaging. For the majority of fluorescence microscopy users, two or more dye colours are required. Each colour labels different proteins or areas of interest within the cell such that the movement and interactions between each dye can be studied with respect to each other. For example, Narendra *et al* (2008)¹ uses mammalian cells expressing YFP-Parkin - a protein linked to Parkinson's disease - and the mitochondrial marker Tom20 conjugated with Alexa Fluor 633 to determine that Parkin accumulates on damaged mitochondria. This is achieved by studying the overlap between where the two dye colours are within the cell under both control and mitochondrial damage protocols - i.e. whether the signal from the YFP-labelled protein and the AF 647 labelled mitochondria overlap in the image.

In standard optical microscopes multicolour images are achieved by sequentially imaging the sample under different wavelengths of light in order to excite optically separate fluorescent molecules² – for example, red, green and blue. Figure 5.1 shows the absorption and emission spectra of three dyes – AF 647, AF 555 and AF 488. These dyes are optically separable from each other: the peak absorption and emission wavelengths for each dye are large, narrow and none significantly overlap the other peaks. If, for example, a 555nm light source is incident on the sample the majority of the signal detected will be from the AF 555 dye. The AF 647 dye absorption spectrum has a small tail at this wavelength value and therefore some of the emission will be unwanted photons emitted from the AF 647 dye¹⁵. However, if optical filters are then applied to the light path only emission from the dye of interest will be detected at the camera. When sequentially imaging the dyes, the filters used must be changed each time the colour is changed. In order to image two colours simultaneously, a dual band pass filter can be used to allow both colours through to the camera.

There are many problems with multicoloured superresolution imaging. Sequentially imaging over one field of view in each different colour channel is the main way that STORM multicolour has been successfully implemented³⁻⁶ so far. Whilst this approach works well for standard optical imaging techniques (e.g. wide field or confocal microscopy) due to the relatively short exposure times required (ms), the slower imaging speed of STORM causes difficulties. Over the time scales that a STORM image needs to be built-up (several minutes), sample drift is a problem - several hundred nanometres is not uncommon⁷. Sample drift occurs when the sample moves relative to the objective lens - either in the xy plane or z plane. This can be due to temperature variations in the room, or mechanical drift of the optical set up. Ways to minimise drift are better than correcting - these

include temperature controlled laboratories and using a motorised stage with 'focus lock' to minimise stage drift. However, there will always be some drift within the image.

To correct for drift, fiducial markers - fluorescent molecules or beads which are present in the sample but do not blink and as such are visible in every frame - can be used. Once an image is taken the positions of the fiducial markers can be tracked to allow the sample movement to be removed. The downside of this technique is that it increases the experimental difficulty, as the fiducial markers must be present in the sample at the same focal plane as the image⁸. Another way to correct for drift is by analytical analysis of the image stacks, using cross-correlation⁹ or Bayesian Inference⁸. Cross-correlation is a technique that looks for similarities between two images and therefore uses fluorophores which are in the bright state over several frames to correct for drift.

Any drift in the image will be compounded when imaging several colours one after the other as this will take tens of minutes to complete - drift becomes more severe with time. These time scales are also make this method of multicolour STORM highly impractical for live cell imaging.

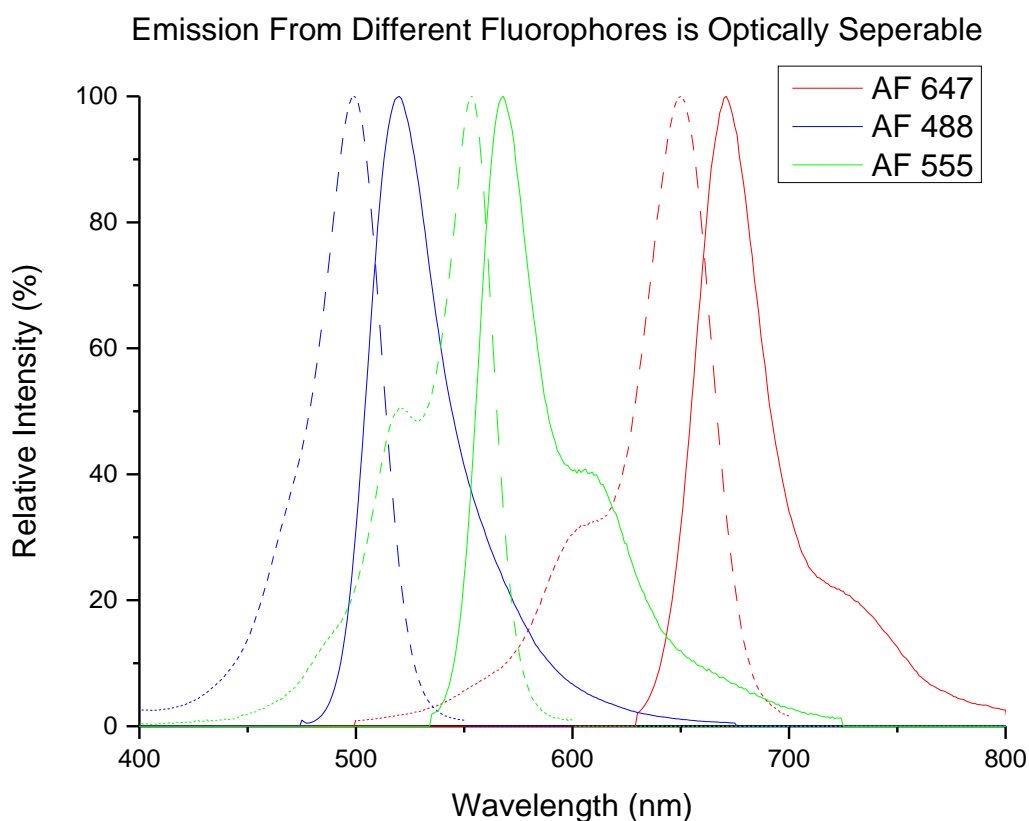


Figure 5.1: Absorption (dashed) and emission (solid) spectra for AF 647 (red), AF 555 (green) and AF 488 (blue). Peaks are optically separable¹⁵

Other methods for superresolution dual colour imaging include illuminating the sample with multiple laser lines at the same time and using filters to split the emitted signal onto multiple cameras¹⁰, using a segmented field of view^{11,12} where the emission from each dye colour is projected onto different areas of the camera detector, or manipulating the PSF to introduce "phase-delay patterns" which change depending on the wavelength of light¹³.

So far, dual colour imaging has been solely used to image different *targets* within the cell - the dyes have been located on different molecules of interest. However: the fluorescent dyes do not have to be attached to different targets. If instead one protein is dual labelled with two different colours this should theoretically allow an increase in imaging speed.

The previous chapter, chapter 4, proposes a cut off time which allows superresolution images to be formed from the smallest possible number of molecules. However, although this method will acquire images as fast as possible for the system, if there are very few molecules localised per frame the imaging speed will still be slow. This is because the limiting factor in STORM imaging is how many molecules can be localised per unit time.

Unfortunately, simply increasing the number of molecules that fluoresce per frame does not solve this problem. STORM works on a principle of single-molecule localisation and if the molecules in the 'on' state are too close together in space their PSFs start to overlap, causing reconstruction issues and the need for complicated reconstruction algorithms(chapter 1.5.2). Additionally, for any particular dye the duty cycle (the fraction of time a dye spends in the 'on' state) is set by its chemistry³ and the chemical environment. This means it is difficult to increase the amount of times a fluorescent molecule turns on in a set length of time. The only way to increase the number of molecules fluorescing per frame is by increasing the fluorophore density.

The fluorophore density refers to the number of fluorophores present in the sample attached to the desired target, and is therefore proportional to the number of molecules which can be found in the 'ON' state at any time during STORM imaging. By changing the density of fluorophores in the sample, the number of molecules in the 'ON' state during STORM imaging can be varied. By carefully optimising the fluorophore density, a maximum number of non-overlapping PSFs per frame can be found. This allows imaging at the overall maximum speed for that particular fluorophore.

Therefore as an alternative to complicated and slow reconstruction programs such as DAOSTORM¹⁴ and 3B¹⁵ which allow fitting to overlapping PSFs, an increased number of molecules can be localised per unit time by splitting the molecules into separate colour channels, i.e. dual labelling one target

molecule with two different dye colours. This, in theory, should allow a twofold increase in imaging speed by allowing both colours to fluoresce at the maximum density simultaneously.

5.2 – Results

To image simultaneously in two colours, the multiple-camera approach was taken. Images were recorded using two Andor 4.3 Zyla sCMOS cameras, mounted at 90 degrees to each other on the optical bench. The images from the microscope side port were relayed to the cameras using a 1:1 4f imaging system. Two readout lasers – 647nm and 532nm – were constantly incident on the sample and a beam splitter (649nm dichroic, FF649-Di01, laser2000) placed at the Fourier plane of the 4f system was used to separate dual colour emissions into separate streams - a different camera for each colour (see figure 5.2). Additionally, a bandpass filter for AF 647 and AF 532 were placed in front of each camera to ensure only light emitted from the correct fluorophore was incident on the sensor.

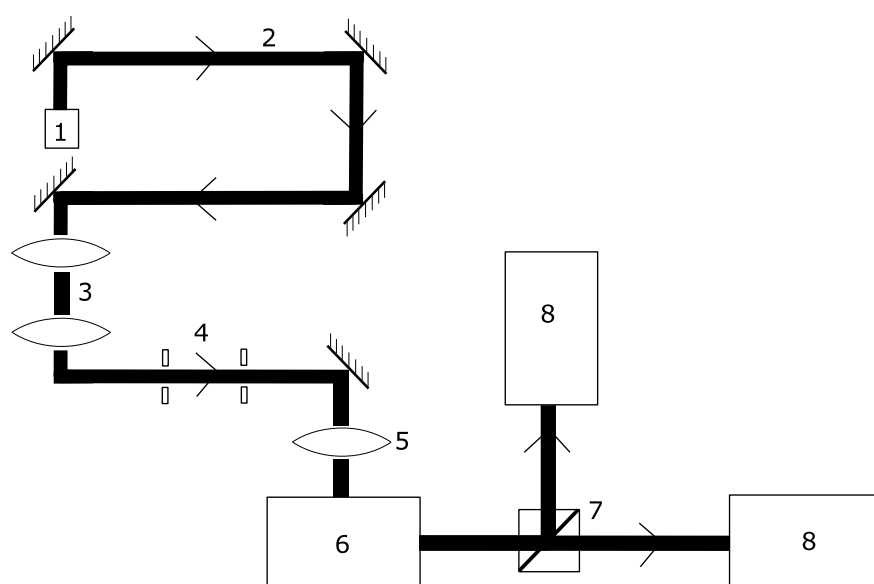


Figure 5.2: Schematic of the Multicolour STORM microscope system. 1. Laser Sources, 2. Laser Light Path, 3. Beam Expander, 4. Pinhole apertures, 5. Focusing Lens, 6. Microscope base, 7. Dichroic Beam Splitter, 8. sCMOS Cameras

To overlap the images from the two colour channels, fluorescent beads with emission visible at both cameras (life technologies, tetraspex) were imaged prior to each sample capture. A custom matlab code (written by previous group members) was then used to map one image onto the other and therefore merge the two final STORM reconstructions into one image. This only worked for specific samples - it was found to be experimentally impossible to label thick NIH 3T3 cells with fiducial markers on the same imaging plane as the cell. Therefore as an alternate, cloud point cross-correlation was used, also written by a previous group member. The cameras were aligned using a grid to maximise overlap, and with a test sample before imaging. The cameras were assumed to be at the same magnification, so this error was ignored.

5.2.1 - Selection of Secondary Fluorophore

A preliminary study of fluorophore candidates suitable for the secondary fluorophore in dual labelling experiments was carried out. As a starting point, the Dempsey *et al* (2011) study³ which compares the STORM performance of many different dyes across the visible spectrum was consulted to choose the secondary colour to work alongside the AF 647 dye.

The chosen dye needed to be

- Optically separate from AF 647 to minimise bleed-through between channels
- Appropriate for use with a GLOX (oxygen scavenging) buffer
- Brightly emissive to ensure a high SNR

Example frames taken from raw STORM data of the dyes tested - AF 488, AF 532, AT 550 and AF 555 - are shown in figure 5.3. As in Chapter 3, each dye was analysed for the average number of localisations per second and the average SNR. In order to achieve the best results with the dual labelling system, it was important to maximise the number of localisations per second. This is because the larger the number of molecules localised per second is, the faster a STORM image can be produced. The results are shown in table 5.1.

The worst performing dye was AF 488. Although this dye had a similar SNR to AF 647, the number of blinks per second was ten times less than for AF 647. Therefore, this dye colour was not used for any further STORM experiments.

Of the other three dyes, AF 532 and AF 555 performed comparatively equally, with similar SNRs and numbers of molecules localised per second. As with the AF 488, these dyes obtained far fewer localisations per second than AF 647.

AT 550 was the best performing dye tested - surpassing that of AF 647, as AT 550 achieved similar numbers of molecules localised per second at a much higher SNR. For this reason, AT 550 was determined to be the best secondary dye for use in dual labelling experiments. However, this dye was only discovered close to the end of the project and therefore all experiments within this chapter were performed using AF 532 instead.

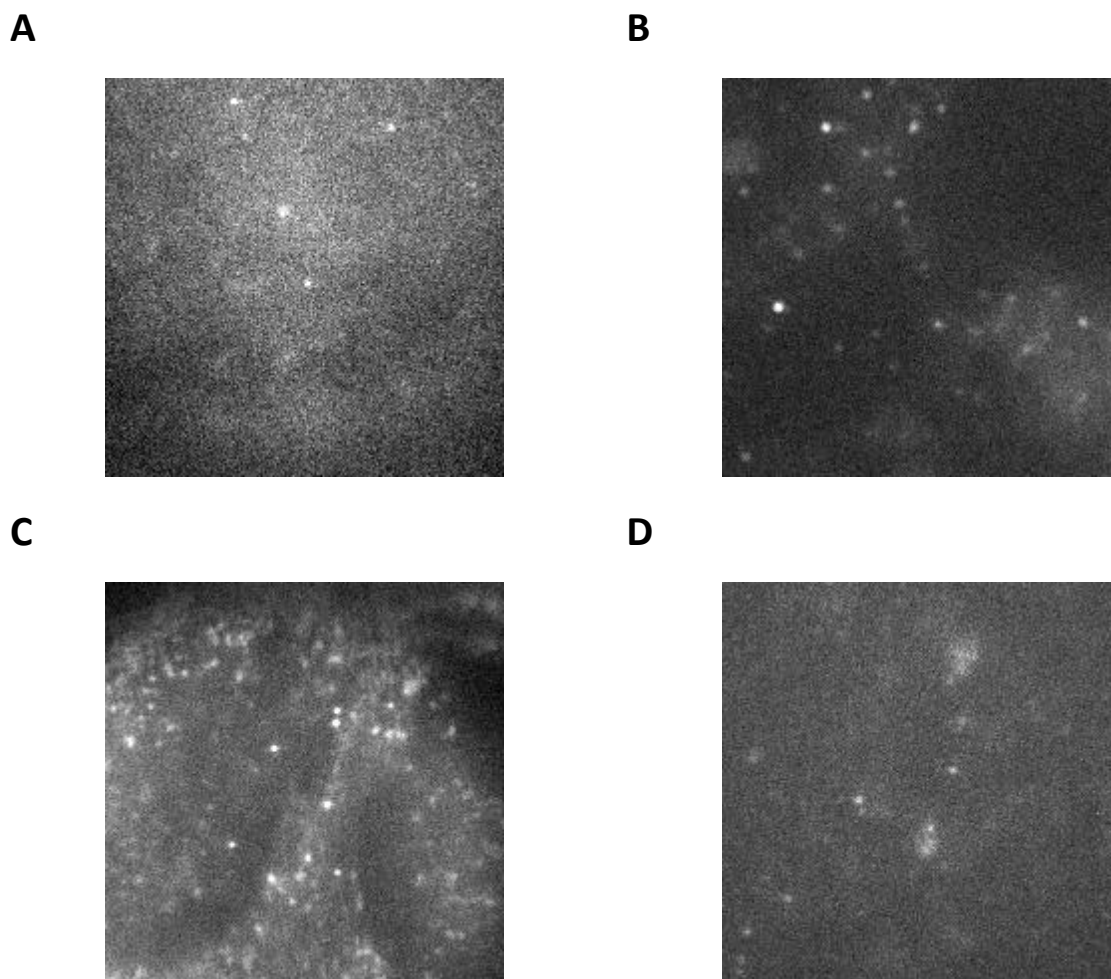


Figure 5.3: Example frames from STORM datasets of 3T3 cells labelled for f-actin using various different fluorescently conjugated phalloidin. (A) AF 488, (B) AF 532, (C) AT 550, (D) AF 555.

| Dye | Average SNR | Average Number of Localisations Per Second |
|--------|-------------|--|
| AF 488 | 6.7 | 24.396 |
| AF 532 | 11.9 | 139.144 |
| AT 550 | 19.5 | 260.48 |
| AF 555 | 12.5 | 183.63 |
| AF 647 | 7.2 | 200-250 |

Table 5.1: Comparison between average SNR and number of localisations per second for different STORM dyes. AF 647 value ranges taken from chapter 4.

To further characterise the blinking properties of AT 550, a custom MATLAB code (Appendix 16) was written to measure the average time the dye spend in the 'off' state. Molecules within ± 10 nm of each other after drift correction (ThunderSTORM¹⁶ cross correlation algorithm) were assumed to be the same molecule. Figure 5.4 (B) shows the range of times spent in the dark state, with the average time 14.6 s. As the data was imaged at 20 fps and the fluorophore was rarely visible in more than one frame, this gives an estimate of the duty cycle as 0.003, which is approximately 10 times larger than for AF 647 as reported by Dempsey *et al* 2011³ but comparable to other ATTO dyes tested in the same paper. Figure 5.4 (C) shows an example trace of the intensity of a pixel over time, where the peak represent when the molecule was in the fluorescent state.

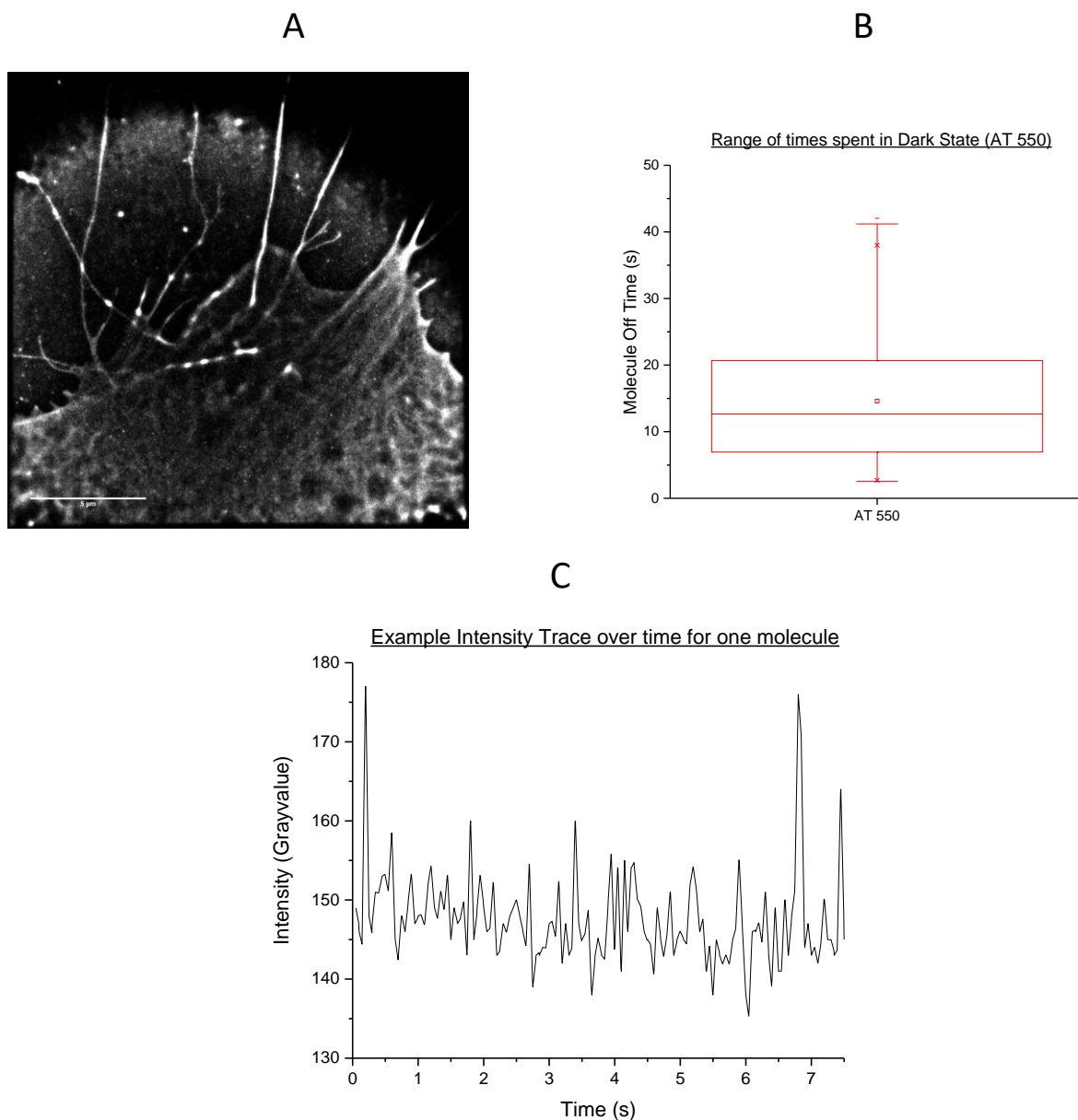


Figure 5.4: (A) Reconstruction of an NIH 3T3 cell labelled with AT 550 phalloidin, (B) Range of times AT 550 spend in the dark state, (C) Example trace of intensity over time for one molecule.

5.2.2 - Testing the Increase in Imaging Speed

In order to test how much faster a STORM image using two colours to image the same molecule of interest can be produced, samples were dual labelled with two dyes to the same target. Figure 5.5 shows an example dual colour image of an axon section of neural outgrowth cultured from E13 mouse DRGs, stained for f-actin using AF 647 and AF 532.

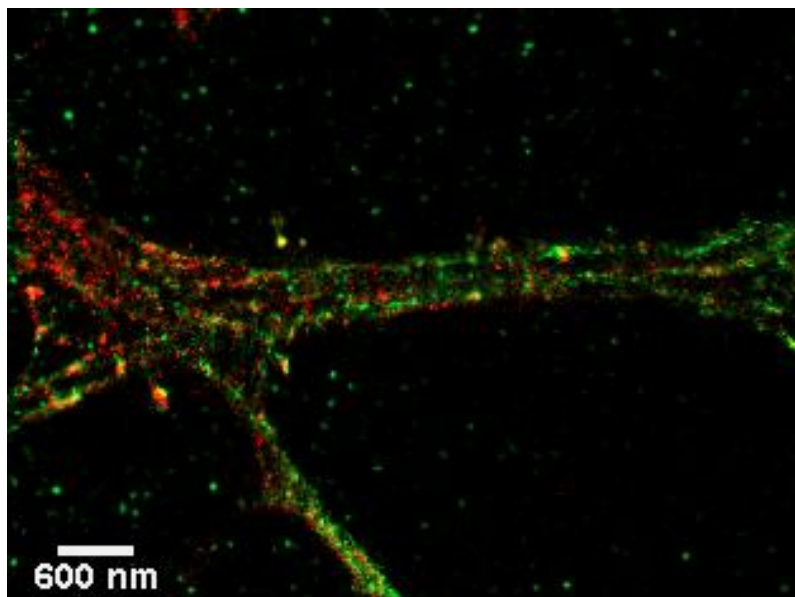


Figure 5.5: Axon segment from E13 mouse DRG neuronal outgrowth, labelled for f-actin in both red and green channels.

Using the same analysis methods as in chapter 4 to determine the cut-off point, the localisation density increase over time for dual labelled samples was calculated (figure 5.6). For each analysis, the same area of cell was chosen in both channels. Figure 5.7 shows example maximum intensity projections of each colour channel. The correlation between these two images is 0.73.

During simultaneous imaging - both readout lasers incident on the sample at the same time - data from the AF 647 (red) and AF 532 (green) channels increase at much the same rate as each other in a linear manner, reaching the cut off limit in 636 s (AF 647) and 652 s (AF 532). This meant that when the data from the two channels was merged, the combined data reached the density cut off limit in 341 s - just slightly over half the amount of time to reach the cut off for each channel separately. That is, the dual labelling technique causes the merged image to be formed almost twice as quickly as the single colour images.

However, the length of time taken to reach the density cut off for the merged image in this experiment (341 s) is only approximately equal to the time taken for single labelled staph and 3T3 samples in the previous chapter (figure 4.17) which tended to range between 100 - 300 s.

To test whether there is, in fact, an increase in imaging speed due to dual labelling, growth cones from DRG explants were imaged using AF 532 and AF 647 dyes labelling f-actin such the samples contained either:

- AF 647 dye only, with only 647 nm laser incident upon the sample (Single labelled sample)
- AF 532 dye only, with only 532 nm laser incident upon the sample (Single labelled sample)
- Both AF 647 and AF 532, with both 647 nm and 532 nm lasers incident upon the sample (Dual labelled sample imaged simultaneously).

Again, the increase in localisation density was calculated as a function of time. Figure 5.8 shows the fitted average localisation density as it increases over time.

In the samples containing a single dye colour (either AF 532 or AF 647) the localisation density increases at a faster rate than samples which are dual labelled. The average time for the single labelled samples to reach the cut-off density was 189.8 s. The average time for dual labelled samples (single channel) to reach the cut-off limit was 408.6 s - over double the amount of time required for single labelled samples.

Therefore, although the localisation density increases approximately twice as quickly when information from two cameras/fluorophores is summed together, the rate of increase with dual labelled samples is much slower than for single labelled samples. This means that the average rate of blinking slows down for dual labelled samples. Overall, there is little difference between the time taken to reach the cut off limit whether the sample is imaged with single or dual fluorophores.

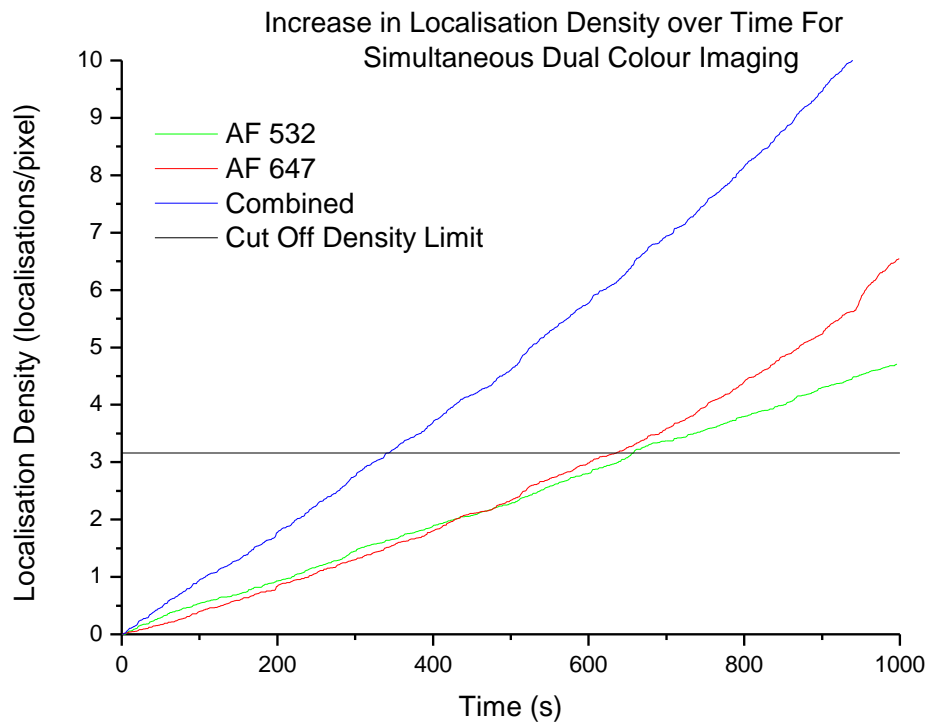


Figure 5.6: Increase in localisation density over time for dual-colour actin filaments

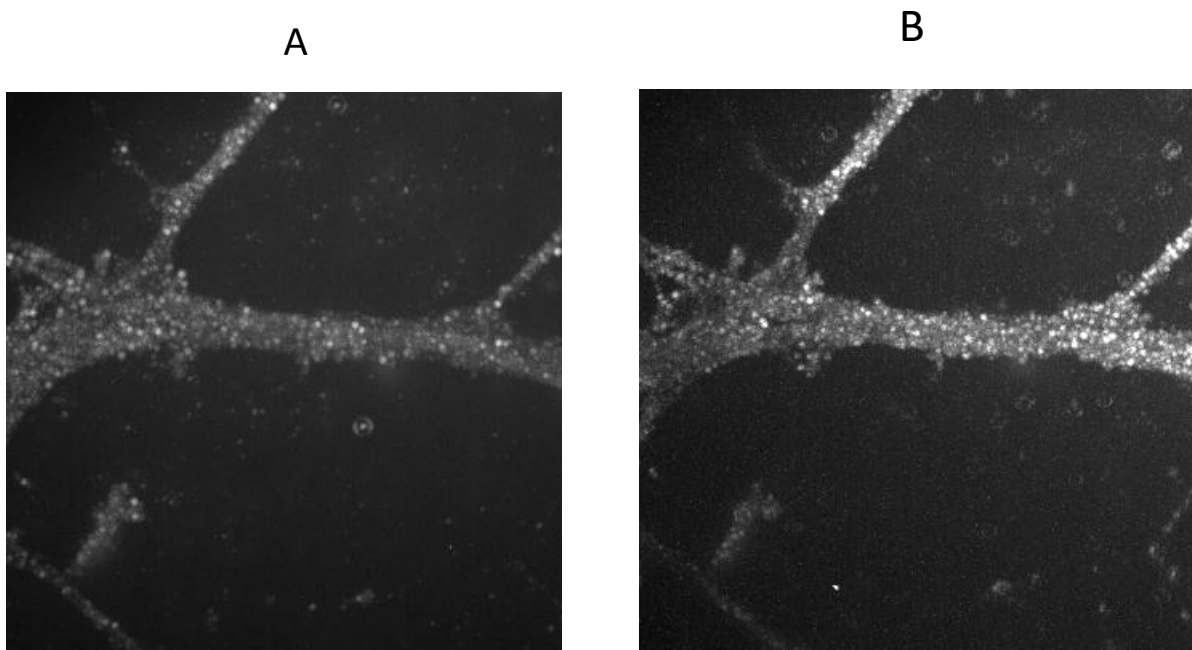


Figure 5.7: Maximum Intensity Projections from (A) Red Channel (AF 647) and (B) Green Channel (AF 532) taken during simultaneous imaging. Images show E13 mouse DRG neuronal outgrowth labelled for f-actin.

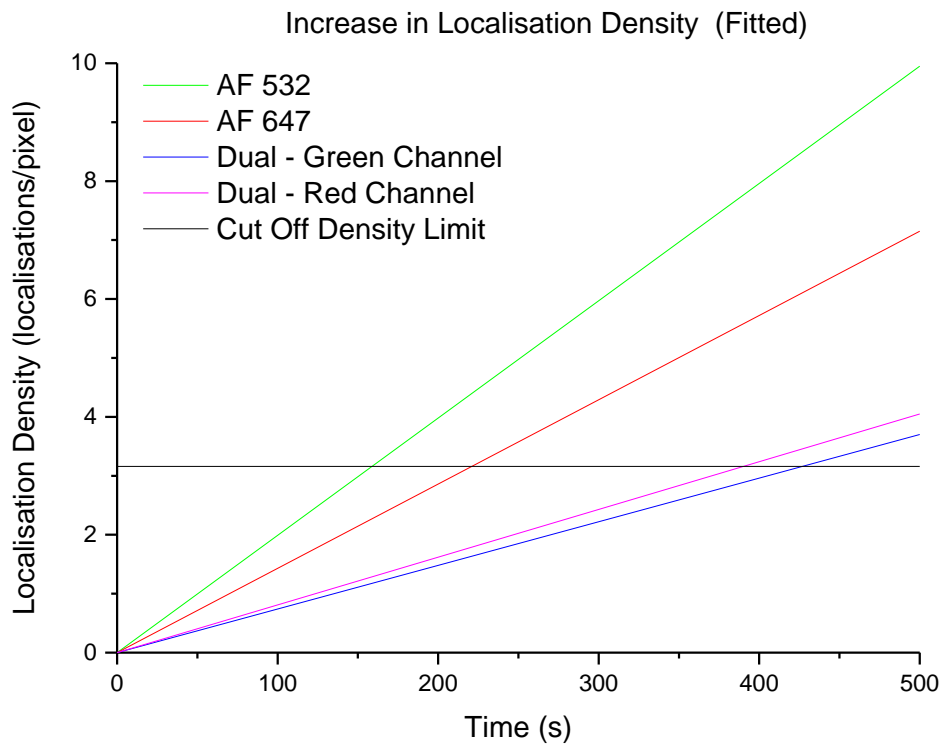


Figure 5.8: Average increase in localisation density over time for single colour and dual labelled samples, linearly fitted. Samples contained (green) AF 532 only, (red) AF 647 only, (blue) Dual labelled, AF 532 and AF 647 - Green Channel, (magenta) Dual labelled, AF 532 and AF 647 - Red Channel. Samples were imaged at the same frame rate and laser power density throughout.

5.2.3 - Investigation of Dual Labelled Blinking Dynamics

When actin filaments are dual labelled with two different fluorophores, the blinking rate appears to be reduced by two as compared to singly labelled samples. There are two possible explanations for this, either the addition of a second dye reduces the effective number of labelling sites in each colour, causing the amount of labelling in each dye colour to be half that of a single-labelled sample, or there could be a photophysics issue due to the close proximity of the two fluorophore types or the two lasers incident simultaneously. For example, there could be some energy exchange between the fluorophores (FRET) causing the light/dark state dynamics to change and the blinking rate to decrease.

In order to test whether the reduction in blink rate when imaging with dual labelled samples is due to a reduced number of labelling sites, samples were prepared and imaged under the following conditions:

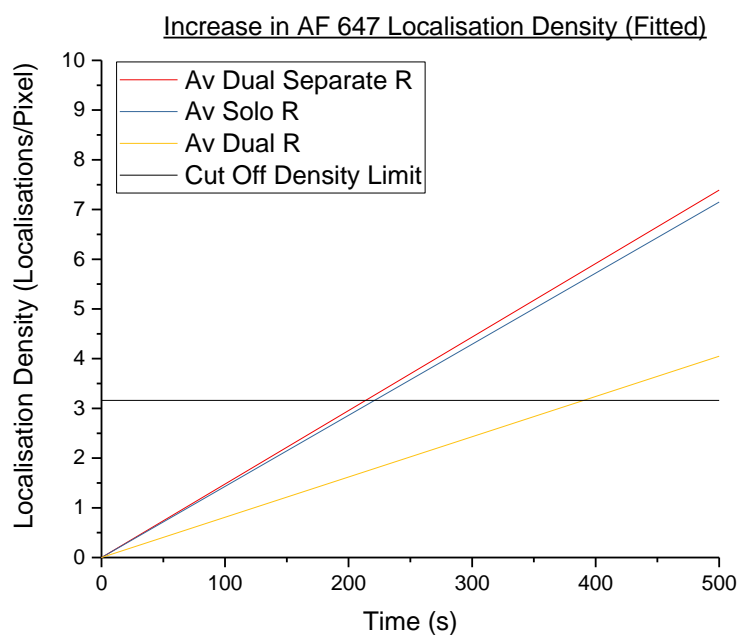
| Single Labelled Samples | Two Colour Samples <i>(Different Targets)</i> | Dual Labelled Samples <i>(Two Dyes to the Same Target)</i> |
|-------------------------|--|---|
| AF 532, Targeting Actin | AF 532, Targeting Actin | AF 532, Targeting Actin |
| AF 647, Targeting Actin | AF 6472, Targeting Transferrin | AF 647, Targeting Actin |

All actin data was analysed as previously. For the two colour sample to different targets, the second target was chosen to be Transferrin (TF) in a pulse-chase experiment of the uptake of fluorescently conjugated TF in 2 minutes of incubation. Transferrin receptors are present on the outer cell membrane. When they encounter the AF 647 conjugated TF, they are brought into the cell via endocytosis in vesicles. To analyse this data, the same MATLAB code used to analyse circular sections of staphylococcus cell wall was used (Appendix 7). This code counts the number of molecules within a circle of a given radius over time. The radius was varied to match the size of each vesicle cluster.

The results from this experiment are shown in figure 5.9. The average blinking rate is very similar for AF 647 (figure 5.9 A) in both the single labelled samples and the two colour (different target) samples, but this rate approximately halves for the dual labelled (same target) samples. The single labelled AF 532 sample has the fastest blinking rate (figure 5.9 B), which drops when a second colour is introduced, and drops again when the two colours target the same structure. Therefore, this

shows that the reduction in speed is likely to be due to both a labelling issue and a quenching issue. This is because the time to reach cut off is halved for AF 647 - indicating a drop in labelling density when dual labelling the same target. The AF 532 drops by over half, indicating both a labelling density issue and that the dye is being quenched. This is expected, as quenching should affect the green dye more as it is at a higher energy.

A



B

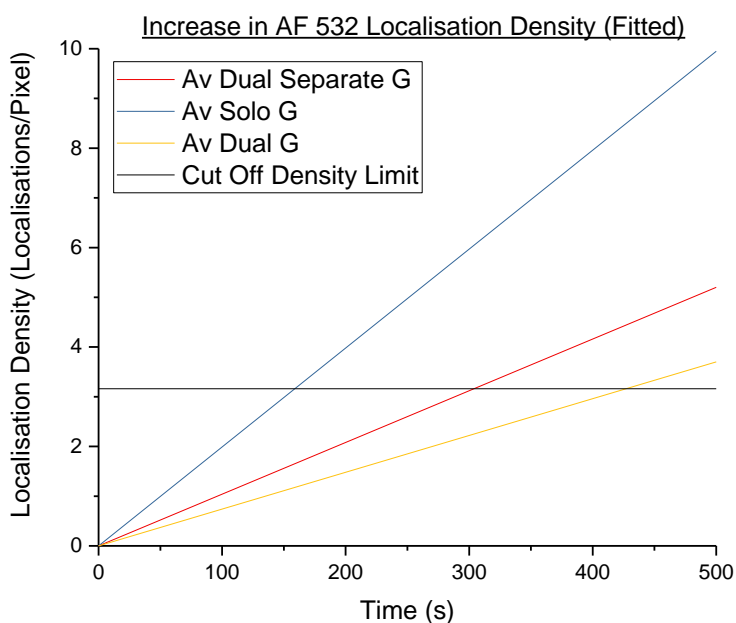


Figure 5.9: Average increase in Localisation Density over time for (A) AF 647 and (B) AF 532. (Blue) Single labelled samples, (Red) Two colour samples - two dyes to different targets, (Yellow) Dual labelled samples - two dyes to the same target. Samples containing two dyes were imaged simultaneously (both colours at once).

5.3 – Conclusions

The limiting factor in STORM imaging is how quickly single molecules can be localised before the PSFs start to overlap and more difficult reconstruction algorithms must be applied to the image^{14,15}. A method of increasing the number of localisations per second was proposed: imaging the same structure at the same time in two colours (i.e. dual labelling a single target). This works by splitting the desired high-density output into two different colour channels so that double the number of molecules can be localised per frame before the PSFs start to overlap.

To test this, AF 647 and AF 532 dyes were added to 3T3 cells with dyes fluorescently conjugated to phalloidin which targets f-actin. The samples were illuminated with both a 532 nm and a 647 nm laser and the emission from both dyes was collected simultaneously using two cameras. Localisation density analysis was performed. It was found that adding the molecules from both channels together (merged reconstruction) approximately halves the amount of time taken to reach the cut off limit (figure 5.6) compared to the time taken for the dual labelled channels separately. However, dual labelled samples take approximately the same amount of time to reach the cut off density as single labelled samples. This means that there is no overall speed increase obtained by dual labelling a single target with two different fluorophores.

To confirm this result, the average increase in localisation density was calculated for samples labelled with only AF 647, only AF 532 or dual labelled with both AF 647 and AF 532 (Figure 5.8). The time taken for the single channel dual labelled samples to reach the cut off is just over double the amount of time that signally labelled samples take. This shows that, although in theory splitting the signal over two different colour channels would allow double the number of molecules to be localised over time, there is no actual reduction in the image acquisition time - images are not built up any faster.

This could be for one of two reasons. The labelling density of the samples is unknown in these experiments, however, there is only a finite number of places along an actin polymer cable that the fluorescently conjugated phalloidin can attach to¹⁷, especially when taking into account the size of the fluorescent molecule. To stain the samples with two colours, both fluorophores were added to the cells at the same time to try and prevent a higher labelling density in whichever fluorophore was added first. However, adding a second colour into the system may reduce the overall number of locations along the actin filament fluorophores of one colour can bind to. This means that adding a second dye colour could effectively half the number of binding sites for each fluorophore. This factor could explain why the single channel data from dual labelled samples have approximately half the number of localisations per second as data from single labelled samples.

Alternatively, the decrease in blinking rate could be due to some kind of interaction between the dye molecules as they are in close proximity to each other along the length of an actin filament. The first STORM paper¹⁸ used Cy5 and Cy3 reporter dye pairs which are structurally very similar to AF 647 and AF 532. In this paper it was the proximity to Cy3 molecules and switching between red and green lasers which caused the characteristic blinking of the STORM technique.

In order to discover whether the reduction in blinking rate with dual labelled samples was due to labelling density or photophysical interactions between the dyes, the results were compared to data taken of a sample labelled with two colours, each to a different target molecule (figure 5.9). This showed that the blinking rate for AF 647 only reduces when the sample is dual labelled. As the drop is a factor of two, this demonstrates the issue is due to half the number of labelling sites being available in each dye colour. The blinking rate for AF 532 drops in both two coloured samples, with the rate dropping over half from the single labelled to the dual labelled sample. This implies that the green dye is both affected by the labelling density decrease and quenching. The red dye is less affected by quenching as it is at a lower energy.

To further probe this issue, the same experiment could be undertaken using microtubules. These have approximately six times the number of binding sites as actin¹⁹, allowing a higher labelling density of each fluorophore colour along the length of the molecule.

5.4 - References

- 1 Narendra, D., Tanaka, A., Suen, D.-F. & Youle, R. J. Parkin is recruited selectively to impaired mitochondria and promotes their autophagy. *Journal of Cell Biology* **183**, doi:10.1083/jcb.200809125 (2008).
- 2 Pawley, J. B. *Handbook of biological confocal microscopy*. 3rd ed. edn, (New York, NY : Springer-Verlag, 2006, 2006).
- 3 Dempsey, G. T., Vaughan, J. C., Chen, K. H., Bates, M. & Zhuang, X. W. Evaluation of fluorophores for optimal performance in localization-based super-resolution imaging. *Nature Methods* **8**, 1027-+, doi:10.1038/nmeth.1768 (2011).
- 4 Bates, M., Huang, B., Dempsey, G. T. & Zhuang, X. Multicolor super-resolution imaging with photo-switchable fluorescent probes. *Science* **317**, doi:10.1126/science.1146598 (2007).
- 5 Huang, B., Wang, W., Bates, M. & Zhuang, X. Three-dimensional super-resolution imaging by stochastic optical reconstruction microscopy. *Science* **319**, doi:10.1126/science.1153529 (2008).
- 6 Bock, H. *et al.* Two-color far-field fluorescence nanoscopy based on photoswitchable emitters. *Applied Physics B* **88**, 161-165, doi:10.1007/s00340-007-2729-0 (2007).
- 7 Mlodzianoski, M. J. *et al.* Sample drift correction in 3D fluorescence photoactivation localization microscopy. *Optics Express* **19**, 15009-15019, doi:10.1364/OE.19.015009 (2011).
- 8 Elmokadem, A. & Yu, J. Optimal Drift Correction for Superresolution Localization Microscopy with Bayesian Inference. *Biophysical Journal* **109**, 1772-1780, doi:10.1016/j.bpj.2015.09.017 (2015).
- 9 Wang, Y. *et al.* Localization events-based sample drift correction for localization microscopy with redundant cross-correlation algorithm. *Optics Express* **22**, 15982-15991, doi:10.1364/OE.22.015982 (2014).
- 10 Lehmann, M. *et al.* Quantitative Multicolor Super-Resolution Microscopy Reveals Tetherin HIV-1 Interaction. *PLOS Pathogens* **7**, e1002456, doi:10.1371/journal.ppat.1002456 (2011).
- 11 Gahlmann, A. a. P. J. L. a. G. G. a. Q. S. a. v. D. A. R. S. a. L. M. K. a. B. M. P. a. S. L. Quantitative Multicolor Subdiffraction Imaging of Bacterial Protein Ultrastructures in Three Dimensions. *Nano Letters* **13**, 987-993, doi:10.1021/nl304071h (2013).
- 12 van den Dries, K. *et al.* Dual-color superresolution microscopy reveals nanoscale organization of mechanosensory podosomes. *Mol Biol Cell* **24**, 2112-2123, doi:10.1091/mbc.E12-12-0856 (2013).

- 13 Shechtman, Y., Weiss, L. E., Backer, A. S., Lee, M. Y. & Moerner, W. E. Multicolour localization microscopy by point-spread-function engineering. *Nat Photon* **10**, 590-594, doi:10.1038/nphoton.2016.137
- <http://www.nature.com/nphoton/journal/v10/n9/abs/nphoton.2016.137.html#supplementary-information> (2016).
- 14 Holden, S. J., Uphoff, S. & Kapanidis, A. N. DAOSTORM: an algorithm for high-density super-resolution microscopy. *Nature Methods* **8**, doi:10.1038/nmeth0411-279 (2011).
- 15 Cox, S. *et al.* Bayesian localization microscopy reveals nanoscale podosome dynamics. *Nature Methods* **9**, doi:10.1038/nmeth.1812 (2012).
- 16 Ovesný, M., Křížek, P., Borkovec, J., Švindrych, Z. & Hagen, G. M. ThunderSTORM: a comprehensive ImageJ plug-in for PALM and STORM data analysis and super-resolution imaging. *Bioinformatics* **30**, 2389-2390, doi:10.1093/bioinformatics/btu202 (2014).
- 17 Vandekerckhove, J., Deboben, A., Nassal, M. & Wieland, T. The phalloidin binding site of F-actin. *The EMBO Journal* **4**, 2815-2818 (1985).
- 18 Rust, M. J., Bates, M. & Zhuang, X. Sub-diffraction-limit imaging by stochastic optical reconstruction microscopy (STORM). *Nature Methods* **3**, doi:10.1038/nmeth929 (2006).
- 19 Wegel, E. *et al.* Imaging cellular structures in super-resolution with SIM, STED and Localisation Microscopy: A practical comparison. *Scientific reports* **6**, 27290 (2016).

6 - Discussion and Conclusions

Contents

| | |
|--|-----|
| 6.1 - Discussion and Conclusions | 153 |
| 6.2 - References | 158 |

6.1 - Discussion and Conclusions

Stochastic Optical Reconstruction Microscopy is a relatively new technique (invented in 2006¹) capable of breaking the diffraction limit and producing superresolution images. This thesis has focused on three simple ways in which to increase the acquisition rate, without the need for complicated analysis methods.

Upon starting this project, the imaging speed of STORM was slow - up to several minutes were required for each image. Currently, the acquisition rate has not improved by much for STORM. The shortest acquisition times remain in the minute to several second range²⁻⁶ and rely on extremely high laser powers or complex reconstruction algorithms. For the standard biological sciences user, times of between 5 - 15 minutes to obtain a single image are common⁷.

The set up used throughout this project was a bespoke STORM system and was built and first optimised (Chapter 3) to find the imaging conditions which are most suitable for imaging at speed. This optimisation was also to see how fast the system could be pushed without any modifications. The experimental variables changed were the readout or excitation laser power density, the camera frame rate and the imaging buffer concentration. The effects of these variables on two different quantities – the signal-to-noise ratio (SNR) and the number of molecules localised per second (NMLpS) – were studied.

From the optimisation experiments it was found that the NMLpS increased with increasing readout laser power density, increasing dramatically at laser power densities higher than 3500 W/cm². The NMLpS peaked between 100 - 150 fps and at buffer concentrations of MEA higher than 100 mM. In contrast, the SNR stayed approximately constant no matter what variable was changed. Therefore as there is no ability to maximise the SNR through these variables, conditions used for imaging should use camera frame rates between 100-150 fps and image using the lowest laser power densities possible to obtain the desired NMLpS. Simply increasing the NMLpS increases the image acquisition rate at the cost of reliability - as more molecules are localised per frame they become overlapping, requiring the use of more complex fitting algorithms. Practically, it was found that samples varied wildly on a sample-by-sample basis, and as such imaging conditions needed to be changed to match the sample to obtain good quality (i.e. well separated PSFs) data.

A consideration which has not been looked at within this work is how the optimised conditions affects the reconstruction accuracy. Future work would be to image a known structure - such as actin filaments - using different laser power and frame rate settings to determine whether images produced at speed represent the sample ground truth as well as samples taken slowly. Imaging at high speeds causes a reduction in data quality as the conditions which allow for quick data collection

tend to increase the background noise and PFSs are no longer as well separated - this can be seen from the raw data throughout Chapter 3.

Factors not considered in the study which may affect STORM imaging and produce the large amount of variability in STORM samples could be temperature, sample preparation, the fluorophore labelling efficiency and the age of STORM buffer used.

A completely different approach to reducing the acquisition time for a STORM image is to consider how many localisations are required to build up a superresolution image. Nieuwenhuizen *et al* (2013)⁸ propose, based on FRC analysis, that there is a trade off between density limited imaging and localisation limited imaging at which the achievable resolution hits a maximum value. This suggests that there is a minimum time required to build a STORM image, and that stopping once this limit has been reached ensures that each STORM image is acquired over the shortest possible time scale. This will indirectly increase the imaging speed as this method ensures molecules are not being wasted - i.e. any molecules which are localised but which are not aiding an increase in resolution. This analysis would work especially well for live STORM imaging as it gives a set localisation density to reach in post-processing before the next superresolution image (the next frame in the movie) can be taken. It also determines the minimum time resolution between images - an important consideration as biological process which occur close to or faster than this time will not be visible by STORM imaging.

To probe the idea of a stopping time or a minimum localisation density in real data, the increase in localisation density was found over time in small areas of cells. The increase in localisation density within small areas was found to be linear, however the rate of increase was found to vary by a large amount over a single image. The stopping time for an entire image is therefore dependent on the slowest area of the sample. Alternatively, the stopping time could be reduced if only a small area of interest is selected.

The localisation density calculated from simulated data by Nieuwenhuizen *et al* (2013) was 3.16 localisations per pixel. To test whether or not this density value represented a useable test for determining when to stop imaging, *staphylococcus aureus* samples were analysed, comparing ten minutes of data to the cut off limit, which for the samples used was between 2 and 3 minutes. The intensity values around *staph* cells which formed a ring or circular structure was plotted for both cases. Although the intensity was higher for the image containing a greater number of frames, both images showed 'flaws' or areas of lower intensity in the same places. This suggests that although the intensity is lower and images therefore do not look as aesthetically accurate by eye, there is actually no more information in the image acquired over a longer time period.

Histograms of radial distance from the cell centre in *staph* cells were analysed to try and determine when the cut off limit occurred using a different method. However, it was found to be statistically difficult to analyse the histograms without knowing the underlying cell structure.

Another method of analysing the data was to split each cell up into different groups based on radial angle and demand that at least 90% (for example) of all groups reach the cut off density limit before the cell was determined to be 'complete'. This was possible for the *staph* cells which formed ring structures as these are known to be continuous (formed from fluorophores being incorporated into the cell wall during growth). As for analysis over single small areas, the percentage number of groups which have reached the density limit increases linearly over time. Data taken at a faster frame rate reaches the stopping time more quickly - which follows from the system optimisation in Chapter 4.

The increase in localisation density over time is a completely random process. This was shown using data simulation which used a random number generator to add molecules to groups over time. The simulated data was very similar to the real data showing that the number of blinks localised in any area of the sample is not biased due to underlying chemical or physical properties.

However, some areas of the cell do reach the cut off density more quickly than other areas. It was hypothesised that this would not be due to variance in laser power across the sample from the experiments in Chapter 4, however to make sure the cut off density across an image was found as a function of distance from the centre of the laser spot. As predicted incident laser power density did not have an effect on the rate at which areas of the cell reached the cut off limit, except to separate areas which blinked from those which did not (i.e. areas where the laser beam was incident compared to areas the laser did not reach). Therefore, differences in stoppage time across a sample are due to sample preparation, for example a non-uniform fluorophore density across a sample.

Most of the experiments were not performed in TIRF mode, which may have caused a greater background signal due to out of focus light from signal elsewhere in the cell. This may have had an effect on the overall number of molecules localised - this is seen in figure 4.22, where the edges of the cell where it is thinner produce a better reconstructed image than in the middle where the cell is thicker. This may have had the effect of extending the time taken to reach the cut-off limit.

All experiments done on *staphylococcus aureus* cells were also repeated in a different test system: actin filaments in mouse fibroblast cells (NIH 3T3). These results were all in agreement to data from *staph* samples.

The use of the FRC limit in STORM imaging has become popular within the superresolution community recently. Fox-Roberts *et al* (2017)⁹ use FRC analysis to determine the differences in time

required to build up images from samples in 0D, 1D and 2D. They show that the dimensionality of the sample has a direct effect on how long it will take to reach the cut off limit density and therefore how long the sample must be imaged to produce an image - a 2D sample requires approximately 30 times the number of frames⁹ compared to a sample with 1D dimensionality. This dimensionality is important to consider when using SMLM, especially when imaging two target structures which have different dimensionality, as the time required to build up an image will be different for the two structures.

Culley *et al* (2017)¹⁰ published an analysis package called NanoJ-SQUIRREL which uses comparisons between the reconstructed SMLM image and the widefield image of the same area to determine which parts of a reconstruction are accurate, and where there are artefacts or errors. It does this by producing an error map. It then calculates the FRC resolution in blocks across the image and compares this to the error map to determine the quality of the reconstructed image. This is an important piece of knowledge for a SMLM image as the 'quality' of the reconstruction is not the same in all areas of the image, as seen in figure 4.3 which shows how different areas of an image reach the cut off density limit at different times.

The method described within this work using the FRC limit is also of use to the microscopy community. The method described in chapter 4 gives a post-processing check to determine whether the localised fluorophore density is large enough to produce an image. Future work in this vein would be to use the cut-off density and the blinking rate to make predictions about how long a sample must be imaged for. If the average NMLpS is known, it should be possible to predict the time the sample will reach the cut-off density. Conversely, if the speed required to be imaged at is known, then the necessary NMLpS can be calculated. It then follows that, if the NMLpS can be determined by the laser power used, the imaging conditions can be varied to suit the sample. For example, live STORM microscopy is difficult as the high laser powers involve damage the cell¹¹ - if however the process being studied was relatively slow, the laser power could potentially be reduced to allow a series of STORM images to be produced with less photodamage to the cell.

The last method to reduce the acquisition time of a STORM image was to image dual labelled samples - one target molecule was labelled with two separate dye colours. The limiting factor in the analysis in Chapter 4 was the NMLpS. Imaging the same target molecule in two different colours will theoretically double the number of localisations found per second which should result in a twofold increase in imaging speed.

Dual labelled samples were imaged in both colour channels simultaneously (two readout lasers incident at the same time) and the time to reach the cut off density limit was halved when

information from two cameras was used compared to just one single channel. However, it was also noted that the time to reach the cut off limit was much longer in dual labelled samples than for single labelled samples. Therefore, although imaging in two colours does double the number of localisations compared to a single channel, this only brings it in line with data obtained from a sample with only one dye. There is no actual improvement to be had for imaging the same object in more than one colour.

This could be due to competition between fluorophores of different colours competing for spaces to attach to the molecule of interest. As there are two colours in the system this automatically requires there to be fewer fluorophores of each colour than in a single dye colour sample. Additionally, there may be some interaction between the dye molecules due to their close proximity to each other attached to the same object. To test this, samples labelled with two coloured dyes to different targets ("two colour") was analysed in the same way as the single and dual labelled samples. For the AF 647 dye the time to reach the cut-off density was unchanged between single labelled samples and two colour samples. The time to reach the cut-off density was doubled when the sample was dual labelled, indicating that the number of AF 647 dye molecules in the sample was halved. The time for AF 532 to reach the cut-off density increased by over two, indicating that not only was the number of fluorescent molecules halved in the dual labelled sample but the AF 532 was also being quenched. This is expected to affect AF 532 more than AF 647 as the green dye is at a higher energy and therefore more susceptible to quenching.

Although the proposed idea to dual label samples in order to increase the imaging speed did not succeed, some positives were highlighted. In the search for a secondary fluorophore capable of STORM imaging, AT 550 was discovered to work on a par with AF 647, generally accepted as the "best" STORM fluorophore by the superresolution community. Further work would be to characterise this dye better. Additionally, the method developed in chapter 3 proved useful in analysing the performance of AF 647 and AF 532. This analysis method could therefore be used to help further characterise the common dyes used for SMLM imaging.

Overall, this work has shown that STORM may not be the best choice for live-cell imaging. This is mainly due to the issues involved in achieving STORM conditions in live cells. The high laser powers required stress and damage the cells, and the imaging buffer is toxic. A third problem is how to label live cells with fluorescent dyes, though there has now been some work done on injection of dyes¹² into live cells. These problems may prove to be surmountable, however if not there are other SMLM techniques such as PALM and fPALM which utilise fluorescent proteins and lower laser powers which may therefore be more suitable for work with live cells.

6.2 - References

- 1 Rust, M. J., Bates, M. & Zhuang, X. Sub-diffraction-limit imaging by stochastic optical reconstruction microscopy (STORM). *Nature Methods* **3**, doi:10.1038/nmeth929 (2006).
- 2 Cox, S. *et al.* Bayesian localization microscopy reveals nanoscale podosome dynamics. *Nature Methods* **9**, doi:10.1038/nmeth.1812 (2012).
- 3 Zhu, L., Zhang, W., Elnatan, D. & Huang, B. Faster STORM using compressed sensing. *Nature Methods* **9**, 721-U286, doi:10.1038/nmeth.1978 (2012).
- 4 Jones, S. A., Shim, S.-H., He, J. & Zhuang, X. Fast, three-dimensional super-resolution imaging of live cells. *Nature Methods* **8**, doi:10.1038/nmeth.1605 (2011).
- 5 Holden, S. J., Uphoff, S. & Kapanidis, A. N. DAOSTORM: an algorithm for high-density super-resolution microscopy. *Nature Methods* **8**, doi:10.1038/nmeth0411-279 (2011).
- 6 Huang, F., Schwartz, S. L., Byars, J. M. & Lidke, K. A. Simultaneous multiple-emitter fitting for single molecule super-resolution imaging. *Biomedical optics express* **2**, 1377-1393 (2011).
- 7 Wegel, E. *et al.* Imaging cellular structures in super-resolution with SIM, STED and Localisation Microscopy: A practical comparison. *Scientific reports* **6**, 27290 (2016).
- 8 Nieuwenhuizen, R. P. J. *et al.* Measuring image resolution in optical nanoscopy. *Nature Methods* **10**, 557-+, doi:10.1038/nmeth.2448 (2013).
- 9 Fox-Roberts, P., Wen, T. Q., Suhling, K. & Cox, S. Fixed Pattern Noise in Localization Microscopy. *Chemphyschem* **15**, 677-686, doi:10.1002/cphc.201300756 (2014).
- 10 Culley, S. *et al.* NanoJ-SQUIRREL: quantitative mapping and minimisation of super-resolution optical imaging artefacts. *bioRxiv* (2017).
- 11 Wäldchen, S., Lehmann, J., Klein, T., van de Linde, S. & Sauer, M. Light-induced cell damage in live-cell super-resolution microscopy. *Scientific Reports* **5**, 15348, doi:10.1038/srep15348 (2015).
- 12 Hennig, S. *et al.* Instant Live-Cell Super-Resolution Imaging of Cellular Structures by Nanoinjection of Fluorescent Probes. *Nano Letters* **15**, 1374-1381, doi:10.1021/nl504660t (2015).

Appendix

Contents

| | |
|----------------------------------|-----|
| Matlab Functions | 160 |
| 1 - Binned_cutoff | 160 |
| 2 - Kmeans_column..... | 164 |
| 3 - Kmeans_position | 168 |
| 4 - KmeansGroups..... | 172 |
| 5 - LM_actin_density_new..... | 176 |
| 6 - LM_BlinksPerSec..... | 180 |
| 7 - LM_CircularAreaDensity | 182 |
| 8 - LM_findPSF | 184 |
| 9 - LM_radialdistances | 186 |
| 10 - Make_binary | 189 |
| 11 - Simulate_seaweed | 190 |
| 12 - Simulate_seaweed_2..... | 192 |
| 13 - Simulate_seaweed_3..... | 194 |
| 14 - SNR_finder | 196 |
| 15- Sortemitters..... | 197 |
| 16 - LM_blinkofftime..... | 199 |

Matlab Functions

1 - Binned_cutoff

```
function [ cornerslist, finallist, frames_onlylist ] = binned_cutoff( fits,
imgsize, sizebins, lasercenterx, lasercentery, camerapositionx,
camerapositiony )
% Splits entire reconstruction into squares (number depends on sizebins)
% and calculates when each square hits 90% confidence density, and the
% radial distance of the square from the laser center

% imgsize ASSUMES SQUARE IMAGE (eg 200x200 pixels)
% sizebins should be in PIXELS eg if sizebins = 10, would have 20 bins of
% size 10x10 pixels

%%%%%%%%%%%%%%%%%%%%%%%%%%%%%%%%%%%%%%%%%%%%%%%%%%%%%%%%%%%%%%%%%%%%%%%%

% PART ONE: CREATING THE BINS/SQUARES

% numsqares = number of bins along 1 axis
% i.e. total number of squares = numsqares^2
numsqares = imgsize / sizebins;

cornerslist = zeros(numsqares^2,4);

coords(1,1) = 0;

% List of potential coordinates
for n = 1:numsqares

    coords((n+1),1) = coords(n,1) + sizebins;

end

% Sequential Coordinates
coordrepeat = zeros((size(coords,1)-1),2);

for n = 1:(size(coords,1) - 1)

    coordrepeat(n,1) = coords(n,1);
    coordrepeat(n,2) = coords((n+1),1);

end

% Y coordinates list
Q = 0;

for n = 1:(size(coordrepeat,1))

    for q = 1:numsqares

        ylist((Q+q),1) = coordrepeat(n,1);
        ylist((Q+q),2) = coordrepeat(n,2);

    end

end
```

```

    Q = Q + numsquares;
end

% X coordinates list
Q = 0;

for n = 1:size(coordrepeat,1)

    cornerslist((n + Q) : (n + Q + (numsquares-1)),3) = coordrepeat(:,1);
    cornerslist((n + Q) : (n + Q + (numsquares-1)),4) = coordrepeat(:,2);

    Q = Q + (numsquares-1);
end

% Flip wrt to y because ~dodgy coord systems
ylist = flipud(ylist);

cornerslist(:,1:2) = ylist;

% SO can now use LM_depthfilter to select out points within each bin

Q = 0;
for n = 1:size(cornerslist,1)

    [ temp ] = LM_depthfilter( fits, cornerslist(n,1), cornerslist(n,2),
4);
    [ temp ] = LM_depthfilter( temp, cornerslist(n,3), cornerslist(n,4),
2);

    % Add column 9 with total # of blinks for that cell
    cornerslist(n,9) = size(temp,1);

    % 1 = x, 2 = y, 3 = frame # (repeats along)
    bins_pointslist(1:size(temp,1), (n+Q)) = temp(:,2);
    bins_pointslist(1:size(temp,1), (n+1+Q)) = temp(:,4);
    bins_pointslist(1:size(temp,1), (n+2+Q)) = temp(:,7);

    frames_onlylist(1:size(temp,1),n) = temp(:,7);

    Q = Q + 2;
end

%%%%%%%%%%%%%%%%%%%%%%%%%%%%%%%%%%%%%%%%%%%%%%%%%%%%%%%%%%%%%%%%%%%%%%%%

% PART TWO: FINDING FRAME WHEN REACHES 90% CONFIDENCE

% Firstly want to calc radial distance from laser center of each box

% Calculate where the laser spot center is wrt to coordinate system
% i.e. need to treat camerapositionx & camerapositiony as '(0,0)'

correctedlaserx = lasercenterx - camerapositionx;
correctedlasery = lasercentery - camerapositiony;

% Calculating center of each box & then radial distance
for n = 1:size(cornerslist,1)

```

```

    cornerslist(n,5) = cornerslist(n,3) + (sizebins/2);
    cornerslist(n,6) = cornerslist(n,1) + (sizebins/2);

    actualx = cornerslist(n,5) + camerapositionx;
    actualy = cornerslist(n,6) + camerapositiony;

    cornerslist(n,7) = sqrt((lasercenterx - actualx)^2 + (lasercentery -
actualy)^2);

    % cornerslist(n,7) = sqrt((correctedlaserx - cornerslist(n,5))^2 +
(correctedlasery - cornerslist(n,6))^2);

end

area = sizebins^2;

% Cut off limit from Dutch Group is 3.16 points/pixel^2
% THEREFORE will need (area * 3.16) points

% Number of points each square requires to be at cutoffpoint
pointsatcutoff = area * 3.16;

% Now need to find what frame each square reaches this number of points.

for n = 1:size(frames_onlylist,2)

    temp = frames_onlylist(:,n);
    frame = temp(ceil(pointsatcutoff),1);

    if frame == 0

        cornerslist(n,8) = 0;

    else

        cornerslist(n,8) = frame;

    end

end

end

% cornerslist
% 1 = bottom y, 2 = top y, 3 = bottom x, 4 = top x, 5 = center x, 6 =
% center y, 7 = radial distance to laser center, 8 = frame reaches cut off
% limit

% % Add column 9 with total # of blinks for that cell
% for n = 1:size(cornerslist,1)
%
%     [ temp2 ] = LM_depthfilter( fits, cornerslist(n,1), cornerslist(n,2),
4);
%     [ temp2 ] = LM_depthfilter( temp2, cornerslist(n,3),
cornerslist(n,4), 2);
%
%     cornerslist(n,9) = size(temp2,1);

```

```

%
% end

% FINALLY put in a list that excludes all 0 values?
Q = 1;
for n = 1:size(cornerslist)

    if cornerslist(n,8) == 0
        continue
    else
        finallist(Q,1) = cornerslist(n,7);
        finallist(Q,2) = cornerslist(n,8);
        finallist(Q,3) = cornerslist(n,5);
        finallist(Q,4) = cornerslist(n,6);
        finallist(Q,5) = cornerslist(n,9);

        % finallist 1 = radial distance, 2 = Cut off Frame, 3 = x value, 4
        % = y value, 5 = total # points

        Q = Q + 1;

    end

end

%%%%%%%%%%%%%%%%%%%%%%%%%%%%%%%%%%%%%%%%%%%%%%%%%%%%%%%%%%%%%%%%%%%%%%%%
end

```

2 - Kmeans_column

```
function [ group1, group2, group3, group4, group5, group6, group7, group8,
group9, group10, group11, group12, group13, group14 ] = Kmeans_column(
listofpoints, column, k )
% Puts groups found from K-means (idx) into separate variables (so can plot
% them, do more k-means calculations on them etc)
%
% Does K-means calculation on a column of choice (eg column 5 - radial
% distances)
%
% Listofpoints: 1 = x, 2 = xnew, 3 = y, 4 = ynew, 5 = Radial Distance, 6 =
% Frame #, 7 = kmeans idx (Position), 8 = angle from upright vertical, 9 =
% kmeans idx (Column)

% K-means
[idx,C,sumd,D] = kmeans(listofpoints(:,column),k, 'replicates', 5);

% Put into groups
listofpoints(:,9) = idx;

m = 1;o = 1;p = 1;q = 1;r = 1;s = 1;t = 1;u = 1;v = 1;w = 1;x = 1;y = 1;z =
;a = 1;

% Sort into groups to plot each k-mean cluster separately
for n = 1:size(listofpoints,1)

    if listofpoints(n,9) == 1

        group1(m,1) = listofpoints(n,1);
        group1(m,2) = listofpoints(n,2);
        group1(m,3) = listofpoints(n,3);
        group1(m,4) = listofpoints(n,4);
        group1(m,5) = listofpoints(n,5);
        group1(m,6) = listofpoints(n,6);
        group1(m,7) = listofpoints(n,7);
        group1(m,8) = listofpoints(n,8);
        group1(m,9) = listofpoints(n,9);
        m = m + 1;
    end
    if listofpoints(n,9) == 2
        group2(o,1) = listofpoints(n,1);
        group2(o,2) = listofpoints(n,2);
        group2(o,3) = listofpoints(n,3);
        group2(o,4) = listofpoints(n,4);
        group2(o,5) = listofpoints(n,5);
        group2(o,6) = listofpoints(n,6);
        group2(o,7) = listofpoints(n,7);
        group2(o,8) = listofpoints(n,8);
        group2(o,9) = listofpoints(n,9);
        o = o + 1;
    end
    if listofpoints(n,9) == 3
        group3(p,1) = listofpoints(n,1);
        group3(p,2) = listofpoints(n,2);
        group3(p,3) = listofpoints(n,3);
        group3(p,4) = listofpoints(n,4);
        group3(p,5) = listofpoints(n,5);
        group3(p,6) = listofpoints(n,6);
        group3(p,7) = listofpoints(n,7);
    end
end
```



```

    group3(p,8) = listofpoints(n,8);
    group3(p,9) = listofpoints(n,9);
    p = p + 1;
end
if listofpoints(n,9) == 4
    group4(q,1) = listofpoints(n,1);
    group4(q,2) = listofpoints(n,2);
    group4(q,3) = listofpoints(n,3);
    group4(q,4) = listofpoints(n,4);
    group4(q,5) = listofpoints(n,5);
    group4(q,6) = listofpoints(n,6);
    group4(q,7) = listofpoints(n,7);
    group4(q,8) = listofpoints(n,8);
    group4(q,9) = listofpoints(n,9);
    q = q + 1;
end
if listofpoints(n,9) == 5
    group5(r,1) = listofpoints(n,1);
    group5(r,2) = listofpoints(n,2);
    group5(r,3) = listofpoints(n,3);
    group5(r,4) = listofpoints(n,4);
    group5(r,5) = listofpoints(n,5);
    group5(r,6) = listofpoints(n,6);
    group5(r,7) = listofpoints(n,7);
    group5(r,8) = listofpoints(n,8);
    group5(r,9) = listofpoints(n,9);
    r = r + 1;
end
if listofpoints(n,9) == 6
    group6(s,1) = listofpoints(n,1);
    group6(s,2) = listofpoints(n,2);
    group6(s,3) = listofpoints(n,3);
    group6(s,4) = listofpoints(n,4);
    group6(s,5) = listofpoints(n,5);
    group6(s,6) = listofpoints(n,6);
    group6(s,7) = listofpoints(n,7);
    group6(s,8) = listofpoints(n,8);
    group6(s,9) = listofpoints(n,9);
    s = s + 1;
end
if listofpoints(n,9) == 7
    group7(t,1) = listofpoints(n,1);
    group7(t,2) = listofpoints(n,2);
    group7(t,3) = listofpoints(n,3);
    group7(t,4) = listofpoints(n,4);
    group7(t,5) = listofpoints(n,5);
    group7(t,6) = listofpoints(n,6);
    group7(t,7) = listofpoints(n,7);
    group7(t,8) = listofpoints(n,8);
    group7(t,9) = listofpoints(n,9);
    t = t + 1;
end
if listofpoints(n,9) == 8
    group8(u,1) = listofpoints(n,1);
    group8(u,2) = listofpoints(n,2);
    group8(u,3) = listofpoints(n,3);
    group8(u,4) = listofpoints(n,4);
    group8(u,5) = listofpoints(n,5);
    group8(u,6) = listofpoints(n,6);
    group8(u,7) = listofpoints(n,7);
    group8(u,8) = listofpoints(n,8);

```

```

    group8(u,9) = listofpoints(n,9);
    u = u + 1;
end
if listofpoints(n,9) == 9
    group9(v,1) = listofpoints(n,1);
    group9(v,2) = listofpoints(n,2);
    group9(v,3) = listofpoints(n,3);
    group9(v,4) = listofpoints(n,4);
    group9(v,5) = listofpoints(n,5);
    group9(v,6) = listofpoints(n,6);
    group9(v,7) = listofpoints(n,7);
    group9(v,8) = listofpoints(n,8);
    group9(v,9) = listofpoints(n,9);
    v = v + 1;
end
if listofpoints(n,9) == 10
    group10(w,1) = listofpoints(n,1);
    group10(w,2) = listofpoints(n,2);
    group10(w,3) = listofpoints(n,3);
    group10(w,4) = listofpoints(n,4);
    group10(w,5) = listofpoints(n,5);
    group10(w,6) = listofpoints(n,6);
    group10(w,7) = listofpoints(n,7);
    group10(w,8) = listofpoints(n,8);
    group10(w,9) = listofpoints(n,9);
    w = w + 1;
end
if listofpoints(n,9) == 11
    group11(x,1) = listofpoints(n,1);
    group11(x,2) = listofpoints(n,2);
    group11(x,3) = listofpoints(n,3);
    group11(x,4) = listofpoints(n,4);
    group11(x,5) = listofpoints(n,5);
    group11(x,6) = listofpoints(n,6);
    group11(x,7) = listofpoints(n,7);
    group11(x,8) = listofpoints(n,8);
    group11(x,9) = listofpoints(n,9);
    x = x + 1;
end
if listofpoints(n,9) == 12
    group12(y,1) = listofpoints(n,1);
    group12(y,2) = listofpoints(n,2);
    group12(y,3) = listofpoints(n,3);
    group12(y,4) = listofpoints(n,4);
    group12(y,5) = listofpoints(n,5);
    group12(y,6) = listofpoints(n,6);
    group12(y,7) = listofpoints(n,7);
    group12(y,8) = listofpoints(n,8);
    group12(y,9) = listofpoints(n,9);

    y = y + 1;
end
if listofpoints(n,9) == 13
    group13(z,1) = listofpoints(n,1);
    group13(z,2) = listofpoints(n,2);
    group13(z,3) = listofpoints(n,3);
    group13(z,4) = listofpoints(n,4);
    group13(z,5) = listofpoints(n,5);
    group13(z,6) = listofpoints(n,6);
    group13(z,7) = listofpoints(n,7);
    group13(z,8) = listofpoints(n,8);

```

```
    group13(z,9) = listofpoints(n,9);  
    z = z + 1;  
end  
if listofpoints(n,9) == 14  
    group14(a,1) = listofpoints(n,1);  
    group14(a,2) = listofpoints(n,2);  
    group14(a,3) = listofpoints(n,3);  
    group14(a,4) = listofpoints(n,4);  
    group14(a,5) = listofpoints(n,5);  
    group14(a,6) = listofpoints(n,6);  
    group14(a,7) = listofpoints(n,7);  
    group14(a,8) = listofpoints(n,8);  
    group14(a,9) = listofpoints(n,9);  
    a = a + 1;  
end  
end  
  
end
```

3 - Kmeans_position

```
function [ group1, group2, group3, group4, group5, group6, group7, group8,
group9, group10, group11, group12, group13, group14 ] = Kmeans_position(
listofpoints, k )
% Puts groups found from K-means (idx) into separate variables (so can plot
% them, do more k-means calculations on them etc)
%
% Does K-means on position (i.e. columns 1 (x) and 3 (y))
%
% Inputs are listofpoints (output from LM_Radialdistances) and idx which
% comes from kmeans calculation ([idx,C,sumd,D] =
% kmeans(listofpoints(:,#), K, 'replicates', 5);)
%
% Listofpoints: 1 = x, 2 = xnew, 3 = y, 4 = ynew, 5 = Radial Distance, 6 =
% Frame #, 7 = kmeans idx (Position), 8 = angle from upright vertical, 9 =
% kmeans idx (Column)

% Make matrix X = x and y values for each point (use this to do 2d k-means)
X(:,1) = listofpoints(:,1);
X(:,2) = listofpoints(:,3);

% K-means
[idx,C,sumd,D] = kmeans(X,k, 'replicates', 5);

% Add K-means groups to dataset (i.e. so each point is on same line as its
% group)

listofpoints(:,7) = idx;

m = 1;o = 1;p = 1;q = 1;r = 1;s = 1;t = 1;u = 1;v = 1;w = 1;x = 1;y = 1;z =
;a = 1;

% Sort into groups to plot each k-mean cluster separately
for n = 1:size(listofpoints,1)

    if listofpoints(n,7) == 1
        group1(m,1) = listofpoints(n,1);
        group1(m,2) = listofpoints(n,2);
        group1(m,3) = listofpoints(n,3);
        group1(m,4) = listofpoints(n,4);
        group1(m,5) = listofpoints(n,5);
        group1(m,6) = listofpoints(n,6);
        group1(m,7) = listofpoints(n,7);
        group1(m,8) = listofpoints(n,8);
        %group1(m,9) = listofpoints(n,9);
        m = m + 1;
    end
    if listofpoints(n,7) == 2
        group2(o,1) = listofpoints(n,1);
        group2(o,2) = listofpoints(n,2);
        group2(o,3) = listofpoints(n,3);
        group2(o,4) = listofpoints(n,4);
        group2(o,5) = listofpoints(n,5);
        group2(o,6) = listofpoints(n,6);
        group2(o,7) = listofpoints(n,7);
        group2(o,8) = listofpoints(n,8);
        %group2(o,9) = listofpoints(n,9);
        o = o + 1;
    end
end
```

```

if listofpoints(n,7) == 3
    group3(p,1) = listofpoints(n,1);
    group3(p,2) = listofpoints(n,2);
    group3(p,3) = listofpoints(n,3);
    group3(p,4) = listofpoints(n,4);
    group3(p,5) = listofpoints(n,5);
    group3(p,6) = listofpoints(n,6);
    group3(p,7) = listofpoints(n,7);
    group3(p,8) = listofpoints(n,8);
    %group3(p,9) = listofpoints(n,9);
    p = p + 1;
end
if listofpoints(n,7) == 4
    group4(q,1) = listofpoints(n,1);
    group4(q,2) = listofpoints(n,2);
    group4(q,3) = listofpoints(n,3);
    group4(q,4) = listofpoints(n,4);
    group4(q,5) = listofpoints(n,5);
    group4(q,6) = listofpoints(n,6);
    group4(q,7) = listofpoints(n,7);
    group4(q,8) = listofpoints(n,8);
    %group4(q,9) = listofpoints(n,9);
    q = q + 1;
end
if listofpoints(n,7) == 5
    group5(r,1) = listofpoints(n,1);
    group5(r,2) = listofpoints(n,2);
    group5(r,3) = listofpoints(n,3);
    group5(r,4) = listofpoints(n,4);
    group5(r,5) = listofpoints(n,5);
    group5(r,6) = listofpoints(n,6);
    group5(r,7) = listofpoints(n,7);
    group5(r,8) = listofpoints(n,8);
    %group5(r,9) = listofpoints(n,9);
    r = r + 1;
end
if listofpoints(n,7) == 6
    group6(s,1) = listofpoints(n,1);
    group6(s,2) = listofpoints(n,2);
    group6(s,3) = listofpoints(n,3);
    group6(s,4) = listofpoints(n,4);
    group6(s,5) = listofpoints(n,5);
    group6(s,6) = listofpoints(n,6);
    group6(s,7) = listofpoints(n,7);
    group6(s,8) = listofpoints(n,8);
    %group6(s,9) = listofpoints(n,9);
    s = s + 1;
end
if listofpoints(n,7) == 7
    group7(t,1) = listofpoints(n,1);
    group7(t,2) = listofpoints(n,2);
    group7(t,3) = listofpoints(n,3);
    group7(t,4) = listofpoints(n,4);
    group7(t,5) = listofpoints(n,5);
    group7(t,6) = listofpoints(n,6);
    group7(t,7) = listofpoints(n,7);
    group7(t,8) = listofpoints(n,8);
    %group7(t,9) = listofpoints(n,9);
    t = t + 1;
end
if listofpoints(n,7) == 8

```

```

    group8(u,1) = listofpoints(n,1);
    group8(u,2) = listofpoints(n,2);
    group8(u,3) = listofpoints(n,3);
    group8(u,4) = listofpoints(n,4);
    group8(u,5) = listofpoints(n,5);
    group8(u,6) = listofpoints(n,6);
    group8(u,7) = listofpoints(n,7);
    group8(u,8) = listofpoints(n,8);
    %group8(u,9) = listofpoints(n,9);
    u = u + 1;
end
if listofpoints(n,7) == 9
    group9(v,1) = listofpoints(n,1);
    group9(v,2) = listofpoints(n,2);
    group9(v,3) = listofpoints(n,3);
    group9(v,4) = listofpoints(n,4);
    group9(v,5) = listofpoints(n,5);
    group9(v,6) = listofpoints(n,6);
    group9(v,7) = listofpoints(n,7);
    group9(v,8) = listofpoints(n,8);
    %group9(v,9) = listofpoints(n,9);
    v = v + 1;
end
if listofpoints(n,7) == 10
    group10(w,1) = listofpoints(n,1);
    group10(w,2) = listofpoints(n,2);
    group10(w,3) = listofpoints(n,3);
    group10(w,4) = listofpoints(n,4);
    group10(w,5) = listofpoints(n,5);
    group10(w,6) = listofpoints(n,6);
    group10(w,7) = listofpoints(n,7);
    group10(w,8) = listofpoints(n,8);
    %group10(w,9) = listofpoints(n,9);
    w = w + 1;
end
if listofpoints(n,7) == 11
    group11(x,1) = listofpoints(n,1);
    group11(x,2) = listofpoints(n,2);
    group11(x,3) = listofpoints(n,3);
    group11(x,4) = listofpoints(n,4);
    group11(x,5) = listofpoints(n,5);
    group11(x,6) = listofpoints(n,6);
    group11(x,7) = listofpoints(n,7);
    group11(x,8) = listofpoints(n,8);
    %group11(x,9) = listofpoints(n,9);
    x = x + 1;
end
if listofpoints(n,7) == 12
    group12(y,1) = listofpoints(n,1);
    group12(y,2) = listofpoints(n,2);
    group12(y,3) = listofpoints(n,3);
    group12(y,4) = listofpoints(n,4);
    group12(y,5) = listofpoints(n,5);
    group12(y,6) = listofpoints(n,6);
    group12(y,7) = listofpoints(n,7);
    group12(y,8) = listofpoints(n,8);
    %group12(y,9) = listofpoints(n,9);
    y = y + 1;
end
if listofpoints(n,7) == 13

```

```

    group13(z,1) = listofpoints(n,1);
    group13(z,2) = listofpoints(n,2);
    group13(z,3) = listofpoints(n,3);
    group13(z,4) = listofpoints(n,4);
    group13(z,5) = listofpoints(n,5);
    group13(z,6) = listofpoints(n,6);
    group13(z,7) = listofpoints(n,7);
    group13(z,8) = listofpoints(n,8);
    %group13(z,9) = listofpoints(n,9);
    z = z + 1;
end
if listofpoints(n,7) == 14
    group14(a,1) = listofpoints(n,1);
    group14(a,2) = listofpoints(n,2);
    group14(a,3) = listofpoints(n,3);
    group14(a,4) = listofpoints(n,4);
    group14(a,5) = listofpoints(n,5);
    group14(a,6) = listofpoints(n,6);
    group14(a,7) = listofpoints(n,7);
    group14(a,8) = listofpoints(n,8);
    %group14(a,9) = listofpoints(n,9);
    a = a + 1;
end

end

end

```

4 - KmeansGroups

```
function [ group1, group2, group3, group4, group5, group6, group7, group8,
group9, group10, group11, group12, group13, group14 ] = KmeansGroups(
listofpoints, k )
% Puts groups found from K-means (idx) into separate variables (so can plot
% them, do more k-means calculations on them etc)
%
% Inputs are listofpoints (output from LM_Radialdistances) and idx which
% comes from kmeans calculation ([idx,C,sumd,D] =
% kmeans(listofpoints(:,#), K, 'replicates', 5);)
%
% Listofpoints: 1 = x, 2 = xnew, 3 = y, 4 = ynew, 5 = Radial Distance, 6 =
% Frame #, 7 = kmeans idx/blank, 8 = angle from upright vertical

% Make matrix X = x and y values for each point (use this to do 2d k-means)
X(:,1) = listofpoints(:,1);
X(:,2) = listofpoints(:,3);

% K-means
[idx,C,sumd,D] = kmeans(X,k, 'replicates', 5);

% Add K-means groups to dataset (i.e. so each point is on same line as its
% group)

listofpoints(:,7) = idx;

m = 1;o = 1;p = 1;q = 1;r = 1;s = 1;t = 1;u = 1;v = 1;w = 1;x = 1;y = 1;z =
;a = 1;

% Sort into groups to plot each k-mean cluster separately
for n = 1:size(listofpoints,1)

    if listofpoints(n,7) == 1
        group1(m,1) = listofpoints(n,1);
        group1(m,2) = listofpoints(n,2);
        group1(m,3) = listofpoints(n,3);
        group1(m,4) = listofpoints(n,4);
        group1(m,5) = listofpoints(n,5);
        group1(m,6) = listofpoints(n,6);
        group1(m,7) = listofpoints(n,7);
        group1(m,8) = listofpoints(n,8);
        %group1(m,9) = listofpoints(n,9);
        m = m + 1;
    end
    if listofpoints(n,7) == 2
        group2(o,1) = listofpoints(n,1);
        group2(o,2) = listofpoints(n,2);
        group2(o,3) = listofpoints(n,3);
        group2(o,4) = listofpoints(n,4);
        group2(o,5) = listofpoints(n,5);
        group2(o,6) = listofpoints(n,6);
        group2(o,7) = listofpoints(n,7);
        group2(o,8) = listofpoints(n,8);
        %group2(o,9) = listofpoints(n,9);
        o = o + 1;
    end
    if listofpoints(n,7) == 3
        group3(p,1) = listofpoints(n,1);
        group3(p,2) = listofpoints(n,2);
    end
end
```



```

    group3(p,3) = listofpoints(n,3);
    group3(p,4) = listofpoints(n,4);
    group3(p,5) = listofpoints(n,5);
    group3(p,6) = listofpoints(n,6);
    group3(p,7) = listofpoints(n,7);
    group3(p,8) = listofpoints(n,8);
    %group3(p,9) = listofpoints(n,9);
    p = p + 1;
end
if listofpoints(n,7) == 4
    group4(q,1) = listofpoints(n,1);
    group4(q,2) = listofpoints(n,2);
    group4(q,3) = listofpoints(n,3);
    group4(q,4) = listofpoints(n,4);
    group4(q,5) = listofpoints(n,5);
    group4(q,6) = listofpoints(n,6);
    group4(q,7) = listofpoints(n,7);
    group4(q,8) = listofpoints(n,8);
    %group4(q,9) = listofpoints(n,9);
    q = q + 1;
end
if listofpoints(n,7) == 5
    group5(r,1) = listofpoints(n,1);
    group5(r,2) = listofpoints(n,2);
    group5(r,3) = listofpoints(n,3);
    group5(r,4) = listofpoints(n,4);
    group5(r,5) = listofpoints(n,5);
    group5(r,6) = listofpoints(n,6);
    group5(r,7) = listofpoints(n,7);
    group5(r,8) = listofpoints(n,8);
    %group5(r,9) = listofpoints(n,9);
    r = r + 1;
end
if listofpoints(n,7) == 6
    group6(s,1) = listofpoints(n,1);
    group6(s,2) = listofpoints(n,2);
    group6(s,3) = listofpoints(n,3);
    group6(s,4) = listofpoints(n,4);
    group6(s,5) = listofpoints(n,5);
    group6(s,6) = listofpoints(n,6);
    group6(s,7) = listofpoints(n,7);
    group6(s,8) = listofpoints(n,8);
    %group6(s,9) = listofpoints(n,9);
    s = s + 1;
end
if listofpoints(n,7) == 7
    group7(t,1) = listofpoints(n,1);
    group7(t,2) = listofpoints(n,2);
    group7(t,3) = listofpoints(n,3);
    group7(t,4) = listofpoints(n,4);
    group7(t,5) = listofpoints(n,5);
    group7(t,6) = listofpoints(n,6);
    group7(t,7) = listofpoints(n,7);
    group7(t,8) = listofpoints(n,8);
    %group7(t,9) = listofpoints(n,9);
    t = t + 1;
end
if listofpoints(n,7) == 8
    group8(u,1) = listofpoints(n,1);
    group8(u,2) = listofpoints(n,2);
    group8(u,3) = listofpoints(n,3);

```

```

    group8(u,4) = listofpoints(n,4);
    group8(u,5) = listofpoints(n,5);
    group8(u,6) = listofpoints(n,6);
    group8(u,7) = listofpoints(n,7);
    group8(u,8) = listofpoints(n,8);
    %group8(u,9) = listofpoints(n,9);
    u = u + 1;
end
if listofpoints(n,7) == 9
    group9(v,1) = listofpoints(n,1);
    group9(v,2) = listofpoints(n,2);
    group9(v,3) = listofpoints(n,3);
    group9(v,4) = listofpoints(n,4);
    group9(v,5) = listofpoints(n,5);
    group9(v,6) = listofpoints(n,6);
    group9(v,7) = listofpoints(n,7);
    group9(v,8) = listofpoints(n,8);
    %group9(v,9) = listofpoints(n,9);
    v = v + 1;
end
if listofpoints(n,7) == 10
    group10(w,1) = listofpoints(n,1);
    group10(w,2) = listofpoints(n,2);
    group10(w,3) = listofpoints(n,3);
    group10(w,4) = listofpoints(n,4);
    group10(w,5) = listofpoints(n,5);
    group10(w,6) = listofpoints(n,6);
    group10(w,7) = listofpoints(n,7);
    group10(w,8) = listofpoints(n,8);
    %group10(w,9) = listofpoints(n,9);
    w = w + 1;
end
if listofpoints(n,7) == 11
    group11(x,1) = listofpoints(n,1);
    group11(x,2) = listofpoints(n,2);
    group11(x,3) = listofpoints(n,3);
    group11(x,4) = listofpoints(n,4);
    group11(x,5) = listofpoints(n,5);
    group11(x,6) = listofpoints(n,6);
    group11(x,7) = listofpoints(n,7);
    group11(x,8) = listofpoints(n,8);
    %group11(x,9) = listofpoints(n,9);
    x = x + 1;
end
if listofpoints(n,7) == 12
    group12(y,1) = listofpoints(n,1);
    group12(y,2) = listofpoints(n,2);
    group12(y,3) = listofpoints(n,3);
    group12(y,4) = listofpoints(n,4);
    group12(y,5) = listofpoints(n,5);
    group12(y,6) = listofpoints(n,6);
    group12(y,7) = listofpoints(n,7);
    group12(y,8) = listofpoints(n,8);
    %group12(y,9) = listofpoints(n,9);
    y = y + 1;
end
if listofpoints(n,7) == 13
    group13(z,1) = listofpoints(n,1);
    group13(z,2) = listofpoints(n,2);
    group13(z,3) = listofpoints(n,3);
    group13(z,4) = listofpoints(n,4);

```

```

    group13(z,5) = listofpoints(n,5);
    group13(z,6) = listofpoints(n,6);
    group13(z,7) = listofpoints(n,7);
    group13(z,8) = listofpoints(n,8);
    %group13(z,9) = listofpoints(n,9);
    z = z + 1;
end
if listofpoints(n,7) == 14
    group14(a,1) = listofpoints(n,1);
    group14(a,2) = listofpoints(n,2);
    group14(a,3) = listofpoints(n,3);
    group14(a,4) = listofpoints(n,4);
    group14(a,5) = listofpoints(n,5);
    group14(a,6) = listofpoints(n,6);
    group14(a,7) = listofpoints(n,7);
    group14(a,8) = listofpoints(n,8);
    %group14(a,9) = listofpoints(n,9);
    a = a + 1;
end

end

end

```

5 - LM_actin_density_new

```
function [ newfits, selected, selected2, holdallz, summed_points,
holdallpoints, finalcellpoints ] = LM_actin_density_new( fits, midtop_x,
midtop_y, midbot_x, midbot_y, x1, y1, x2, y2, x3, y3, x4, y4 )
% Calculates little boxes and how many points are in each box.
% newfits = rotated fits, 1 = x, 2 = y, 7 = frame
% selected = selected area of newfits, 1 = x, 2 = y, 7 = frame
% selected2 = selected, in the form that we can use 'LM_blinksperspec' on it
% holdallz = binned matrix, each # represents how many points were found in
% that binned area
% summed_points = sum of all points along a column (to calc width from)

sizestep=20;
pixelsize=100;

% % This is a v simple way to rotate, doesn't rotate enough
% % op=y1-y4;
% % ad=x4-x1;
% % theta=atan(op/ad);
%
% % This method finds the midpoint of the top and bottom short sides and
fits
% % a line between. ALSO NOT VERY ACCURATE. Really just depends on how well
% % select outside points.....
% midtop_x = x4 + ((x4 - x1)/2);
% midtop_y = y1 - ((y1 - y4)/2);
%
% midbot_x = x3 + ((x3 - x2)/2);
% midbot_y = y2 - ((y2 - y3)/2);

% ACTUALLY. WHY DON'T I JUST ADD ANOTHER INPUT FOR THE MIDDLE OF THE CABLE
% AT THE TOP AND BOTTOM:

opp = midtop_y - midbot_y;
adj = midtop_x - midbot_x;

theta = atan(adj/opp);

% Translate all point such that (midtop_x, midtop_y) is the origin
% i.e. subtract from all points

for i = 1:size(fits,1)

    fits(i,2) = fits(i,2) - midtop_x;
    fits(i,4) = fits(i,4) - midtop_y;

end

newfits = zeros(size(fits,1),16);
% Rotates all points by angle THETA
newfits(:,2)=cos(theta).*fits(:,2)-sin(theta).*fits(:,4);
newfits(:,4)=sin(theta).*fits(:,2)+cos(theta).*fits(:,4);
newfits(:,7) = fits(:,7);

% Retranslate the points so the actual origin is the origin again
```

```

for i = 1:size(newfits,1)

    newfits(i,2) = newfits(i,2) + midtop_x;
    newfits(i,4) = newfits(i,4) + midtop_y;

end

% Again, need to translate before we rotate
x1 = x1 - midtop_x;
x2 = x2 - midtop_x;
x3 = x3 - midtop_x;
x4 = x4 - midtop_x;
y1 = y1 - midtop_y;
y2 = y2 - midtop_y;
y3 = y3 - midtop_y;
y4 = y4 - midtop_y;

% Recalculate the corners of the wanted area (commented out unused points)
%x1n=cos(theta)*x1-sin(theta)*y1;
y1n=sin(theta)*x1+cos(theta)*y1;

x2n=cos(theta)*x2-sin(theta)*y2;
%y2n=sin(theta)*x2+cos(theta)*y2;

%x3n=cos(theta)*x3-sin(theta)*y3;
y3n=sin(theta)*x3+cos(theta)*y3;

x4n=cos(theta)*x4-sin(theta)*y4;
%y4n=sin(theta)*x4+cos(theta)*y4;

% Translate back (commented out unused points)
%x1n = x1n + midtop_x;
x2n = x2n + midtop_x;
%x3n = x3n + midtop_x;
x4n = x4n + midtop_x;
y1n = y1n + midtop_y;
%y2n = y2n + midtop_y;
y3n = y3n + midtop_y;
%y4n = y4n + midtop_y;

% x2nn=x1n;
% y2nn=y2n;
% x3nn=x4n;
% y3nn=y2n;
%
% selected=LM_depthfilter(newfits,x1n,x4n,1);
% selected=LM_depthfilter(selected,y1n,y2n,2);

% Want to reselect the correct points, i.e. the square xwidth (x2 - x4),
% ywidth (y1 - y3)
selected2=LM_depthfilter(newfits,x4n,x2n,2);
selected2=LM_depthfilter(selected2,y3n,y1n,4);

selected(:,1) = selected2(:,2);
selected(:,2) = selected2(:,4);
selected(:,3) = selected2(:,7);

plot(selected(:,1),selected(:,2),'g. ');
hold on;

```

```

% Initialise holdallz
holdallz=zeros(10,10);
holdallx=zeros(100,10);
holdally=zeros(100,10);

% Calculates bin sizes
diffy=abs(y1n-y3n);
numbery=round(diffy.*pixelsize/sizestep);
diffx=abs(x2n-x4n);
numberx=round(diffx.*pixelsize/sizestep);

% Calculates # points in each bin box (holdallz). Also draws it
for i=1:numberx
    for j=1:numbery
temp=LM_depthfilter(selected,x4n+((i-
1)*sizestep/pixelsize),x4n+((i)*sizestep/pixelsize),1);
temp1=LM_depthfilter(temp,y3n+((j-
1)*sizestep/pixelsize),y3n+((j)*sizestep/pixelsize),2);

plot(temp1(:,1),temp1(:,2),'rp');
rectangle('Position',[x4n+((i-1)*sizestep/pixelsize),y3n+((j-
1)*sizestep/pixelsize),sizestep/pixelsize,sizestep/pixelsize]);
holdallz(i,j)=size(temp1,1);
holdallx(i,j)=(x4n+((i-1)*sizestep/pixelsize)+((sizestep/pixelsize)/2));
holdally(i,j)=(y3n+((j-1)*sizestep/pixelsize)+((sizestep/pixelsize)/2));

% Save as a cell array all the points that make up holdallz
% Will read these out later in the program (y)
holdallpoints(i,j) = {temp1};

drawnow;
    end
end
% final(:,1)=reshape(holdallz,1,[]);
% final(:,2)=reshape(holdallx,1,[]);
% final(:,3)=reshape(holdally,1,[]);
% figure
% scatter(final(:,2),final(:,3),(final(:,1)*50)+1,'b')

% SO - now to sum the points in each bin along the rows (i.e. along the
% length of the cable. Idk why it's like that but it is

summed_points = zeros (size(holdallz,1),1);
rowsum = 0;

for j = 1:(size(holdallz,1))
    for i = 1:size(holdallz,2)
        rownum = holdallz(j,i);
        rowsum = rowsum + rownum;
        summed_points(j,2) = rowsum;
    end
    summed_points(j,1) = holdallx(j,1);
    rownum = 0;
    rowsum = 0;
    % summed_points: 1 = midway point of bins, 2 = # points in that row
end

```

```

% Sum over all width & every (numsplits) (10) cells in length
numsplits = 10;
temppoints = [];

for k = 1:10:((floor(size(holdallz,2)/numsplits))*10)

    for i = 1:numsplits

        m = k + i - 1;

        for j = 1:size(holdallz,1)

            % Getting the info out of the cell into a useable format
            x = cell2mat(holdallpoints(j,m));
            X = zeros(size(x,1),16);
            X(:,2) = x(:,1);
            X(:,4) = x(:,2);
            X(:,7) = x(:,3);

            temppoints = [ temppoints ; X ];

        end

    end

    K = floor(k/numsplits) + 1;

    finalcellpoints(K,1) = { temppoints };

    % Reset temppoints
    temppoints = [];

end

end

```

6 - LM_BlinksPerSec

```
function [ list2, Blist, sumlist ] = LM_BlinksPerSec( BX, BY, width,
height, fits, framespersec )
%Calculates # of localisations per second

q = 1;
p = 0;

% Filtering on X

for q = 1:size(fits,1)

    if fits(q,2) > BX && fits(q,2) < (BX+width)
        p = p + 1;
        list1(p,1) = fits(q,2);
        list1(p,2) = fits(q,4);
        list1(p,3) = fits(q,7);
    end
end

% Filering on Y

k = 1;
m = 0;

for k = 1:size(list1,1)

    if list1(k,2) > BY && list1(k,2) < (BY+height)
        m = m + 1;
        list2(m,1) = list1(k,1);
        list2(m,2) = list1(k,2);
        list2(m,3) = list1(k,3);
    end
end

% List2 - xvalues, yvalues, framenumber

%%
% Sort into frame order - this means the frame and the xy position no
% longer relate to each other, but I don't think that matters?
% I can always remove this section if needs be
% Mainly adding this section for 90% confidence on actin strips

F = fits(:,7);
F = sort(F);

fits(:,7) = F;

%%
%Initialises List
Blist = zeros(fits((size(fits,1)),7),2);

% Not sure if this is necessary tbh, this just makes a list that goes
% 1,2,3... etc
Blist(1,1) = 1;
r = 1;
```



```

for r=1:(fits((size(fits,1)),7)+1)

    Blist((r+1),1) = Blist(r,1) + 1;

end

%% this reads the frame number off list2 and puts it next to the frame
% number in a big ol' list as a series of 1's (i.e. was a blink in that
% frame) or 0's (no blink in that frame).
% Can then sum the 1's and 0's in lumps of (framespersec) to find out how
% many blinks per second there are
n = 1;

for n=1:size(list2,1)

    b = list2(n,3);
    if Blist(b,2) >= 0
        Blist(b,2) = Blist(b,2) + 1;
    end

end

%% Attempting to sum the 1's and 0's...
a = 0;

Number = size(Blist,1)/framespersec - fix(size(Blist,1)/framespersec);
Subtractthis = Number*framespersec;
numwholeframes = size(Blist,1) - Subtractthis;

for a = 0:framespersec:(numwholeframes-framespersec)

    c = fix(a/framespersec) + 1;
    sumlist(c,2) = sum((Blist((a+1):(a+framespersec),2)));
    sumlist(c,1) = c;

end

%% Cumulative # blinks

sumlist(1,3) = sumlist(1,2);

for i = 2:(size(sumlist,1))

    sumlist(i,3) = sumlist((i-1),3) + sumlist(i,2);

end

end

```

7 - LM_CircularAreaDensity

```
function [ rvalues, pointspersec ] = LM_CircularAreaDensity( xvalue,
yvalue, radius, framespersec, fits )
% LM_Circular Area Density
% Inputs x & y values of an point in a STORM image, along with a given
% radius. Radius must be in PIXELS (1pixel = 100nm).
% Calculates the number of points within that radius of the points and
% outputs # of points, area and density
% Headings of 'rvalues' : x, newx, y, newy, r, frame#, y/n

m = 1;

rvalues = zeros(size(fits,1),7);
rvalues(:,1) = fits(:,2);
rvalues(:,3) = fits(:,4);

for m = 1:size(rvalues,1)

    % Subtract x values i.e. xnew = xm - xvalue
    rvalues(m,2) = rvalues(m,1) - xvalue;

    % Subtract y values
    rvalues(m,4) = rvalues(m,3) - yvalue;

end

n = 1;

for n = 1:size(rvalues,1)

    % Calculate radial distance away from point, i.e. r = SQRT(newx^2 +
newy^2)
    rvalues(n,5) = sqrt(rvalues(n,2).^2 + rvalues(n,4).^2);

    % rvalues(n,2) = frame#
    rvalues(n,6) = fits(n,7);

end

l = 1;

% Counting overall # of points - Change points outside of desired area to 0
for l = 1:size(rvalues,1)

    if rvalues(l,5) > radius
        rvalues(l,7) = 0;
    else rvalues(l,7) = 1;
    end

end

% Total # of frames in dataset fits
totalframes = rvalues(size(rvalues,1),6);

% Calculating density/# of points per second
totalseconds = ceil(totalframes/framespersec);
```

```

pointsperssec = (zeros(totalseconds, 4));

q = 0;
k = 0;

for q = 1:totalseconds

    pointsperssec(q,1) = q;

    for k = 1:size(rvalues,1)

        if ceil(rvalues(k,6)/framesperssec) == q
            pointsperssec(q,2) = pointsperssec(q,2) + rvalues(k,7);
        end

    end

end

end

% Calculate overall density in pixels
area = pi*radius.^2;
total_sumpoints = sum(rvalues(:,7));
rvalues(1,8) = total_sumpoints;
rvalues(2,8) = total_sumpoints / area;

u = 0;

% Calc how density changes over time
for u=1:totalseconds

    if (u-1) == 0
        pointsperssec(u,3) = pointsperssec(u,2);
        pointsperssec(u,4) = pointsperssec(u,3)/area;
    else
        pointsperssec(u,3) = pointsperssec((u-1),3) + pointsperssec(u,2);
        pointsperssec(u,4) = pointsperssec(u,3)/area;
    end

end

end

end

```

8 - LM_findPSF

```
function [ frames ] = LM_findPSF( files, x, y, fits )
% Chops out blinks and saves them into a stack
% Files from code
% Fits from reconstruction
% x & y are how large the image is (i.e. 200x200)

% Import only required frames into a 3D matrix

q = 2; %q = size(files,1);
frames = zeros(x,y,q); %initialise empty matrix
% x = width of image, y = height of image (i.e. 200x200px)
% q = # of tiffs to average signal over (i.e. them all)

%Want to import every frame
for m = 2 %1:size(files,1)

    %import frame
    frame = double(importdata(char(files{m})));

    % Save frame
    frames(:,:,m) = frame;

end

% Find the pixel value of each event point found by 'LM_dofiles'

e = 1;

for i = 1%i = 1:size(fits,1) % loop round all fits

    % find suggested pixel values for where the signal is
    xvalue = fits(i,15);
    yvalue = fits(i,16);

    % Want to chop out a square containing the signal and save as a
    % .tiff stack

    cutsize = 4; % I.e. size of cut squares will be cutsize*2 + 1

    coords = zeros(2,4);
    % Coords = TL, TR, BR, BL coords of square to cut out

    xplus = xvalue + cutsize;
    xminus = xvalue - cutsize;
    yplus = yvalue + cutsize;
    yminus = yvalue - cutsize;

    % Move onto the next point if too close to edge of image
    if xplus >= x
        continue
    elseif xminus <= 0
        continue
    elseif yplus >= y
        continue
    else
        continue
    end
end
```

```

elseif yminus <= 0
    continue
end

image = zeros(9,9);

k = 1;
l = 1;

d = fits(i,7); % What frame is the blink located on

for k = 1:9

    for l = 1:9

        % x value changes with each loop
        currentx = xminus + l - 1;

        % y value stays the same for whole row
        currenty = yplus - k + 1;

        image(k,l) = frames(currenty, currentx, d);

    end

end

i
intimage = uint8(image);

formatspec = 'img_%d.tif';
filename = sprintf(formatspec, i)
imwrite(intimage, filename, 'tif');

end

end

```

9 - LM_radialdistances

```
function [ distances_sorted, listofpoints, radialdistances_setframe ] =
LM_radialdistances( xvalue, yvalue, radius, fits, setframe )
% LM_radialdistances
% Inputs a point (i.e. center of a cell) and calculates the distance of all
% points from the center

% INPUT: setframe = FRAME at which to stop radial distances (for
histograms)
% OUTPUT: radialdistances_settime: Use this for the histograms

listofpoints = zeros(size(fits,1),6);
distances = zeros(size(fits,1),1);
listofpoints(:,1) = fits(:,2);
listofpoints(:,3) = fits(:,4);
listofpoints(:,6) = fits(:,7);

for m = 1:size(listofpoints,1)

    % Subtract x values i.e. xnew = xm - xvalue
    listofpoints(m,2) = listofpoints(m,1) - xvalue;

    % Subtract y values
    listofpoints(m,4) = listofpoints(m,3) - yvalue;

end

n = 1;

for n = 1:size(listofpoints,1)

    % Calculate radial distance away from point, i.e. r = SQRT(newx^2 +
newy^2)
    listofpoints(n,5) = sqrt(listofpoints(n,2).^2 + listofpoints(n,4).^2);

end

m = 1;

for m = 1:size(listofpoints,1)

    if listofpoints(m,5) <= radius
        distances(m,1) = listofpoints(m,5);
    end

end

distances_sorted = sort(distances, 'descend');

%%
% List of points. 1 = x, 2 = xnew, 3 = y, 4 = ynew, 5 = Radial Distance,
% 6 = Frame #, 7 = kmeans idx/blank, 8 = angle from upright vertical

%% Add angle into listofpoints
p = 1;
```

```

for m = 1:size(listofpoints,1)

    % If listofpoints(m,2) > 0 i.e. if xnew is POSITIVE
    if listofpoints(m,2) > 0

        % listofpoints(m,4) > 0 i.e. ynew positive
        if listofpoints(m,4) > 0

            % Listofpoints(m,8) = angle from upright vertical
            % See LabBook 3 Page 117
            % Tan theta = x/y
            %listofpoints(m,8) = atan(listofpoints(m,4)/listofpoints(m,2));
            listofpoints(m,8) =
abs(atan(listofpoints(m,2)/listofpoints(m,4)));
            one(p,1) = listofpoints(m,1);
            one(p,2) = listofpoints(m,3);
            one(p,3) = listofpoints(m,8);

            p = p + 1;

        else % I.e. if ynew is negative

            % tan theta = y/x
            %listofpoints(m,8) = (pi/2) +
atan(listofpoints(m,4)/listofpoints(m,2));
            listofpoints(m,8) = 90 +
abs(atan(listofpoints(m,4)/listofpoints(m,2)));
            two(p,1) = listofpoints(m,1);
            two(p,2) = listofpoints(m,3);
            two(p,3) = listofpoints(m,8);

            p = p + 1;
        end

    end

    % If listofpoints(m,2) < 0 i.e. if xnew is NEGATIVE
    if listofpoints(m,2) < 0

        % listofpoints(m,4) < 0 i.e. ynew negative
        if listofpoints(m,4) < 0

            % Tan theta = x/y
            %listofpoints(m,8) = (2*pi) +
atan(listofpoints(m,2)/listofpoints(m,4));
            listofpoints(m,8) = 180 +
abs(atan(listofpoints(m,2)/listofpoints(m,4)));
            three(p,1) = listofpoints(m,1);
            three(p,2) = listofpoints(m,3);
            three(p,3) = listofpoints(m,8);

            p = p + 1;

        else % I.e. if ynew is positive

            % tan theta = y/x

```

```

        %listofpoints(m,8) = (3*pi/2) +
atan(listofpoints(m,2)/listofpoints(m,4));
        listofpoints(m,8) = 270 +
abs(atan(listofpoints(m,4)/listofpoints(m,2)));
        four(p,1) = listofpoints(m,1);
        four(p,2) = listofpoints(m,3);
        four(p,3) = listofpoints(m,8);

        p = p + 1;

    end

end

end

%% Output radial distances chopped off at a certain time (for histograms)

for k = 1:size(listofpoints,1)

    radialdistances_setframe(k,1) = listofpoints(k,5);

    if listofpoints(k,6) > setframe

        break

    end

end

end

end

```


10 - Make_binary

```
function [ image2 ] = make_binary( image, threshold )
% After importing an image (i.e. A = imread('img.jpg'))
% This program turns any pixel value over a threshold into 1/under = 0

Size = size(image);
width = Size(1,1);
length = Size(1,2);

for n = 1:length

    for m = 1:width

        if image(n,m) >= threshold
            image(n,m) = 1;
        else image(n,m) = 0;

        end

    end

end

image2 = logical(image);

end
```

11 - Simulate seaweed

```
function [ GROUP, seaweed, percentages ] = simulate_seaweed( cutoff )
% Simulates seaweed data graphs (i.e. % of groups that have reached the cut
% off limit density against time)
% Input 'cutoff' changes how many molecules are required to be added to
% each group before reaches the cut off (i.e. 10 molecules. Or whatever)

% FOR TESTING PURPOSES: initialise random numbers for repeatability
% rng(0,'twister');

% initialise groups. GROUP is a 1x16 area, 1x20, whatever
group = zeros(1,2);
GROUP = { group; group; group; group; group; group; group; group; group; group;
group; group; group; group; group; group; group; group; group; group;
group};

% Number of groups
Q = 20;

% Add Molecules to groups
for a = 1:1000

    % Add a 'time' to each group
    for b = 1:Q

        % Column 1 = time (i.e. # of iterations)
        GROUP{b,1}(a,1) = a;

        % Column 2 = number of molecules in that group so far (i.e. same #
        % of molecules as the last time point.
        % Once generated random number will potentially add another number
        if a == 1
            GROUP{b,1}(a,2) = 0;
        else
            GROUP{b,1}(a,2) = GROUP{b,1}((a-1),2);
        end

    end

    % Generate a random number between 1 & 16
    RANDNUM = randi(Q);

    % Add one to group specified by RANDNUM
    GROUP{RANDNUM,1}(a,2) = GROUP{RANDNUM,1}(a,2) + 1;

end

% Order data into something useable
% initialise seaweed output
seaweed = zeros (Q, 2);

for a = 1:Q

    sizeloop = size(GROUP{a,1},1);

    for b = 1:sizeloop
```

```

num_mol = GROUP{a,1}(b,2);

if num_mol == cutoff
    TIME = GROUP{a,1}(b,1);
    break
end

end

% Column 1 = group, column 2 = time rreaches cut off
seaweed(a,1) = a;
seaweed(a,2) = TIME;

end

% Output percentages

percentages = zeros(Q,2);

percentages(:,2) = sort(seaweed(:,2));

for a = 1:Q
    percent = (a/Q)*100;
    percentages(a,1) = percent;
end

end

```

12 - Simulate_seaweed_2

```
function [ GROUP, seaweed, percentages ] = simulate_seaweed_2( cutoff )
%Exactly the same as seaweed only this time there doesn't have to have a
%point added to every group each time

% FOR TESTING PURPOSES: initialise random numbers for repeatability
% rng(0,'twister');

% initialise groups. GROUP is a 1x20, whatever (can change this by
% adding/subtracting groups from GROUP and changing the value of Q)
group = zeros(1,2);
GROUP = { group; group; group; group; group; group; group; group; group;
group; group; group; group; group; group; group; group; group;
group};

% Number of groups
Q = 20;

% Add Molecules to groups
for a = 1:1000

    % Add a 'time' to each group
    for b = 1:Q

        % Column 1 = time (i.e. # of iterations)
        GROUP{b,1}(a,1) = a;

        % Column 2 = number of molecules in that group so far (i.e. same #
        % of molecules as the last time point.
        % Once generated random number will potentially add another number
        if a == 1
            GROUP{b,1}(a,2) = 0;
        else
            GROUP{b,1}(a,2) = GROUP{b,1}((a-1),2);
        end

    end

    % Generate a random number between 1 & Q+5.
    RANDNUM = randi((Q+5));

    % If the random number generated corresponds to a group - add a
    % molecule to that group.
    % This allows a for Q = 20 and generating between 1-Q+5 gives a 20%
    % chance for a molecule to not be added to a group each "second"
    if RANDNUM <= (Q)
        % Add one to group specified by RANDNUM
        GROUP{RANDNUM,1}(a,2) = GROUP{RANDNUM,1}(a,2) + 1;
    end

end

% Order data into something useable
% initialise seaweed output
seaweed = zeros (Q, 2);

for a = 1:Q
```

```

sizeloop = size(GROUP{a,1},1);

for b = 1:sizeloop

    num_mol = GROUP{a,1}(b,2);

    if num_mol == cutoff
        TIME = GROUP{a,1}(b,1);
        break
    end

end

% Column 1 = group, column 2 = time rreaches cut off
seaweed(a,1) = a;
seaweed(a,2) = TIME;

end

% Output percentages

percentages = zeros(Q,2);

percentages(:,2) = sort(seaweed(:,2));

for a = 1:Q

    percent = (a/Q)*100;
    percentages(a,1) = percent;

end

end

```

13 - Simulate_seaweed_3

```
function [ GROUP, seaweed, percentages ] = simulate_seaweed_3( cutoff )
%Exactly the same as seaweed only this time there doesn't have to have a
%point added to every group each time & groups 1-5 weighted more heavily

% FOR TESTING PURPOSES: initialise random numbers for repeatability
% rng(0,'twister');

% initialise groups. GROUP is a 1x20, whatever (can change this by
% adding/subtracting groups from GROUP and changing the value of Q)
group = zeros(1,2);
GROUP = { group; group; group; group; group; group; group; group; group;
group; group; group; group; group; group; group; group; group;
group};

% Number of groups
Q = 20;

% Add Molecules to groups
for a = 1:1000

    % Add a 'time' to each group
    for b = 1:Q

        % Column 1 = time (i.e. # of iterations)
        GROUP{b,1}(a,1) = a;

        % Column 2 = number of molecules in that group so far (i.e. same #
        % of molecules as the last time point.
        % Once generated random number will potentially add another number
        if a == 1
            GROUP{b,1}(a,2) = 0;
        else
            GROUP{b,1}(a,2) = GROUP{b,1}((a-1),2);
        end

    end

    % Generate a random number between 1 & Q+10.
    RANDNUM = randi((Q+10));

    % If the random number generated corresponds to a group - add a
    % molecule to that group.
    % This allows a for Q = 20 and generating between 1-Q+5 gives a 20%
    % chance for a molecule to not be added to a group each "second"
    % If random number = 20-25, recall this as a number between 1 - 5 to
    % weight groups 1-5 more heavily than other groups

    if RANDNUM >20
        if RANDNUM >= 25
            RANDNUM = randi(5);
        end
    end

    if RANDNUM <= (Q)

        % Add one to group specified by RANDNUM
        GROUP{RANDNUM,1}(a,2) = GROUP{RANDNUM,1}(a,2) + 1;
    end
end
```

```

end

end

% Order data into something useable
% initialise seaweed output
seaweed = zeros (Q, 2);

for a = 1:Q

    sizeloop = size(GROUP{a,1},1);

    for b = 1:sizeloop

        num_mol = GROUP{a,1}(b,2);

        if num_mol == cutoff
            TIME = GROUP{a,1}(b,1);
            break
        end

    end

    % Column 1 = group, column 2 = time rreaches cut off
    seaweed(a,1) = a;
    seaweed(a,2) = TIME;

end

% Output percentages

percentages = zeros(Q,2);

percentages(:,2) = sort(seaweed(:,2));

for a = 1:Q

    percent = (a/Q)*100;
    percentages(a,1) = percent;

end

end

```

14 - SNR_finder

```
function [ frames, signallist ] = SNR_finder( files, x, y, fits)
% Finds the Signal of each point
% Import only required frames into a 3D matrix

q = size(files,1);
frames = zeros(x,y,q); %initialise empty matrix
% x = width of image, y = height of image (i.e. 200x200px)
% q = # of tiffs to average signal over (i.e. every 500th)

%Want to import every 500th frame (i.e. 1, 501, 1001, 1501)
for m = 1:size(files,1)

    %import frame
    frame = double(importdata(char(files{m})));

    % Code for placing frames into correct sections (so don't put into a
    % 1501 leaflet matrix, only want 4 leaflets!)
    % B = fix(m/500); %'fix' command = round down
    frames(:, :,m) = frame;

end

% Find the pixel value of each event point found by 'LM_dofiles'

%signallist = zeros(size(fits2,1),2); % initialise empty matrix

% n = fits2(1,7); % use to calc. frame number (so starts at 1)
% No need for this if assuming all frame #'s start from 1...
e = 1;

for i = 1:size(fits,1) % loop round all fits

    %if fits2(i,7) == 3500 || fits2(i,7) == 4000
    % find suggested pixel values for where the signal is
    xvalue = fits(i,15);
    yvalue = fits(i,16);

    % Find which leaflet of matrix we need
    % A = fix((fits(i,7)-fits(1,7))/500);

    % use suggested pixel values to find actual intensity from frame
    % where frame1 = double(importdata(char(files{1})));
    % signal_value = frames(yvalue, xvalue, (A+1));
    d = fits(i,7);
    signal_value = frames(yvalue, xvalue, d);

    % Save signal values into list
    signallist(e,1) = fits(i,7);
    signallist(e,2) = signal_value;
    e = e + 1;
%end

end

end
```


15- Sortemitters

```
function [ last_emitter_ident, emitter_identifiers, filtered_emitters ] =
sortemitters( emitters )
% Takes output of 'LM_emitters' code and makes it useable

sorted = sort(emitters(:,10));

sorted2 = zeros(size(emitters,1),7);

% These may be called 'sorted2' but none of them are ACTUALLY sorted into
% order
% 1 = emitter identifying #, 2 = x, 3 = y, 4 = frame #
sorted2(:,1) = emitters(:,10);
sorted2(:,2) = emitters(:,2);
sorted2(:,3) = emitters(:,4);
sorted2(:,4) = emitters(:,7);

sorted2(:,6) = emitters(:,3); % x width
sorted2(:,7) = emitters(:,5); % y width

% A = number of points
A = size(sorted,1);

last_emitter_ident = sorted(A, 1);

emitter_identifiers = zeros(last_emitter_ident,7);

for n = 1:last_emitter_ident

    % List emitter ident. from 0 - largest value
    emitter_identifiers(n,1) = n;

end

% loop through all points
for n = 1:A

    % Temp = emitter identifier we're looking for this time
    temp = sorted2(n,1);

    emitter_identifiers(temp,2) = emitter_identifiers(temp,2) + 1;

    if emitter_identifiers(temp,5) == 0

        emitter_identifiers(temp,5) = sorted2(n,4);

    end

    % these two lines of code should place the last x & y value found for
    % the emitter identifier as the x & y value to be plotted....
    emitter_identifiers(temp,3) = sorted2(n,2);
    emitter_identifiers(temp,4) = sorted2(n,3);

end
```

```

emitter_identifiers(temp,6) = sorted2(n,6);
emitter_identifiers(temp,7) = sorted2(n,7);

% Emitter_identifiers
% 1 = emitter ident. #, 2 = # of blinks @ that location, 3 = x position
% of last emitter found @ that location, 4 = y position, 5 = frame
% number of last emitter found @ that location

end

% In order to use 'LM_BlinksPerSec' with the filtered emitters, need to
% reorder into 'filtered_emitters'

Q = size(emitter_identifiers,1);

filtered_emitters = zeros(Q,16);

filtered_emitters(:,10) = emitter_identifiers(:,1);
filtered_emitters(:,2) = emitter_identifiers(:,3);
filtered_emitters(:,4) = emitter_identifiers(:,4);
filtered_emitters(:,7) = emitter_identifiers(:,5);

filtered_emitters(:,3) = emitter_identifiers(:,6);
filtered_emitters(:,5) = emitter_identifiers(:,7);

end

```

16 - LM_blinkofftime

```
function [ timeslist ] = LM_blinkofftime( data )
%Analyses ThunderSTORM data - finds all points within (+-) 10 nm and
calculates time difference between turning off/on.

overalltimesfound = 0;
timeslist = zeros();
q = 1;

for i = 1:size(data,1)

    if data(i, 1) == 0

        continue

    end

    id = data(i, 1);
    lowerx = data(i, 3) - 10;
    upperx = data(i, 3) + 10;

    lowery = data(i, 4) - 10;
    uppery = data(i, 4) + 10;

    [ newout ] = LM_depthfilter( data, lowerx, upperx, 3);
    [ newout ] = LM_depthfilter( newout, lowery, uppery, 4);

    % If there are no points or only 1 point without, delete the datapoint
    % and continue to the next one
    if size(newout, 1) == 1

        data(i, :) = zeros();
        continue

    end

    numpointsfound = size(newout,1);
    numtimesfound = numpointsfound - 1;

    for m = 1:numtimesfound

        overalltimesfound = overalltimesfound + 1;
        timeslist(q, 1) = id;
        timeslist(q, 2) = newout((m+1),2) - newout(m,2);
        q = q + 1;

    end

    for n = 1: size(newout);

        S = newout(n,1);
        data(S,:) = zeros();

    end

end
end
```